UNIVERSITAT POLITÈCNICA DE VALÈNCIA

DOCTORAL THESIS

NUMERICAL AND OPTICAL ASSESSMENT OF DIFFERENT SOLUTIONS FOR POLLUTANT EMISSION REDUCTION IN COMPRESSION IGNITION ENGINES

WRITTEN BY

USAMA BIN KHALID

SUPERVISED BY

Dr. CARLOS MIĆO RECHE

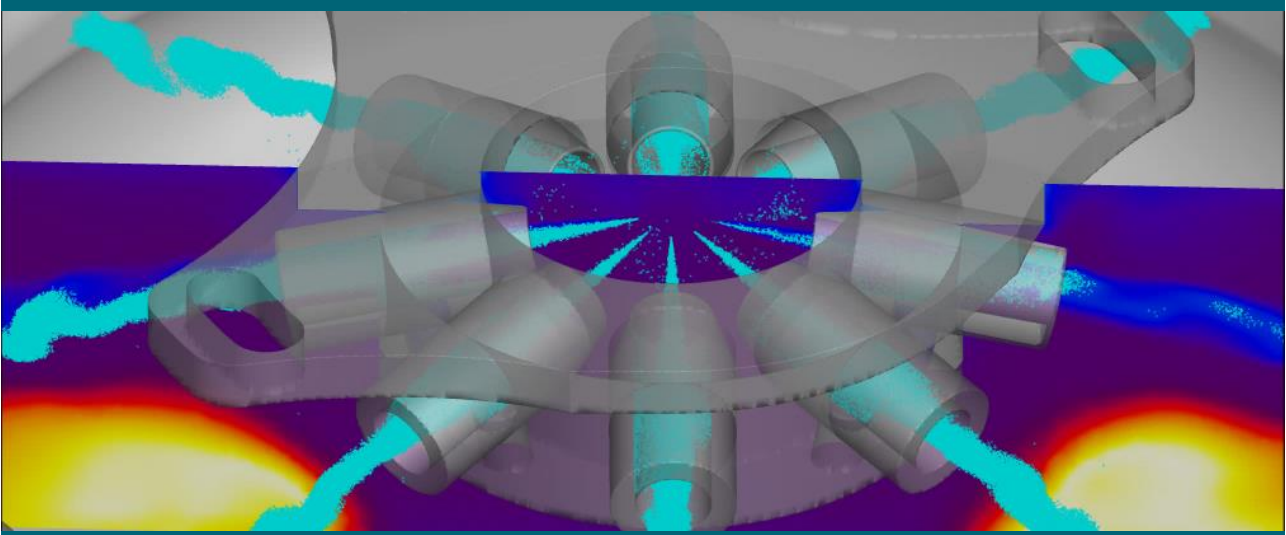

JUNE 2024

CMT - CLEAN MOBILITY & THERMOFLUIDS

Universitat Politècnica de València
I.U.I. CMT – Clean Mobility & Thermofluids

Doctoral Thesis

NUMERICAL AND OPTICAL ASSESSMENT OF DIFFERENT SOLUTIONS FOR POLLUTANT EMISSION REDUCTION IN COMPRESSION IGNITION ENGINES

Written by:
Usama Bin Khalid

Supervised by:
Dr. Carlos Mićo Reche

in fulfillment of the requirements for the degree of
Doctor of Philosophy in Transport Propulsion Systems

Valencia, June 2024

Ph.D. Thesis

NUMERICAL AND OPTICAL ASSESSMENT OF DIFFERENT SOLUTIONS FOR POLLUTANT EMISSION REDUCTION IN COMPRESSION IGNITION ENGINES

Written by: Usama Bin Khalid
Supervised by: Dr. Carlos Mićo Reche

Examination committee:

Chairman: Dr. José Javier López Sánchez
Secretary: Dr. Blanca Gimenez Olavarria
Member: Dr. Elna Heimdal Nilsson

Reviewing board:

Dr. Luciano Rolando
Dr. Elna Heimdal Nilsson

Valencia, June 2024

Abstract

The reduction of the carbon footprint of internal combustion engines and the pollutant emissions is mandatory for the survival of this technology, especially for medium and heavy-duty applications. In the last decade, researchers and manufacturers have explored different approaches to achieve this goal. In this sense, the use of alternative fuels and alternative technologies is considered as a potential pathway to reach this objective.

Within the scope of alternative fuels, e-fuels and biofuels are gaining relevance as they can be utilized without major modifications of the internal combustion engine technology. The former term refers to fuels that can be both gaseous or liquid and are produced from renewable electricity in a synthetic process consuming carbon dioxide and water. The latter refers to fuels produced from biomass and organic waste. Among e-fuels, oxymethylene dimethyl ethers stand out, and among biofuels, hydrotreated vegetable oil is particularly notable. On the one hand, oxymethylene dimethyl ethers drastically reduce pollutant emissions however suffer challenges like lower energy density, and compatibility with conventional engines when utilized in pure form. On the other hand, hydrotreated vegetable oil presents similar properties as compared to diesel and is considered a good drop in fuel for fossil diesel despite providing a lesser pollutant reduction when compared with oxymethylene dimethyl ethers. However, these fuels, when produced solely from renewable resources, can drastically reduce the carbon footprint.

Another way to address pollutant emission reduction, which has provided great advances in the past, is the design of new hardware directly involved with the combustion process. From complex piston bowl geometries or injector nozzles to new concepts like ducted fuel injection for heavy-duty applications, which improves the air-fuel mixing process increasing efficiency and reducing pollutant formation. Nevertheless, a better understanding of their impact on the combustion process and engine performance is required for proper implementation in commercial solutions.

In light of the aforementioned text, the current thesis is focused on advancing the knowledge of the behaviour of alternative fuels and new hardware concepts under operating conditions of compression ignition engines and their impact on combustion performance and pollutant formation. These assessments are done both by detailed numerical simulations and experiments carried out in an optically accessible compression ignition engine, utilizing a variety of optical techniques. Results highlight that these two promising approaches can greatly reduce the pollutant formation inside the compression

ignition engine and can be a potential solution to the ever-increasing carbon footprint and pollutant emissions problem of compression ignition engines.

Resumen

La reducción de la huella de carbono de los motores de combustión interna así como de sus emisiones contaminantes es necesaria para la supervivencia de esta tecnología, especialmente para aplicaciones de uso medio y pesado. En la última década, investigadores y fabricantes han explorado diferentes enfoques para lograr este objetivo. En este sentido, el uso de combustibles alternativos y tecnologías alternativas se considera una vía potencial para alcanzarlo.

Dentro del ámbito de los combustibles alternativos, los e-fuels y los biocombustibles están ganando relevancia, ya que pueden ser utilizados sin modificaciones importantes en la tecnología de motores de combustión interna. El primer término se refiere a combustibles que pueden ser tanto gaseosos como líquidos y que se producen a partir de electricidad renovable mediante un proceso sintético que consume dióxido de carbono y agua. El segundo se refiere a combustibles producidos a partir de biomasa y residuos orgánicos. Entre los e-fuels, destacan los éteres dimetílicos de oximetileno, y entre los biocombustibles, es particularmente notable el aceite vegetal hidrotratado. Por un lado, los primeros destacan por reducir drásticamente las emisiones contaminantes, aunque presentan problemas como una menor densidad energética y compatibilidad con los motores convencionales cuando se utilizan en estado puro. Por otro lado, el aceite vegetal hidrotratado presenta propiedades similares a las del diésel y se considera un buen sustituto de este a pesar de reducir menos las emisiones contaminantes que los éteres de dimetileno de oximetileno. Sin embargo, ambos combustibles, cuando se producen exclusivamente a partir de recursos renovables, pueden reducir drásticamente la huella de carbon.

Otra forma de abordar la reducción de las emisiones contaminantes, que ha proporcionado grandes avances en el pasado, es el diseño de nuevo hardware directamente implicado en el proceso de combustión. Desde geometrías complejas del cuenco del pistón o de toberas de los inyectores hasta nuevos conceptos como la inyección de combustible por conductos para aplicaciones pesadas, que mejoran el proceso de mezcla aire-combustible aumentando la eficiencia y reduciendo la formación de contaminantes. No obstante, es necesario comprender mejor su impacto en el proceso de combustión y en el rendimiento del motor para su correcta aplicación en soluciones commercials.

A la luz de lo anterior, la presente tesis se centra en avanzar en el conocimiento del comportamiento de los combustibles alternativos y los nuevos conceptos de hardware en las condiciones de funcionamiento de los motores de encendido por compresión y su impacto en el rendimiento de la combustión y la formación de contaminantes. Estas evaluaciones se realizan tanto medi-

ante simulaciones numéricas detalladas como mediante experimentos llevados a cabo en un motor de encendido por compresión ópticamente accesible, utilizando diversas técnicas ópticas. Los resultados ponen de relieve que estos dos enfoques prometedores pueden reducir en gran medida la formación de contaminantes en el interior del motor de encendido por compresión y pueden ser una solución potencial al problema cada vez mayor de la huella de carbono y las emisiones contaminantes de los motores de encendido por compresión.

Resum

La reducció de la petjada de carboni dels motors de combustió interna així com de les seues emissions contaminants és necessària per a la supervivència d'esta tecnologia, especialment per a aplicacions d'ús mitjà i pesat. En l'última dècada, investigadors i fabricants han explorat diferents enfocaments per a aconseguir este objectiu. En este sentit, l'ús de combustibles alternatius i tecnologies alternatives es considera una via potencial per a aconseguir-ho.

Dins de l'àmbit dels combustibles alternatius, els e-fuels i els biocombustibles estan guanyant rellevància, ja que poden ser utilitzats sense modificacions importants en la tecnologia de motors de combustió interna. El primer terme es refereix a combustibles que poden ser tant gasosos com líquids i que es produeixen a partir d'electricitat renovable mitjançant un procés sintètic que consumeix diòxid de carboni i aigua. El segon es refereix a combustibles produïts a partir de biomassa i residus orgànics. Entre els e-fuels, destaquen els èters dimetílics d'oximetilè, i entre els biocombustibles, és particularment notable l'oli vegetal hidrotratat. D'una banda, els primers destaquen per reduir dràsticament les emissions contaminants, encara que presenten problemes com una menor densitat energètica i compatibilitat amb els motors convencionals quan s'utilitzen en estat pur. D'altra banda, l'oli vegetal hidrotratat presenta propietats similars a les del dièsel i es considera un bon substitut d'este malgrat reduir menys les emissions contaminants que els èters dimetílics d'oximetilé. No obstant això, tots dos combustibles, quan es produïxen exclusivament a partir de recursos renovables, poden reduir dràsticament la petjada de carboni.

Una altra manera d'abordar la reducció de les emissions contaminants, que ha proporcionat grans avanços en el passat, és el disseny de nou maquinari directament implicat en el procés de combustió. Des de geometries complexes del bol del pistó o de toveres dels injectors fins a nous conceptes com la injecció de combustible per conductes per a aplicacions pesades, que milloren el procés de mescla aïre-combustible augmentant l'eficiència i reduint la formació de contaminants. No obstant això, és necessari comprendre millor el seu impacte en el procés de combustió i en el rendiment del motor per a la seua correcta aplicació en solucions comercials.

A la llum de l'anterior, la present tesi se centra en avançar en el coneixement del comportament dels combustibles alternatius i els nous conceptes de maquinari en les condicions de funcionament dels motors d'encesa per compressió i el seu impacte en el rendiment de la combustió i la formació de contaminants. Estes avaluacions es realitzen tant mitjançant simulacions numèriques detallades com mitjançant experiments duts a terme en un motor

d'encesa per compressió òpticament accessible, utilitzant diverses tècniques òptiques. Els resultats posen en relleu que estos dos enfocaments prometedors poden reduir en gran manera la formació de contaminants a l'interior del motor d'encesa per compressió i poden ser una solució potencial al problema cada vegada major de la petjada de carboni i les emissions contaminants dels motors d'encesa per compressió.

*"**Work, work and work and we are bound to succeed.**"*

Muhammad Ali JINNAH

Dedicated to my family...
Specially to my mother.

Acknowledgements

First and foremost, I would like to praise and thank Allah (God), The Almighty, for granting me life and guidance, as well as for surrounding me with supportive and knowledgeable individuals throughout the course of my Ph.D. thesis.

I would like to then acknowledge my supervisor Dr. Carlos Mico without his guidance and support, my PhD journey wouldn't have been possible especially during the first years, when I was reluctant to continue at CMT. Despite not being physically present in valencia for the duration of my PhD, his regular participation in team meetings ensured that his guidance and supervision were always felt and greatly valued. Thank you for that Professor.

Further, I would like to extend my gratitude to Prof. Jose Pastor, Prof. Garcia-Oliver and Prof. Ricardo Novella who were involved throughout my thesis. Very special thanks to Dr. Dario Lopez at Sandia National Laboratories, whose role was very incremental in developing my interest in chemical kinetics alongside CFD which led to my stay in the USA.

I would like to express my special thanks to Frank and Felipe as these two guided me really to understand optical techniques and optical engine operation. Frank, thanks for letting me accompany you in the lab during the campaign with Duramax in the first year and helping me throughout my PhD journey, especially in post-processing algorithms. Felipe thanks for your support during the campaign with DFI in the last year. Further, I would like to thank my friends and colleagues at CMT who were beside me, especially Aditya, Waqas and Daiana.

I express my heartfelt appreciation to Omar and Dani for conducting the experimental tests alongside me, and to all the members of CMT, including the researchers, professors, technicians, and administrative staff. Special thanks to Amparo for her dedication, responsibility, and clear guidance through all the administrative procedures.

Lastly special gratitude to my beloved family; my dear parents Khalid Saeed and Samina Yasmin who wanted me to be a Dr. (PhD), my beloved wife Rida who supported me throughout and my brothers Awais, Ans and Ayyaz. Thank you everyone.

Funding Acknowledgements

The author would like to acknowledge the financial support received through contract UPV - Subprograma 2 (PAID-01-22) del Vicerrectorado de Investigaciòn, which was incremental in the development of this thesis at I.U.I. CMT – Clean Mobility & Thermofluids, Universitat Politècnica de València. Furthermore, author also acknowledges the grant Ayudas Para Movilidad de Estudiantes de Doctorado de la Universitat Politècnica de València - 2022, which made his research stay possible at Sandia National Laboratories.

List of Publications

Usama Bin Khalid is co-author of the publications detailed in this section, with the supervision of other members of the I.U.I CMT – Clean Mobility & Thermofluids (CMT), and specially by the thesis director, Dr.Carlos Mićo Reche. The publications in this section are merely the publications resulting from the researching activities performed during the candidate's doctorate. The respondent solely carried out both numerical analyses and experimental studies, which were presented in the publications. The analysis and discussion of results and procedures were done in collaboration with the thesis director (Dr.Carlos Mićo Reche) and with the co-authors of each publication. Any requirement to guarantee the fulfilment of the Ph.D. works, such as materials, software licenses, computational resources and test benches were provided by the UPV and CMT. The results of the publications mentioned in this section have been improved, ordered, linked, completed, and further discussed in the present thesis manuscript. The part of the contents, figures and discussions of this thesis have been partially taken from the PhD candidate publications. The last publication was carried out on candidate's doctoral research stay at Sandia National Laboratories, USA in collaboration with Dr.Dario lopez-pintor utilizing Sandia's computational resources. The methodology outlined in that publication served as a partial guide for the development of the present thesis manuscript. However, its results were not incorporated, as the study primarily delved into fundamental aspects rather than directly addressing applications in CI engines, unlike other publications. This section compensates and justifies that the basis of the innovative component that has already been presented in the publications specified in this section, therefore constituting Mr. Usama's thesis document. The signature of PhD candidate follows the CMT members seniority signing order protocol. Hence, in most publications, the PhD candidate becomes the last signer according to this protocol. The following journal and conference papers have been published in chronological order:

1. J. M. Garcıa-Oliver, R. Novella, C. Micó, and **Bin-Khalid, Usama**, "A numerical investigation of the performance of oxymethylene ethers blended with fossil diesel to reduce soot emissions in compression ignition engines", Fuel, vol. 324, p. 124 768, 2022. DOI: https://doi.org/10.1016/j.fuel.2022.124768.

2. J. M. Garcia-Oliver, R. Novella, D. L. Pintor, C. Micó, and **Bin-Khalid, Usama**, "A numerical approach for the analysis of hydrotreated vegetable oil and dimethoxy methane blends as low-carbon alternative fuel

in compression ignition engines", SAE Technical Paper 2023-01-0338, 2023, DOI: https://doi.org/10.4271/2023-01-0338.

3. J. M. García-Oliver, R. Novella, C. Micó, **Bin-Khalid, Usama**, and D. Lopez-Pintor, "A numerical analysis of hydrotreated vegetable oil and dimethoxymethane (OME1) blends combustion and pollutant formation through the development of a reduced reaction mechanism",International Journal of Engine Research, vol. 0, no. 0, p. 14 680 874 231 226 321, 0. DOI: https://doi.org/10.1177/14680874231226321.

4. J. M. García-Oliver, R. Novella, C. Micó, and **Bin-Khalid, Usama**, "Development of a reduced primary reference fuel – oxymethylene dimethyl ether (PRF-OMEx) mechanism for diesel engine applications",International Journal of Engine Research, vol. 0, no. 0, p. 14 680 874 241 255 755, 0. DOI: https://doi.org/10.1177/14680874241255755.

5. **Bin-Khalid, Usama**, D. Lopez-Pintor, C. Micó, and S. Lee, "Potential of 2-ethylhexyl nitrate (ehn) and di-tert-butyl peroxide (dtbp) to enhance the cetane number of ethanol, a detailed chemical kinetic study," Fuel, vol. 363, p. 130 928, 2024. DOI: https://doi.org/10.1016/j.fuel.2024.130928.

Contents

List of Figures

List of Tables

Nomenclature

Acronyms

AHRR	Apparent heat release rate.
AMR	Adaptive mesh refinement.
ATDC	After top dead center.
BTE	Brake thermal efficiency.
CAD	Crank angle degree.
CDS	Controlled diffusive nozzle.
CFD	Computational fluid dynamics.
CI	Compression ignition.
CO_2	Carbon dioxide.
CO	Carbon monoxide.
CVCV	Constant volume combustion chamber.
D100	100% Diesel.
D50O50	50% Diesel-50% OME_x in mass.
D70O30	70% Diesel-30% OME_x in mass.
D80O20	80% Diesel-20% OME_x in mass.
D90O10	90% Diesel-10% OME_x in mass.
DFI	Ducted fuel injection.
DNS	Direct numerical simulation.
DOC	Diesel oxidation catalyst.
DPF	Diesel particulate filter.
DRGEPSA	DRGEP with sensitivity analysis.

DRGEP	Direct relation graph with error propagation.
DRGPFA	Direct relation graph with path flux analysis.
DRG	Direct relation graph.
E-fuel	electro fuel.
EGR	Exhaust gas re-circulation.
EQ	Equivalence ratio.
EU	European union.
EVO	Exhaust valve opening.
FPS	Frame per second.
FS	Free spray.
FWHM	Full width half maximum.
GHG	Green house gas.
H100	100% HVO.
H70M30	70% HVO-30% OME_1 in mass.
H80M20	80% HVO-20% OME_1 in mass.
H90M10	90% HVO-10% OME_1 in mass.
HCCI	Homogeneous charge compression ignition.
HC	Hydrocarbon.
HVO	Hydrotreated vegetable oil.
ICE	Internal combustion engine.
ID	Ignition delay.
IHRR	Integrated heat release rate.
IMEP	Indicated mean effective pressure.
IR	Infrared.
IVC	Inlet valve closing.
LCA	Life cycle analysis.
LES	Large eddy simulation.
LFS	Laminar flame speed.
LHV	Lower heating value.
LLFC	Leaner lifted-flame combustion.
LLNL	Lawrence livermore national laboratory.
LOL	Lift-off length.
NL	Natural luminosity.
NO_x	Nitrogen oxides.

OHV	Over head valve.
OH	Hydroxyl radical.
OME_1	Dimethoxymethane or Methylal.
OME_x	Oxymethylene dimethyl ethers where x>1.
PAH	Poly aromatic hydrocarbon.
PCCI	Premixed Charge Compression Ignition.
PM	Particulate matter.
PRF	Primary reference fuel.
RANS	Reynolds averaged navier stokes.
RCCI	Reactivity controlled compression ignition.
RoHR	Rate of heat release.
SCR	Selective catalyst reduction.
SNL	Sandia national laboratories.
SOC	Start of combustion.
SOE	Start of energizing.
SOI	Start of ignition.
TER	Total energy released.
TKE	Turbulent kinetic energy.
TRF	Tertiary reference fuel.
UV	Ultra violet.
WDF	Wide distillation fuel.

Greek symbols

λ	Wavelength.
μ	Micro.
ϕ	Spray cone angle.
ρ	Density.
τ	Reynolds stress.
ε	Emissivity.

Latin symbols

μ_t	Turbulent viscosity.
A	Pre-exponential factor.
A_r	Area of ring.
D_t	Turbulent diffusion.

I	Radiance (general).
K_t	Turbulent conductivity.
K_{eng}	Engagement coefficient.
K_{ins}	Insertion coefficient.
KL	Optical thickness related to soot.
OH^*	Excited state hydroxyl radical.
P	Pressure (general).
Pr_t	Turbulent prandtl number.
Sc_t	Turbulent schmidt number.
T	Temperature (general).
u	velocity (general).
$\overline{KL}_{\text{acc}}$	Mean accumulated KL.
KL_{mean}	Mean KL.

Chapter 1

Introduction

1.1 Introduction

This chapter provides a framework which justifies the relevance of the thesis, the hypothesis addressed and the work done focusing on internal combustion engines for transportation. The first section gives an overview of the global context in today's transportation landscape and the problems with internal combustion engines that motivated this study. Additionally, a brief description of new technologies and solutions that aim to keep internal combustion engines alive has also been addressed. It further offers insight into previous research conducted within the research group, providing valuable background context. Finally, the objectives of the thesis and the general structure of this document are addressed, highlighting the novelties of this work.

1.2 General context and motivations

In recent decades, with all technological advancements and increasing industrialization, our world has experienced a remarkable surge in energy consumption. Figure 1.1 shows the increase of energy demand during the past decades until now [1]. Considering the latest period (leaving aside the decrease caused by the COVID-19 pandemic), the trend clearly shows that this consumption will continue to increase.

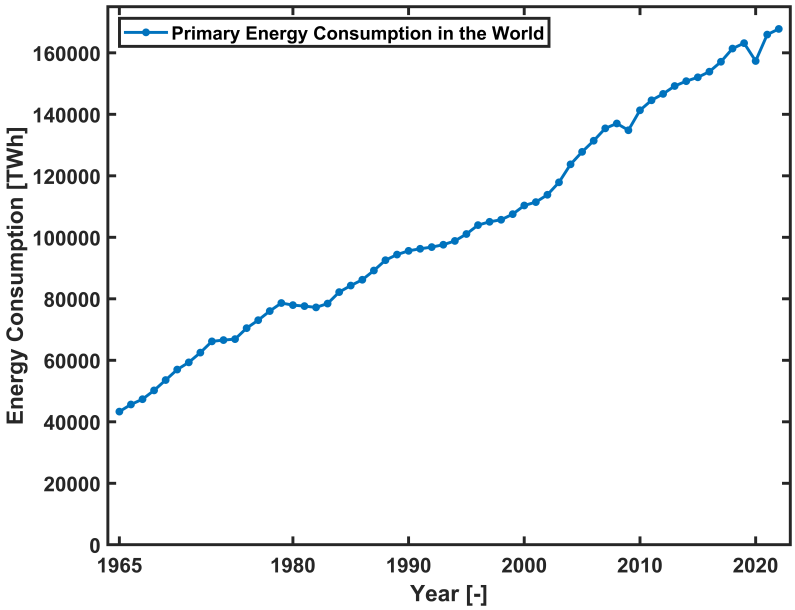

Figure 1.1: Primary energy consumption of the world measured in terawatt-hours. Source [1]

However, it is also important to consider where does this energy comes from, and what are the different sources of energy. Figure 1.2 the energy source breakdown from the past decades. It is clear that this escalating demand for energy is predominantly met by the extraction and utilization of fossil fuels. These non-renewable resources, such as coal, oil, and natural gas, have historically served as the backbone of the energy infrastructure. However, as society delves into the reliance on fossil fuels to sustain our energy needs, it becomes evident that this practice is not only finite but also raises significant environmental challenges.

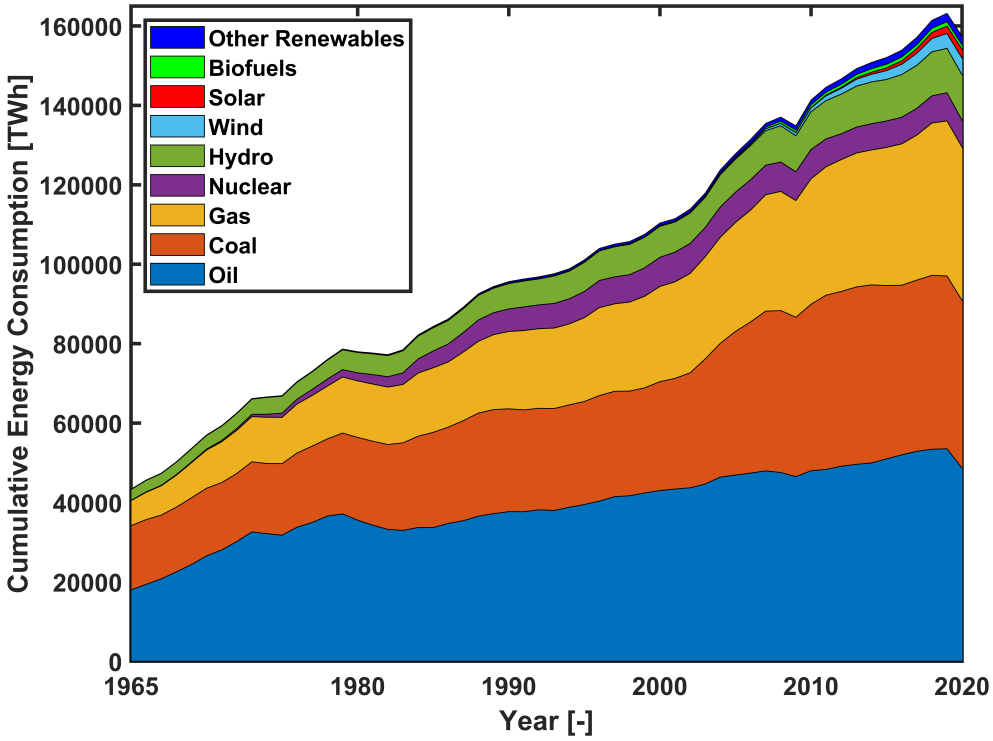

Figure 1.2: Primary energy consumption by different sources around the world measured in terawatt-hours. Source [2]

One of the primary sectors significantly contributing to overall energy consumption is transportation. This includes energy used in various modes of transportation such as road, air, rail, and maritime. Alongside transportation, industrial activities, residential, and commercial sectors also play substantial roles in primary energy consumption. It is estimated that around 99.8% of the current transport sector is powered by internal combustion engines (ICE) [3]. Besides it is also reported that around 70% of the energy used to power these ICE's comes from fossil-based fuels [4]. During the recent decade, the ICE engines have been a topic of attention for the different regulatory bodies owing to their high reliance on fossil-based fuels and in turn their contribution to greenhouse gas (GHG) emissions. The data from World Resources Institute reveals that the transport sector contributes around 16% of total GHG emissions when compared to other sectors such as industry, agriculture, etc [5] as also shown in Figure 1.3. It is crucial to understand the broader impact of

these emissions on climate change as these emissions from transportation significantly contribute to it, posing a pressing global challenge with far-reaching consequences for ecosystems, economies, and societies. Alongside GHG emissions from the transport sector, tailpipe emissions, including nitrogen oxides (NO_x), particulate matter (PM), and other pollutants pose significant threats to public health and the environment. These emissions cause air pollution, respiratory diseases, and environmental degradation, affecting both urban and rural residents globally. As a result, there has been a growing emphasis on implementing stricter emission regulations globally, pushing researchers and automakers to their limits in terms of controlling emissions and finding innovative solutions.

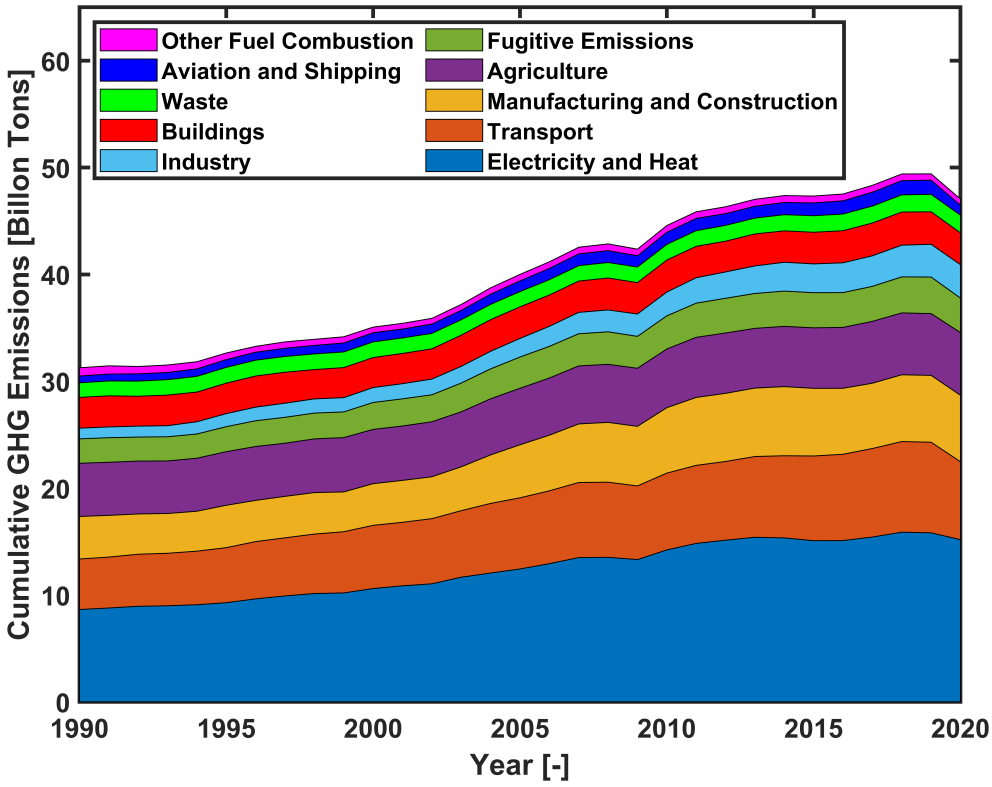

Figure 1.3: Greenhouse gas emission by sector measured in tonnes of carbon dioxide-equivalents. Source [6]

Only in Europe, according to a recent study, the ICE engines are mainly responsible for around 24% of total GHG emissions [7]. In addition to GHG

emissions, as mentioned earlier, the ICEs also contribute to tailpipe emissions mainly including particulate matter, NO_x, hydrocarbons (HC), carbon monoxide (CO), etc. In order to tackle these, the European Union (EU) introduced back in 1992 the emission regulation standard named as EURO standard. The EURO I, II, and III standards played a pivotal role in advancing the mitigation of pollutant exhaust gases. Additionally, EURO IV and V standards marked a significant milestone by introducing catalytic control mechanisms. Euro VI, implemented in January 2013, stands as the most recent and rigorous emission standard in effect. The implementation of the Euro Normative until now has resulted in substantial reductions, with NO_x and PM limits being curtailed by 95% and 97%, respectively. The EU intends to implement Euro VII, a significant improvement to emission regulatory regulations, in early 2030. Extending the framework of earlier EURO standards, Euro VII aims to set even more stringent limits on pollutant exhaust emissions [8]. This upcoming standard reflects ongoing efforts to combat air pollution and promote cleaner and more sustainable transportation systems. Figure 1.4 visually depicts the evolution of emissions standards over the past three decades, illustrating a notable decrease in emissions from current engines compared to their predecessors.

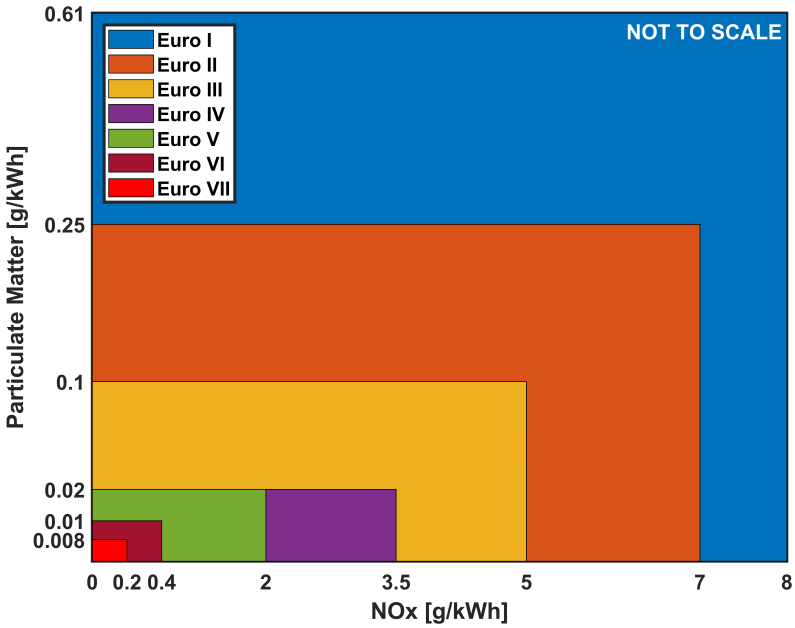

Figure 1.4: European emission standard classification. Source [9]

In this current scenario, keeping into perspective the ever-increasing stricter regulations regarding emissions and the impact of the greenhouse effect, one of the main objectives of the automotive community has been to search for different ways to reduce the GHG and tailpipe emissions from the ICEs. In recent years, the research community has extensively covered various emerging technologies aiming to replace internal combustion engines. Among these alternatives, electrification and hybridization of the powertrain have gained attention. A significant reduction in tailpipe emissions is indeed achieved by moving from full combustion-powered vehicles to hybrid or fully electric vehicles. However, a full life cycle analysis (LCA) is necessary to claim this statement as LCA evaluates all environmental effects linked to a vehicle's lifespan, covering raw material extraction, production, transport, usage, upkeep, and disposal [10–14]. LCA reveals that the energy source for electric generation and battery manufacturing and charging are key to these statements. This approach is crucial to consider as it differs from focusing solely on tailpipe emissions during vehicle operation, as it provides a comprehensive view of environmental impacts across all stages of a vehicle's life. As mentioned before, currently most of the global electricity production is carried out via fossil fuels (around 60%) and renewable energy sources are only 10% of the global energy mix. Therefore, as long as the primary source of electricity for the production of hybrid and electric vehicles as well as for the charging of batteries is not fully transformed into a renewable energy mix, it is wise to consider that the future of transportation is not fully electric, rather it's a mix and one single solution is not enough to stop this problem of global warming. Especially, in the case of heavy-duty applications including construction, agriculture, mining, shipping, etc, full electrification is not a viable option yet and these applications significantly contribute to GHG emissions. The emissions produced by these heavy-duty vehicles worsen climate change and require a more nuanced approach to sustainability. Furthermore, these applications require a higher degree of autonomy in terms of battery and the fact that the infrastructure related to long haul drives needed for these sectors is still lacking. Therefore, The future of transportation is still uncertain and indicates a long life for the ICE.

Therefore, as mentioned earlier a significant amount of research is being carried out in the ICE field to sustain this technology for the future. Focusing on the compression ignition (CI) engines mainly which are widely used in heavy-duty transport owing to their higher thermal efficiency and good power performance [15], new technologies and alternative solutions have been investigated to tackle their emissions problem. These include different modes of combustion like homogeneous charge compression ignition (HCCI), premixed

controlled compression ignition (PCCI), and reactivity controlled compression ignition (RCCI) [16, 17], as well as better exhaust after treatment and newer injection systems [18]. However, with ever-increasing emission regulations, the cost of these after-treatment systems has significantly increased [19]. Dealing with pollutants outside the combustion chamber requires various devices like diesel Oxidation catalyst (DOC), diesel particulate filter (DPF), and selective catalyst reduction (SCR), which can be expensive due to the high cost of raw materials. Therefore, reducing pollutant formation within the engine cylinder has been seen as a very interesting alternative.

Controlling the pollutant formation within the combustion chamber has been lately proposed through the use of different alternative fuels and also by doing innovations in the field of engine hardware, mainly related to air management, fuel injection and air-fuel mixing process. Alternative fuels such as biofuels i.e., ethanol, hydrotreated vegetable oil (HVO), biodiesel, and electro fuels (e-fuels) such as dimethyl ethers, ammonia, oxymethylene dimethyl ethers, etc. have proven to be effective in curtailing not only the in-cylinder pollutant emissions but also the carbon footprint justified by the lifecycle analysis as these fuels are produced from organic matter or biomass or renewable resources. [20–24]. Similarly, different hardware improvements like changes in piston geometry to improve the combustion process inside the chamber[25], or more recently, the ducted fuel injection (DFI) concept [26] have shown great potential in curtailing in cylinder pollutant emissions in CI engines.

The role of computational fluid dynamics (CFD) simulations coupled with detailed chemistry is very crucial in terms of understanding the combustion process and emissions formation inside the combustion chamber [27–30]. CFD with detailed chemistry has been widely utilized in the past involving these alternative fuels and new advancements inside the engine as it can provide a wide variety of parameters related to mixture formation, combustion and pollutant formation inside the combustion chamber [4, 31–33]. Similarly, the utilization of various optical techniques to visualize the combustion process inside an optical engine also serves as an important aspect in understanding the in-cylinder phenomenon [34–36]. These advanced optical techniques also help in analyzing the mixing, combustion, and pollutant formation process inside the chamber which is otherwise impossible inside a metal engine. Both of these approaches are crucial for gaining insights into the complex processes occurring within the combustion chamber.

In summary, the above discussion underscores the ongoing uncertainty surrounding the future energy carrier for transportation. ICE will maintain dominance in this sector until the challenges associated with electrifi-

cation are effectively addressed. Within ICEs, CI engines, known for their higher efficiency and power, are extensively employed in heavy-duty industries. However, stringent regulations concerning GHG and tailpipe emissions have spurred researchers and automakers to seek viable solutions for powering these vehicles. Alternative fuels and modifications to engine hardware emerge as promising approaches for addressing these issues. CFD simulations coupled with detailed chemistry as well as optical techniques present themselves as viable tools to access these potential solutions. Therefore, the focus of the current thesis is on utilizing state-of-the-art numerical simulations and optical techniques to assess the potential of these two promising solutions, including alternative fuels and hardware modifications, in mitigating pollutant emissions within a CI engine.

1.3 Background

As discussed in the previous section the use of alternative fuels and modifications in the hardware design of the engine seems to be a viable solution to tackle the pollutant emissions. For this reason, the current thesis aims to implement two different approaches including numerical and optical techniques to assess these promising solutions. However, before delving into the investigation conducted in this work, it is important to review the existing research conducted within the author's research group at CMT.

Alternative fuels and alternative technologies applied to engine hardware have been the focus of the research group for a few years now due to the promising results achieved by them in terms of pollutant mitigation in CI engines. In this context, the thesis conducted by Lewiski [37] and Tejada [38] serve as predecessors to the current doctoral dissertation.

Focusing on the former one, Lewiski carried out a detailed experimental analysis of the combustion process and soot formation in a single-cylinder light-duty optical engine fueled with e-fuels and using different piston geometries. The thesis on one hand evaluated the potential of different Diesel-OME_x blends and on the other hand, analyzed the potential of an unconventional piston geometry (reference to hardware modification in an engine) in reducing soot formation when using pure diesel. The results presented in Lewiski's thesis offer valuable insights into the advantages of utilizing Diesel-OME_x blends as well as unconventional piston geometries to diminish soot emissions and enhance combustion processes.

A more recent Tejada's thesis [38] was focused on experimentally analysing the fuel effects on the diffusive flame structure using optical techniques in a

medium-duty optical engine. In contrast to Lewiski's thesis, the work carried out by Tejada was more focused on bigger-size engines (the same engine which is utilized in the current dissertation). The thesis was also focused on evaluating the potential of Diesel-OME_x blends as well as unconventional piston geometry in mitigating pollutant emissions. One of Tejada's works was also focused on other alternative fuels including HVO alonside OME_x [34]. The findings of Tejeda's thesis also offer valuable knowledge in terms of utilizing alternative fuels and unconventional piston geometries in a medium-duty optical engine platform to tackle pollutant formation.

These findings of both theses are instrumental in advancing the development of internal combustion engines that are both more efficient and environmentally friendly. Both these theses were more focused towards utilizing advanced optical techniques to carry out experimental campaigns. The theses established a database of experimental findings, which the current dissertation leverages mainly in its numerical (CFD) approach. Furthermore, in terms of hardware modifications, these theses mainly focused on unconventional piston geometries. Building on that the current dissertation aims to evaluate experimentally a totally new hardware proposal, the Ducted fuel injection (DFI) concept in a CI engine platform.

In summary, the current thesis primarily seeks to numerically assess the potential of alternative fuels that have previously been examined only experimentally within the research group. Additionally, it aims to evaluate the potential of a novel hardware modification (DFI concept) using advanced optical techniques, an area not previously explored within the group. The specific objectives related to the current thesis are further summarized in the next section.

1.4 Objectives of the study

In light of the aforementioned text, the present thesis aims to address the mitigation of pollutant emissions in an optically assessed CI engine in two ways, by utilizing alternative fuels (biofuels and e-fuels) and through hardware development like DFI inclusion in the engine. These assessments are done both by detailed numerical simulations and experiments utilizing optical techniques. Therefore, the fundamental objective of the current thesis is to advance the knowledge of the behaviour of alternative fuels and new hardware concepts under operating conditions of compression ignition engines and their impact on combustion performance and pollutant formation. The

particular objectives addressed in this thesis required to achieve the main one are also listed below:

- To develop robust chemical reaction mechanisms that can be utilized to perform high fidelity 3D CFD simulations for the blends of different fuels i.e., Diesel-OME_x and HVO-OME_1.
- To develop an accurate 3D CFD model of the optical engine which, when coupled with chemical kinetics mechanisms, can be used to perform 3D CFD simulations of fuel blends.
- To investigate the effect of blends of different fuels on the combustion and emission aspects like ignition delay, heat release rate and soot formation in a single-cylinder optical engine through rigorous 3D CFD simulations.
- To design, develop and implement the new hardware concept, the ducted fuel injection (DFI) in a medium duty CI optical engine.
- To investigate the DFI concept by performing a rigorous experimental campaign utilizing optical techniques in a CI engine to see its effect on combustion aspects like ignition delay, heat release rate, and emission aspects like soot formation, etc.

1.5 Thesis outline

The thesis is organized into six chapters, starting with this **Chapter 1**, which presents the general overview of the future of transport and the alternate solutions to keep internal combustion engines running in the long term. Further, a general context, background and primary objectives of the work carried out have been presented.

Chapter 2 is focused on describing the literature review regarding the different solutions for pollutant mitigation in CI engines. It starts with a general description of the conventional diesel combustion process overlying the different stages of the combustion and the different pollutant emissions associated with it. Then a detailed review of the use of alternative fuels in CI engines is given which can be used to overcome the pollutant problem. In the same context, a review of different hardware improvements done in the CI engine to mitigate pollutant emissions is given. The chapter ends with proposing two different approaches including different fuel blends and hardware improvements as potential solutions to tackling pollutant emissions in CI engines.

Chapter 3 outlines the experimental and numerical tools and their corresponding methodologies utilized in this thesis. Primarily, the different fuels utilized in the thesis have been described. In terms of experimental tools, the optical engine test cell that serves as the basis of this thesis, enabling the utilization of various optical techniques and image processing methodologies has been discussed. Furthermore, the incorporation of the ducted fuel injection (DFI) device within the optical engine setup is outlined. As far as numerical tools are concerned, the description of 0D and 1D modelling tools alongside the different mechanism reduction techniques has been given. In terms of 3D tools, a detailed description regarding the development of the 3D CFD model utilized in this work has been included with a focus given on the combustion and turbulence models utilized in the framework of this thesis.

In **Chapter 4**, the detailed numerical analysis regarding the use of blends of different fuels inside the CI engine i.e., Diesel-OME_x and HVO-OME_1 has been carried out. The analysis starts with the development of a chemical mechanism necessary to perform numerical simulations of the blends. Then the developed mechanism is utilized to perform simulations, the results of which are used to analyze the combustion and emission behaviour of these promising blends. In the end, a conclusion is made regarding this numerical study and the potential of the fuels proposed to fulfil the pollutant reduction target.

Chapter 5 focuses on the detailed experimental analysis of the DFI concept. The chapter starts by comparing the combustion evolution achieved with the DFI and FreeSpray cases. Then a detailed parametric investigation is carried out regarding different geometrical parameters of DFI and their effect on soot KL formation inside the engine. It is followed by the incorporation of different fuel blends along with DFI. In the end, conclusions are made regarding its performance and the most optimum design to fulfil the pollutant reduction target.

Lastly, **Chapter 6** presents a review of the work carried out, as well as the main conclusions. In addition, some ideas for future directions are proposed from the knowledge and experience acquired during the development of this thesis.

References

[1] Ritchie, Hannah, Rosado, Pablo, and Roser, Max. “Energy”. In: *Our World in Data* (2023). https://ourworldindata.org/energy.

[2] Ritchie, Hannah, Rosado, Pablo, and Roser, Max. "Energy Production and Consumption". In: *Our World in Data* (2020). https://ourworldindata.org/energy-production-consumption.

[3] Leach, Felix, Kalghatgi, Gautam, Stone, Richard, and Miles, Paul. "The scope for improving the efficiency and environmental impact of internal combustion engines". In: *Transportation Engineering* 1 (2020), p. 100005.

[4] Reitz, Rolf D et al. *IJER editorial: The future of the internal combustion engine*. 2020.

[5] Ritchie, Hannah. "Sector by sector: where do global greenhouse gas emissions come from?" In: *Our World in Data* (2020). https://ourworldindata.org/ghg-emissions-by-sector.

[6] Ritchie, Hannah, Rosado, Pablo, and Roser, Max. "CO2 and Greenhouse Gas Emissions". In: *Our World in Data* (2023). https://ourworldindata.org/co2-and-greenhouse-gas-emissions.

[7] *Transport sector contribution to total GHG emissions, 2009 (EEA-32) — European Environment Agency, https://www.eea.europa.eu/data-and-maps/figures/transport-sector-contribution-to-total.*

[8] *Euro 7: Deal on new EU rules to reduce road transport emissions, Dec 2023, https://www.europarl.europa.eu/news/en.*

[9] *Heavy-duty Vehicles - AECC - Legislative updates Feb 2024, https://www.aecc.eu/legislation/heavy-duty-vehicles/.*

[10] Hawkins, Troy R, Singh, Bhawna, Majeau-Bettez, Guillaume, and Strømman, Anders Hammer. "Comparative environmental life cycle assessment of conventional and electric vehicles". In: *Journal of industrial ecology* 17.1 (2013), pp. 53–64.

[11] Girardi, Pierpaolo, Gargiulo, Alessia, and Brambilla, Paola Cristina. "A comparative LCA of an electric vehicle and an internal combustion engine vehicle using the appropriate power mix: the Italian case study". In: *The International Journal of Life Cycle Assessment* 20 (2015), pp. 1127–1142.

[12] Kawamoto, Ryuji et al. "Estimation of CO2 emissions of internal combustion engine vehicle and battery electric vehicle using LCA". In: *Sustainability* 11.9 (2019), p. 2690.

[13] Farzaneh, Farhad and Jung, Sungmoon. “Lifecycle carbon footprint comparison between internal combustion engine versus electric transit vehicle: A case study in the US”. In: *Journal of Cleaner Production* 390 (2023), p. 136111.

[14] Verma, Shrey, Dwivedi, Gaurav, and Verma, Puneet. “Life cycle assessment of electric vehicles in comparison to combustion engine vehicles: A review”. In: *Materials Today: Proceedings* 49 (2022), pp. 217–222.

[15] Liu, Junheng et al. “An overview of polyoxymethylene dimethyl ethers as alternative fuel for compression ignition engines”. In: *Fuel* 318 (2022), p. 123582.

[16] Zhao, Fuquan et al. “Homogeneous charge compression ignition (HCCI) engines”. In: (2003).

[17] Kokjohn, Sage L, Hanson, Reed M, Splitter, DA, and Reitz, RD. “Fuel reactivity controlled compression ignition (RCCI): a pathway to controlled high-efficiency clean combustion”. In: *International Journal of Engine Research* 12.3 (2011), pp. 209–226.

[18] Boccardo, Giulio et al. “Experimental investigation on a 3000 bar fuel injection system for a SCR-free non-road diesel engine”. In: *Fuel* 243 (2019), pp. 342–351.

[19] Posada, Francisco, Chambliss, Sarah, and Blumberg, Kate. “Costs of emission reduction technologies for heavy-duty diesel vehicles”. In: *ICCT White paper* (2016).

[20] Khan, Nida, Sudhakar, Kumarasamy, and Mamat, Rizalman. “Role of biofuels in energy transition, green economy and carbon neutrality”. In: *Sustainability* 13.22 (2021), p. 12374.

[21] Mathews, John A. “Carbon-negative biofuels”. In: *Energy policy* 36.3 (2008), pp. 940–945.

[22] Chum, Helena L and Overend, Ralph P. “Biomass and renewable fuels”. In: *Fuel processing technology* 71.1-3 (2001), pp. 187–195.

[23] Kranenburg-Bruinsma, KJ van et al. “E-fuels-Towards a more sustainable future for truck transport, shipping and aviation”. In: (2020).

[24] Garcia, Antonio, Monsalve-Serrano, Javier, Villalta, David, and Guzman-Mendoza, Maria. “Parametric assessment of the effect of oxygenated low carbon fuels in a light-duty compression ignition engine”. In: *Fuel Processing Technology* 229 (2022), p. 107199.

[25] Pastor, José V et al. "Effect of a novel piston geometry on the combustion process of a light-duty compression ignition engine: An optical analysis". In: *Energy* 221 (2021), p. 119764.

[26] Mueller, Charles J et al. "Ducted fuel injection: A new approach for lowering soot emissions from direct-injection engines". In: *Applied energy* 204 (2017), pp. 206–220.

[27] Gong, Y, Kaario, O, Tilli, A, Larmi, M, and Tanner, FX. *A computational investigation of hydrotreated vegetable oil sprays using RANS and a modified version of the RNG k-ε model in OpenFOAM*. Tech. rep. SAE Technical Paper, 2010.

[28] Zhang, Zhichao et al. "Investigation of the macroscopic characteristics of Hydrotreated Vegetable Oil (HVO) spray using CFD method". In: *Fuel* 237 (2019), pp. 28–39.

[29] Ren, Shuojin, Wang, Zhi, Li, Bowen, Liu, Haoye, and Wang, Jianxin. "Development of a reduced polyoxymethylene dimethyl ethers (PODEn) mechanism for engine applications". In: *Fuel* 238 (2019), pp. 208–224.

[30] Gao, Wanying et al. "Numerical simulation on NO and soot formation process of a diesel engine with polyoxymethylene dimethyl ethers-diesel blend fuel". In: *Energy Sources, Part A: Recovery, Utilization, and Environmental Effects* (2020), pp. 1–16.

[31] Novella, Ricardo, Bracho, Gabriela, Gomez-Soriano, Josep, Fernandes, Cássio S, and Lucchini, Tommaso. "Combustion system optimization for the integration of e-fuels (Oxymethylene Ether) in compression ignition engines". In: *Fuel* 305 (2021), p. 121580.

[32] Lin, Qinjie, Tay, Kun Lin, Zhao, Feiyang, and Yang, Wenming. "Enabling robust simulation of polyoxymethylene dimethyl ether 3 (PODE3) combustion in engines". In: *International Journal of Engine Research* 23.9 (2022), pp. 1522–1542.

[33] Liu, Xinlei, Im, Hong G, Mueller, Charles J, and Nyrenstedt, Gustav. "A computational parametric study of ducted fuel injection implementation in a heavy-duty diesel engine". In: *Fuel* 358 (2024), p. 130228.

[34] Pastor, Jose V, Garcia-Oliver, Jose M, Micó, Carlos, and Tejada, Francisco J. *Combustion behaviour of blends of synthetic fuels in an optical single cylinder engine*. Tech. rep. SAE Technical Paper, 2021.

[35] Pastor, José V, García, Antonio, Micó, Carlos, and Lewiski, Felipe. "An optical investigation of Fischer-Tropsch diesel and Oxymethylene dimethyl ether impact on combustion process for CI engines". In: *Applied Energy* 260 (2020), p. 114238.

[36] Li, Feng, Lee, Chia-fon, Wang, Ziman, Liu, Fushui, and Lu, Guoxiang. "Optical investigation on impacts of ambient pressure on macroscopic spray characteristics of ducted fuel injection under non-vaporizing conditions". In: *Fuel* 268 (2020), p. 117192.

[37] Vargas Lewiski, Felipe de. "Analysis of the combustion process and soot formation in a single cylinder optical engine fueled with e-fuels and using different piston geometries". PhD thesis. Universitat Politècnica de València, 2021.

[38] Tejada Magraner, Francisco José. "Analysis of Fuel Effects on the Diffusive Flame Structure Using Advanced Optical Techniques in a Single Cylinder Optical Engine". PhD thesis. Universitat Politècnica de València, 2024.

Chapter 2

Different solutions for pollutant emission reduction in CI engines

2.1 Introduction

The CI engines are facing big challenges in terms of pollutant emissions. Ever-increasing stricter pollutant regulations are being placed every year. Thus, the research community and the automotive sector are continuously trying to find feasible solutions for this problem. They span from the use of different alternative fuels with conventional CI technology to tackle pollutant and/or CO_2 emissions to utilizing different hardware improvements in order to ultimately affect the combustion process in a way to reduce the emissions.

The following chapter aims to establish the framework for the work included in this thesis. Thus, an overview of the different alternatives that can be found in the literature to reduce pollutant emission in CI engines is presented and discussed. This chapter is organized as follows; primarily an overview of conventional diesel combustion alongside the major pollutant emissions has been carried out. Then a review of different alternative fuels that are being utilized in recent times to tackle pollutant emissions problems has been presented. After that, a review of changes in hardware design that ultimately affect the formation of harmful pollutants has been performed. Finally, information has been summarized in the conclusion section with the identification of different strategies for pollutant reduction in CI engines to be applied in this thesis.

2.2 Conventional diesel combustion

2.2.1 Combustion process

The combustion process is characterized by the release of the fuel's energy within the engine cylinder for conversion to useful work. One of the classical ways to describe the combustion process is by analyzing the rate of heat release rate (RoHR). It represents the intensity of the chemical energy released by the fuel per unit time. Thus Figure 2.1 is used here to describe the different phases of diesel combustion. The injection rate curve is also included here which makes it possible to determine the initiation and completion of fuel injection into the combustion chamber. A comparison with the RoHR reveals a delay between the start of injection and the initial signs of heat release, indicating the onset of chemical reactions. RoHR curve is derived from direct measurement of in-cylinder pressure concerning crank angle degree and by the application of the first law of thermodynamics during a closed cycle between intake valve closing (IVC) to exhaust valve opening (EVO)[1].

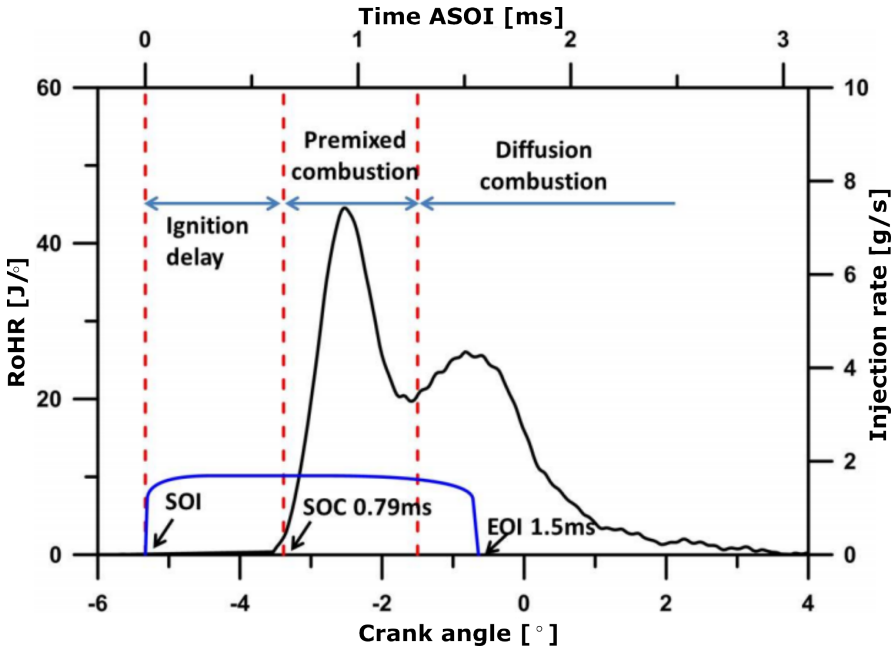

Figure 2.1: Rate of heat release (ROHR) and Injection rate for a conventional diesel combustion. Source [2]

Taking this RoHR into consideration, conventional diesel combustion is divided into three different stages as per the literature :

- **Ignition Delay:** In general, the ignition delay (ID) is defined as the time interval in crank angle degrees (CAD) between the start of injection (SOI), and the start of combustion (SOC). This interval is marked in the Figure 2.1. Ignition delay is caused by two different phenomena where one corresponds to physical ignition delay and the other one is chemical ignition delay. The former involves phenomena like atomization (breakup of liquid fuel into droplets), vaporization, and mixing of air-fuel mixture while the latter corresponds to the period where pre-reactions occur and create favorable conditions for triggering the autoignition. In the context of this thesis, the ID is comprised both of physical and chemical delays starting when the first drop of fuel is injected until the autoignition occurs in the combustion chamber. It is important to understand that the ID period is greatly dependent on numerous factors like injection pressure, nozzle diameter, ambient temperature, density, composition of fuel, etc. and it greatly affects the combustion evolution in the latter stages.

- **Premixed Combustion:** This phase is comprised of an abrupt increase in the rate of heat release. During the ID period, the injected fuel gets mixed with the air and creates an ignitable mixture which results in an abrupt increase in RoHR when it suddenly reacts and is characterized by the first peak of the curve as shown in Figure 2.1. The end of the premixed phase occurs when the RoHR drops to relatively low values. Hence its duration can be defined as the difference between SOC and the first local minimum in ROHR. The main factors that affect this premixed combustion phase are injection rate, mixing rate, and ID as described by authors in [3].
- **Diffusion Combustion:** After the completion of the premixed combustion, a mixing-controlled process occurs. The RoHR is governed by the rate at which the air mixture becomes available for burning. With a sufficiently long injection, the diesel jet in free spray configuration reaches stationary conditions, maintaining a relatively consistent flame structure until the end of injection [1, 4] except in real diesel engine conditions where flame-to-flame interactions occur. This stage is known as diffusion combustion and is marked in Figure 2.1.

This definition of the diesel combustion process provides a global overview of how it develops along each engine cycle. However, to offer a detailed view of some of the phenomena occurring in this process including the air-fuel mixture formation, atomization and evaporation, diesel flame structure, and the formation of different pollutants, the description is given in the following sections.

2.2.2 Formation of air-fuel mixture

Diesel engines are generally characterized by internal mixture formation and auto-ignition, which necessitate the use of highly ignitable fuels and the assurance of high temperatures. The process of energy conversion in these kinds of engines is mainly controlled by the rate of air-fuel mixing as well as the injection rate. That is the reason the formation of a proper air-fuel mixture plays a pivotal role in defining the combustion performance and emissions formation in CI engines.

Taking into consideration the heterogeneity of the mixture, different air-fuel ratios (λ) are formed. The core regions of the spray tend to be extremely rich, characterized by λ approaching 0, while the peripheral regions exhibit λ approaching ∞, indicating pure air. These λ gradients also result in temperature variations within the combustion chamber. Given the limited time

available to achieve a fully homogeneous mixture, the presence of rich regions makes it challenging to entirely prevent soot formation. In modern diesel engines, approximately 95% of the generated soot undergoes oxidation primarily during the expansion stroke.

Internal mixture formation is predominantly influenced by the injection process. Hence, the injection system plays a crucial role in ensuring sufficient injection pressure, facilitating fuel introduction inside the chamber, promoting spray propagation, and distributing it effectively within the chamber in a short period of time. Subsequently, the liquid fuel undergoes rapid breakup, forming droplets, evaporating, and mixing with the air, ultimately triggering combustion through autoignition. The ongoing burning process relies on the air-fuel mixing to create an ideal combustion environment. Therefore, the air-fuel mixing dictates the combustion characteristics of diesel engines [1, 5].

2.2.3 Atomization and Evaporation

During the injection process, the fuel jet forms a cone-shaped configuration as it exits the nozzle. The liquid fuel is injected at a high velocity in the combustion chamber, where it interacts with the high-density, high-temperature air. It undergoes atomization, resulting in considerably smaller droplets than the nozzle diameter [1, 2]. The initial phase of atomization, where the first droplets appear is known as a primary breakup. The volatility property, a critical parameter in spray breakup, is determined by the temperature and composition of the fuel.

The primary breakup is followed by a secondary breakup, where the primary droplets undergo further breakup into much smaller particles. This process is essential for rapidly heating and evaporating the fuel, directly impacting the ignition delay. Aerodynamic forces are the primary driving mechanism behind secondary atomization, with factors such as air density, spray cone angle, and injection pressure exerting significant influence.

In addition to the spray break-up process, fuel evaporation plays a crucial role in both pollutant formation and combustion evolution. After the spray is atomized, and the droplets are fully enveloped by the hot air within the combustion chamber, the heat transfer process from the air to the droplets intensifies. This process is directly impacted by the kinetic energy of the fuel spray. The high velocity between the droplets and the air facilitates mass transport and heat transfer. Consequently, the droplet temperature rises, leading to an increase in its vapor pressure and the amount of evaporated fuel. Through the evaporation process, the droplets progressively decrease in size until they are entirely evaporated.

The penetration of the liquid phase of the spray stops when the rates of fuel injection and evaporation become equal. The liquid length, defined as the distance between the nozzle exit and the tip of the liquid region, is a crucial parameter in the combustion process of the diesel engine. Prolonged liquid lengths may lead to impingement inside the piston bowl, contributing to higher emission formation.

2.2.4 Autoignition

Autoignition is characterized by the spontaneous ignition of unburned gases ahead of the flame front. Autoignition takes place in regions of the combustion chamber where thermodynamic conditions including but not limited to local temperatures, and vapor concentration are proper to initiate chemical reactions. In these areas, intermediate species are generated, and energy is released, resulting in a positive RoHR. Higgins et al. [6] classified the chain of different processes occurring during the autoignition named physical induction, first-stage ignition, and second-stage ignition.

- Physical induction period: This period is mainly driven by the physical process involved during the spray breakup. The process of fuel vaporization absorbs heat, rapidly lowering the temperature within the chamber of combustion. Any form of chemical reaction is prevented from happening at this point. Pressure and chemiluminescence increase simultaneously as soon as the air mixture temperature begins to rise once more and the necessary conditions are met. With this, the physical induction phase comes to an end and the first step of ignition begins.

- First-stage ignition: This phase spans from the point at which a minor pressure increase and chemiluminescence become detectable until the onset of rapid heat release. At this instant, the fuel is consumed due to the chain-branching reactions under rich conditions of air mixture between the liquid length and the penetration tip of the spray. These reactions result in the generation of radicals and the release of small amounts of energy, leading to an elevation in temperature and pressure. Various authors have categorized this period as the low-temperature ignition process or cool flame [7, 8].

- Second-stage ignition: This phase begins with a significant heat release followed by a sudden increase in premixed burn pressure. Because of the elevated temperatures resulting from the heat released in the first

stage, the hydrogen peroxide dissociation reaction prevails in the chemistry, leading to the production of OH radicals and contributing to a substantial heat release [9].

2.2.5 Diesel flame structure

After progressing through the various stages of autoignition which dictates the premixed phase, the combustion process enters the diffusion combustion phase as described earlier which is governed by the rate at which the air mixture becomes available for burning. This phase persists until all the injected fuel is consumed. Upon completion, the combustion process attains conditions that are favorable to the establishment of a self-sustained reaction. A diffusion flame front emerges and stabilizes, maintaining its fundamental structure as fuel injection continues.

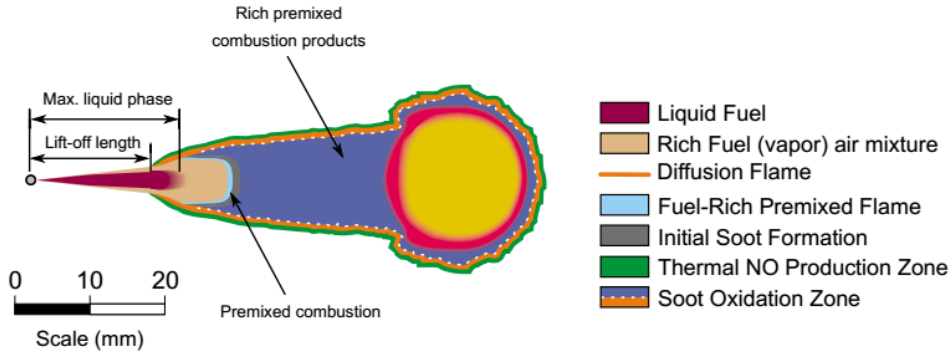

Figure 2.2: Diffusive flame structure according to the conceptual model proposed by Dec. [10]

Figure 2.2 shows the most widely accepted conceptual model of a reactive diesel flame structure as proposed by Dec et al. [10] and later extended by Flynn et al. [11]. The hot air is drawn into the jet as fuel enters the cylinder, shaping a cone-like spray. The fuel undergoes heating and complete evaporation, defining the characteristic liquid length. A fuel-rich premixed combustion region (cyan) appears downstream of the liquid fuel penetration and extends to a fixed distance from the nozzle which is known as Lift-off length (LOL). The fuel-air mixture in this region is rich, exhibiting an equivalence ratio between 2-4. In this region, most of the previously entrained oxygen is

consumed increasing local temperature. During this phase, the breakdown of the fuel into droplets and polyaromatic hydrocarbons (PAH) formation occurs followed by the low level of soot formation in the form of small particles. Carbon monoxide (CO) and unburned hydrocarbons (HC) are also likely to be produced in the zone. However, because of the lower availability of oxygen and lower adiabatic flame temperatures than required for thermal NO production, these conditions are unfavorable for NO_x formation. In this combustion stage, as reported by Flynn et al. [11], approximately 10-15% of the chemical energy from the fuel is released. Subsequently, these combustion products continue moving downstream, entraining other combustion products and diffusing towards the surrounding diffusion flame front. The LOL is directly responsible for the amount of oxygen present inside the premixed combustion zone.

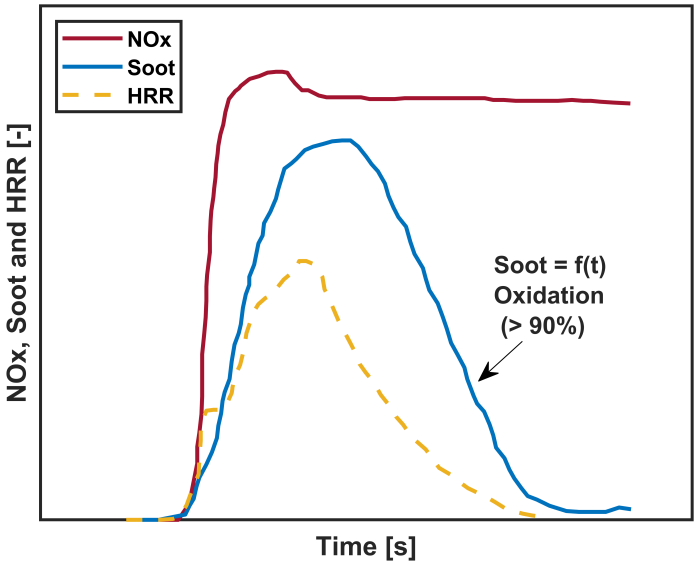

Figure 2.3: Soot and NO_x concentrations in a combustion chamber as a function of time. Source [12]

The typical structure of the diffusive flame is established downstream of the LOL, where the internal volume contains intermediate combustion products, unburned fuel, and soot precursors (blue). The diffusion flame front (orange) is characterized by a thin layer of the stoichiometric surface with a high concentration of available oxygen [13]. The partial products of combustion undergo oxidation upon reaching the flame front. In this region, a significant portion of the fuel's chemical energy is released. Moreover, the

presence of oxygen in the outer region of the spray (depicted in green) results in lean mixtures and elevated temperatures, thereby promoting the formation of nitrogen oxides NO_x. The evolution of soot and NO_x is depicted in Figure 2.3.

2.2.6 Soot formation

Soot can be considered as a solid substance mainly composed of carbon particles. According to Tree et al., [14], the composition ratio of soot in terms of carbon to hydrogen is roughly 8 to 1. Unburned fuel nucleates at high temperatures above 1600K in fuel-rich areas to transition from a vapor to a solid phase, forming soot. Depending on the environment, hydrocarbons or other accessible molecules may condense on or be absorbed into soot.

Figure 2.4 shows the schematic of the soot formation process proposed by Tree et al. [14]. The first step is fuel pyrolysis, which produces precursors like acetylene (C_2H_2) and PAH by causing organic substances to change structurally at high temperatures without significantly oxidizing. Nucleation is the following stage, where gas-phase reactants are converted to create soot particles. The formation of first aromatic ring by the combination of two C_3H_3 propynyl radicals marks the beginning of this stage. The nucleation is limited to the areas close to the reaction zone because of elevated temperatures, and concentrations of radicals and ions during the two stages of combustion [15]. The amount of soot created in this step is determined by the first aromatic rings to form.

Surface growth is the subsequent phase, which takes place simultaneously with nucleation without a clear difference between the end of nucleation and the beginning of surface growth. During this phase, mass is added to the surface of the soot particle produced during the nucleation. The heated surface of soot particles absorbs the gas-phase hydrocarbons, which are often acetylenes, increasing the mass of soot and keeping the number of particles constant. Agglomeration and coalescence come together to form the final stage. Particles collide during coalescence, reducing the total number of particles while keeping the total mass constant. The process of primary particles adhering to one another to produce a sizable group of primary particles is known as agglomeration.

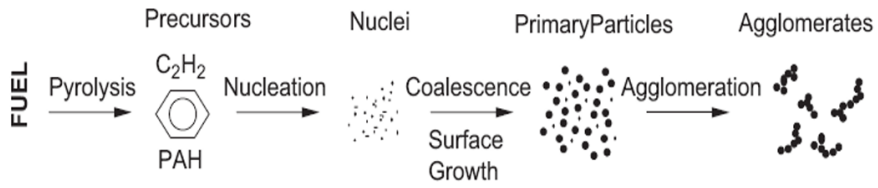

Figure 2.4: Soot formation process. Source [14]

2.2.7 NO_x formation

The oxides of nitrogen consisting of NO and NO_2 are collectively termed as NO_x in the context of diesel engine combustion. In contrast, N_2O is not considered a regulated emission. The dominant source of NO emission is the combustion process while the NO_2 is formed as a consequence of further oxidation. Elevated temperatures reached inside the combustion chamber make the nitrogen present to react with oxygen forming these nitrogen oxides.

Numerous pathways describe the formation pathway of NO as adapted from [16]. These include thermal or zeldovich mechanism which is dominant for high-temperature combustion over a wide range of equivalence ratios. Another mechanism is Fenimore or prompt one which is mainly predominant in rich fuel mixtures. On the other hand, very lean low-temperature combustion is characterized by N_2O sub mechanism. Lastly, the NNH mechanism is a more recent addition to the formation of NO mechanisms.

Regardless of how it forms, NO in diesel engines is a byproduct of combustion rather than a substance in motion like CO. Depending on the dominant equilibrium direction, NO creation can either be preserved or destroyed, although it can occur through any method. In general, the process of NO generation in diesel combustion is linked to the extended zeldovich mechanism, which is more prevalent in equilibrium diffusion flames at high (local) temperatures [17]. The chain reactions in Equation 2.1 and Equation 2.2 describe the zeldovich mechanism with an extended reaction in Equation 2.3. The N_2 reacts with atomic oxygen in Equation 2.1 followed by oxidation of atomic nitrogen in Equation 2.2 and Equation 2.3. The thermal mechanism requires temperatures above 1800 K and excess oxygen to be efficient which is the case of a diffusion flame in a diesel engine combustion where most of the NO_x is formed.

$$O + N_2 \longleftrightarrow NO + N \tag{2.1}$$

$$N + O_2 \longleftrightarrow NO + O \tag{2.2}$$

$$N + OH \longleftrightarrow NO + H \tag{2.3}$$

Keeping this into account, it is understood that the burning of diesel results in the formation of many harmful pollutants during the onset of its combustion phases, where the soot and NO_x emissions are one of the main drawbacks. Researchers and automakers have developed and tested different solutions to tackle these pollutants which span from the burning of alternative fuels to utilizing different combustion strategies. Some of them are described in detail and discussed in the following paragraphs.

2.3 Role of alternative fuels in tackling pollutant emissions

The ongoing debates about the next-generation energy source for combustion engines, amid the increasing global energy demand, lack a consensus. This uncertainty still exists, especially about the transportation sector's potential effects on greenhouse gas emissions. Diverse alternatives for cutting greenhouse gas emissions are being researched, one of them evidences the necessity of exploring the potential of alternative fuels.

These alternative fuels present themselves as a viable choice over the traditional fossil-based fuels which are constantly depleting and significantly contribute towards global GHG emissions. Researchers and automakers have been constantly researching on this potential solution now for decades. In the case of the automotive sector, the search for alternative fuels gradually emerged in the 1980s along with the ICE development [18]. Since then a variety of solutions in terms of these fuels have been explored and are currently being utilized.

Before jumping into the role of different alternative fuels in pollutant reduction, it is important to understand them. Alternative fuels are those fuels that can directly replace their fossil counterparts. These include different alcohol-based fuels (ethanol, methanol, alcohol mixtures), biofuels (bioethanol, biodiesel, hydrotreated vegetable oil) and recently explored fuels like ammonia, hydrogen, etc [19]. According to Bae et al., [19] the alternative fuel's significance can be attributed to the following three aspects:

- Achieving energy sustainability by using more alternative fuels from renewable sources and addressing the challenges of limited fossil fuel energy.
- Enhancing engine efficiency and reducing emissions by utilizing alternative fuels with superior physical or chemical properties when compared to conventional fuels.
- Alleviating the disproportionate reliance on traditional petroleum-based fossil fuels.

These aspects clearly describe the significance of alternative fuels. In particular, the second one is closely related to the purpose of this thesis and reflects the relevance of alternative fuels in the current work. Alternative fuels can be further classified into two different categories. i.e., biofuels and e-fuels. Biofuels are those alternative fuels that are produced from organic matter or biomass [20]. However, e-fuels (electro-fuels) are the ones that are produced using renewable energy resources [21].

Focusing on the first ones, biofuels have been considered as a way forward for the replacement of fossil diesel in CI engines. In general, the fuels that are produced from organic sources such as biomass and organic waste are termed biofuels. Depending on the feedstock and the procedure utilized for their production, biofuels have been classified into different generations as shown in Figure 2.5. The first generation is produced by using agricultural products i.e., soybean, rapeseed, corn, etc. of which the most common are biodiesel, and ethanol [22]. As this first generation is made of food, it presents ethical problems which motivated the development of new generations. The second generation of biofuels is produced from non-feed stocks and overcomes the problems related to climatic and social dilemmas. Examples include cellulosic ethanol, algal biofuel, etc. The more advanced biofuels is the third-generation which is produced by more sustainable feedstock sources of which the prominent ones are waste-based biofuels, cyanobacterial biofuels, etc. They can be considered carbon neutral fuels as the CO_2 released by them when burning is roughly equal to what they absorb during their growth phase. However, the CO_2 generated with the production method and the feedstock obtaining method greatly influence how close they are to the real carbon neutrality [23].

Among these biofuels, the most commonly utilized in CI engines include alcohol fuels like ethanol [24–26] and methanol [27–29], biodiesel [30–32], hydrotreated vegetable oil [33–35], etc. For the scope of this thesis, hydrotreated vegetable oil (HVO) has been considered a promising biofuel to replace fossil

diesel and ultimately reduce pollutant emissions. Henceforth a detailed literature review on the use of HVO in CI engines and its potential advantages in terms of reduction in pollutant emissions is carried out later in the proceeding sections.

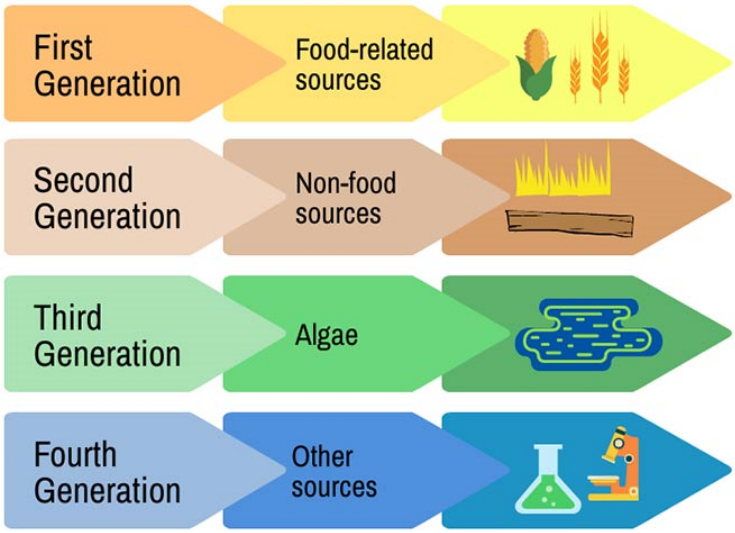

Figure 2.5: Different generations of biofuels depending upon the source of production. Source [36]

The second type of alternative fuels, the e-fuels, are also termed synthetic fuels. They can be also considered as carbon-neutral fuels if they are produced from renewable energy resources. The main components for their production are hydrogen and CO_2 where the first comes from electrolysis of water and the second is obtained from carbon capture either from the combustion of fossil fuel sources (industrial plants) or directly from the atmosphere (biomass or direct capturing of air) [37]. Both of these operations, including carbon capture and electrolysis, along with the process of combining hydrogen and CO_2 commonly known as fischer-trop synthesis consume a significant amount of electricity, emphasizing the importance of utilizing renewable energy sources. This utilization is essential for realizing the advantages of reducing CO_2 emissions [38]. Figure 2.6 highlights the different production pathways of various e-fuels which include the utilization of clean electricity, green hydrogen, and carbon capture technologies as discussed earlier. In addition to the carbon neutrality that these e-fuels provide, they are also particularly advantageous

as they can be a direct substitution of their fossil counterparts [21] and reduce pollutant emission by a considerable amount [39].

Among the numerous e-fuels, the most prominent ones that are being utilized in CI engines include fischer-trop diesel [40–42], ammonia [43–45], synthetic natural gas [46–48], dimethyl ether [49–51], oxymethylene dimethyl ethers [52–54], etc. For the scope of this thesis, oxymethylene dimethyl ethers have been considered as a promising synthetic fuel to replace fossil diesel and ultimately reduce pollutant emissions. Henceforth a detailed literature review on the use of oxymethylene dimethyl ethers in CI engines and its potential advantages in terms of reduction in pollutant emissions is carried out later in the proceeding sections.

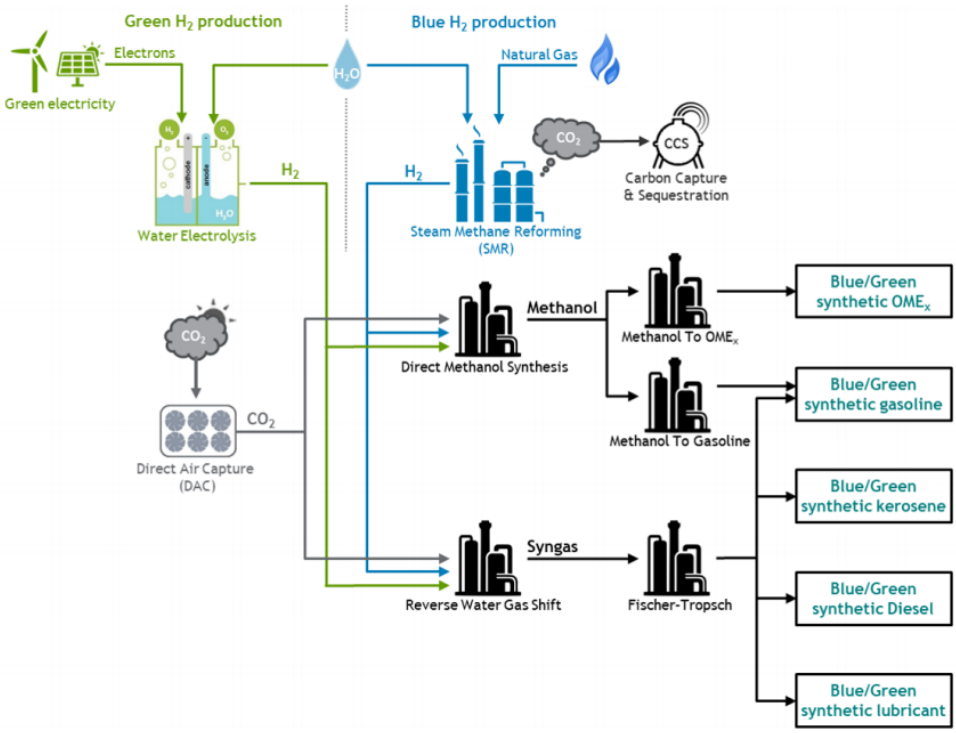

Figure 2.6: Different production pathways for various e-fuels. Adapted from [55]

2.3.1 Hydrotreated vegetable oil as a promising biofuel

Hydrotreated vegetable oil is a high cetane number biofuel composed mainly of straight chain paraffinic hydrocarbons, with a chemical formula of C_nH_{2n+2}. However, it is free of sulfur and aromatic compounds [56]. HVO can be manufactured using a variety of feedstocks, including vegetable oils, animal fats, and waste oils, with minimal impact on the end product's characteristics. HVO is considered a second-generation biofuel, as the feedstock that is used for its production does not come from the human food chain. According to Hartikka et al. [57], high-quality HVO can be produced when feedstocks like algal oils and microbial oils from waste materials are introduced into the production process. The raw material or feedstock necessary for the production of HVO has been the biggest hurdle. Nonetheless, HVO production technology is fully developed and operational at a large commercial scale, with over one million tons produced in Europe. The technology closely resembles catalytic processes utilized in conventional oil refining and is accessible from numerous process technology suppliers. Neste currently dominates the production volume, holding the largest share. However, companies like Preem, Eni, and Cespa have also joined the HVO production sector [58, 59]. Further Companies like DAF, Volvo, and MAN have verified that their latest trucks can use HVO without any issues [60–62].

Due to its similar properties to fossil diesel, HVO is regarded as green or renewable diesel, despite coming from renewable sources [63]. HVO is also considered a good drop in fuel for fossil diesel in CI engines, as no hardware modifications are required for utilizing this fuel. However, due to the absence of sulfur, the lubricity of HVO is low which requires the use of lubricating agents as used in conventional diesel to protect the injection system [64]. Regarding the lower heating value of the HVO, it contains slightly higher energy content as compared to fossil diesel. Furthermore, similar to fossil diesel, there aren't many challenges associated in terms of storage and implementation in vehicle fuel tanks. It has been observed that the driving economy of HVO-powered vehicles is quite similar to that of fossil diesel [65]. These are the reasons why researchers consider HVO as one of the best alternative fuels to fossil diesel [66, 67].

An extensive amount of research has been carried out in the past decade regarding HVO performance in CI engines. Sugiyama et al. [67] experimentally studied the effects of HVO utilization on the combustion and emission performance of a diesel engine. They concluded that HVO possesses similar spray characteristics as fossil diesel, increases fuel consumption by 5%, and due to high cetane number, it decreases the HC and PM emissions. Kim et

al. [68] studied HVO performance inside a light-duty diesel engine experimentally. Their finding indicated that HVO blended fuels show lower HC and CO emissions, however, similar levels of NO_x and PM emissions were obtained as compared to biodiesel. Chau et al. [34] studied HVO blends with diesel inside an optical CI engine under various EGR conditions. Their findings highlighted that ID, flame temperature along with soot, and NO_x emissions are decreased when the HVO percentage in the blend with diesel is increased. Dimitradis et al. [33] carried out a diesel engine optimization study fueled with HVO experimentally. The author's results included a decrease in PM and HC emissions as compared to fossil diesel. The NO_x emissions were found to be similar to fossil diesel. In a study conducted by Bortel et al. [69], the impact of this fuel on passenger cars was investigated, with different substitution ratios tested, including pure HVO (100% HVO) and a blend consisting of 30% HVO and 70% diesel. The findings indicated a 10% reduction in CO, unburned HC, and PM emissions. In certain operating conditions, there was no significant effect observed, either on emissions or engine performance. The influence on NO emissions was slightly positive but minimal. As the substitution rate increased, the power output also increased, although adjustments to operating parameters, such as EGR, injection pressure, injection timing, and others, were required to optimize performance. The authors from [66] identified HVO as a superior substitute for fossil diesel in terms of emissions reductions related to HC, CO, and NO_x. According to their findings, the lack of aromatics, sulfur, and cycloalkanes in the chemical structure of HVO contributed to the reported pollutant reductions. However, they also highlighted the poor lubricity problems of this fuel which were also addressed in [70], where authors suggested the use of lubricating agents for injection system protection. Pinto et al. [35] presented a rather quantitative analysis of pollutant reduction achieved by utilizing HVO inside a 0.418l, single-cylinder diesel engine. Their results suggested that HVO reduced NO_x emissions by around 2.5%, PM emissions by 54%, CO emissions by 35%, and CO_2 emissions by 2.3% as compared to fossil diesel.

In line with experimental research carried out, a few numerical studies also exist in the literature that utilize computational fluid dynamics (CFD) simulations to better understand the fundamental characteristics and performance of HVO or its blends. In a study conducted by Gong et al. [71], the spray characteristics of HVO were examined under non-evaporating (room temperature) and evaporating (high temperature) conditions using both Reynolds-averaged Navier-Stokes (RANS) and large eddy simulation (LES). The findings revealed that HVO exhibited similar droplet sizes and spray tip penetration as diesel fuel at room temperature, but slightly smaller droplets and penetration than

diesel at high temperatures. Zhang et al. [72] also studied the spray characteristics of HVO utilizing a waver breakup model and RNG k-epsilon turbulence model, where their numerical model proved to be effective in replicating the experimental behavior. The numerical studies regarding HVO are limited to only 1D spray simulations. One of the main reasons for this limitation is the unavailability of a proper chemical reaction mechanism which is required for detailed CFD simulations.

To summarize, the research carried out in the literature with regards to the use of HVO in a CI engine highlights its potential in improving combustion and reducing pollutant emissions including soot, NO_x, and other harmful species like CO, HC, etc. HVO both in pure or blended form can be considered a promising and most immediate biofuel to replace fossil diesel. However, there exists a clear literature gap in terms of numerical studies related to HVO utilization in CI engines. Therefore, this aspect related to a detailed numerical analysis of HVO or its blends with conventional or alternative fuels along with the construction of appropriate chemical reaction mechanism can be explored. All these arguments justify the consideration of this fuel in the scope of this thesis.

2.3.2 Oxymethylene dimethyl ethers as promising e-fuels

Oxymethylene dimethyl ethers also termed polyoxymethylene dimethyl ethers are promising diesel alternative e-fuels. They have a molecular structure of $CH_3O\text{-}(CH_2O)_x\text{-}CH_3$ where x ranges from 1 to 6 [73, 74]. The first OME molecule where x is 1 is termed dimethoxymethane or methylal and denoted by OME_1 in the context of this thesis. Higher OME molecules where x>1 will be denoted by OME_x. OME_1 can be produced from methanol and formaldehyde [75, 76], which further undergoes polymerization to produce OME_x. Methanol that is utilized is produced by combining the captured CO_2 from the atmosphere with the hydrogen produced by electrolysis through processes like direct methanol synthesis. Formaldehyde is obtained then by dehydrogenation of methanol [77]. The trioxane process involves the trimerization of formaldehyde, typically catalyzed by sulphuric acid H_2SO_4, followed by processing the reactor output. This processing can include techniques such as pressure-swing distillation sequences [78]. The preferred method for producing OME_1 from formaldehyde and methanol is a heterogeneously catalyzed reactive distillation [79]. Subsequently, both formaldehyde-based products, trioxane and OME_1, are transformed into OME_x. The blockchain diagram in Figure 2.7 taken from [75] highlights the above-mentioned pathways to synthesize these fuels.

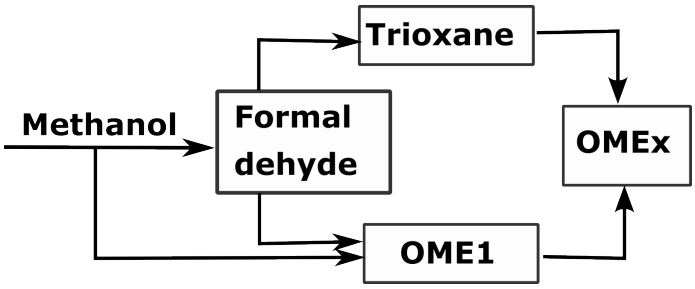

Figure 2.7: Oxymethylene dimethyl ethers production pathway. Source [75]

The physicochemical properties of these fuels are strongly dependent on the chain length. When x in OME_x is $\geq$2, the cetane number exceeds 60 [80]. However, OME_1 has a relatively lower cetane number of 28 and is highly volatile. Thus it cannot be utilized in an engine unless blended [73, 81]. It poses greater challenges in terms of lubricity and lower cetane number however, due to its lower emissions potential it is used in blended form with other higher cetane number fuels like diesel, HVO, etc. The increment of chain length greater than 1 comes with the benefit of soot reduction, increase in cetane number, lubricity, and flash point [41]. However, with the increase in chain length above 5, OME_x presents problems with cold flow properties i.e., melting point [82]. Therefore, oxymethylene dimethyl ethers where x is between 2 to 5 present characteristics more similar to diesel and are hence more appropriate for use in the current injection systems [81]. In terms of LHV, these fuels possess rather lower energy as compared to fossil diesel so they require longer injection durations to compensate for energy loss. In contrast, these fuels generally exhibit a faster combustion phase due to the higher content of oxygen present inside them. Furthermore, oxymethylene dimethyl ethers contain over 40 % oxygen in their molecular structure [83]. All of these characteristics make them a potential choice for the replacement of fossil diesel in CI engines either in pure form or in the form of blends.

A wide amount of research has been carried out in the past decade regarding the analysis of combustion and emission behavior of these fuels in CI engines. Focusing first on OME_1, Ogawa et al. [52] performed experiments to explore the potential of OME_1 under stoichiometric conditions by using EGR and three-way catalyst. Results indicated that the NO_x emissions were reduced significantly by utilizing 30% EGR without deteriorating the brake-specific energy consumption (BSEC). Song et al.[84] studied the effects of the addition of OME_1 in diesel on soot production in an optically accessed diesel

engine. An increase of ID and premixed combustion phase along with significant soot reduction was observed. Zhu et al. [85] investigated experimentally the effect of OME_1 addition and EGR on the combustion and emission performance of a direct injection diesel engine. The results matched previous literature indicating that the addition of OME_1 results in an increase in ignition delay, an increase in premixed combustion phase, and effectively reduced CO and PM emissions. The use of EGR results in longer ID but it helped reduce the NO_x emissions. Deepenraj et al. [86] studied the influence of the addition of OME_1 on the combustion and emission characteristics of diesel engines. The authors concluded that a better performance in terms of combustion efficiency and exhaust emissions reductions was achieved by the addition of 20% of OME_1 in the blend with diesel. They reported further that CO, HC, and smoke levels were decreased. The combustion and emission effect of blends of OME_1 with diesel was also investigated by pan et al. [87]. The results suggested that the OME_1 addition improves the brake thermal efficiency and reduces significantly the soot emissions.

When it comes to OME_x, experimental research has also been carried out in a significant amount. Pellegrini et al. [54] studied the combustion and emission behavior of neat and blended OME_x in a CI engine. The results indicated that OME_x increases the oxidation rate of soot and it helps in the decrement of soot and NO_x formation. Authors reported that around 40% reduction in PM emission was achieved by the addition of 10-12% of OME_x in the blend. Barro et al. [53] conducted research on the combustion characteristics of OME_x (80% OME_3, 20% OME_4) on a heavy-duty single-cylinder engine. The results showed that the high cetane number of OME_x caused its ignition delay to be shorter than that of diesel fuel, and the proportion of premixed combustion was reduced, while the diffusion combustion was faster. Thus, the brake thermal efficiency (BTE) of OME_x was higher than that of diesel without considering EGR. Liu et al. [88] investigated the OME_x-diesel blends inside a heavy-duty diesel engine. Authors highlighted that the late combustion phase is accelerated by the addition of OME_x, and the HC, CO, and soot emissions are decreased by a significant amount. Omari et al.[89] studied the potential of long-chain OME_x and OME_x-diesel blends in a CI engine in terms of emissions reduction. Authors concluded that OME_x shows soot-free combustion and can break the famous soot-NO_x trade-off. An Optical Investigation of the performance of OME_x was carried out by authors in [41] where they highlighted that OME_x helps to increase the intensity of OH* chemiluminescence which directly relates to faster combustion. Further investigation from the same authors indicated that OME_x produces soot-free combustion. Recently, authors in [90] studied the Diesel-OME_x blends inside

a common rail diesel engine. The findings of the investigation included the reduction of smoke emissions, diesel particle size, and total particle number.

In addition to the experimental research being carried out both on OME_1 and OME_x, a significant amount of numerical studies also exists in the literature highlighting the combustion and emission aspects of these fuels. Focusing on OME_1 first, yang et al. [91] investigated the application of OME_1 in a truck diesel engine by means of 1D simulation. The results highlighted the perfect soot suppression effect for OME_1 as well as a slight decrease in NO_x emissions. A combustion system optimization was carried out by Novella et al. in [92] for OME_1 fuel using 3D CFD simulations, where authors concluded that this fuel produces soot-free combustion and can help decrease NO_x emissions. The effect of the addition of OME_1 in blends with diesel was investigated numerically by Ghadamkhier et al. [93] using 3D CFD simulations, where the authors concluded that Diesel-OME_1 blends can effectively finish the soot-NO_x trade-off. Furthermore, the findings demonstrated that a 60% blend of Diesel-OME_1 can significantly reduce soot and NO_x emissions by up to 89% and 90%, respectively. However, with an increase in OME_1 content in the fuel, there was a decrease in peak pressure and peak rate of heat release, primarily due to the lower LHV of the fuel mixture. As a result, authors advised that if performance degradation is a concern in a particular application, the OME_1 content should not exceed 25 to 30%.

Regarding the numerical research carried out for OME_x or its blends, Ren et al. [94] studied the primary reference fuel (PRF)-OME_x blends numerically by developing a reduced reaction mechanism. 3D CFD results indicated that the soot reduction tendency is three orders of magnitude smaller than that of pure diesel. Lv et al. [95] also studied Diesel-OME_x blends through the development of a reduced reaction mechanism. Authors reaffirmed the soot-reducing tendency of OME_x with the tendency increasing as the OME_x percentage in the blend was increased. The same approach was followed by Lin et al. [96] recently, where authors primarily developed a reduced reaction mechanism and further analyzed gasoline/diesel/OME_x blends. Conclusions included the soot emissions were decreased reaffirming the advantages of OME_x as a fuel additive. A numerical simulation of the NO and soot formation process of a diesel engine with OME-diesel blend fuel was carried out by Gao et al. [97]. The research findings highlighted, that as the blending ratio of OME_x increases, the range of soot generation distribution of the blends is decreased. When compared to diesel, a blend having 20% OME_x exhibits a 46% reduction in ultimate soot generation, while a blend having 30% OME_x experiences a nearly 80% reduction under rated operating conditions. Recently A numerical analysis of combustion and emission performance of OME_x was

carried out by authors in [98] inside an optical CI engine. Results highlighted that OME_x fuel produces large amounts of fuel at equivalence ratios less than 2 which ultimately contributed towards less soot formation. Furthermore, it was also seen that intense levels of OH regions were observed for OME_x which hinted towards faster oxidation of soot.

To summarize, the research carried out in the literature with regards to the use of oxymethylene dimethyl ethers in a CI engine highlights their potential in improving combustion and reducing pollutant emissions including soot, NO_x, and other harmful species like CO, HC, etc. Both experimental and numerical studies exist in the literature which complement the advantages achieved in terms of utilizing these promising e-fuels. However, another aspect in terms of detailed numerical analysis along with the construction of appropriate chemical reaction mechanisms, when these fuels are blended with other conventional and alternative fuels can be explored. Hence, a part of this thesis will be dedicated to analyzing the combustion and emission performance of these fuels.

2.4 Role of hardware improvements in tackling pollutant emissions

In conjunction with the exploration of alternative fuels for combustion engines, the optimization of combustion system hardware offers itself a promising strategy to mitigate pollutant emissions. Over many years, researchers and automakers have developed and implemented many hardware improvements related to CI engines to affect the in-cylinder combustion process and ultimately reduce pollutant emissions. These hardware improvements include but are not limited to changes in piston bowl design, optimization of the combustion chamber, optimizing cylinder head design, changing the injector nozzle design, etc. One of the proven examples is the evolution of piston bowl geometry as the development of CI engines has progressed. In the past, CI engines featured straightforward bowl shapes. However, contemporary designs have undergone a transformative shift, integrating sophisticated elements such as optimized bowl shapes, well-defined squish areas, and crevice volumes ultimately affecting the in-cylinder air-fuel mixing in turn decreasing pollutant formation. The launch of wave piston by Volvo, where protrusions located around the bowl circumference helped push the flames toward the bowl center where fresh oxygen was available serves as a recent example of the implication of bowl changes to improve the combustion process [99, 100]. This helped reduce not only soot emissions but also HC and CO emissions. Other examples

include the utilization of different types of nozzles as compared to the conventional conical nozzles which result in improvement in spray distribution in turn improving the air-fuel mixing and reducing the formation of soot [101]. A more recent addition to the improvements done to the CI engine hardware is the Ducted fuel injection (DFI) concept, which has shown a significant potential to affect the air-fuel mixing process ultimately reducing soot emissions and also breaking the soot-NO_x tradeoff [102].

As the improvements done to CI engine hardware have proven to be effective in reducing pollutant formation by affecting the combustion process, therefore, during the context of this thesis, the more recent concept of DFI is explored in detail including its basics to the application in a CI engine. Henceforth a detailed literature review on the use of DFI in CI engines and its potential advantages in terms of reduction in pollutant emissions is carried out in the proceeding section.

2.4.1 The Ducted Fuel Injection concept

Ducted fuel injection is a concept that conceives to enhance the air/fuel mixing inside the combustion chamber of a CI engine, which ultimately leads to increased efficiency and reduced pollutant formation. This concept was first proposed by Mueller et al. [102] in 2017. It consists of driving the spray, formed by a high-pressure fuel injection, through a small duct co-axial to the spray itself. The authors reported the first evidence of the DFI performance in a constant volume combustion vessel (CVCV), with a single-hole nozzle and utilizing natural luminosity (NL) and OH* chemiluminescence. Their results showed that this new concept was able to enhance air-fuel mixing, resulting in leaner combustion with much lower soot formation than that observed with a conventional free spray (FS) configuration. Figure 2.8 shows the improvements achieved in terms of soot incandescence for the DFI configuration as compared to free spray as first reported by Mueller et al. [102] in the proof of concept stage of DFI.

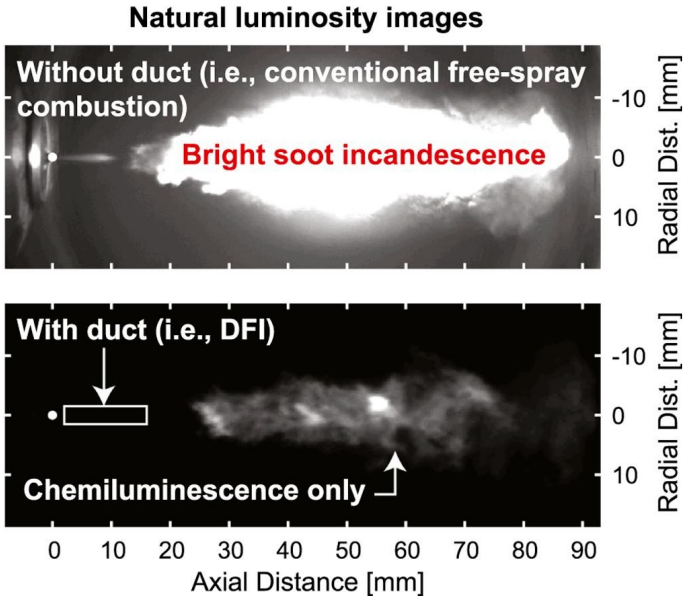

Figure 2.8: Natural luminosity images for Free spray and DFI configuration. Source [102]

The idea of injecting the fuel through a tube to enhance premixing and reduce soot formation is at least 160 years old, as evidenced by the invention of the Bunsen burner. Fuel is added to a Bunsen burner through a tube, which draws in air at the tube's base and mixes the fuel along its length. A premixed flame stabilizes and burns cleanly near the tube's exit. Bunsen was able to maintain a reliable and repeatable light source for his photochemical investigations because of this design. Comparably, in DFI, the duct should ideally encourage efficient fuel and charge-gas premixing before autoignition, completely avoiding the formation of soot. The schematic of DFI taken from [102] is shown in Figure 2.9.

The idea of DFI is based on leaner lifted-flame combustion (LLFC) strategy which is an advanced combustion strategy where the injection timing is used to control the ignition of the fuel. With LLFC, the fuel spray mixes with air inside the cylinder before reaching the flame so to say a controlled premixing happens in contrast to the conventional combustion strategy. This strategy is believed to eliminate soot if the equivalence ratios achieved near the lift-off length are maintained below 2 [103–105] as it is suggested in the literature that soot is unlikely to be formed where equivalence ratio values are below 2 [106]. Referring to Figure 2.9, authors stated that the implementation of

the duct could lead to LLFC in a way that the presence of the duct improves the entrainment of charge gas inside the spray and promotes leaner fuel/air mixtures near the LOL (equivalence ratios below 2).

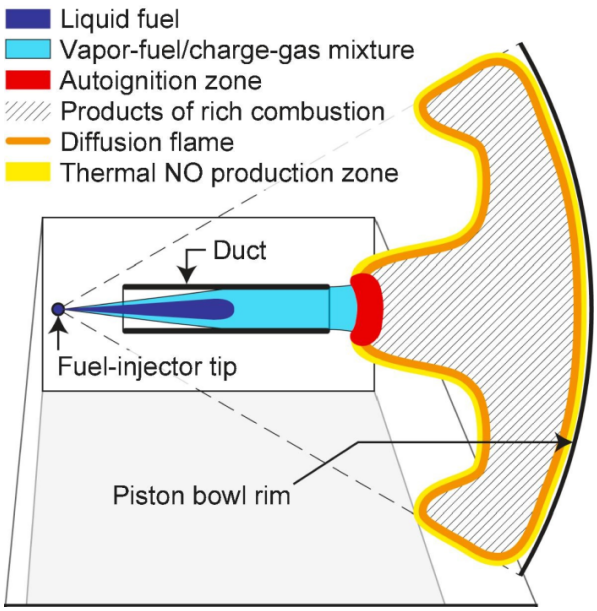

Figure 2.9: Schematic of the ducted fuel injection (DFI) concept on one fuel spray within a compression-ignition, direct-injection engine. Source [102]

From the proposal of the first DFI concept in 2017 till now, limited yet both fundamental and applied research has been carried out by numerous researchers. Gehmlich et al. [107] continued the previous work of Mueller et al. [102] providing more insight into the effects of this new concept. The authors reported that the DFI caused an increase of the ID and LOL, while reaching up to 35-100% of soot reduction over a wide range of operating conditions. Fitzgerald et al. [108] confirmed that the DFI provided longer ID but also faster initial jet penetration. This resulted in a larger LOL, where equivalence ratios were lower than those found at the LOL for a Free spray configuration. Other authors have also evaluated the impact of DFI on spray development. Liu et al. [109] explored the influence of the device over a wide range of ambient and injection pressures, concluding that an increase in spray penetration was observed especially for high injection pressures. In addition, the authors also reported an increase of the spray cone angle. All in all, the results suggested an improvement in the air-fuel mixing process, as was suggested in

previous works. Similar conclusions were reported by Millo et al. [110], who confirmed the mixing improvement also highlighting an intensification of the turbulent mixing when compared to FS. These authors also report a reduction of soot up to 80% when using this new technology.

One of the main aspects that has been identified as critical for the DFI performance is its geometry. Gehmlich et al. [107] reported that the duct length (L) $>$ 8 mm had minimal effects on DFI performance. However, additional features like a rounded inlet flange provided improvement because it allowed a jet-pumping effect that increased the air entrainment driven into the duct. The results by Svensson et al. [111] confirmed the benefits of the DFI concept, however, in contrast, they reported that larger ducts were better at soot reduction as compared to smaller ducts in terms of length. Svensson et al. [111] also reported a decrease in soot luminosity when the axial distance between the nozzle orifice exit and duct inlet plane (G, or stand-off distance) was decreased. This was in agreement with the conclusions of Gehmlich et al. [107], who also highlighted that a much smaller axial gap (G $<$ 2 mm) could actually reverse this relation because it will limit the entrainment of the air into the duct, resulting in higher soot formation. In contrast, Li et al. [112] reported that larger G increased the spray velocity which would result in better DFI performance in terms of soot reduction. In the same way, Nilsen et al. [113] while conducting a study inside a compression ignition (CI) engine found that a larger G duct provided higher soot attenuation. However, they compared 1.6 mm and 3 mm G distance, which is close to the range limits proposed in [107]. Li et al. [112] also explored the impact of duct inner diameter (D). Their findings indicated that a narrower duct exhibits better spray diffusion, longer liquid length, and a broader spray cone angle which would result in better DFI performance. Further, in other studies [109, 114], they confirmed that a smaller D performs better, provided that the spray diameter doesn't exceed that of the duct inlet. More recently, Svensson et al. [115] conducted an experimental study in order to find an optimum duct size to be utilized with DFI concept. They also highlighted the importance of ambient temperature, which plays a key role in DFI performance. Besides, they confirmed that DFI efficacy in reducing soot formation is decreased when increasing D and ambient temperature.

The first study inside a CI engine related to DFI was performed by Nilsen et al. [113] where authors studied DFI performance inside a 1.7 litres single cylinder heavy duty CI engine with 2 orifice injector nozzle at injection pressure of 180 MPa utilizing NL imaging technique. DFI was effective in curtailing soot emissions and also in terms of breaking the soot-NO_x trade-off. This study proved the efficacy of DFI concept to reduce soot emissions in

engine application and matched the previous results of spray vessels. Nilsen et al. [116] presented later, a similar work with 4 orifice fuel injectors. Their study was conducted on a wide range of operating conditions including injection pressure sweep, intake oxygen mole fraction sweep, injection duration sweep, start of combustion timing sweep, intake pressure, and temperature sweep. They concluded that DFI decreased the soot emissions in all the operating conditions tested. Svensson et al. [117] performed experiments with a 6-hole nozzle injector inside a heavy-duty engine. However, in this case, their results were in contrast with previous literature findings as DFI consistently produced more soot than FS configuration at high load conditions. For this reason, they suggested that a proper design optimization of the combustion system was necessary. The application of DFI was combined with oxygenated fuel blended with diesel by Mueller et al. [118] in the same CI engine as previous work conducted by the same group [113, 116]. The authors utilized two blends containing oxygenated fuels alongside conventional diesel fuel at various oxygen concentrations with a two-orifice fuel injector. They were able to achieve a sort of incandescence attenuation of up to around 100 times, indicating DFI combined with oxygenated fuels can curtail soot emissions by a substantial amount. Recently Nyrenstedt et al. [119] studied DFI alongside low net carbon fuels inside a CI engine utilized in [113, 116, 118] at different oxygen dilution levels and at two different load conditions. Conclusions highlighted that independent of load being used, DFI along with low net carbon fuels can break the soot-NO_x trade-off and can be presented as a solution to future stricter emissions regulations.

In parallel to the experimental work done related to DFI, a series of numerical investigations has been also carried out by different authors in order to better understand the DFI concept. A numerical investigation of DFI and FS was carried out by Liu et al. [120] where authors simulated DFI and FS under CI engine conditions using n-dodecane as a diesel surrogate. Their conclusions were in line with previous literature, highlighting that DFI strategy reduced the combustion duration and increased the ignition delay. In fact, the use of this new concept increased the low-temperature heat release region and decreased the high-temperature one, leading to soot reduction. Piano et al. [87] investigated the DFI device inside a light-duty diesel engine at various engine operating points. Despite observing a reduction of soot formation, they identified certain oxidation problems. For this reason, they highlighted that a proper optimization of the combustion system would be necessary before the full advantage of DFI in terms of soot mitigation can be obtained. Recently, another numerical study related to DFI was performed by Sener et al. in [121, 122], where authors findings complemented the experimental literature

results. DFI was able to achieve up to 66.7% attenuation in soot with respect to FS and it was also effective in decreasing CO and HC emissions.

Taking into account all the work done on the DFI concept, it is understood that DFI can attenuate soot emissions and can break the soot-NO_x trade-off in most cases. However, the studies conducted so far are limited to spray vessels and heavy-duty engines utilizing 2-to-4-hole nozzle injectors and have shown some limitations when this number has been increased up to 6 holes. In addition, among the different studies, there are contradictory conclusions regarding the influence of the main geometrical parameters of DFI. Therefore, the investigation of this DFI concept has been considered within the scope of this thesis in order to better understand the working principle of this concept and explore the advantages achieved in terms of soot reduction in a CI engine.

2.5 Summary and Conclusions

During this chapter, a brief overview of conventional diesel combustion with a focus on different combustion stages and pollutant formation is given. The overview is followed by a description of the role of alternative fuels in tackling pollutant emissions. In that sense, focus has been given to promising fuels including HVO, OME_1, and OME_x as an alternative to fossil diesel in reducing harmful pollutants. This is followed by an overview of the different hardware improvements applied to the combustion chamber which resulted in lowering the emissions. In that sense, a detailed literature review has been presented on the DFI concept which has proven to reduce CI engine pollutant problem. Henceforth, in summary, two different kinds of approaches have been presented in this chapter to tackle pollutant emissions (the use of alternative fuels particularly HVO, OME_1, OME_x and the use of the DFI concept). Although some studies were already carried out with these technologies, there are still some topics that must be explored, and they are summarized as follows:

- In the case of the use of alternative fuels (HVO, OME_1, OME_x), the literature was mainly focused on experimental studies, with a few numerical studies. Furthermore, the literature related to numerical studies was confined to either 1D spray simulations or to the use of specific blends of these fuels in 3D CI engine simulations. This was partially due to the absence of appropriate chemical reaction mechanisms necessary to perform detailed numerical simulations of different blends of these fuels. So, a different perspective in terms of numerical modeling of these fuel blends can be explored, which involves the development

of a reduced and robust chemical reaction mechanism followed by detailed combustion and emission analysis performed based on an optical CI engine.

- In the case of the use of the DFI concept, the literature was also focused mainly on experimental studies and was mainly confined to spray vessels with some studies performed in heavy-duty engines as it is a relatively new concept. Hence, a different perspective in terms of experimental modeling of the DFI concept applied to an optical CI engine can be explored, which can improve the understanding of the working principle and combustion and emission behavior of DFI.

References

[1] Heywood, John B. *Internal combustion engine fundamentals*. McGraw-Hill Education, 2018.

[2] Tiemin, Xuan. "Optical investigations on diesel spray dynamics and in-flame soot formation". PhD thesis. Universitat Polit'ecnica de Val'encia, 2017.

[3] Plee, Steven L and Ahmad, Tanvir. "Relative roles of premixed and diffusion burning in diesel combustion". In: *SAE transactions* (1983), pp. 892–909.

[4] Musculus, Mark PB, Miles, Paul C, and Pickett, Lyle M. "Conceptual models for partially premixed low-temperature diesel combustion". In: *Progress in energy and combustion science* 39.2-3 (2013), pp. 246–283.

[5] Stone, R. and Ball, J.K. *Automotive Engineering Fundamentals*. Premiere Series Bks. SAE International, 2004.

[6] Higgins, Brian, Siebers, Dennis, and Aradi, Allen. "Diesel-spray ignition and premixed-burn behavior". In: *SAE transactions* (2000), pp. 961–984.

[7] Skeen, Scott, Manin, Julien, and Pickett, Lyle M. "Visualization of ignition processes in high-pressure sprays with multiple injections of n-dodecane". In: *SAE International Journal of Engines* 8.2 (2015), pp. 696–715.

[8] Pickett, Lyle M, Kook, Sanghoon, and Williams, Timothy C. "Visualization of diesel spray penetration, cool-flame, ignition, high-temperature combustion, and soot formation using high-speed imaging". In: *SAE international journal of engines* 2.1 (2009), pp. 439–459.

[9] Westbrook, CK et al. "The effects of pressure, temperature, and concentration on the reactivity of alkanes: Experiments and modeling in a rapid compression machine". In: *Symposium (international) on combustion*. Vol. 27. 1. Elsevier. 1998, pp. 371–378.

[10] Dec, John E. "A conceptual model of DL diesel combustion based on laser-sheet imaging". In: *SAE transactions* (1997), pp. 1319–1348.

[11] Flynn, Patrick F et al. "Diesel combustion: an integrated view combining laser diagnostics, chemical kinetics, and empirical validation". In: *SAE transactions* (1999), pp. 587–600.

[12] Mollenhauer, Klaus, Tschöke, Helmut, and Johnson, Krister GE. *Handbook of diesel engines*. Vol. 1. Springer Berlin, 2010.

[13] Dec, John E and Coy, Edward B. "OH radical imaging in a DI diesel engine and the structure of the early diffusion flame". In: *SAE transactions* (1996), pp. 1127–1148.

[14] Tree, Dale R and Svensson, Kenth I. "Soot processes in compression ignition engines". In: *Progress in energy and combustion science* 33.3 (2007), pp. 272–309.

[15] Bartok, William and Sarofim, Adel F. "Fossil fuel combustion: a source book". In: (1991).

[16] Turns, Stephen R et al. *Introduction to combustion*. Vol. 287. McGraw-Hill Companies New York, NY, USA, 1996.

[17] Alozie, Nehemiah Sabinus and Ganippa, Lionel Christopher. "Diesel Exhaust Emissions and Mitigations". In: *Introduction to Diesel Emissions*. Ed. by Richard Viskup. Rijeka: IntechOpen, 2019. Chap. 1. DOI: 10.5772/intechopen.85248.

[18] Heywood, John B. "Automotive engines and fuels: a review of future options". In: *Progress in Energy and Combustion Science* 7.3 (1981), pp. 155–184.

[19] Bae, Choongsik and Kim, Jaeheun. "Alternative fuels for internal combustion engines". In: *Proceedings of the Combustion Institute* 36.3 (2017), pp. 3389–3413.

[20] Chum, Helena L and Overend, Ralph P. "Biomass and renewable fuels". In: *Fuel processing technology* 71.1-3 (2001), pp. 187–195.

[21] Kranenburg-Bruinsma, KJ van et al. "E-fuels-Towards a more sustainable future for truck transport, shipping and aviation". In: (2020).

[22] Khan, Nida, Sudhakar, Kumarasamy, and Mamat, Rizalman. "Role of biofuels in energy transition, green economy and carbon neutrality". In: *Sustainability* 13.22 (2021), p. 12374.

[23] Mathews, John A. "Carbon-negative biofuels". In: *Energy policy* 36.3 (2008), pp. 940–945.

[24] Jamuwa, DK, Sharma, D, and Soni, SL. "Performance, emission and combustion analysis of an ethanol fuelled stationary CI engine". In: *Biofuels* (2016).

[25] Taghizadeh-Alisaraei, Ahmad and Rezaei-Asl, Abbas. "The effect of added ethanol to diesel fuel on performance, vibration, combustion and knocking of a CI engine". In: *Fuel* 185 (2016), pp. 718–733.

[26] Fraioli, Valentina, Mancaruso, Ezio, Migliaccio, Marianna, and Vaglieco, Bianca Maria. "Ethanol effect as premixed fuel in dual-fuel CI engines: experimental and numerical investigations". In: *Applied energy* 119 (2014), pp. 394–404.

[27] Wei, Jiangjun et al. "Impact of methanol alternative fuel on oxidation reactivity of soot emissions from a modern CI engine". In: *Fuel* 268 (2020), p. 117352.

[28] Verhelst, Sebastian, Turner, James WG, Sileghem, Louis, and Vancoillie, Jeroen. "Methanol as a fuel for internal combustion engines". In: *Progress in Energy and Combustion Science* 70 (2019), pp. 43–88.

[29] Zhou, Feng et al. "The application prospect and challenge of the alternative methanol fuel in the internal combustion engine". In: *Science of The Total Environment* (2023), p. 169708.

[30] Arunkumar, M, Kannan, M, and Murali, G. "Experimental studies on engine performance and emission characteristics using castor biodiesel as fuel in CI engine". In: *Renewable Energy* 131 (2019), pp. 737–744.

[31] Rajasekar, E and Selvi, S. "Review of combustion characteristics of CI engines fueled with biodiesel". In: *Renewable and Sustainable Energy Reviews* 35 (2014), pp. 390–399.

[32] Shahir, VK, Jawahar, CP, and Suresh, PR. "Comparative study of diesel and biodiesel on CI engine with emphasis to emissions—a review". In: *Renewable and Sustainable Energy Reviews* 45 (2015), pp. 686–697.

[33] Dimitriadis, Athanasios et al. "Improving PM-NOx trade-off with paraffinic fuels: A study towards diesel engine optimization with HVO". In: *Fuel* 265 (2020), p. 116921.

[34] Chau, Vo Tan, Chinda, Charoenphonphanich, Preechar, Karin, Sato, Susumu, and Kosaka, Hidenori. "Optical study on combustion characteristics of hydrotreated vegetable oil and blends under simulated CI engine conditions and various EGR". In: *Journal of Mechanical Science and Technology* 31 (2017), pp. 4521–4531.

[35] Pinto, GM et al. "Combustion, performance and emission analyses of a CI engine operating with renewable diesel fuels (HVO/FARNESANE) under dual-fuel mode through hydrogen port injection". In: *International Journal of Hydrogen Energy* 48.51 (2023), pp. 19713–19732.

[36] *Howden Backing Bioenergy for a Low Carbon Future,2023, https://www.howden.com/en-us/articles/renewables/backing-bioenergy.*

[37] Ueckerdt, Falko et al. "Potential and risks of hydrogen-based e-fuels in climate change mitigation". In: *Nature Climate Change* 11.5 (2021), pp. 384–393.

[38] Garcia, Antonio, Monsalve-Serrano, Javier, Villalta, David, and Guzman-Mendoza, Maria. "Parametric assessment of the effect of oxygenated low carbon fuels in a light-duty compression ignition engine". In: *Fuel Processing Technology* 229 (2022), p. 107199.

[39] Lepperhoff, Gerhard et al. *Potential of synthetic fuels in future combustion systems for HSDI diesel engines.* Tech. rep. SAE Technical Paper, 2006.

[40] Gill, SS, Tsolakis, Athanasios, Dearn, KD, and Rodríguez-Fernández, J. "Combustion characteristics and emissions of Fischer–Tropsch diesel fuels in IC engines". In: *Progress in Energy and Combustion Science* 37.4 (2011), pp. 503–523.

[41] Pastor, José V, García, Antonio, Micó, Carlos, and Lewiski, Felipe. "An optical investigation of Fischer-Tropsch diesel and Oxymethylene dimethyl ether impact on combustion process for CI engines". In: *Applied Energy* 260 (2020), p. 114238.

[42] Cai, Panpan et al. "Effects of Fischer-Tropsch diesel blending in petrochemical diesel on combustion and emissions of a common-rail diesel engine". In: *Fuel* 305 (2021), p. 121587.

[43] Nadimi, Ebrahim et al. "Effects of using ammonia as a primary fuel on engine performance and emissions in an ammonia/biodiesel dual-fuel CI engine". In: *International Journal of Energy Research* 46.11 (2022), pp. 15347–15361.

[44] Chiong, Meng-Choung et al. "Advancements of combustion technologies in the ammonia-fuelled engines". In: *Energy Conversion and Management* 244 (2021), p. 114460.

[45] Dimitriou, Pavlos and Javaid, Rahat. "A review of ammonia as a compression ignition engine fuel". In: *International Journal of Hydrogen Energy* 45.11 (2020), pp. 7098–7118.

[46] Chen, Hao, He, Jingjing, and Zhong, Xianglin. "Engine combustion and emission fuelled with natural gas: a review". In: *Journal of the Energy Institute* 92.4 (2019), pp. 1123–1136.

[47] Sattarzadeh, Mehran, Ebrahimi, Mojtaba, and Jazayeri, Seyed Ali. "A detail study of a RCCI engine performance fueled with diesel fuel and natural gas blended with syngas with different compositions". In: *International Journal of Hydrogen Energy* 47.36 (2022), pp. 16283–16296.

[48] Wahbi, A, Tsolakis, A, and Herreros, J. "Emissions control technologies for natural gas engines". In: *Natural Gas Engines: For Transportation and Power Generation* (2019), pp. 359–379.

[49] Park, Su Han and Lee, Chang Sik. "Applicability of dimethyl ether (DME) in a compression ignition engine as an alternative fuel". In: *Energy Conversion and Management* 86 (2014), pp. 848–863.

[50] Putrasari, Yanuandri and Lim, Ocktaeck. "Dimethyl ether as the next generation fuel to control nitrogen oxides and particulate matter emissions from internal combustion engines: A review". In: *ACS omega* 7.1 (2021), pp. 32–37.

[51] Agarwal, Avinash Kumar et al. "Ultra-low soot/particulate emissions from a dimethyl ether-fueled agricultural tractor engine". In: *Fuel* 356 (2024), p. 129637.

[52] Ogawa, Hideyuki, Nabi, Md Nurun, Minami, Masahiro, Miyamoto, Noboru, and Bong-Seock, Kim. "Ultra low emissions and high performance diesel combustion with a combination of high EGR, three-way catalyst, and a highly oxygenated fuel, dimethoxy methane (DMM)". In: *SAE transactions* (2000), pp. 1019–1027.

[53] Barro, Christophe, Parravicini, Matteo, and Boulouchos, Konstantinos. "Neat polyoxymethylene dimethyl ether in a diesel engine; part 1: Detailed combustion analysis". In: *Fuel* 256 (2019), p. 115892.

[54] Pellegrini, Leonardo et al. *Combustion behaviour and emission performance of neat and blended polyoxymethylene dimethyl ethers in a light-duty diesel engine*. Tech. rep. SAE Technical Paper, 2012.

[55] García, Antonio, Monsalve-Serrano, Javier, Sari, Rafael Lago, and Martinez-Boggio, Santiago. "Energy sustainability in the transport sector using synthetic fuels in series hybrid trucks with RCCI dual-fuel engine". In: *Fuel* 308 (2022), p. 122024.

[56] Aatola, Hannu, Larmi, Martti, Sarjovaara, Teemu, and Mikkonen, Seppo. "Hydrotreated vegetable oil (HVO) as a renewable diesel fuel: trade-off between NOx, particulate emission, and fuel consumption of a heavy duty engine". In: *SAE International Journal of Engines* 1.1 (2009), pp. 1251–1262.

[57] Hartikka, Tuukka, Kuronen, Markku, and Kiiski, Ulla. *Technical performance of HVO (hydrotreated vegetable oil) in diesel engines*. Tech. rep. SAE Technical Paper, 2012.

[58] *ERTRAC Working Group. Energy Carriers for Powertrains for a clean and efficient mobility. European Road Transport Research Advisory Council (ERTRAC) Working Group: Energy and Environment*. 2014.

[59] *Cepsa begins supply of HVO (100% renewable diesel) for professional customers*. 2023.

[60] *New Generation DAF trucks ready for 100% HVO, 2023, https://www.daf.com/en/news-and-media/news-articles/global/2023/20-07-2023-new-generation-daf-trucks-ready-for-100-procent-hvo*.

[61] *Volvo Trucks certify HVO synthetic diesel for all engines, 2015, https://www.fleetnews.co.uk/news/latest-news/2015/06/25/volvo-trucks-certify-hvo-synthetic-diesel-for-all-engines*.

[62] *MAN Engines approves off-road engines for use with regenerative diesel/HVO, 2023, https://press.mantruckandbus.com/corporate/man-engines-approves-off-road-engines-for-use-with-regenerative-dieselhvo/*.

[63] Bjørgen, Karl Oskar Pires, Emberson, David Robert, and Løvås, Terese. "Combustion and soot characteristics of hydrotreated vegetable oil compression-ignited spray flames". In: *Fuel* 266 (2020), p. 116942.

[64] McCaffery, Cavan, Karavalakis, George, Durbin, Tom, Jung, Heejung, and Johnson, Kent. *Engine-out emissions characteristics of a light duty vehicle operating on a hydrogenated vegetable oil renewable diesel*. Tech. rep. SAE Technical Paper, 2020.

[65] Karavalakis, George et al. "Emissions and fuel economy evaluation from two current technology heavy-duty trucks operated on HVO and FAME blends". In: *SAE International Journal of Fuels and Lubricants* 9.1 (2016), pp. 177–190.

[66] Szeto, Wai and Leung, Dennis YC. "Is hydrotreated vegetable oil a superior substitute for fossil diesel? A comprehensive review on physicochemical properties, engine performance and emissions". In: *Fuel* 327 (2022), p. 125065.

[67] Sugiyama, Kouseki, Goto, Isamu, Kitano, Koji, Mogi, Kazuhisa, and Honkanen, Markku. "Effects of hydrotreated vegetable oil (HVO) as renewable diesel fuel on combustion and exhaust emissions in diesel engine". In: *SAE International Journal of Fuels and Lubricants* 5.1 (2012), pp. 205–217.

[68] Kim, Duckhan, Kim, Seonghwan, Oh, Sehun, and No, Soo-Young. "Engine performance and emission characteristics of hydrotreated vegetable oil in light duty diesel engines". In: *Fuel* 125 (2014), pp. 36–43.

[69] Bortel, Ivan, Vávra, Jiří, and Takáts, Michal. "Effect of HVO fuel mixtures on emissions and performance of a passenger car size diesel engine". In: *Renewable Energy* 140 (2019), pp. 680–691.

[70] Mikkonen, Seppo, Honkanen, Markku, and Kuronen, Markku. "HVO, hydrotreated vegetable oil. A premium renewable biofuel for diesel engines". In: (2013).

[71] Gong, Y, Kaario, O, Tilli, A, Larmi, M, and Tanner, FX. *A computational investigation of hydrotreated vegetable oil sprays using RANS and a modified version of the RNG k-ε model in OpenFOAM*. Tech. rep. SAE Technical Paper, 2010.

[72] Zhang, Zhichao et al. "Investigation of the macroscopic characteristics of Hydrotreated Vegetable Oil (HVO) spray using CFD method". In: *Fuel* 237 (2019), pp. 28–39.

[73] Pastor, Jose V, Garcia-Oliver, Jose M, Micó, Carlos, and Tejada, Francisco J. *Combustion behaviour of blends of synthetic fuels in an optical single cylinder engine*. Tech. rep. SAE Technical Paper, 2021.

[74] Iannuzzi, Stefano Emanuele, Barro, Christophe, Boulouchos, Konstantinos, and Burger, Jakob. "Combustion behavior and soot formation/oxidation of oxygenated fuels in a cylindrical constant volume chamber". In: *Fuel* 167 (2016), pp. 49–59.

[75] Burger, Jakob, Siegert, Markus, Ströfer, Eckhard, and Hasse, Hans. "Poly (oxymethylene) dimethyl ethers as components of tailored diesel fuel: Properties, synthesis and purification concepts". In: *Fuel* 89.11 (2010), pp. 3315–3319.

[76] Burger, Jakob, Ströfer, Eckhard, and Hasse, Hans. "Production process for diesel fuel components poly (oxymethylene) dimethyl ethers from methane-based products by hierarchical optimization with varying model depth". In: *Chemical Engineering Research and Design* 91.12 (2013), pp. 2648–2662.

[77] Walker, Joseph Frederic and Frederic, Joseph. *Formaldehyde*. Vol. 26. Reinhold New York, 1964.

[78] Grützner, Thomas, Hasse, Hans, Lang, Neven, Siegert, Markus, and Ströfer, Eckhard. "Development of a new industrial process for trioxane production". In: *Chemical Engineering Science* 62.18-20 (2007), pp. 5613–5620.

[79] Masamoto, Junzo and Matsuzaki, Kazuhiko. "Development of methylal synthesis by reactive distillation". In: *Journal of chemical engineering of Japan* 27.1 (1994), pp. 1–5.

[80] Zheng, Yanyan, Tang, Qiang, Wang, Tiefeng, Liao, Yuhui, and Wang, Jinfu. "Synthesis of a green fuel additive over cation resins". In: *Chemical Engineering & Technology* 36.11 (2013), pp. 1951–1956.

[81] Härtl, Martin, Seidenspinner, Philipp, Jacob, Eberhard, and Wachtmeister, Georg. "Oxygenate screening on a heavy-duty diesel engine and emission characteristics of highly oxygenated oxymethylene ether fuel OME1". In: *Fuel* 153 (2015), pp. 328–335.

[82] Schemme, Steffen, Samsun, Remzi Can, Peters, Ralf, and Stolten, Detlef. "Power-to-fuel as a key to sustainable transport systems–An analysis of diesel fuels produced from CO2 and renewable electricity". In: *Fuel* 205 (2017), pp. 198–221.

[83] Pélerin, Dominik, Gaukel, Kai, Härtl, Martin, Jacob, Eberhard, and Wachtmeister, Georg. "Potentials to simplify the engine system using the alternative diesel fuels oxymethylene ether OME1 and OME3- 6 on a heavy-duty engine". In: *Fuel* 259 (2020), p. 116231.

[84] Song, Ki Hoon and Litzinger, Thomas A. "Effects of dimethyoxymethane blending into diesel fuel on soot in an optically accessible DI diesel engine". In: *Combustion science and technology* 178.12 (2006), pp. 2249–2280.

[85] Zhu, Ruijun, Wang, Xibin, Miao, Haiyan, Yang, Xiaofeng, and Huang, Zuohua. "Effect of dimethoxy-methane and exhaust gas recirculation on combustion and emission characteristics of a direct injection diesel engine". In: *Fuel* 90.5 (2011), pp. 1731–1737.

[86] Deepanraj, B, Sankaranarayanan, G, Senthilkumar, N, and Pugazhvadivu, M. "Influence of dimethoxymethane addition on performance, emission and combustion characteristics of the diesel engine". In: *International Journal of Ambient Energy* 38.6 (2017), pp. 622–626.

[87] Pan, Mingzhang, Qian, Weiwei, Wang, Yuke, Wu, Changkun, and Huang, Haozhong. "Effect of dimethoxymethane (DMM) additive on combustion and emission characteristics under different working conditions in CI engines". In: *Fuel* 284 (2021), p. 119304.

[88] Liu, Jialin et al. "Effects of diesel/PODE (polyoxymethylene dimethyl ethers) blends on combustion and emission characteristics in a heavy duty diesel engine". In: *Fuel* 177 (2016), pp. 206–216.

[89] Omari, Ahmad, Heuser, Benedikt, Pischinger, Stefan, and Rüdinger, Christoph. "Potential of long-chain oxymethylene ether and oxymethylene ether-diesel blends for ultra-low emission engines". In: *Applied energy* 239 (2019), pp. 1242–1249.

[90] Liu, Junheng et al. "Effects of PODE/diesel blends on particulate matter emission and particle oxidation characteristics of a common-rail diesel engine". In: *Fuel processing technology* 212 (2021), p. 106634.

[91] Yang, Qirui, Grill, Michael, and Bargende, Michael. *The application of e-fuel oxymethylene ether OME1 in a virtual heavy-duty diesel engine for ultra-low emissions*. Tech. rep. SAE Technical Paper, 2020.

[92] Novella, Ricardo, Bracho, Gabriela, Gomez-Soriano, Josep, Fernandes, Cássio S, and Lucchini, Tommaso. "Combustion system optimization for the integration of e-fuels (Oxymethylene Ether) in compression ignition engines". In: *Fuel* 305 (2021), p. 121580.

[93] Ghadamkheir, Kourosh, Zareei, J, Yang, Xiaohu, and Hatami, Mohammad. "The effects of diesel-OME1 blended fuel on combustion characteristics of a heavy-duty compression ignition engine by a numerical study". In: *Alexandria Engineering Journal* 64 (2023), pp. 493–503.

[94] Ren, Shuojin, Wang, Zhi, Li, Bowen, Liu, Haoye, and Wang, Jianxin. "Development of a reduced polyoxymethylene dimethyl ethers (PODEn) mechanism for engine applications". In: *Fuel* 238 (2019), pp. 208–224.

[95] Lv, Delin et al. "Development of a reduced diesel/PODEn mechanism for diesel engine application". In: *Energy Conversion and Management* 199 (2019), p. 112070.

[96] Lin, Qinjie, Tay, Kun Lin, Zhao, Feiyang, and Yang, Wenming. "Enabling robust simulation of polyoxymethylene dimethyl ether 3 (PODE3) combustion in engines". In: *International Journal of Engine Research* 23.9 (2022), pp. 1522–1542.

[97] Gao, Wanying et al. "Numerical simulation on NO and soot formation process of a diesel engine with polyoxymethylene dimethyl ethers-diesel blend fuel". In: *Energy Sources, Part A: Recovery, Utilization, and Environmental Effects* (2020), pp. 1–16.

[98] García-Oliver, José M, Novella, Ricardo, Micó, Carlos, and De Leon-Ceriani, Daiana. "Numerical analysis of the combustion process of oxymethylene ethers as low-carbon fuels for compression ignition engines". In: *International Journal of Engine Research* 24.5 (2023), pp. 2175–2186.

[99] Eismark, Jan and Balthasar, Michael. *Device for reducing emissions in a vehicle combustion engine*. US Patent 8,499,735. 2013.

[100] Eismark, Jan, Christensen, Magnus, Andersson, Mats, Karlsson, Anders, and Denbratt, Ingemar. "Role of fuel properties and piston shape in influencing soot oxidation in heavy-duty low swirl diesel engine combustion". In: *Fuel* 254 (2019), p. 115568.

[101] Pastor, José V et al. "Influence of the radial-lip concept design to achieve ultra-low soot emission reductions: An optical analysis". In: *Fuel* 345 (2023), p. 128161.

[102] Mueller, Charles J et al. "Ducted fuel injection: A new approach for lowering soot emissions from direct-injection engines". In: *Applied energy* 204 (2017), pp. 206–220.

[103] Pickett, Lyle M and Siebers, Dennis L. "Non-sooting, low flame temperature mixing-controlled DI diesel combustion". In: *SAE transactions* (2004), pp. 614–630.

[104] Polonowski, Christopher J et al. "An experimental investigation of low-soot and soot-free combustion strategies in a heavy-duty, single-cylinder, direct-injection, optical diesel engine". In: *SAE International Journal of Fuels and Lubricants* 5.1 (2012), pp. 51–77.

[105] Manin, Julien, Skeen, Scott, Pickett, Lyle, Kurtz, Eric, and Anderson, James E. "Effects of oxygenated fuels on combustion and soot formation/oxidation processes". In: *SAE International Journal of Fuels and Lubricants* 7.3 (2014), pp. 704–717.

[106] Kitamura, Takaaki, Ito, T, Senda, Jiro, and Fujimoto, Hajime. "Mechanism of smokeless diesel combustion with oxygenated fuels based on the dependence of the equivalence ration and temperature on soot particle formation". In: *International Journal of Engine Research* 3.4 (2002), pp. 223–248.

[107] Gehmlich, RK et al. "Using ducted fuel injection to attenuate or prevent soot formation in mixing-controlled combustion strategies for engine applications". In: *Applied energy* 226 (2018), pp. 1169–1186.

[108] Fitzgerald, Russell, Svensson, Kenth, Martin, Glen, Qi, Yongli, and Koci, Chad. "Early investigation of ducted fuel injection for reducing soot in mixing-controlled diesel flames". In: *SAE International Journal of Engines* 11.6 (2018), pp. 817–834.

[109] Li, Feng, Lee, Chia-fon, Wu, Han, Wang, Ziman, and Liu, Fushui. "An optical investigation on spray macroscopic characteristics of ducted fuel injection". In: *Experimental Thermal and Fluid Science* 109 (2019), p. 109918.

[110] Millo, F et al. "Ducted fuel injection: Experimental and numerical investigation on fuel spray characteristics, air/fuel mixing and soot mitigation potential". In: *Fuel* 289 (2021), p. 119835.

[111] Svensson, Kenth I and Martin, Glen C. "Ducted fuel injection: effects of stand-off distance and duct length on soot reduction". In: *SAE International Journal of Advances and Current Practices in Mobility* 1.2019-01-0545 (2019), pp. 1074–1083.

[112] Li, Feng, Lee, Chia-fon, Wang, Ziman, Pei, Yiqiang, and Lu, Guoxiang. "Impacts of duct inner diameter and standoff distance on macroscopic spray characteristics of ducted fuel injection under non-vaporizing conditions". In: *International Journal of Engine Research* 22.5 (2021), pp. 1702–1713.

[113] Nilsen, Christopher W, Biles, Drummond E, and Mueller, Charles J. "Using ducted fuel injection to attenuate soot formation in a mixing-controlled compression ignition engine". In: *SAE International Journal of Engines* 12.3 (2019), pp. 309–322.

[114] Li, Feng, Lee, Chia-fon, Wang, Ziman, Liu, Fushui, and Lu, Guoxiang. "Optical investigation on impacts of ambient pressure on macroscopic spray characteristics of ducted fuel injection under non-vaporizing conditions". In: *Fuel* 268 (2020), p. 117192.

[115] Svensson, Kenth, Fitzgerald, Russell, and Martin, Glen. *Ducted Fuel Injection: An Experimental Study on Optimal Duct Size*. Tech. rep. SAE Technical Paper, 2022.

[116] Nilsen, Christopher W, Biles, Drummond E, Yraguen, Boni F, and Mueller, Charles J. "Ducted Fuel Injection versus Conventional Diesel Combustion". In: *SAE International Journal of Engines* 13.3 (2020), pp. 345–362.

[117] Svensson, Kenth, Kim, Charlie, Seiler, Patrick, Martin, Glen, and Koci, Chad. *Performance and emission results from a heavy-duty diesel engine with ducted fuel injection*. Tech. rep. SAE Technical Paper, 2021.

[118] Mueller, Charles J, Nilsen, Christopher W, Biles, Drummond E, and Yraguen, Boni F. "Effects of fuel oxygenation and ducted fuel injection on the performance of a mixing-controlled compression-ignition optical engine with a two-orifice fuel injector". In: *Applications in Energy and Combustion Science* 6 (2021), p. 100024.

[119] Nyrenstedt, Gustav, Nilsen, Christopher W, Biles, Drummond E, and Mueller, Charles J. "Ducted fuel injection with Low-Net-Carbon fuels as a solution for meeting future emissions regulations". In: *Fuel* 338 (2023), p. 127167.

[120] Liu, Xinlei, Mohan, Balaji, and Im, Hong G. "Numerical investigation of the free and ducted fuel injections under compression ignition conditions". In: *Energy & Fuels* 34.11 (2020), pp. 14832–14842.

[121] Şener, R. "Numerical investigation of ducted fuel injection strategy for soot reduction in compression ignition engine". In: *Journal of Applied Fluid Mechanics* 15.2 (2022), pp. 475–489.

[122] Şener, Ramazan. "Ducted fuel injection: Numerical study of soot formation and oxidation using detailed soot modeling approach in a compression ignition engine at different loads". In: *Journal of the Brazilian Society of Mechanical Sciences and Engineering* 44.1 (2022), p. 45.

Chapter 3

Tools and Methodology

3.1 Introduction

This chapter is focused on presenting a detailed overview of different experimental and numerical tools as well as methodology utilized in the framework of this thesis. The chapter starts by a description of different fuels utilized in this thesis and then a detailed description of experimental and numerical tools is given. The experimental tools include the medium-duty optical engine, different optical techniques, and the DFI device, and the numerical tools include the 0D/1D modeling approach, reaction mechanisms development tools, and the approach for 3D CFD modeling of the optical engine. In terms of methodology, a detailed explanation has been provided regarding the development of the 3D CFD model. This model will serve as the basis of this thesis for the numerical assessment of potential solutions to reduce pollutant emissions. Additionally, detail is also included for the design of the DFI device and the optical setup utilized.

3.2 Fuels

The general background and advantages achieved in terms of using different alternative fuels including OME_x, OME_1 and HVO has already been presented in section 2.3. In the context of this thesis, several numerical investigations of blends of different fuels have been carried out. On one hand, blends of OME_x with fossil diesel have been utilized and on the other hand, the blends of OME_1 with HVO have been utilized. It must be noted that as established earlier in section 2.3, the first OME molecule when x is 1 in (CH_3O-$(CH_2O)_x$-CH_3) is termed as dimethoxymethane or methylal and denoted by OME_1 in the context of this thesis. Higher OME molecules where x>1 are denoted by OME_x in this thesis which are in fact a combination of different OMEs

having x>1. The composition of the OME_x fuel utilized in this thesis has been summarized in Table 3.1. As it can be seen the major part of OME_x fuel corresponds to OME molecules where x>1, specially OME_3 and OME_4.

Table 3.1: Composition of OME_x fuel utilized .

OME_x molecule	**% by weight**
OME_1	0.01
OME_2	< 0.01
OME_3	57.90
OME_4	28.87
OME_5	10.08
OME_6	1.91

As discussed in Section 2.3, OME_x emerges as a promising e-fuel for CI engines. However, due to its lower LHV, its blends with fossil diesel have presented themselves as promising alternatives to reduce pollutant emissions as well as improve combustion process [1–6]. Hence, in this thesis, different blends of OME_x with fossil diesel have been utilized. From here on, they will be represented as DXXOYY, where D refers to fossil diesel and XX represents the % of this fuel by mass in the blend. Similarly, O refers to OME_x and YY represents the % of this fuel by mass in the blend. For example, D70O30 identifies a blend of 70% diesel and 30% OME_x by mass. In this study, the OME_x fraction in blends starts from 10% and has been limited up to 50% owing to energy reduction caused by the lower LHV of this fuel. These different blends are identified by D90O10, D80O20, D70O30 and D50O50.

Similar to the OME_x, the advantages achieved by utilizing OME_1 have also been discussed in section 2.3. However in contrast to OME_x, OME_1 cannot be utilized directly in CI engines unless blended due to its high volatility [7, 8]. HVO also presents itself as a promising biofuel to replace fossil diesel which was discussed in detail in section 2.3. Hence, during the context of this thesis, different blends of OME_1 with HVO have been studied. This has been done in order to achieve the advantages both from HVO which has similar physical properties as diesel and from oxygenated fuel OME_1. From here on, they will be represented as HAAMBB, where H refers to HVO and AA represents the % of this fuel by mass in the blend. Similarly, M is used to represent OME_1

as it is also termed as Methylal and BB refers to % of this fuel by mass in the blend. For example, H70M30 identifies a blend of 70% HVO and 30% OME_1 by mass. In this case, the OME_1 fraction in blends has been limited up to 30% owing to both energy reduction caused by the lower LHV of this fuel and its high volatile characteristics. These different blends are represented as pure HVO (H100), H90M10, H80M20 and H70M30. Additionally, n-Dodecane has also been utilized specifically for studying HVO-OME_1 blends, the details of which will be discussed in the corresponding section.

The numerical investigations related to blends of Diesel-OME_x and HVO-OME_1 constitute the first part of this thesis. During the second part, commercial diesel alongwith Diesel-OME_x blends have also been utilized mainly to study the DFI concept. Table 3.2 summarizes the main properties of the utilized fuels.

Table 3.2: Properties of different fuels utilized.

Parameter	**Diesel**	**OME_x**	**OME_1**	**HVO**	**n-Dodecane**
Viscosity @40°C (mm^2/s)	2.80	1.08	0.36	2.70	1.439
Density @15°C (kg/m^3)	835.20	1057.10	866.7	779.9	751.2
Lubricity (μm)	386	320	747	460	563
Cetane number (-)	54.18	68.6	28	75.5	74
Oxygen content (%m/m)	0	45	42.1	0	0
Lower heating value [LHV] (MJ/kg)	39.79	19.21	19.248	44.046	44.2
Initial boiling point (°C)	155.10	144.90	37.4	185.5	214
Final boiling point (°C)	363.1	242.4	38	302	218

3.3 Experimental Tools and Methodology

In this subsection, a description of different experimental tools and well as the methodology utilized has been given. These include the experimental optical engine, the optical techniques, the optical setup utilized, and lastly the DFI design and implementation inside the optical engine.

3.3.1 Optical Engine

The sketch of the optical engine that has been utilized during the development of the current thesis is shown in Figure 3.1. The engine is a single-cylinder medium-duty optical engine based on the bowditch-type design having a capacity of 0.8 liters. This engine is an overhead valve (OHV) type and has 2 intake and 2 exhaust valves per cylinder inside the cylinder head. The design comprises an elongated piston, formed by an extension bolted on top of the standard engine piston as shown in Figure 3.1. This provides optical access from below the combustion chamber through a transparent window located at the bottom of the piston bowl. Moreover, the optical engine utilizes the same cylinder head as the conventional engine, featuring four valves and a centred solenoid injector per cylinder. The main characteristics of the optical engine are summarized in Table 3.3.

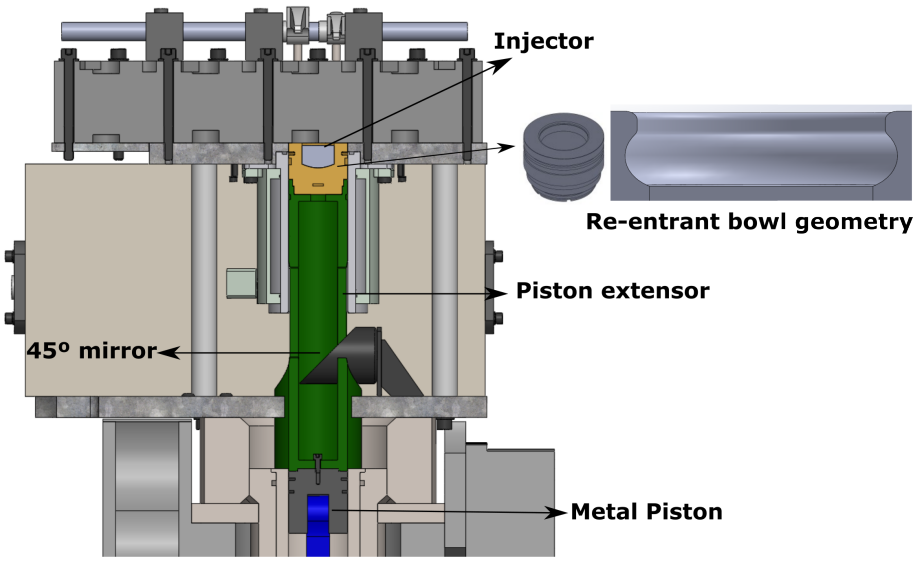

Figure 3.1: Optical engine assembly with parts.

Table 3.3: Optical engine characteristics.

Parameter	**Description/Value**
Operational mode	Diesel engine
Number of cylinders	1
Number of valves	4
Bore (mm)	103
Stroke (mm)	99
Displacement (l)	0.825
Effective compression ratio (-)	13.3
Connecting rod length (mm)	163.63

A re-entrant piston with a flat bottom was utilized throughout this thesis development as visualized in the Figure 3.1. Furthermore, a standard 8-hole conical nozzle was used with an orifice diameter of approximately 138 μm, with a common rail delivering the fuel to the injector. Regarding the operation of the engine, a skip fire mode was chosen to operate the engine which means only 1 out of 20 cycles was a firing cycle. This ensured a proper renovation of in-cylinder air during each cycle before the start of combustion, while limiting the thermal stress applied to the engine and the different parts. Furthermore, to cancel out the effect of cycle-to-cycle variability on the analysis, ten successive combustion cycles were recorded.

Regarding the equipment used in engine operation, an electric dynamometer was used to motor the engine. To achieve the required intake air pressure, a screw compressor was employed, and a valve located in the exhaust pipe was used to simulate a backpressure of 0.2 bar compared to the intake. Moreover, an air heater, positioned just before the intake port, ensured the intake air reached the desired temperature. A piezoelectric transducer (Kistler-6124A) was utilized to obtain the in-cylinder pressure. Similarly, a piezoresistive transducer (Kistler-4049A5) was used to measure the instantaneous intake and exhaust pressures. An oscilloscope (Yokogawa DL708E) which was synchronized with a crankshaft encoder, recorded the pressure signal, providing a 0.5 CAD resolution. The measured in-cylinder pressure was used to calculate the apparent heat release rate (aHRR) by applying the standard first law thermodynamic analysis [9] by utilizing an in-house developed zero-dimensional single zone thermodynamic model named CALMEC [10].

3.3.2 Optical Techniques

In the context of this thesis, three different optical techniques have been utilized to study the combustion evolution inside the combustion chamber as well as the soot formation. These techniques include natural luminosity, OH* chemiluminescence, and 2-color pyrometry. The working principle of these techniques is described below individually.

3.3.2.1 Natural Luminosity

Natural luminosity (NL) imaging was utilized to study the combustion process of alternative fuel blends inside the optical engine in this thesis. This technique was chosen as visible radiation emitted by hydrocarbon diffusion flames is usually related to soot thermal radiation and is considered to be dependent upon the soot volume fraction and its temperature. Thus, this technique can provide valuable information about the soot formation of the fuel blends used in this study. For this reason, it has been widely used in literature to study the evolution of soot for different fuels [11–15].

There are two radiation sources associated with the NL signal, one being soot incandescence and the other chemiluminescence. As described earlier, the hot soot particles emit visible thermal radiation, which is considered the dominant luminosity source during diffusion combustion. Chemiluminescence refers to the emission of non-thermal radiation by molecules as they transition from an excited energy state to the ground state during chemical reactions. In the context of diesel combustion, various intermediate species release light in this manner across specific, limited spectral ranges [16]. In general, thermal radiation is the dominant source of NL, and chemiluminescence in the visible range is usually negligible. Hence, during this thesis, the NL imaging constitutes mainly thermal radiation. The details about the cameras utilized to register NL imaging are discussed while describing the optical setup.

3.3.2.2 OH* Chemiluminiscene

The OH* Chemiluminescence technique was applied in both parts of this thesis i.e., numerical investigation of alternative fuels and the DFI concept. The OH* radical has been identified in the literature as a good tracer for the high-temperature reactions in diffusion combustion [17]. This technique has been widely used in literature to trace high-temperature zones and soot oxidation regions inside the combustion chamber utilizing different fuels [18–21]. Therefore, OH* chemiluminescence high-speed imaging was utilized.

In the process of combustion involving typical hydrocarbon fuels, the energetic reactions and elevated temperatures lead to the formation of excited state species, including excited state OH (OH*). Following its formation, the radical OH* returns to its ground state, releasing energy through either spontaneous fluorescence (chemiluminescence) or physical quenching through collisions. The spontaneous radiation from OH* primarily exists in the UV region, ranging from 280 to 350 nm, with a peak at 310 nm. In the same range, it is possible to find the emission of other radicals (like CO_2*). However, they are relatively weak compared to that of OH*. It has been reported to represent approximately 3.5% of the total radiation measured at this wavelength range [22, 23]. The details about the cameras utilized to register OH* imaging are discussed while describing the optical setup.

3.3.2.3 2-Color Pyrometry

As discussed earlier, NL imaging is utilized in this thesis as it gives valuable information about soot evolution inside the combustion chamber. However, there are certain limitations to NL imaging. NL imaging relies on capturing the natural light emitted by combustion processes, which can be influenced by various factors such as ambient lighting conditions and background noise, leading to potential inaccuracies in temperature measurements. Furthermore, it serves as a qualitative technique rather than quantitative. Therefore, a more state-of-the-art optical technique named, the 2-color (2C) pyrometry has been employed in this thesis to measure the amount of soot present within the combustion chamber mainly in the second part of the thesis (DFI concept). This technique involves detecting the thermal radiation emitted by the soot at two distinct wavelengths. Then the soot surface temperature and its optical density are determined by the application of Plank's law [24] and the combination of these two distinct wavelengths. This technique has been employed previously in literature by numerous researchers to quantify soot in a CI engine [25–28].

The assumption that the radiation emitted by a sooting flame with uniform spatial temperature and soot distributions depends on wavelength, the temperature, and the amount of soot present within the flame, serves as a starting point of 2C pyrometry. The Plank's law for a black body emitting radiation at a certain wavelength is given by Equation 3.1:

$$I_b(T,\lambda) = \frac{C_1}{\lambda^5\left[e^{\frac{C_2}{\lambda T}} - 1\right]} \tag{3.1}$$

where the emitted radiance by a black body is represented by I_b. The first Plank's constant is C_1 having a value of $1.1910439\text{X}10^{-16}\ Wm^2/sr$. C_2 is the second Plank's constant having a value of $1.4388\text{X}10^{-2}\ mk$ and λ is wavelength. Soot is a grey body with an emissivity ϵ below 1. Thus the flame emission can be represented by the Equation 3.2 as

$$I(T, \lambda) = \varepsilon I_b(T, \lambda) \tag{3.2}$$

In this context, the term emissivity (ε) represents the fraction of radiation emitted by a surface at a specific wavelength (λ) compared to that of a black body at the same wavelength and temperature T. Specifically, $I(T, \lambda)$ denotes the emissivity of a non-black body, while $I_b(T, \lambda)$ represents the emissivity of a black body, both emitting radiation at the same temperature (T) and wavelength (λ).

In the 2C technique, the process involves the calculation of an apparent temperature T_a, defined as the temperature of the black body that emits radiation with the same intensity as a non-black body at temperature T. Considering the definition of T_a, it is possible to assume that $I(T, \lambda) = I_b(T_a, \lambda)$. Considering this assumption and combining it with Equation 3.1, we get the following equation for the emissivity of a nonblack body:

$$\varepsilon_\lambda = \frac{e^{(\frac{C_2}{\lambda T})} - 1}{e^{(\frac{C_2}{\lambda T_a})} - 1} \tag{3.3}$$

However, the emissivity of soot particles can be estimated also by correlation proposed by Hottel and Broughton [29] as:

$$\varepsilon_\lambda = 1 - e^{-(\frac{KL}{\lambda^\alpha})} \tag{3.4}$$

where K represents the absorption co-efficient proportional to the number density of soot particles and L is the geometric thickness of the flame along the optical axis of the detection system. Furthermore, the parameter α depends upon the soot's physical and optical properties. This parameter stands at a value of 1.39 within the visible range as reported by Zhao et al. [30]. The parameter KL characterizes the relationship between emissivity and the quantity of soot. It encompasses the overall influence of soot along the optical path, no matter either its distribution or geometrical size [31].

Equation 3.3 and Equation 3.4 can be combined to obtain the KL parameter, which is represented in Equation 3.5 as:

$$KL = -\lambda^a ln\left[1 - \left(\frac{e^{(\frac{C_2}{\lambda T})} - 1}{e^{(\frac{C_2}{\lambda T_a})} - 1}\right)\right] \tag{3.5}$$

Assuming that the KL parameter remains constant and α parameter remains unchanged along the wavelength range considered in this work, Equation 3.5 can be written for the two registered wavelengths λ_1 and λ_2 to determine the temperature T of the soot particles, as illustrated in Equation 3.6

$$\left[1 - \left(\frac{e^{(\frac{C_2}{\lambda_1 T})} - 1}{e^{(\frac{C_2}{\lambda_1 T_{a1}})} - 1}\right)\right]^{\lambda_1{}^{\alpha_1}} = \left[1 - \left(\frac{e^{(\frac{C_2}{\lambda_2 T})} - 1}{e^{(\frac{C_2}{\lambda_2 T_{a2}})} - 1}\right)\right]^{\lambda_2{}^{\alpha_2}} \tag{3.6}$$

Once T is calculated the value of KL can be obtained from Equation 3.5. The details about the cameras utilized to register 2C imaging are discussed while describing the optical setup.

3.3.3 Optical Setup

Two different optical setups were utilized in the context of this thesis. One was used in the first part of the thesis, focused on the potential of alternative fuels. The other was designed for the second part of the thesis, which focuses on the DFI concept. These setups are explained below.

3.3.3.1 Optical Setup A

In order to study the potential of blends of different fuels i.e., Diesel-OME_x and HVO-OME_1, the optical setup A has been utilized. The setup consists of one high-speed camera which is used to capture the natural luminosity and the other camera equipped with a high-speed intensifier to register OH* chemiluminescence. Figure 3.2 shows the details of the optical setup A.

Flame radiation coming from the quartz piston bottom gets reflected by the 45-degree elliptical mirror and then reaches the dichroic mirror as shown in Figure 3.2. The dichroic mirror transmits the visible radiation and reflects the ultraviolet (UV) one. The range of the UV radiation reflected by the dichroic mirror falls in line with the most intense excited state hydroxyl OH* radical emission band, which is 310 nm. This allows OH* chemiluminescence radiation to reach a high-speed camera equipped with a high-speed intensifier and narrow-band interference filter (labeled as OH* camera) shown in Figure 3.2. The visible light that goes through the dichroic mirror reaches the

high-speed NL camera which registers the NL images (labeled as High-Speed Photron-Fastcam NL in Figure 3.2).

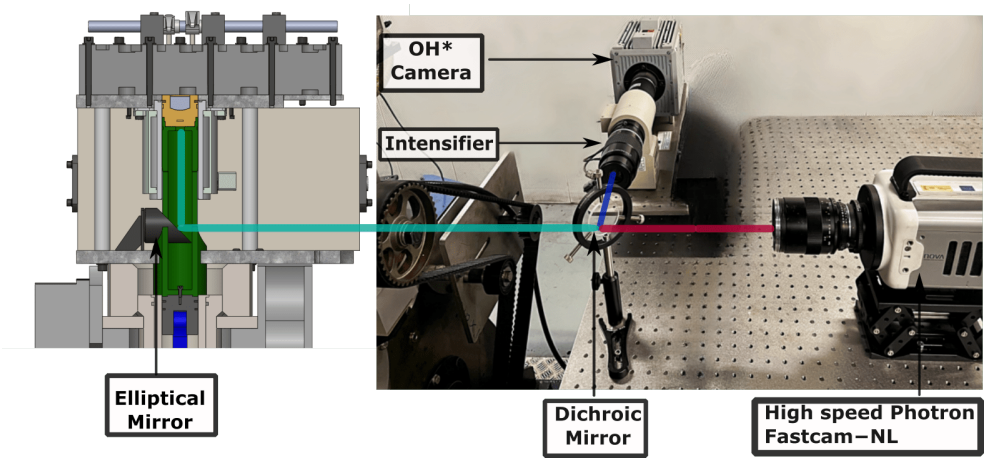

Figure 3.2: Optical components involved in Optical setup A.

For OH* chemiluminescence, a Photron Fastcam SA-5 high-speed camera labeled as OH* camera in Figure 3.3 equipped with Hamamatsu C10880-03F high-speed intensifier was utilized. This high-speed camera was also equipped with a narrowband interference filter having a central wavelength of 310 nm and a 10 nm full-width half maximum (FWHM). The purpose of this filter was to selectively capture only the radiation corresponding to the OH* emission peak while rejecting others. The intensifier's gating was synchronized with a camera exposure time of 39.75μs, and the intensifier gain remained at 62.5% of maximum value for the tests. The camera's acquisition speed was set at 25,000 fps, ensuring high temporal resolution. Additionally, this camera had a resolution of 4.15 pixels per millimeter. For the case of NL imaging, a Photron Fastcam Nova-S12 equipped with a 100 mm f2 Karl-Zeiss makroplanar lens was utilized. This camera shutter speed was also set at 25000 frames per second (fps) with an exposure time of 0.3 μs. Furthermore, the camera had a resolution of 5.60 pixels/mm. To ensure the image-by-image correlation between the two cameras, they were simultaneously triggered with the SOE and were synchronized on a frame basis. The images from the optical setup were registered from SOE to the end of combustion.

3.3.3.2 Optical Setup B

The optical setup B was specifically used to study the DFI concept in the second part of the thesis. Figure 3.3 shows the elements involved in Optical setup B. This setup differs from the optical setup A in a way that it involves additional optical elements necessary for carrying out the 2C pyrometry technique. Similar to Optical setup A, flame radiation coming from the quartz piston bottom gets reflected by the 45-degree elliptical mirror as shown in Figure 3.3, and then reaches this optical setup. The very first element in the optical setup is a dichroic mirror which transmits the visible radiation and reflects the ultraviolet (UV) one. The reflected radiation reaches the high-speed camera equipped with a high-speed intensifier and narrow-band interference filter (labeled as OH* camera). The details of this camera are the same as described in optical setup A. The visible light that goes through the dichroic mirror then reaches the beam splitter which is an additional element in this setup, that reflects half of the light and transmits the other half. These two halves of the visible light are then registered by two high-speed cameras as shown in Figure 3.3.

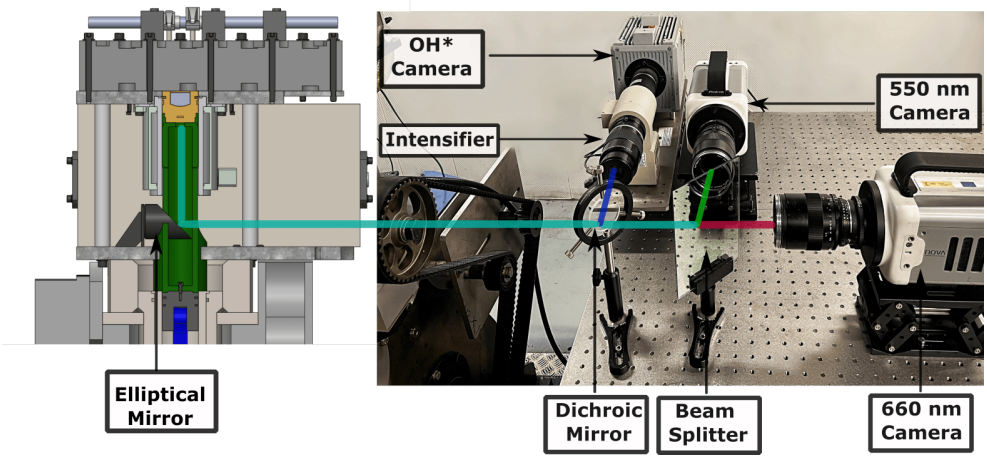

Figure 3.3: Optical components involved in Optical setup B.

For OH* chemiluminescence, the same settings as described in optical setup A have been utilized. A difference occurs in terms of the intensifier gain which remained at 62.5% of maximum value for the tests with 21% and 18% O_2, while for the case of 15% O_2, the gain was increased to 87.5% of the maximum value to ensure proper visualization.

For the 2C technique, two Photron NOVA-S9 high-speed cameras, labeled as 550 nm and 660 nm in Figure 3.3, were utilized. Both cameras were configured with a frame rate of 25,000 fps and were equipped with a 100 mm f/2 Karl-Zeiss Makroplanar camera lens. One of them incorporated a narrowband interference filter, which had its transmission peak centered at 660 nm with a FWHM of 10 nm. In contrast, the other camera utilized a filter centered at 560 nm with a 10 nm FWHM. Each camera was synchronized with a specific exposure time to get the most out of their dynamic range. To ensure the image-by-image correlation among the three cameras, they were simultaneously triggered with the SOE and were synchronized on a frame basis. Here also, the images from the optical setup were registered from SOE to the end of combustion.

- **2C Calibration procedure**

As the 2C system generates a specific digital level for each of the utilized cameras in the system which corresponds to radiation of flame at two different wavelengths. Hence the system can be calibrated by determining the apparent temperatures T_{a1} and T_{a2} corresponding to the digital level from each camera. This calibration is achieved by establishing a curve that relates the digital level to the blackbody temperature for each wavelength. In this thesis, a tungsten-ribbon calibration lamp (Osram Wi17G) serves as the blackbody source, and a previously validated procedure, utilized in other studies, is followed for calibration [31, 32]. The lamp operates using an electrical setup comprising a voltage source and a variable resistor, which enables precise control of the electrical power supply with an accuracy of 0.1 A, ensuring it stays within the lamp's operational range. To conduct spectral calibration, three distinct electric currents (9.1 A, 11.7 A, and 13.0 A) were applied to the tungsten lamp. These currents were selected to cover the expected radiance levels of a Diesel flame. Through this calibration process, the emitted radiance from the lamp was determined for a specific area measuring 25 mm in diameter located at the lamp center.

To ensure accurate calibration, the radiance measured for the three currents must match that of the two wavelengths used in the experimental campaign, which are 560 nm and 660 nm. The radiance-versus-wavelength curves of the Osram Wi17G lamp are shown in Figure 3.4.

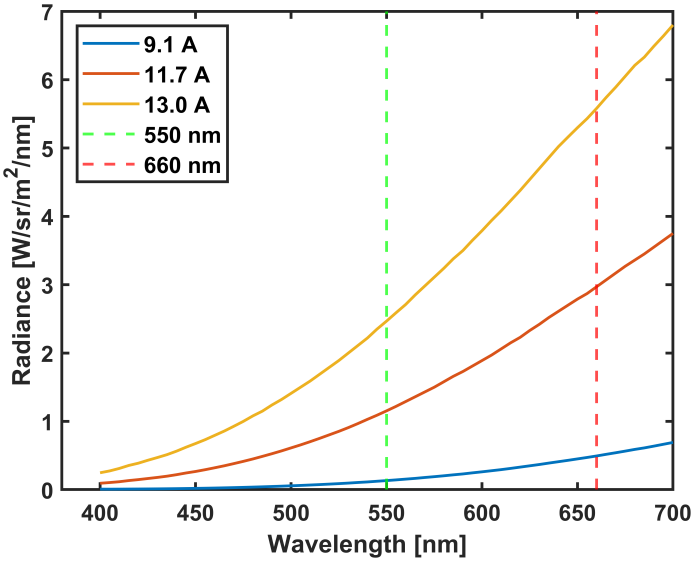

Figure 3.4: Calibration lamp curves. Vertical lines represent the wavelengths used for 2C method.

The calibration procedure is conducted using the same optical setup employed to capture images in the optical engine (Figure 3.3), ensuring consistency in the distance between the lamp, the optical system, and the flame. Twenty images of the lamp filament are captured for each calibrated current (9.1 A, 11.7 A, and 13.0 A). An example of the filament image captured by the camera for each current is illustrated in Figure 3.5. The digital levels of pixels within a 25 mm diameter area are averaged and compared with the lamp's calibration values. This process enables the derivation of a calibration curve for each wavelength. It is important to consider that camera parameters, such as shutter speed, aperture, etc., affect the pixels digital level, so each configuration has its respective calibration curve.

Figure 3.5: Images of lamp filament for different electrical currents.

3.3.3.3 Image Processing

During this thesis, the analysis of the accumulated NL, OH* radiation, and KL collected from the 10 combustion cycles was performed. Matrices representing the spatial distribution and accumulated value of these species were obtained by accumulating NL, OH*, and KL data for each recorded instant across the 10 combustion cycles. These matrices were later used to calculate the temporal evolution of the in-cylinder accumulated NL, OH* chemiluminescence, and KL.

Furthermore, it is important to discuss the application of the 2C algorithm to obtain KL evolution. As discussed for the 2C technique two different cameras were used namely 550 nm and 660 nm as highlighted in Figure 3.3. Primarily, image correction is carried out by overlapping frames captured by cameras operating at 550 nm and 660 nm wavelengths. This correction is performed using a Matlab code, which calculates a spatial transformation matrix accounting for translation, rotation, and scaling to achieve a perfect pixel-by-pixel match between the images. Additionally, background segmentation of the images is implemented. Once the green and red images are overlapped to achieve the best match, the equation mentioned earlier Equation 3.5 is applied to each wavelength. This equation enables the determination of both temperature and KL values.

Figure 3.6 illustrates an example of the composition of instantaneous natural luminosity images captured at 550 nm and 660 nm, along with the outcomes of the KL calculations and a map highlighting error zones. The yellow color observed in the overlap between the 660 nm and 550 nm images signifies a perfect alignment between the two distinct wavelength images. However, the darker areas denote regions where the code failed to identify a satisfactory match, potentially introducing uncertainties in the KL calculation from various sources [25]. Within the error map, zones depicted in red consist of pixels where the combination of the two wavelengths may yield radiation intensities lacking physical solutions. In such instances, a value of 3 is assigned for the KL.

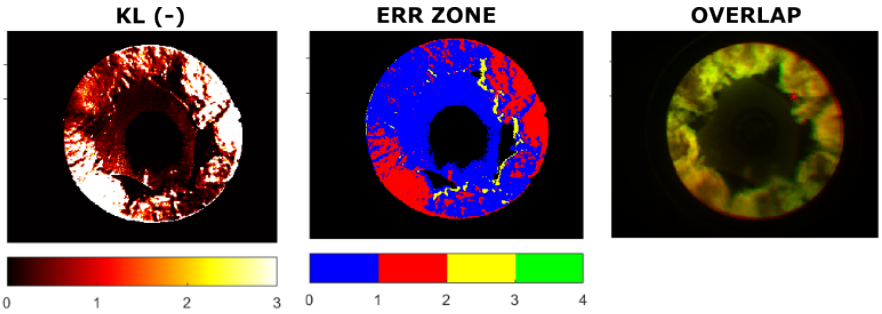

Figure 3.6: Overlapping of images and erros in KL calculation.

Figure 3.7 shows the steps involved in the methodology to obtain the different KL evolution depictions. KL evolution as an image is obtained following the procedure described earlier. Later, Equation 3.7 is further used to determine the Mean accumulated KL ($\overline{KL}_{\text{acc}}$) evolution, which is in fact the mean of the Accumulated KL ($\sum KL$: sum of all soot pixels) for 10 combustion cycles (here represented by repetitions).

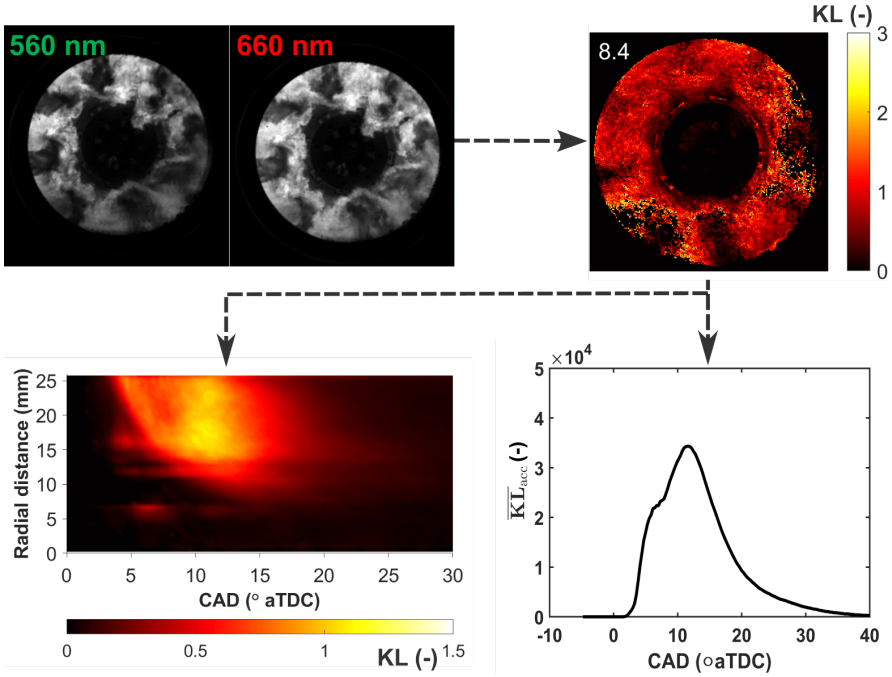

Figure 3.7: Description of various steps involved in obtaining KL evolution.

$$\overline{KL}_{\text{acc}} = \frac{(\sum KL)_{repititions}}{no.of repititions} \tag{3.7}$$

In order to visualize the temporal and spatial evolution of soot formation and oxidation, KL radial maps were created as shown in bottom left of Figure 3.7. It must be noted that the procedure to build the OH^* and NL radial maps is the same as followed in creating the KL radial maps. The KL registered images, which are in fact an average of ten combustion cycles, are divided into rings of 0.5 mm radius. KL_{mean} for each ring is obtained using the Equation 3.8, where $KL_{\text{Accumulated r}}$ is the sum of all soot pixels in the specific ring and A_r represents the total amount of pixels present in that certain ring.

$$KL_{mean} = \frac{KL_{Accumulatedr}}{A_r} \tag{3.8}$$

Finally, this information regarding the mean KL of each ring is summarized into spatial and temporal maps, where the row corresponds to all the ring regions into which the images were divided, which are in fact the respective distance from the nozzle and the column depicts the registered instants i.e., CAD. An example of this procedure is illustrated in Figure 3.8. The image represents the average KL evolution for 10 combustion cycles at 8.4 °aTDC. The mean KL values for various rings of 0.5mm radius at 8.4 °aTDC are depicted by the two white lines in the image on the right. The value for the specific ring, shown in light green in the left image, has been illustrated using the same color on the 2D map.

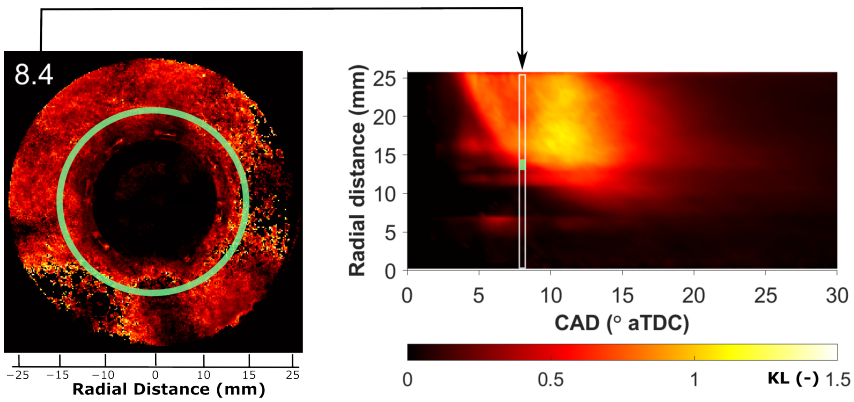

Figure 3.8: A sketch of methodology to obtain KL radial maps.

3.3.4 DFI Design and Implementation

The detailed literature review regarding DFI has been discussed already in section 2.4. In the context of this thesis, a DFI device was designed and implemented in the optical engine. The DFI design developed on purpose consisted of two distinct parts named holder and ducts (Figure 3.9). The holder is attached to the cylinder head which ensures the same alignment throughout the experimental campaign, while the different ducts can be removed and replaced. The holder was built of stainless steel while an aluminum alloy was used for the ducts which were black anodized in order to avoid undesired reflections from the soot radiation.

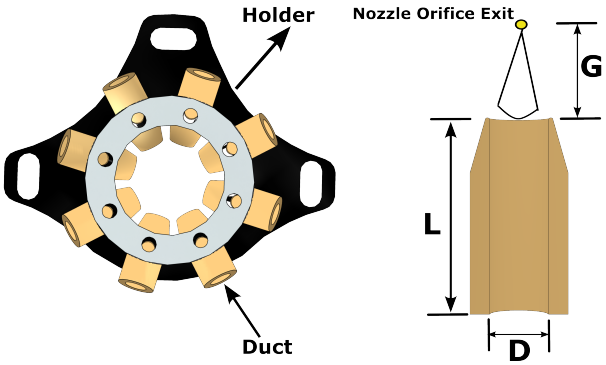

Figure 3.9: DFI device along with duct and holder.

The flange at the inlet orifice of the duct was rounded in order to gain the advantage of the pumping effect as suggested by [33]. Ducts with four different combinations of length (L), diameter (D), and stand-off distance (G) were tested. These dimensions are indicated in Figure 3.9. The DFI device was assembled by inserting the ducts in their designated space inside the holder and tightening them with a screw. To change the stand-off distance for a specific duct, simply the screw was tightened in a different hole located at a different position on the duct surface. From here onwards in the thesis, the four duct designs will be identified by the nomenclature L##D##G##, including the value of each dimension. The proposed designs are presented in Table 3.4

Table 3.4: Description of different duct designs utilized.

Duct Design	**Length [L] (mm)**	**Diameter [D] (mm)**	**Stand-off distance [G] (mm)**
L8D2G4.28	8	2	4.28
L8D2G3.33	8	2	3.33
L10D2G4.28	10	2	4.28
L10D3G4.28	10	3	4.28

The combinations of L, D, and G were chosen based on previous literature research where many authors reported different dimensions but falling in a similar range. In addition, the dimensionless parameters named insertion (K_{ins}) and engagement (K_{eng}) co-efficient defined in [33, 34] as well as the G/D ratio were used as reference to compare with previous proposals. The first one represents the axial distance from the duct inlet to the first contact point between the spray and duct wall and is non-dimensionalized by dividing it by the duct's inner diameter. Similarly, the second one is defined as the axial distance over which spray would interact with the duct wall and is again non-dimensionalized by dividing it by the duct's inner diameter. Table 3.5 shows a summary of the comparison of K_{eng} and K_{ins} between the designs studied in this work and other proposals from the literature. Here ϕ represents the spray cone angle in degrees.

It can be seen that the dimensionless parameters considered as a reference are comparable with those of other designs in the literature. Only the one identified as L10D3G4.28 has a lower K_{eng} value compared to all other designs. In addition, it must be highlighted that a rather larger G was used in this study as compared to the literature. The possible collision between ducts at their inlet region due to the large number of nozzle holes limited the use of a smaller G. Similarly, the possible interference with valves limited the maximum length to 10 mm.

As mentioned earlier, the same optical engine as shown in Figure 3.1 was utilized for the investigation of the DFI concept. However, a few modifications were made to the cylinder head. Holes were drilled on the head to attach the DFI. Figure 3.10 shows a cut-section view of the utilized piston with DFI installed in the optical engine.

Table 3.5: Comparison of dimensionless parameters between duct designs found in literature and utilized.

Duct Design	**L (mm)**	**D (mm)**	**G (mm)**	ϕ (°)	**G/D (-)**	K_{ins} (-)	K_{eng} (-)
Gehmlich et al. [33]	6	1.5	3.25	15	2.17	1.631	2.39
Gehmlich et al. [33]	14	3	4	21	1.33	1.364	3.302
Millo et al. [35]	14	2	1.0	13	0.50	3.888	3.112
Svensson et al. [36]	14	2	2.2	15	1.1	2.697	4.302
L8D2G4.28	8	2	4.28	15	2.14	1.658	2.342
L8D2G3.33	8	2	3.33	15	1.67	2.133	1.867
L10D2G4.28	10	2	4.28	15	2.14	1.658	3.342
L10D3G4.28	10	3	4.28	15	1.43	2.371	0.962

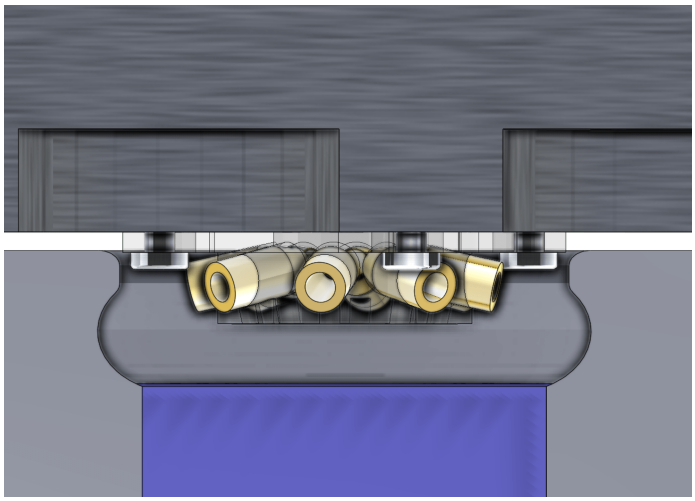

Figure 3.10: Cut section view of DFI device installed in the optical engine.

3.4 Numerical Tools and Methodology

In this subsection, a description of different numerical tools as well as the methodology utilized has been presented. These include the numerical tools for the development of reaction mechanisms and the numerical tools for the analysis of the behavior of different fuels utilized in this thesis.

3.4.1 0D/1D Modeling

All the necessary simulations related to 0D/1D modeling were performed using the ANSYS CHEMKIN Pro package [37]. For the case of 0D ignition delay simulations, an adiabatic closed homogenous constant volume reactor model was utilized where ignition delay is referred to as the time when the temperature reaches above 400 K as compared to the initial temperature. This ignition delay definition is a standard definition utilized in ANSYS CHEMKIN Pro and is commonly followed in literature while performing 0D calculations [5, 38–41].

For the case of 1D flame speed calculations, a flame simulator available in CHEMKIN Pro with a mixture averaged transport model accompanying the soret effect, which considers thermal diffusions, has been utilized. Furthermore, the simulations related to species concentration profile validations were done using CHEMKIN Pro's premixed model. To simulate the premixed flame, the measured temperature profile is employed as the initial condition. The calculations also utilize the mixture-average transport model, incorporating soret diffusion.

3.4.2 Reaction Mechanism Development

During this thesis, SAGE detailed chemistry solver has been utilized to model combustion inside the engine [42] which is discussed later in the thesis. However, one of the compulsory aspects of this solver is the incorporation of chemical reaction mechanisms. Therefore, it is important to discuss the mechanism itself in the context of numerical simulations. A chemical reaction mechanism refers to a detailed set of elementary chemical reactions that describe the complex chemical processes occurring during combustion. These reactions involve the transformation of reactants, typically fuel and oxidizer (such as air), into various intermediate species and eventually into the final products of combustion, including water vapor, carbon dioxide, nitrogen oxides, soot, etc. A chemical reaction mechanism includes rate expressions for each elementary reaction, specifying how reaction rates depend on factors such as

temperature, pressure, and species concentrations. These chemical reactions are generally detailed in the sense that they include numerous species and reactions. For example, a state-of-the-art mechanism for gasoline-like surrogate fuel is the Lawrence Livermore National Laboratory (LLNL) Co-optima 2021 mechanism that consists of 4164 species and 18636 reactions [43]. In order to improve the computational efficiency which allows for faster simulations, these detailed mechanisms are reduced. The reduction of the chemical mechanism involves applying several literature-proven techniques to remove unimportant species and reactions that finally result in the reduced mechanism which can drastically reduce the computational cost.

The major part of the reaction mechanism development in this thesis corresponds to the reduction of the detailed mechanisms. Once the detailed mechanisms are reduced, they are further combined with other mechanisms. The reduction and combination of the reaction mechanisms during this thesis is carried out by utilizing the ANSYS CHEMKIN Pro package [37]. The detailed mechanism is reduced by utilizing different reduction techniques like Direct relation graph with error propagation (DRGEP)[44], Direct relation graph with path flux analysis (DRGPFA)[45], and sensitivity analysis [46] using ANSYS CHEMKIN Pro constant volume homogeneous reactor model as reference. These reduction techniques have been widely used previously in other works for mechanism reductions and are recognized in the literature [5, 39–41]. In the reduction process, ignition delay has been used as the target parameter with a certain relative tolerance. As an example, a tolerance of 10% for ID means the reduction technique will continue until the relative difference between IDs of two consecutive steps in the reduction process (before and after removing unimportant species and reactions) doesn't reach 10%. The principles behind these reduction techniques are summarized here.

3.4.2.1 Mechanism Reduction Techniques

One of the first reduction techniques that is utilized is DRGEP. DRGEP is an extension of a simpler technique which is the Direct relation graph (DRG). It works by identifying the unimportant species in a chemical mechanism by resolving the species coupling without having prior knowledge of the system. However, the DRG is simple and can result in many problems leading to inconsistencies in the reduced mechanism. An improvement of the DRG technique is DRGEP. The working principle is the same as of DRG however, the criteria to decide whether a species can be removed from the mechanism is different. It involves propagating the errors from the reduced mechanism to the simulation results, providing a measure of the reliability of the reduced mechanism

in predicting system behavior. DRGEP stops when the tolerance threshold is reached and is recommended for the first stage of large mechanism reduction as it is computationally less expensive and faster than other techniques resulting in reasonable reduction.

DRGFPA, known as direct relation graph by path flux analysis, is another more rigorous reduction technique proposed by authors in [45]. This technique differs from DRGEP in way that instead of considering the error from only the first generation (direct relation) of pre-selected species, it takes into account both the first and second-generation or higher-generation species which are considered important based on path flux analysis. This method is considered more time-consuming and memory-intensive than DRGEP and that is why it is recommended to be utilized after larger mechanisms are already reduced via DRG or DRGEP. This technique along with DRGEP has been utilized in the context of this thesis.

Sensitivity analysis can be employed along with the DRGEP and DRGEPFA reduction techniques. This is an effective but severe reduction technique requiring a lot of computational resources. As described earlier, the DRGEP or DRGPFA techniques stop the reduction process when a certain threshold is reached which, in the context of this thesis, is the ignition delay's relative tolerance. However, in some cases, the error dramatically increases with the removal of a group of certain species making these techniques halt. In reality, among this group of species, there are only a few ones that are responsible for the increased error but as the DRGEP and DRGPFA techniques cannot differentiate between them, they altogether remove the group of species and stop the reduction process. This is where the sensitivity analysis comes in handy as it differentiates between species in such a group, identifying their effect on error. This technique has also been utilized in the context of this thesis.

3.4.3 Computational Fluid Dynamics Modelling

Computational Fluid Dynamics (CFD) is recognized as a scientific discipline that utilizes computer-based numerical simulations to provide quantitative forecasts of fluid-flow phenomena, including heat transfer and chemical reactions [47]. Renowned for its potential, CFD offers a valuable means to overcome many constraints associated with experimental analysis, thereby streamlining research efforts and complementing experimental findings. This has led to the widespread adoption of CFD tools in the aerospace engineering sector, where they have been integral to aircraft and jet engine design, research, and development since the 1960s. More recently, CFD techniques

have found application across various domains, notably in the optimization and modeling of internal combustion engines (ICEs) and combustion systems. Here, CFD serves as a crucial tool in the design process, offering the potential for swift and cost-effective analysis to optimize key performance parameters.

It is worth mentioning that, in the context of IC engine simulations, given the complexity of the combustion process, the computational study itself becomes a challenge. The accurate modeling of different processes involved in combustion including spray, heat transfer, turbulence, combustion, and emission formation is really important. Therefore, 3D CFD simulations were performed by using the commercial CFD code CONVERGE CFD [48]. This software has gained extensive adoption in the Internal Combustion Engine community owing to its ability to simulate moving boundaries and its integrated Adaptive Mesh Refinement (AMR) tool. This enables the computational mesh to be scaled in real-time, enhancing the resolution of relevant physical and thermodynamic properties within the flow. Keeping this into prospective, the following subsections explain the modeling strategy followed throughout this thesis. Primarily the fundamentals of CFD modeling in the form of the classical equations of computational fluid dynamics of Navier-Stokes are outlined. After that, a description of the different sub-models utilized is given that ultimately leads to the development of a 3D CFD model which serves as a base for the first part of the thesis, i.e., numerical analysis of different fuel blends.

3.4.3.1 Navier-Stokes equations

The dynamics of the fluid flow involved in the combustion process are governed by the classical Navier-Stokes conservation equations of mass, momentum, and energy. For numerical resolution, the equations are adapted to the problem to be studied, and the equations can be simplified by disregarding some terms. The compressible transport equations for mass and momentum can be expressed according to Equation 3.9 and Equation 3.10 respectively.

$$\frac{\rho}{\partial t} + \frac{\rho u_j}{\partial x_j} = 0 \tag{3.9}$$

and

$$\frac{\rho u_i}{\partial t} + \frac{\rho u_i u_j}{\partial x_j} = -\frac{\partial P}{\partial x_i} + \frac{\partial}{\partial x_j}\left[\mu\left(\frac{\partial u_i}{\partial x_j} + \frac{\partial u_j}{\partial x_i}\right) - \frac{2}{3}\mu\frac{\partial u_k}{\partial x_k}\delta_{ij}\right] + \frac{\partial}{\partial x_j}(\tau_{ij}) \tag{3.10}$$

In the above equations, u represent the velocity of the fluid, ρ corresponds to the density, P is the pressure, μ reflects the viscosity, δ_{ij} is the Kronecker delta and τ_{ij} denotes the Reynolds stresses of the system $\tau_{ij} = \rho u_i' u_j'$ which need to be modeled to provide mathematical closure and to account for turbulence effects (discussed later).

As discussed earlier, the combustion process inside the CI engine is highly turbulent. Thus the adequate prediction of the in-cylinder turbulence field is critical in order for the proper reproduction of combustion evolution [49]. In the context of fluid mechanics, the characterization of turbulence is considered a very complex yet delicate phenomenon, provided that it convectively enhances the rate of mixing of momentum, energy, and species which has the ultimate effect on flow characterization [50, 51].

Currently, the CFD simulations can be performed via Direct numerical simulation (DNS), Large eddy simulation (LES) and Reynolds averaged navier stokes (RANS) modeling. The computational cost decreases as we move from DNS to RANS, however, the complexity of modeling is also decreased. In the context of this thesis, RANS modeling is used to model the complex turbulent flow inside the combustion chamber.

- **Reynolds-Averaged Navier-Stokes (RANS)**

RANS methods are characterized by employing the average value of the flow variables, thus modeling the full range of turbulent scales. The approach considers that all of the unsteadiness in the flow is averaged out i.e., all unsteadiness is regarded as part of the turbulence. Traditionally this modification is accomplished by representing the flow variables (i.e., velocity) into two terms, mean and fluctuating. Mathematically Equation 3.11 describes the decomposition where u_i is instantaneous velocity, $\bar{u}_i$ ensemble mean velocity, and u_i' the fluctuating velocity term.

$$u_i = \bar{u}_i + u_i' \tag{3.11}$$

The compressible RANS transport equations and average are then computed by substitution of Equation 3.11 into the mass and momentum conservation navier stokes equations i.e., Equation 3.9 and Equation 3.10, which yield Equation 3.12 and Equation 3.13:

$$\frac{\partial \bar{\rho}}{\partial t} + \frac{\partial \bar{\rho} \tilde{u}_j}{\partial x_j} = 0 \tag{3.12}$$

and

$$\frac{\partial \bar{\rho}\tilde{u}_i}{\partial t} + \frac{\partial \bar{\rho}\tilde{u}_i\tilde{u}_j}{\partial x_j} = -\frac{\partial \bar{P}}{\partial x_i} + \frac{\partial}{\partial x_j}\left[\mu\left(\frac{\partial \tilde{u}_i}{\partial x_j} + \frac{\partial \tilde{u}_j}{\partial x_i}\right) - \frac{2}{3}\mu\frac{\partial \tilde{u}_k}{\partial x_k}\delta_{ij}\right] + \frac{\partial}{\partial x_j}(-\bar{\rho}\widetilde{u_i'u_j'}) \tag{3.13}$$

where $\tilde{u}_i = \frac{\overline{\rho u_i'}}{\bar{\rho}}$ represents the Favre average. Some additional terms are introduced then by doing the ensemble average which are known as Reynolds stresses that represent the turbulence effect. The Reynold stress as discussed earlier τ_{ij} is given by Equation 3.14.

$$\tau_{ij} = -\bar{\rho}\widetilde{u_i'u_j'} \tag{3.14}$$

This term is included on the last on the right-hand side of Equation 3.13. The turbulence model must be able to model this Reynolds stress to obtain closure for the Equation 3.13. This is where the RANS model comes into the equation, which solves additional transport equations for turbulence modeling to close this term together with the governing Navier-Stokes equations. The treatment of this new term depends on the RANS turbulence model used and this selection is outlined later on while describing turbulence model configuration.

3.4.3.2 Computational Domain

The computational domain was built based on the geometry of the optical engine utilized that has been described in the section 3.3. The computational domain represents the combustion chamber of the engine that is delimited by the inner piston surface (bowl and squish region), the cylinder liner, and the cylinder head plane as shown in Figure 3.11.

3.4.3.3 Domain Boundary Conditions

Simulations were run from inlet valve closing to exhaust valve opening (IVC-EVO) i.e., [-148 °aTDC to 115.5 °aTDC]. Thus, only compression, combustion, and expansion processes were simulated while air management was excluded. An initial swirl ratio of 1.5 was defined to take into account the air movement at IVC. Thermodynamic conditions used to initialize pressure and temperature fields in simulations were obtained from the experimental measurements in the same optical engine. For this purpose, an in-house developed zero-dimensional single zone thermodynamic model [10] was utilized named CALMEC. Based on the intake, exhaust, and in-cylinder pressures as well as

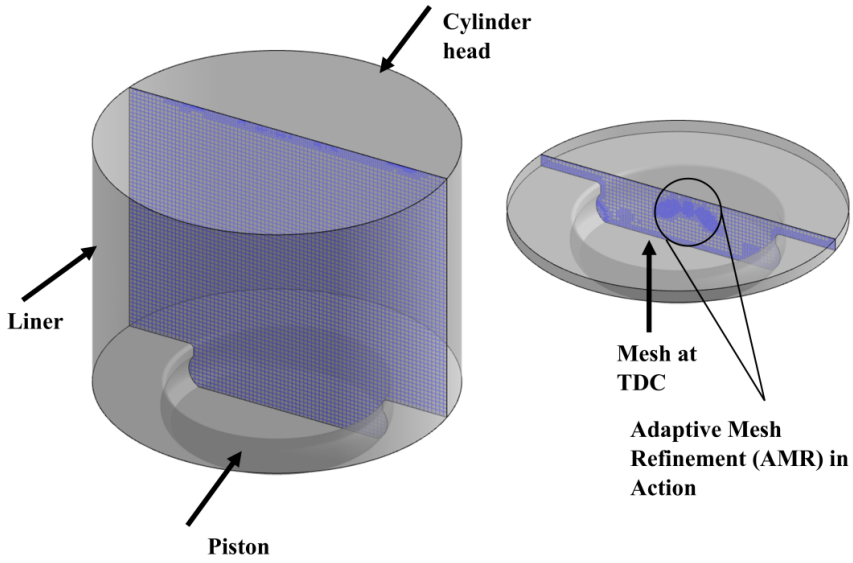

Figure 3.11: Computational Domain and Mesh characteristics.

the intake temperature and air mass flow rate, the model is able to calculate in-cylinder thermodynamic conditions at IVC which are later used to define an initial pressure and temperature homogeneous field within the computational domain. The same model was also used to calculate in-cylinder surface temperatures. It uses a nodal model to calculate the liner, piston, and head mean temperatures, which were later used as the boundary conditions for the CFD model. Blowby and combustion chamber deformations were not taken into account while fitting the CALMEC model. Instead, the compression ratio in the simulation was adjusted to match the effective compression ratio of the real engine. In order to confirm the accuracy of IVC conditions used for the CFD model, the simulation was first run for the motored (no combustion) case. Figure 3.12 (a) shows the in-cylinder pressure comparison between CFD and experimental data between -20 to 20 $^{\circ}$aTDC; injection and combustion takes place within this range. Figure 3.12 (b) represents the in-cylinder temperature evolution comparison. By looking at both pressure and temperature comparisons, it can be seen that the simulation was able to replicate the in-cylinder conditions with accuracy.

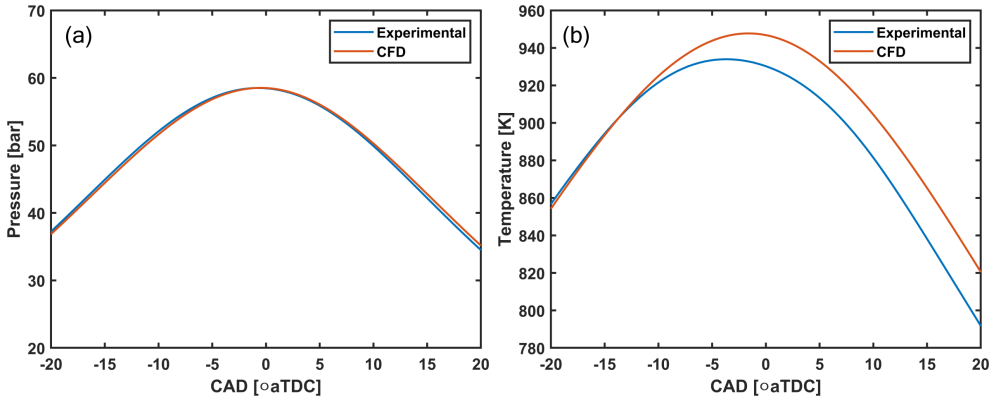

Figure 3.12: Numerical and experimental in-cylinder pressure evolution (a) and temperature evolution (b) in motored conditions.

3.4.3.4 Mesh Configuration

To define an appropriate mesh size, a mesh sensitivity analysis was performed. Its effect on the HRR and pressure was used as a reference. CONVERGE allows the incorporation of embedding in various regions. As an example an embedding scale of 2 means the base mesh size is reduced by 2 times in the specific region. In this context, the basic configuration of the utilized mesh included a fixed embedding scale of 2 around the nozzles as well as AMR. The AMR allowed to automatically refine the grid based on local fluctuations of temperature and velocity with a maximum configured embedding scale of 3. For the case of temperature, the minimum temperature sub-grid value above which a cell was embedded was set to 1K, and for velocity, this value was defined to be 2.5m/s. Table 3.6 shows the different mesh configurations evaluated, where the main parameter modified was the base grid size.

The results of the mesh sensitivity analysis are shown in Figure 3.13. Data corresponds to the simulation of a blend of 50% Diesel and 50% OME_x (in mass) i.e., D50O50. It can be seen that HRR and pressure are different for Mesh A when compared to the others, which are much more similar among them. However, with Mesh B still, some small discrepancies in comparison to Mesh C and Mesh D are observed. Therefore, it can be concluded that results were almost not affected by the base mesh size when it was lower than 1.5 mm.

Table 3.6: Different Mesh parameters used in Mesh sensitivity analysis.

Mesh Type	**Mesh A**	**Mesh B**	**Mesh C**	**Mesh D**
Base grid size (mm)	2.0	1.5	1.25	1.15
Mesh size around nozzle [Fixed embedding] (mm)	0.5	0.375	0.3125	0.2875
Total number of cells without embedding and AMR	111664	264685 (+137%)	457376 (+310%)	587367 (+426%)
Computational time	18.5h	30.5h (+64.3 %)	36.0h (+91.9 %)	38.5h (+106 %)

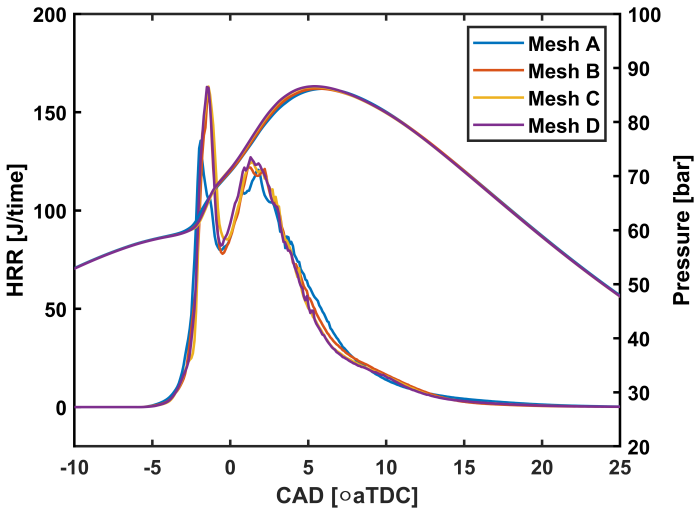

Figure 3.13: Mesh Sensitivity check for the case of blend of 50%Diesel and 50%OME_x D50O50.

Considering this, a base mesh size of 1.25 mm with the fixed embedding and AMR previously described, leading to a minimum grid size of 0.3125 mm. Figure 3.14 shows the mesh within a plane that represents half of the computational domain at 0°aTDC. It is possible to see the effect of AMR and fixed embedding around one of the fuel sprays as well as at some regions close to the walls.

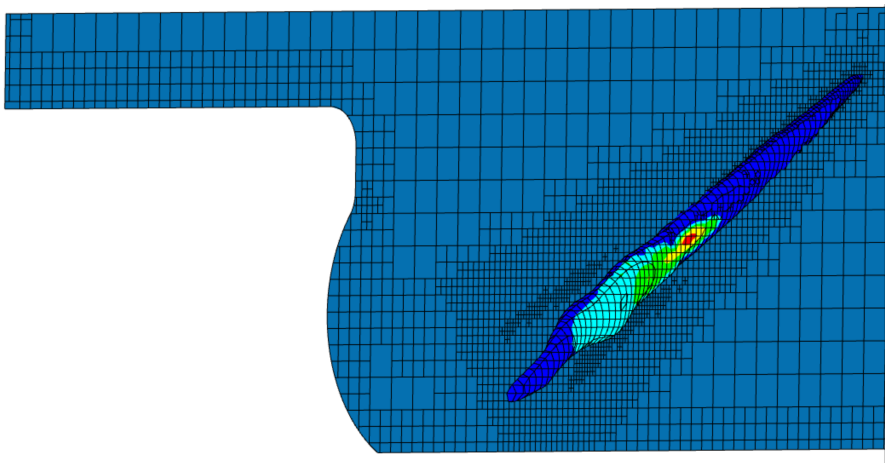

Figure 3.14: Mesh distribution at TDC.

3.4.3.5 Injector Configuration

During this thesis, a similar injection strategy has been utilized for the whole study of the fuel blends. These injection parameters replicate the experimental injection utilized. The main parameters of this strategy have been summarized in the Table 3.7. It should be noted that a separate experimental campaign was performed at the injection test bench to measure the injection profiles. For this purpose, the same injector that was utilized inside the engine was disassembled and incorporated into the injection test bench. An in-house developed software to obtain the injection rate shapes.

Table 3.7: Main injection spray parameters.

Injection parameters	**Configuration**
Start of Energizing [SOE](°aTDC)	-9
Start of Injection [SOI](°aTDC)	-6.804
Injection profile	Single main injection
Injection Pressure (bar)	1000
Number of nozzles	1
Nozzle holes	8
Discharge coefficient	0.9
Orifice diameter (μm)	138
Spray cone angle ϕ (°)	14
Angle between spray axis and cylinder head (°)	30

Figure 3.15 shows the injection profiles for the case of D100 and D50O50 as well as for H100 and H50M50 blend. Looking at Figure 3.15 (a), it can be observed that the main effects when increasing the OME_x content was that the instantaneous mass flow rate increased while its duration was slightly shortened (2% of total duration). These resulted in a noticeable increase of the total injected mass when increasing the OME_x content. For the sake of simplification, it was decided to use the D50O50 normalized injection rate profile of Diesel-OME_x blends. However, to take into account the described behavior, a total injected mass was calculated for D90O10, D80O20, and D70O30 (as no measured values were available). For this purpose, a linear relation between OME_x content and total injected mass variation was assumed and the values corresponding to 10%, 20% and 30% of this fuel were calculated using a linear interpolation procedure. These values are also shown in the Figure 3.15. Similar behavior can be observed between the injection profiles of H100 and H50M50 (It was shortened by 2% for the H50M50 case as compared to H100).

Therefore, the injection profile of H100 was used for simplification for HVO-OME_1 blends and injected mass was calculated accordingly following a similar procedure as for Diesel-OME_x blends.

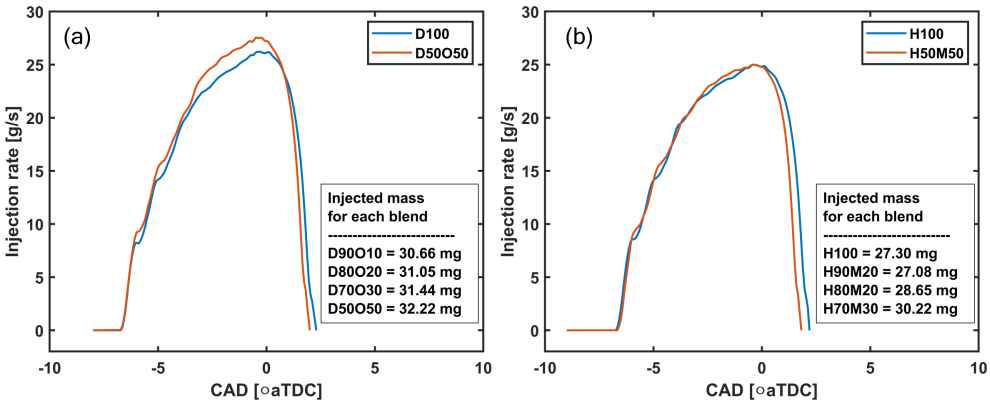

Figure 3.15: Experimentally measured injection profiles for injector configuration used for the case of D100 and D50O50 alongside injected mass for different Diesel-OME_x blends utilized (a), and for the case of H100 and H50M50 alongside injected mass for different HVO-OME_1 blends utilized (b).

3.4.3.6 Spray Model Configuration

In CI engines, the liquid fuel is injected near the end of the compression stroke inside the combustion chamber. So, after injection, the fuel spray undergoes numerous processes like atomization, vaporization, etc. There are numerous models available for each phenomenon in the CONVERGE CFD library to handle these processes. Table 3.8 shows a summary of the ones used in this work.

The liquid injection model employed here was the blob injection model [48] that simply defines the parcels (a group of identical drops having the same radius, velocity, temperature, etc., and are used to statistically represent the entire spray field) that are injected inside the computational domain with a characteristic size equal to the size of the nozzle diameter. The modified Kelvin-Helmholtz Rayleigh-Taylor (Modified KH-RT) was used as a spray breakup model [48]. In this model, the primary breakup of injected liquid blobs is due to the aerodynamic instabilities. During this process, child drops are formed and the secondary breakup of these drops is modeled by assessing the competing effects of KH and RT Mechanisms. The droplet collision was

based on the No Time Counter (NTC) model by Schmitz and Rutland [48]. This method involves the stochastic sub-sampling of the parcels within each cell which results in much faster collision calculations. Finally, a rebound/slide model was used to model the spray wall interaction. It is worth mentioning that all these tools related to spray models are extensively used in literature and are recommended by CONVERGE for diesel engine simulations.

Table 3.8: Different Spray Models used.

Liquid Injection	Blob Injection
Spray breakup	Modified KH-RT
Drop Drag	Dynamic Drag Model
Collision Outcome models	Post collision outcome
Turbulent dispersion	O'Rourke model
Collision Model	No time counter (NTC) collision
Spray/wall interaction model	Rebound/slide

3.4.3.7 Heat Transfer Model Configuration

Accurate modeling of heat transfer is an important aspect during the CFD simulations of IC engines. CONVERGE library includes different models named O'Rourke and Amsden, Han and Reitz, Angelberger, and GruMo-UniMORE for this purpose. Figure 3.16 depicts the comparison between different heat transfer models implementation in simulation along with the experimentally obtained heat transfer through combustion chamber walls obtained through CALMEC. It is evident that two of the models including O'Rourke and Amsden and GruMo-UniMORE replicate the experimental heat transfer rate accurately. However, for this thesis, heat transfer during the simulations was modeled by O'Rourke and Amsden [52, 53] model as it both replicates the experimental data and is also recommended for diesel engine applications [48].

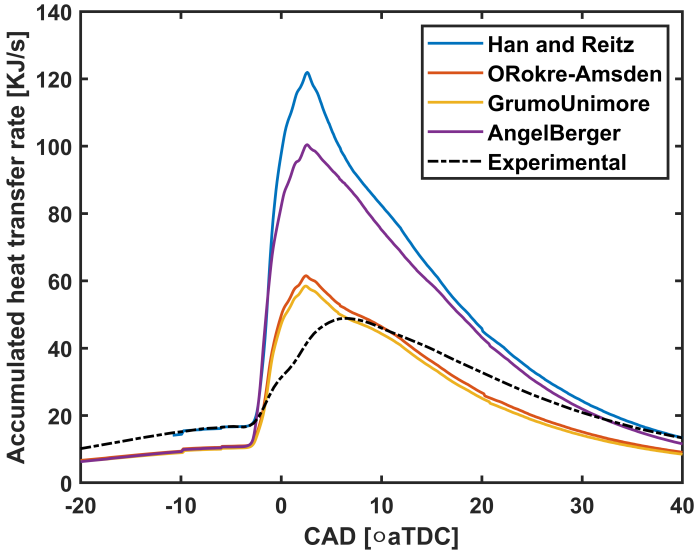

Figure 3.16: Accumulated heat transfer through combustion chamber (piston, cylinder walls, cylinder head) by using different heat transfer models.

3.4.3.8 Turbulence Model Configuration

As discussed in the beginning while describing the CFD modeling approach for this thesis, RANS modeling was utilized to model turbulence inside the combustion chamber. There are many RANS CFD models available in the CONVERGE library to effectively perform combustion simulations. However, in the context of this thesis, the Re-normalization group (RNG) k-epsilon model has been utilized which has been recommended for engine applications.

The RNG k-epsilon model [54] belongs to the class of two equation turbulence models and it to similar to the standard k-epsilon model [51]. The RNG model boasts several enhancements that not only enhance its accuracy but also broaden its applicability to various flow scenarios:

- Incorporates an extra term in the equation to enhance accuracy in high vorticity flows.
- Integrates the swirl effect to better handle swirling flows.
- Provides an analytical formula for turbulent Prandtl numbers.
- Presents an analytical differential equation for effective viscosity, considering the impacts of low Reynolds numbers.

As established the RANS models should be able to model the Reynolds stress introduced in Equation 3.13. The modeled Reynolds stress τ_{ij} for the standard k-ε and RNG K-ε model is given by Equation 3.15.

$$\tau_{ij} = -\bar{\rho}\widetilde{u_i'u_j'} = 2\mu_t S_{ij} - \frac{2}{3}\delta_{ij}\left(\rho k + u_t\frac{\partial \tilde{u}_i}{\partial x_i}\right) \tag{3.15}$$

Here, k represents turbulent kinetic energy and μ_t represents turbulent viscosity.

The standard k-ε and RNG k-ε models further require additional transport equations to obtain turbulent viscosity as given in Equation 3.15. Hence, one equation is needed for TKE i.e., k, which determines the energy in turbulence, and other for turbulent dissipation rate (ε), which determines the rate of dissipation of turbulent kinetic energy. That is why these are known as 2 equation models, because, in addition to the conservation equations (Equation 3.12 and Equation 3.13), they solve two transport equations, which account for the historical effects like convection and diffusion of turbulent energy.

The RNG k-ε model differs from the standard K-εmodel in a way that the equation of ε contains an additional term that attempts to account for the different scales of motion through changes to the production term (high vorticity flows as discussed earlier and these are characteristic of CI engine combustion). Therefore, in summary, due to the reasons described above and the recommendation from CONVERGE, the turbulence is modeled by the RNG k-ε model.

3.4.3.9 Combustion Model Configuration

In order to model the combustion inside the CI engine, SAGE detailed chemistry solver has been utilized in the context of this thesis. SAGE [42] solves the detailed chemical kinetic through the CHEMKIN formatted input files on each computational cell. These CHEMKIN formatted input files are in fact the reaction mechanism files that constitute the set of species and elementary reactions as also discussed earlier in reaction mechanism development subsection. SAGE works by calculating the elementary reaction rate while CONVERGE solves the transport equations. Depending on the accuracy of the mechanisms, SAGE can be used to model different combustion regimes including ignition, premixed, mixing controlled, etc. However, the size of the provided reaction mechanisms can affect the computational time needed for simulation. In general, SAGE solver happens to provide accurate results in terms of diesel combustion, which has been utilized in performing

CFD simulations in this thesis. It has been considered important to further discuss this model in detail. The way SAGE operates is:

- Reads the chemical mechanisms in CHEMKIN format and solves the ordinary differential equations (ODEs) to find the reaction rates
- Couples with transport solver via source term in the species transport equation
- At each time step, the new species mass fractions and the reaction rates for each elementary reaction are calculated prior to solving transport equations. The change in the mass fraction of species is taken as a source.

Having discussed these details about the prerequisites of the SAGE solver, the further theory about how SAGE works is reported now. It has been considered important to describe this as this thesis involves work related to chemical reaction mechanisms which are a compulsory part of SAGE solver. Equation 3.16 represents the forward rate co-efficient for the i-th reaction in the Arrhenius form, which is utilized in SAGE.

$$k_{fi}(T) = A_i.T^b.e^{\frac{-E_{a,i}}{RT}} \tag{3.16}$$

where A_i is the pre-exponential factor, b is the exponent of temperature, E is the activation energy (in cal/mol) and R is the ideal gas constant. Similar to the forward rate co-efficient, the reverse rate co-efficient can also be specified in the analogous fashion or can be determined via the equilibrium co-efficient K_{ci}, which is given as:

$$k_{ri}(T) = \frac{k_{fi}}{K_{ci}} \tag{3.17}$$

The equilibrium co-efficient K_{ci} is determined via the thermodynamics properties and is given as:

$$k_{K_{ci}} = K_{pi}\left(\frac{P_{atm}}{RT}\right)^{\sum_{j=1}^{N} v_{ij}} \tag{3.18}$$

where P_{atm} is the atmospheric pressure. The equilibrium constant K_{pi} is calculated via:

$$K_{pi} = exp\left(\frac{\Delta S_i^0}{R} - \frac{\Delta H_i^0}{RT}\right) \tag{3.19}$$

Here, S and H represent entropy and enthalpy respectively. The δ represents the change that occurs in the i-th reaction when passing completely from reactants to products. These changes in entropy and enthalpy are given by Equation 3.20 and Equation 3.21 respectively.

$$\frac{\Delta S_i^0}{R} = \sum_j^N v_{ji} \frac{S_j^0}{RT} \tag{3.20}$$

$$\frac{\Delta H_i^0}{R} = \sum_j^N v_{ji} \frac{H_j^0}{RT} \tag{3.21}$$

With the above information, the conservation equations of continuity and energy can be solved for a given computational cell. The equations for mass is:

$$\frac{d[X_j]}{dt} = \dot{\omega_j} \tag{3.22}$$

The energy equation is given by:

$$\frac{dT}{dt} = \frac{V\frac{dp}{dt} - \sum_j^N (\bar{h_j}\dot{\omega_j})}{\sum_j^N ([X_j]\bar{c_{p,j}})} \tag{3.23}$$

where V is the volume, T is the temperature, and p is the pressure. The molar specific enthalpy and molar constant pressure specific heat of species j are represented by $\bar{h_j}$ and $\bar{c_{p,j}}$ respectively. These equations are solved at each computational time step and the species are updated accordingly. It must be noted that the temperature obtained via Equation 3.23 is only used to update the rate coefficients and is not used to update the cell temperature. For the cell temperature, the update is done using the computed series concentration when all the detailed chemistry calculation is finished.

3.4.3.10 Emissions Model Configuration

CI engines can result in different types of pollutant emissions as described earlier in section 2.2. In particular, soot and NO_x emissions are considered in the context of this thesis.

The Hiroyasu soot model has been utilized to simulate soot emissions [55]. It is the most popular, simple, and easy model to implement in CFD applications and has been widely used in literature [56–58]. Hiroyasu provided a simple formulation to calculate the rate of soot mass formation, given by the difference between the formation and oxidation rate of soot during combustion [59]. This is an empirical soot model that is coupled with the Nagle and Strickland-Constable NSC model to simulate soot oxidation [60]. The soot formation is modeled in the sense that C_2H_2 is being treated as soot formation species. This treatment of the soot formation is compatible with the SAGE detailed chemistry solver. To model soot oxidation, as described earlier the NSC model was utilized which considers the arrangement and location of carbon atoms over the surface of soot particles.

The NO_x emissions are modeled by the extended Zeldovich model as presented by [9]. This model has been widely used in literature [61–63]. The principle behind the NO_x formation using this model has already been discussed in section 2.1. The extended Zeldovich model is an enhancement of the original Zeldovich mechanism, which describes the formation of nitrogen oxides during combustion processes. The Zeldovich mechanism primarily focuses on the formation of nitric oxide through thermal nitrogen fixation. The extended Zeldovich model incorporates additional reactions and considerations to improve the accuracy of NO_x predictions, especially in CI engine conditions.

3.5 Summary

This chapter presents all the experimental and numerical tools and their corresponding methodologies utilized in this thesis. In the beginning, the experimental optical engine along with the fuels utilized, different optical techniques, and the optical setup used in the context of this thesis have been described. Then the DFI implementation inside the optical engine along with the DFI design has been elaborated. In terms of numerical tools, the 0D/1D modeling tools including the tools for mechanisms reduction have been described. A more detailed explanation has been given of the development of the CFD model which serves as the basis of the numerical part of this thesis, including a description of different sub-models utilized.

References

[1] Pellegrini, Leonardo et al. *Combustion behaviour and emission performance of neat and blended polyoxymethylene dimethyl ethers in a light-duty diesel engine*. Tech. rep. SAE Technical Paper, 2012.

[2] Liu, Jialin et al. "Effects of diesel/PODE (polyoxymethylene dimethyl ethers) blends on combustion and emission characteristics in a heavy duty diesel engine". In: *Fuel* 177 (2016), pp. 206–216.

[3] Omari, Ahmad, Heuser, Benedikt, Pischinger, Stefan, and Rüdinger, Christoph. "Potential of long-chain oxymethylene ether and oxymethylene ether-diesel blends for ultra-low emission engines". In: *Applied energy* 239 (2019), pp. 1242–1249.

[4] Liu, Junheng et al. "Effects of PODE/diesel blends on particulate matter emission and particle oxidation characteristics of a common-rail diesel engine". In: *Fuel processing technology* 212 (2021), p. 106634.

[5] Lv, Delin et al. "Development of a reduced diesel/PODEn mechanism for diesel engine application". In: *Energy Conversion and Management* 199 (2019), p. 112070.

[6] Liu, Haoye, Wang, Zhi, Wang, Jianxin, and He, Xin. "Improvement of emission characteristics and thermal efficiency in diesel engines by fueling gasoline/diesel/PODEn blends". In: *Energy* 97 (2016), pp. 105–112.

[7] Pastor, Jose V, Garcia-Oliver, Jose M, Micó, Carlos, and Tejada, Francisco J. *Combustion behaviour of blends of synthetic fuels in an optical single cylinder engine*. Tech. rep. SAE Technical Paper, 2021.

[8] Härtl, Martin, Seidenspinner, Philipp, Jacob, Eberhard, and Wachtmeister, Georg. "Oxygenate screening on a heavy-duty diesel engine and emission characteristics of highly oxygenated oxymethylene ether fuel OME1". In: *Fuel* 153 (2015), pp. 328–335.

[9] Heywood, John B. *Internal combustion engine fundamentals*. McGraw-Hill Education, 2018.

[10] Payri, Francisco, Olmeda, Pablo, Martín, Jaime, and García, Antonio. "A complete 0D thermodynamic predictive model for direct injection diesel engines". In: *Applied Energy* 88.12 (2011), pp. 4632–4641.

[11] Mueller, Charles J and Martin, Glen C. "Effects of oxygenated compounds on combustion and soot evolution in a DI diesel engine: broadband natural luminosity imaging". In: *SAE Transactions* (2002), pp. 518–537.

[12] Ueckerdt, Falko et al. "Potential and risks of hydrogen-based e-fuels in climate change mitigation". In: *Nature Climate Change* 11.5 (2021), pp. 384–393.

[13] Jakob, Markus et al. "Simultaneous high-speed visualization of soot luminosity and OH* chemiluminescence of alternative-fuel combustion in a HSDI diesel engine under realistic operating conditions". In: *Combustion and Flame* 159.7 (2012), pp. 2516–2529.

[14] Jalilimehr, M, Behzadan, H, Javadi Mal Abad, SM, Moghiman, M, and Niazmand, H. "Investigating the effects of natural gas preheating on soot formation, flame luminosity, and nox emissions: a combined experimental and numerical approach". In: *Heat Transfer—Asian Research* 46.7 (2017), pp. 895–912.

[15] Li, Zheming et al. *Comparison of laser-extinction and natural luminosity measurements for soot probing in diesel optical engines*. Tech. rep. SAE Technical Paper, 2016.

[16] Gaydon, A. *The Spectroscopy of Flames*. Springer Netherlands, 2012.

[17] Higgins, Brian and Siebers, Dennis. "Measurement of the flame lift-off location on DI diesel sprays using OH chemiluminescence". In: *SAE Transactions* (2001), pp. 739–753.

[18] White, CM. "OH* chemiluminescence measurements in a direct injection hydrogen-fuelled internal combustion engine". In: *International Journal of Engine Research* 8.2 (2007), pp. 185–204.

[19] Yu, Xin, Zha, Kan, Luo, Xi, Taraza, Dinu, and Jansons, Marcis. *Simulation and experimental measurement of CO2*, OH* and CH2O* chemiluminescence from an optical diesel engine fueled with n-heptane*. Tech. rep. SAE Technical Paper, 2013.

[20] Pastor, José V, García, Antonio, Micó, Carlos, and Lewiski, Felipe. "An optical investigation of Fischer-Tropsch diesel and Oxymethylene dimethyl ether impact on combustion process for CI engines". In: *Applied Energy* 260 (2020), p. 114238.

[21] Pastor, José V et al. "Effect of a novel piston geometry on the combustion process of a light-duty compression ignition engine: An optical analysis". In: *Energy* 221 (2021), p. 119764.

[22] Zhao, Mengmeng, Buttsworth, David, and Choudhury, Rishabh. "Experimental and numerical study of OH* chemiluminescence in hydrogen diffusion flames". In: *Combustion and Flame* 197 (2018), pp. 369–377.

[23] Liu, Yao, Tan, Jianguo, Wan, Minggang, Zhang, Lang, and Yao, Xiao. "Quantitative measurement of OH^* and CH^* chemiluminescence in jet diffusion flames". In: *ACS omega* 5.26 (2020), pp. 15922–15930.

[24] Riedl, Max J. *Optical design fundamentals for infrared systems*. Vol. 48. SPIE press, 2001.

[25] Musculus, Mark PB, Singh, Satbir, and Reitz, Rolf D. "Gradient effects on two-color soot optical pyrometry in a heavy-duty DI diesel engine". In: *Combustion and flame* 153.1-2 (2008), pp. 216–227.

[26] Lopez, J Javier et al. *Characterization of in-cylinder soot oxidation using two-color pyrometry in a production light-duty diesel engine*. Tech. rep. SAE Technical Paper, 2016.

[27] Piano, A et al. "Numerical and optical soot characterization through 2-color pyrometry technique for an innovative diesel piston bowl design". In: *Fuel* 333 (2023), p. 126347.

[28] Pastor, José V et al. "Influence of the radial-lip concept design to achieve ultra-low soot emission reductions: An optical analysis". In: *Fuel* 345 (2023), p. 128161.

[29] Hottel, Hoyt C and Broughton, FP. "Determination of true temperature and total radiation from luminous gas flames". In: *Industrial & Engineering Chemistry Analytical Edition* 4.2 (1932), pp. 166–175.

[30] Zhao, Hua and Ladommatos, Nicos. "Optical diagnostics for soot and temperature measurement in diesel engines". In: *Progress in energy and combustion science* 24.3 (1998), pp. 221–255.

[31] Pastor, Jose V, Garcia-Oliver, Jose M, Garcia, Antonio, Mico, Carlos, and Möller, Sebastian. "Application of optical diagnostics to the quantification of soot in n-alkane flames under diesel conditions". In: *Combustion and Flame* 164 (2016), pp. 212–223.

[32] Xuan, Tiemin et al. "In-flame soot quantification of diesel sprays under sooting/non-sooting critical conditions in an optical engine". In: *Applied Thermal Engineering* 149 (2019), pp. 1–10.

[33] Gehmlich, RK et al. "Using ducted fuel injection to attenuate or prevent soot formation in mixing-controlled combustion strategies for engine applications". In: *Applied energy* 226 (2018), pp. 1169–1186.

[34] Mueller, Charles J et al. "Ducted fuel injection: A new approach for lowering soot emissions from direct-injection engines". In: *Applied energy* 204 (2017), pp. 206–220.

[35] Millo, F et al. “Ducted fuel injection: Experimental and numerical investigation on fuel spray characteristics, air/fuel mixing and soot mitigation potential”. In: *Fuel* 289 (2021), p. 119835.

[36] Svensson, Kenth I and Martin, Glen C. “Ducted fuel injection: effects of stand-off distance and duct length on soot reduction”. In: *SAE International Journal of Advances and Current Practices in Mobility* 1.2019-01-0545 (2019), pp. 1074–1083.

[37] ANSYS, Chemkin. *Reaction Workbench 17.0*. 2016.

[38] Lin, Qinjie, Tay, Kun Lin, Zhou, Dezhi, and Yang, Wenming. “Development of a compact and robust Polyoxymethylene Dimethyl Ether 3 reaction mechanism for internal combustion engines”. In: *Energy Conversion and Management* 185 (2019), pp. 35–43.

[39] Lin, Qinjie, Tay, Kun Lin, Zhao, Feiyang, and Yang, Wenming. “Enabling robust simulation of polyoxymethylene dimethyl ether 3 (PODE3) combustion in engines”. In: *International Journal of Engine Research* 23.9 (2022), pp. 1522–1542.

[40] Jing, Zheng, Zhang, Chunhua, Cai, Panpan, Li, Yangyang, and Wang, Jibai. “Construction of a Reduced Diesel/Polyoxymethylene Dimethyl Ether 3 (PODE3) Reaction Mechanism for Combustion and Emission Analysis”. In: *Energy & Fuels* 35.5 (2021), pp. 4437–4446.

[41] He, Tanjin et al. “Development of surrogate model for oxygenated wide-distillation fuel with polyoxymethylene dimethyl ether”. In: *SAE International Journal of Fuels and Lubricants* 10.3 (2017), pp. 803–814.

[42] Senecal, PK et al. “Multi-dimensional modeling of direct-injection diesel spray liquid length and flame lift-off length using CFD and parallel detailed chemistry”. In: *SAE transactions* (2003), pp. 1331–1351.

[43] Cheng, Song et al. “Autoignition and preliminary heat release of gasoline surrogates and their blends with ethanol at engine-relevant conditions: Experiments and comprehensive kinetic modeling”. In: *Combustion and Flame* 228 (2021), pp. 57–77.

[44] Pepiot-Desjardins, Perrine and Pitsch, Heinz. “An efficient error-propagation-based reduction method for large chemical kinetic mechanisms”. In: *Combustion and Flame* 154.1-2 (2008), pp. 67–81.

[45] Sun, Wenting, Chen, Zheng, Gou, Xiaolong, and Ju, Yiguang. “A path flux analysis method for the reduction of detailed chemical kinetic mechanisms”. In: *Combustion and Flame* 157.7 (2010), pp. 1298–1307.

[46] Niemeyer, Kyle E, Sung, Chih-Jen, and Raju, Mandhapati P. "Skeletal mechanism generation for surrogate fuels using directed relation graph with error propagation and sensitivity analysis". In: *Combustion and flame* 157.9 (2010), pp. 1760–1770.

[47] Versteeg, Henk Kaarle and Malalasekera, Weeratunge. *An introduction to computational fluid dynamics: the finite volume method*. Pearson education, 2007.

[48] Richards, KJ, Senecal, PK, and Pomraning, E. "CONVERGE (v3. 0), Convergent Science". In: *Inc., Madison, WI* (2021).

[49] Peters, N. "Turbulent combustion. Cambridge, UK: Cambridge University Press."" In: (2000).

[50] Cant, Stewart. "SB Pope, Turbulent Flows, Cambridge University Press, Cambridge, UK, 2000, 771 pp." In: *Combustion and Flame* 4.125 (2001), pp. 1361–1362.

[51] Launder, Brian Edward and Spalding, Dudley Brian. "The numerical computation of turbulent flows". In: *Numerical prediction of flow, heat transfer, turbulence and combustion*. Elsevier, 1983, pp. 96–116.

[52] O'rourke, PJ and Amsden, AA. "A particle numerical model for wall film dynamics in port-injected engines". In: *SAE transactions* (1996), pp. 2000–2013. DOI: 10.4271/961961.

[53] Amsden, Anthony A and Findley, Margaret. *KIVA-3V: A block-structured KIVA program for engines with vertical or canted valves*. Tech. rep. Lawrence Livermore National Lab.(LLNL), Livermore, CA (United States), 1997. DOI: 10.2172/505339.

[54] Yakhot, VSASTBCG, Orszag, SA, Thangam, Siva, Gatski, TB, and Speziale, CG1167781. "Development of turbulence models for shear flows by a double expansion technique". In: *Physics of Fluids A: Fluid Dynamics* 4.7 (1992), pp. 1510–1520.

[55] Hiroyasu, H and Kadota, To. "Models for combustion and formation of nitric oxide and soot in direct injection diesel engines". In: *SAE transactions* (1976), pp. 513–526.

[56] Dempsey, Adam B, Seiler, Patrick J, Svensson, Kenth I, and Qi, Yongli. "A comprehensive evaluation of diesel engine CFD modeling predictions using a semi-empirical soot model over a broad range of combustion systems". In: *SAE International Journal of Engines* 11.6 (2018), pp. 1399–1420.

[57] Ibrahim, Fadzli, Mahmood, Wan Mohd Faizal Wan, Abdullah, Shahrir, and Mansor, Mohd Radzi Abu. *Comparison of simple and detailed soot models in the study of soot formation in a compression ignition diesel engine*. Tech. rep. SAE Technical Paper, 2017.

[58] Tang, Meng et al. "Numerical Investigation of Fuel Effects on Soot Emissions at Heavy-Duty Diesel Engine Conditions". In: *Internal Combustion Engine Division Fall Technical Conference*. Vol. 51999. American Society of Mechanical Engineers. 2018, V002T06A019.

[59] Singh, Rahul Kumar and Agarwal, Avinash Kumar. "Soot and NOx modelling for diesel engines". In: *Engine Modeling and Simulation*. Springer, 2021, pp. 195–217.

[60] Nagle, J and Strickland-Constable, RF. "Oxidation of carbon between 1000–2000 C". In: *Proceedings of the fifth conference on carbon*. Elsevier. 1962, pp. 154–164.

[61] Aithal, SM. "Modeling of NOx formation in diesel engines using finite-rate chemical kinetics". In: *Applied Energy* 87.7 (2010), pp. 2256–2265.

[62] Rao, Varun and Honnery, Damon. "A comparison of two NOx prediction schemes for use in diesel engine thermodynamic modelling". In: *Fuel* 107 (2013), pp. 662–670.

[63] Wei, Wu, Zhou, Tingyu, Zhao, Lun, Ba, Jin, and Zhang, Long. "Numerical study on the injection strategy on combustion and emission characteristics of a non-road diesel engine under different altitude conditions". In: *Case Studies in Thermal Engineering* 53 (2024), p. 103838.

Chapter 4

Numerical study on the potential of different fuel blends to tackle pollutant emissions

4.1 Introduction

In this chapter, a detailed numerical study has been carried out. It is focused on evaluating the potential/performance of the different blends identified in this thesis to replace conventional fossil diesel to tackle pollutant emissions. These blends specifically are of Diesel-OME_x and HVO-OME_1 as discussed in previous chapters. In both cases, the analysis begins with the identification and development of a reaction mechanism necessary for accurate numerical simulations of the combustion process of these blends. It is followed by a detailed analysis of the combustion performance and emissions formation inside the combustion chamber by means of 3D CFD simulations. In the end, a summary and conclusions are presented.

It should be taken into account that the numerical analysis has been complimented by experiments that have been performed with the fuel blends identified in this thesis. Some of this data was obtained directly from the one included in [1]. Specifically, the one corresponding to Diesel-OME_x blends. In contrast, the data of HVO-OME_1 was specifically measured for this work, following a similar experimental procedure, which has been described in chapter 3. The experiments were performed by utilizing the Optical setup A as described in Figure 3.2. Table 4.1 depicts the operating conditions used for analyzing the fuel blends.

Table 4.1: Engine operating conditions for analyzing fuel blends.

Parameter	**Value**
Injection profile (-)	Single pulse
Engine speed (rpm)	1250
Intake pressure (bar)	1.8
Exhaust pressure (bar)	2
Injection pressure (bar)	1000
SOE (°aTDC)	-9
Injection duration (μs)	900

The CFD model utilized in doing the numerical analysis of these fuel blends has already been described in detail in section 3.4. In doing so, the injection parameters presented in Table 3.7 have been utilized together with injection profiles shown earlier in Figure 3.15.

4.2 Diesel-OME$_x$ Blends

The advantages achieved in terms of using OME$_x$ in CI engines have been discussed in detail in section 2.3. Based on that, as discussed in section 3.3, different blends of Diesel-OME$_x$ blends have been utilized in the context of this thesis in order to evaluate the advantages of OME$_x$ as an oxygenated fuel. Specifically, the blends ranging from 10% to 50% of OME$_x$ have been utilized. They are identified as D90O10, D80O20, D70O30, and D50O50. The OME$_x$ fraction in blends has been limited up to 50% owing to energy reduction caused by the lower LHV of this fuel as discussed earlier.

4.2.1 Fuel Definition and Mechanism development

In order to perform the detailed numerical analysis of Diesel-OME$_x$ blends using 3D CFD simulations, it is necessary to identify an appropriate surrogate and a proper chemical mechanism to properly replicate the behaviour of the blends. It should be noted that in doing numerical analysis via 3D CFD simulations, the general practice is to use surrogates that have a simpler chemical composition as compared to actual fuel. For instance, n-heptane is widely used as a surrogate for diesel fuel [2, 3]. So the primary step in doing

the analysis is the definition of fuel surrogates and a proper mechanism to perform the numerical simulations. Taking into account the literature, for this work, n-heptane was chosen as a surrogate to model the vapor phase of diesel fuel. For the case of OME_x two different approaches have been followed. Primarily only OME_3 was used as a surrogate to model OME_x, which allowed the evaluation of different mechanisms from literature. Secondly a more realistic surrogate consisting of blend of several OME molecules was chosen which resembled the real OME_x fuel tested. The later approach relates to the development of a reaction mechanism. These two approaches are described in proceeding sections.

4.2.1.1 Evaluation of reaction mechanisms from literature

Numerous chemical reaction mechanisms can be found in the literature that have been proposed to perform the numerical simulations of the Diesel-OME_x blends. These works have been already discussed in section 2.3. He et al. [4] constructed and validated a wide distillation fuel (WDF)-OME_x mechanism, consisting of 354 species and 943 reactions which covered the surrogates of OME_x, iso-octane, n-heptane etc. Following his work, Ren et al. [5] formed and validated a primary reference fuel (PRF)-OME_3 chemical mechanism consisting of 145 species and 585 reactions, to predict the combustion and emission behavior of Gasoline/Diesel-OME_x blends. A very compact PRF-OME_3 mechanism including only 61 species and 190 reactions was proposed by Lin et al. [6]to be utilized in a CI engine application. Another Diesel-OME_3 mechanism consisting of 179 species and 769 reactions was developed by Lv et al. [7], for CI engine applications. Recently, the authors from [6] published another work on tertiary reference fuel (TRF)-OME_3 mechanism consisting of 120 species and 560 reactions to better explain Gasoline/Diesel-OME_x blends behavior [8].

Table 4.2: Details of reaction mechanisms utilized for Diesel-OME_x blends.

Mechanism	**Number of species**	**Number of reactions**
He 2017 [4]	354	943
Ren 2019 [5]	145	585
Lin 2019 [6]	61	190
Lin 2021 [8]	120	360

To the author's knowledge, these are most of the reaction mechanisms that exist in literature which can be utilized to perform numerical simulations regarding blends of Diesel with OME_x i.e., [4–8]. A common point among these mechanisms is that all of these use only OME_3 as a surrogate to represent OME_x fuel. Table 4.2 summarizes the details of the reaction mechanisms which are primarily evaluated for Diesel-OME_x blends simulations.

In evaluating these reaction mechanisms, CFD simulations were performed utilizing the model and operating conditions as described earlier and the results were compared with experimental data from [1]. In doing so, the liquid phase of fossil diesel was modeled by using a pre-defined fluid found in CONVERGE CFD named DIESEL2, however, n-heptane was chosen as a surrogate to model the vapor phase which as mentioned earlier is a widely used surrogate for diesel. For the case of OME_x, OME_3 was used as a surrogate to model it, as the mentioned mechanisms have the limitation of having only OME_3 molecule present in them to model OME_x. Figure 4.1 shows the heat release rate and in-cylinder pressure for the case of the D50O50 blend utilizing different reaction mechanisms.

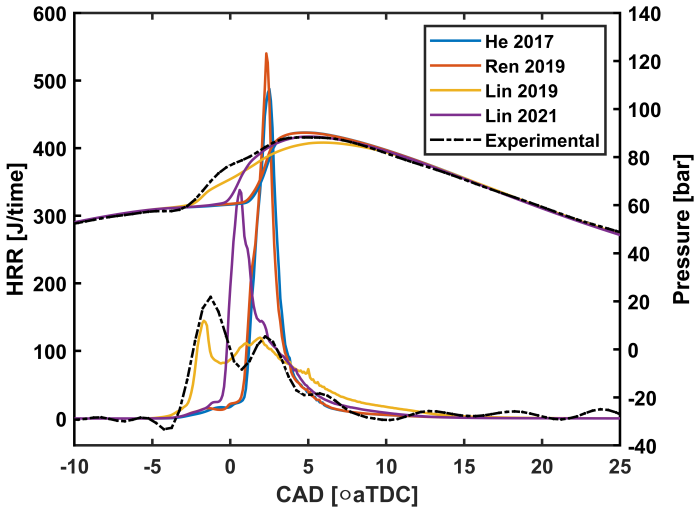

Figure 4.1: Numerically obtained heat release rate and in-cylinder pressure for the case of D50O50 blend by utilizing different reaction mechanisms compared with experimental data from [1].

It is possible to see that only one of the four mechanisms was able to predict a rather similar behavior as of experimental data, which is the compact mechanism provided by Lin et al. [6]. However, it also suffers a slightly

longer ignition delay prediction. The other three mechanisms perform badly in terms of predicting the combustion phasing. The reasons could be related to the improper fuel surrogate definition for the case of OME_x. As mentioned earlier, the part of the mechanism related to OME_x was only represented by one molecule i.e., OME_3. However, OME_x is a combination of different OME chain lengths. Table 3.1 shows that the experimental OME_x fuel consists of OME chain lengths with prominent ones being OME_3 and OME_4. Another reason can be that the mechanisms evaluated here were only validated individually (as no fundamental data was available for mixtures) under the assumption that if both individual mechanisms can predict the neat fuels, the combined one would also perform reasonably well in predicting the fuel blends as suggested by Klotz et al. [9] which is not always true and can lead to problems especially in ignition delay prediction in case of fuel blends as seen here. Hence, keeping this in perspective, there exists a margin of improvement in literature in terms of the definition of a more representative chemical mechanism, to be used to simulate blends of OME_x with diesel, where the first fuel is not only represented by the OME_3 molecule but by a more realistic composition of different OME chain lengths. Therefore, a new PRF-OME_x mechanism was constructed to overcome all these limitations, the detail of which is described in the following sections.

4.2.1.2 PRF sub-mechanism

The PRF surrogate mechanisms are designed to reproduce iso-octane and n-heptane oxidation processes, which can be used to simulate the oxidation of diesel and gasoline respectively. Several validated PRF mechanisms exist in the literature to date, including a 33 species and 55 reactions mechanism proposed by Tanaka et el. [10], 41 species and 130 reactions PRF mechanism proposed by Ra and Reitz [11], a 33 species ad 38 reaction PRF compact mechanism proposed by Tsurushima [12], 41 species and 124 reactions PRF mechanism proposed by Liu et al. [13] and a 73 species 296 reactions PRF mechanism constructed by Wang et al. [14].

For the purpose of this work, the PRF mechanism from the work of Lin et al. [6] was chosen. As discussed earlier the authors [6] proposed a robust PRF-OME_3 mechanism consisting of 61 species and 190 reactions, which was able to reproduce the experimental behavior of the Diesel-OME_x reference blend with more accuracy than the others. These authors constructed the mechanism by individually developing a PRF and OME_3 mechanism and merging them together. The PRF part was constructed based on the PRF oxidation mechanism proposed by Liu et al. [13] and the diesel surrogate mechanism

by Chang et al. [15]. Specifically, authors integrated the n-heptane sub-mechanism from [13] and iso-octane sub-mechanism from [15] into reduced C_2-C_3 mechanism and detailed $H_2/CO/C_1$ taken from [15] to form a baseline PRF oxidation mechanism consisting of 50 species and 170 reactions. This practice was done by authors in order to ensure the accurate prediction of laminar flame speed and species concentration profiles. It was validated extensively in terms of ignition delay times, laminar flame speed, and species concentration profiles. Hence, in this work, this PRF mechanism was utilized. Furthermore, this selection of utilizing the same PRF mechanism allows us to identify the contribution of our proposal (OME_x with PRF) to the behavior of the mechanism in comparison with other proposals where only OME_3 is used with PRF.

4.2.1.3 OME_x sub-mechanism

As discussed earlier, the main motive for the development of a new mechanism for Diesel-OME_x blends was to incorporate a reduced mechanism for OME_x that includes not only OME_3 but also other OME molecules, to get as close as possible to real OME_x fuels. For this reason, an already published $OME_{2\text{-}4}$ detailed mechanism by Cai et al. [16] was chosen for reduction. It has been utilized by various authors in the past to represent OME_x fuel [17–19]. The detailed mechanism was generated on the basis of $OME_{2\text{-}4}$ autoignition. This work included the individual validation of different OME molecules in terms of ignition delay times. A wide range of initial conditions including temperature (650-1150K), pressure (10,20 bars), and equivalence ratios (0.5,1.0,2.0) were used. From here onwards it will be referred to as the master mechanism consisting of 322 species and 1611 reactions. Unfortunately, the master mechanism was too large to be utilized in numerical simulations, therefore, it was reduced.

Starting with the master mechanism, a set of different initial conditions were selected to reduce it by utilizing different techniques like DRGEP and DRGPFA as discussed in section 3.4. These reduction techniques have been widely used previously in other works for mechanism reductions and are recognized in literature [5–8]. A set of different combinations of fuel composition were used in the reduction process to ensure that the resulting mechanism behaves well for all $OME_{2\text{-}4}$ molecules in each single, binary or ternary fuel composition. They are summarized in Table 4.3. Note that composition 8 was chosen as it corresponds closely to the experimental fuel OME_x utilized in this thesis as described in Table 3.1. In addition, the pressure range was increased as compared to the one used to develop the master mechanism. The

pressures of 40 and 50 bars were also included to make sure the mechanism behaves properly in realistic CI engine conditions.

Table 4.3: Different fuel compositions utilized for OME_x mechanism reduction.

Fuel Composition	**OME_2 mol. frac**	**OME_3 mol. frac**	**OME_4 mol. frac**
Composition 1	1.0	0.0	0.0
Composition 2	0.0	1.0	0.0
Composition 3	0.0	0.0	1.0
Composition 4	0.5	0.5	0.0
Composition 5	0.5	0.0	0.5
Composition 6	0.0	0.5	0.5
Composition 7	0.33	0.33	0.33
Composition 8	0.017	0.622	0.360

OME_x master mechanism reduction is based on a large dataset of ignition delay data calculated in an adiabatic, closed, constant-volume, homogeneous reactor at the following conditions:

- Pressure variation: 10, 20, 40, and 50 bar.
- Temperature variation: from 650 K to 1150 K.
- Equivalence ratio variation: 0.5, 1.0, 2.0, and 3.0.

Considering all these conditions, a set of 640 parameters was established for the reduction of the master mechanism. During the iterative process, ignition delay was used as the target parameter with a relative tolerance of 10%. The following sequence of reduction techniques was utilized. The process started with DRGEP applied to the master mechanism, which reduced it to 273 species and 1352 reactions. Further, DRGPFA, which is considered a more rigorous reduction technique, was applied to further reduce the mechanism to 190 species and 777 reactions to its final state. It must be noted that the ignition delay error during each step was kept under the tolerance defined. During the reduction, care was taken to keep all the important species like OH, CH_2O, CO inside the reduced mechanism.

4.2.1.4 Mechanism Merging

The final step after the identification and development of both PRF and reduced OME$_x$ mechanism was the formation of a PRF-OME$_x$ mechanism. The merging was done using the Ansys CHEMKIN Pro merging tool [20]. The PRF one was used as a baseline. Thus, the species and reactions that were duplicated in the OME$_x$ mechanism were deleted. In the end, a PRF-OME$_x$ mechanism consisting of 213 species and 840 species was obtained. The process of developing the PRF-OME$_x$ mechanism is summarized in Figure 4.2.

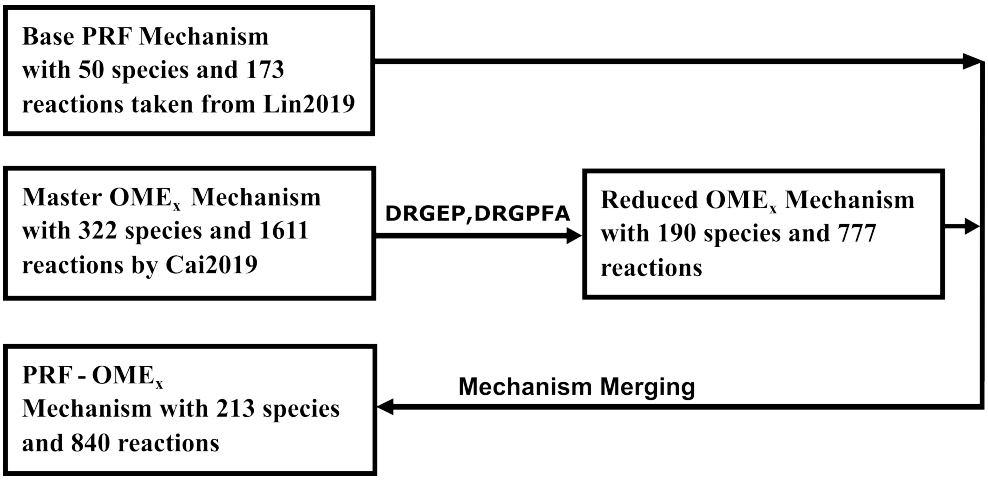

Figure 4.2: Pathway followed to develop PRF-OME$_x$ mechanism required for Diesel-OME$_x$ blends simulations.

4.2.1.5 Mechanism Validations

The proposed PRF-OME$_x$ mechanism was validated through all the available experimental data in the literature, including the ignition delay times, laminar flame speeds and species concentration profiles. The fundamental validations were carried out both before and after merging both PRF and OME$_x$ sub mechanisms following the reasons as described while evaluating the reaction mechanisms in Figure 4.1. Hence, the discussion below will be structured in three parts: ignition delay times, laminar flame speeds and species concentration. It should be noted that during the validations the developed PRF-OME$_x$ will be identified as a merged PRF-OME$_x$ mechanism.

- **Ignition delay validations**

One of the important combustion parameters that can affect the degree of fuel mixing before combustion and the consequent heat release is Ignition delay (ID). As mentioned earlier, a total of 640 parameters were utilized to reduce the master OME_x mechanism. So, the ignition delay comparison between master OME_x, reduced OME_x, and merged PRF- OME_x mechanism can be applied to each condition. However, owing to the scarce availability of experimental data, only limited comparison including experimental conditions is presented here.

Figure 4.3 shows the comparison of the ignition delay as a function of the inverse of temperature for the case of mixtures of air with OME_2, OME_3 and OME_4 between master OME_x, reduced OME_x, merged PRF-OME_x and experimental data measured in shock tube, at different conditions that can be found in [16]. It can be seen that the master, reduced and merged mechanisms behave quite similarly and close to experimental data among each other at most of the initial conditions. The difference with experimental data arises at low temperatures, particularly for the case of OME_2. The simulated mechanisms seem to predict longer ignition delay at low temperatures. However, it must be noted these discrepancies were already presented by the master mechanism. Therefore, it can be concluded that the merged mechanism is able to reproduce experimental data in most of the initial conditions evaluated and behaves very similar to the master mechanism.

The comparison of ignition delay was also extended to the pure n-heptane case. Figure 4.4 shows the comparison of ignition delay for the case of this fuel mixed with air at two different initial conditions of 0.5 and 1 equivalence ratio at 40 bars. Experimental data of shock tube was taken from various sources including Shen et al. [21], Fieweger et al. [22], Hartmann et al.[23], and Herzler et al. [24]. Here the base mechanism represents the base PRF mechanism which has been already discussed earlier and the merged one represents the PRF-OME_x mechanism. It can be seen that both base and merged mechanisms behave quite similarly to each other and also show small differences with the experimental data.

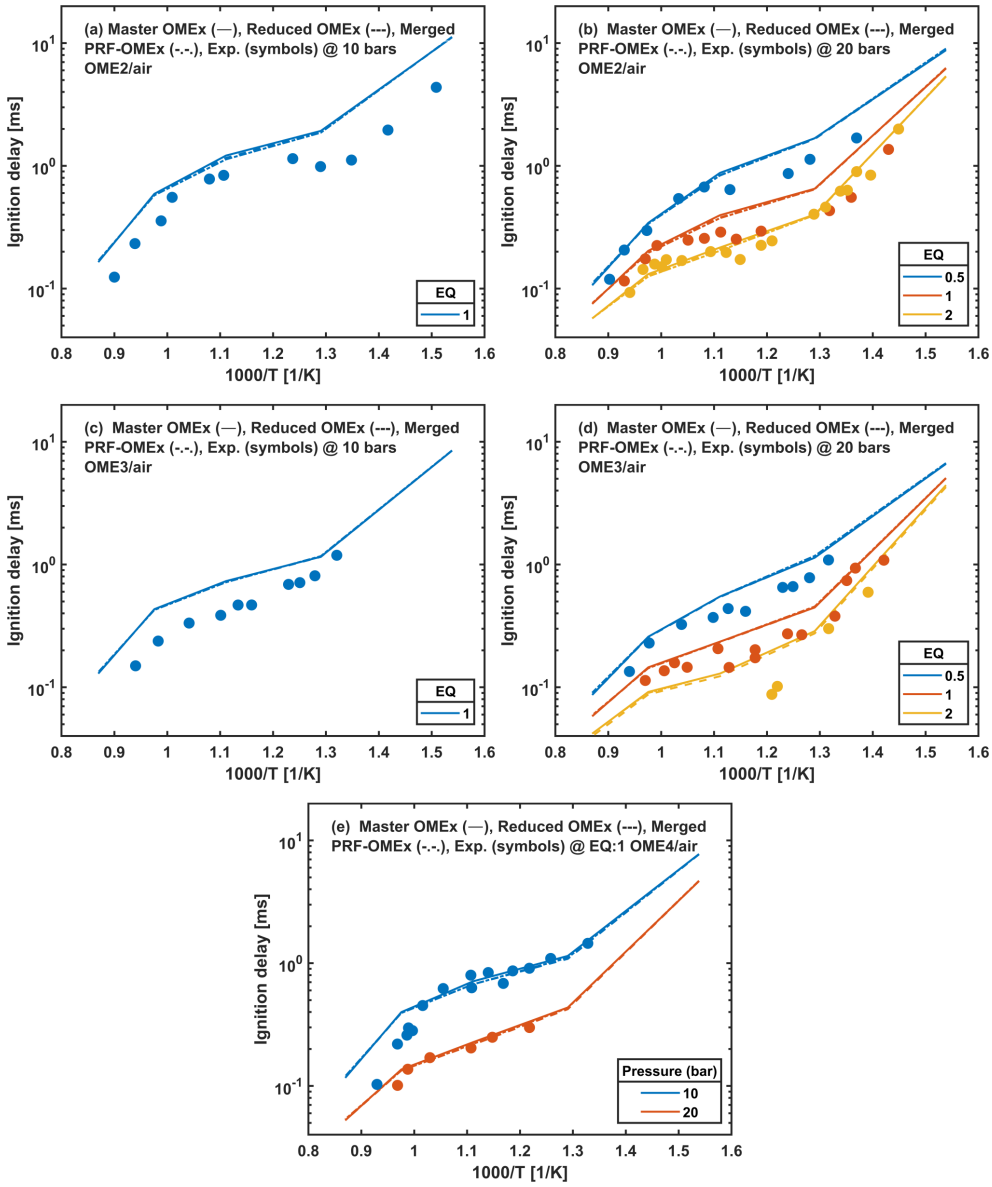

Figure 4.3: Ignition delay validations of master OME$_x$, reduced OME$_x$ and merged PRF-OME$_x$ mechanism against experimental data for the case of OME$_2$/air, OME$_3$/air and OME$_4$/air mixtures at different equivalence ratios and pressures.

.

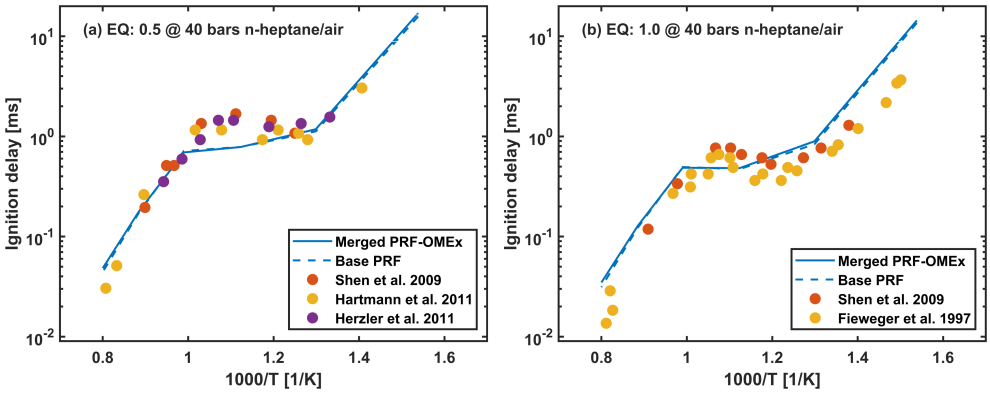

Figure 4.4: Ignition delay validations of base PRF and merged PRF-OME$_x$ mechanism against experimental data for the case of n-heptane/air mixture at 40 bars pressure and equivalence ratio of 0.5 (a), 1.0 (b).

To extend validation further, Figure 4.5 shows the simulated ignition delay times of n-heptane and iso-octane mixtures compared with experimental data taken from [22], where experiments were performed in a shock tube at a pressure of 40 bars and equivalence ratio of 1. The number beside PRF shows the percentage of iso-octane in the mixture. As an example, PRF0 refers to pure n-heptane and PRF100 represents pure iso-octane. It can be seen that both base PRF and merged PRF-OME$_x$ mechanisms show very little differences among themselves and with experiments in the case of PRF0, PRF60, PRF80 cases. However, some differences arise for the case of PRF90 and PRF100 (pure iso-octane) at temperatures of around 700-900K, when the merged PRF-OME$_x$ mechanism underpredicts ignition delay. Nevertheless, in general, it can be said that simulation results matched their respective experimental results quite accurately.

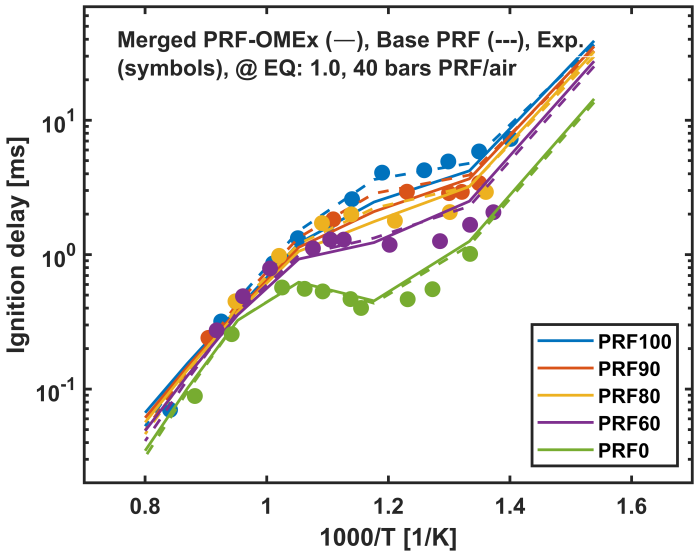

Figure 4.5: Ignition delay validations of base PRF and merged PRF-OME$_x$ mechanism against experimental data for the case of PRF0, PRF60, PRF80, PRF90 and PRF100 at 40 bars pressure and equivalence ratio of 1.0.

- **Laminar flame speed validations**

The present PRF-OME$_x$ mechanism has also been validated for the predictions of laminar flame speed (LFS). The newly developed mechanism must be able to predict the experimentally obtained LFS values in order to reproduce the actual diesel engine combustion. LFS simulations were carried out according to the methodology described in section 3.4.

Figure 4.6 depicts the simulated LFS values obtained from master OME$_x$, reduced OME$_x$, merged PRF-OME$_x$ mechanisms for the case of OME$_2$/air, OME$_3$/air and OME$_4$/air mixtures compared with available experimental data. The experimental data for the case of OME$_2$ was taken from [25, 26] , for the case of OME$_3$ from [26, 27] and for the case of OME$_4$ from [28]. It is possible to see that the merged PRF-OME$_x$ mechanism overpredicts both master OME$_x$ and reduced OME$_x$ simulations in every case i.e., OME$_2$, OME$_3$ and OME$_4$. However, it is interesting to see that the merged PRF-OME$_x$ replicates the experimental data quite accurately in almost all cases. This is particularly evident in the case of OME$_4$/air mixtures. Therefore, it can be said that the merged PRF-OME$_x$ mechanism performs quite accurate in terms of LFS predictions for different OME/air mixtures.

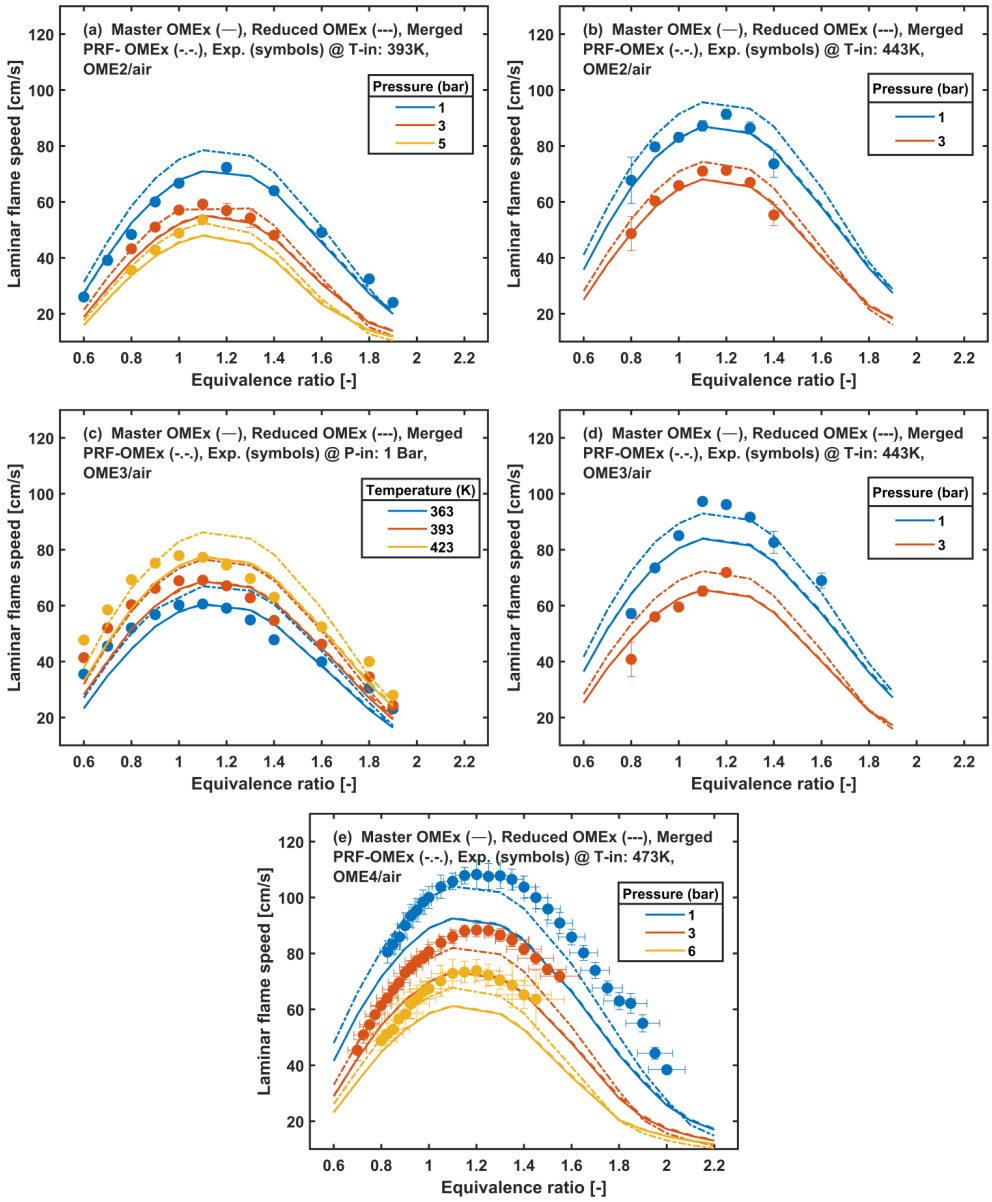

Figure 4.6: Laminar flame speed validations of master OME_x, reduced OME_x and merged PRF-OME_x mechanism against experimental data for the case of OME_2/air, OME_3/air and OME_4/air mixtures at different temperatures and pressures.

The LFS validations are also extended to PRF mixtures. Figure 4.7 shows the simulated LFS values for the case of PRF0, PRF50 and PRF100, compared against experimental data taken from [29–31]. It can be observed that the merged PRF-OME$_x$ mechanism overpredicts both experimental data and base PRF simulated data particularly around near stoichiometric equivalence ratios. However, differences between simulated data are smaller as compared to differences with experimental data.

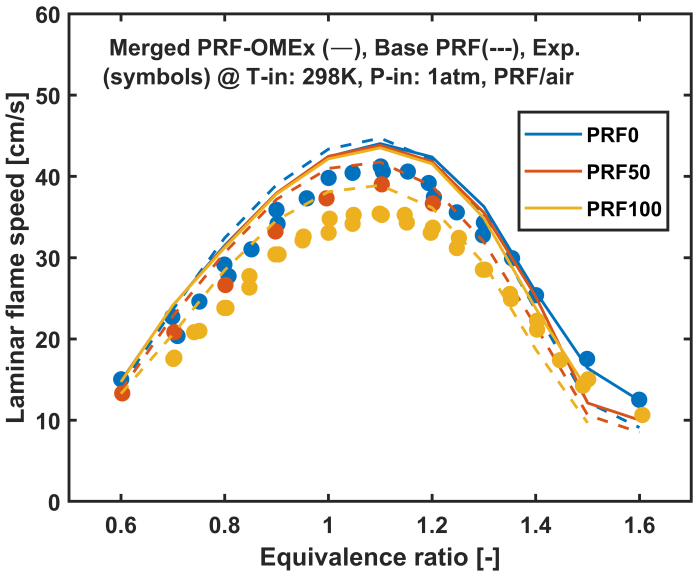

Figure 4.7: Laminar flame speed validations of base PRF and merged PRF-OME$_x$ mechanism against experimental data for the case of PRF0, PRF50 and PRF100 at 1 atm pressure 298K temperature.

- **Species concentration profiles validations**

The flame species concentration is also an important metric for the validation of the chemical kinetic mechanism. Species concentration profile simulations were carried out according to the methodology described in section 3.4. Note that, for the case of OME$_x$, simulations were limited to OME$_3$ only due to the scarcity of available experimental data for other OME chain lengths. The experimental data for the case of OME$_3$ was taken from [32] where experiments were conducted at 25.0 torr pressure with Mckenna burner under stoichiometric flame conditions.

Figure 4.8 shows the comparison between experimental data and simulated values for the case of master OME$_x$, reduced OME$_x$ and merged PRF-OME$_x$

mechanism for the important species including H_2, CO, O_2, CO_2, H_2O and Ar. It is possible to see that a very good agreement is reached between simulated species profiles and their experimental counterparts, especially at the steady-state region beyond 15 mm above the burner. The predicted consumption of OME_3 and O_2 is well captured, in turn forming H_2, CO_2, CO and H_2O before reaching a steady state condition. Only overestimation can be seen in the case of CO and a slight underestimation in the case of Ar. Nevertheless, it can be said that the newly developed PRF- OME_x mechanism reproduced the detailed OME_3 flame structure to a reasonably good accuracy.

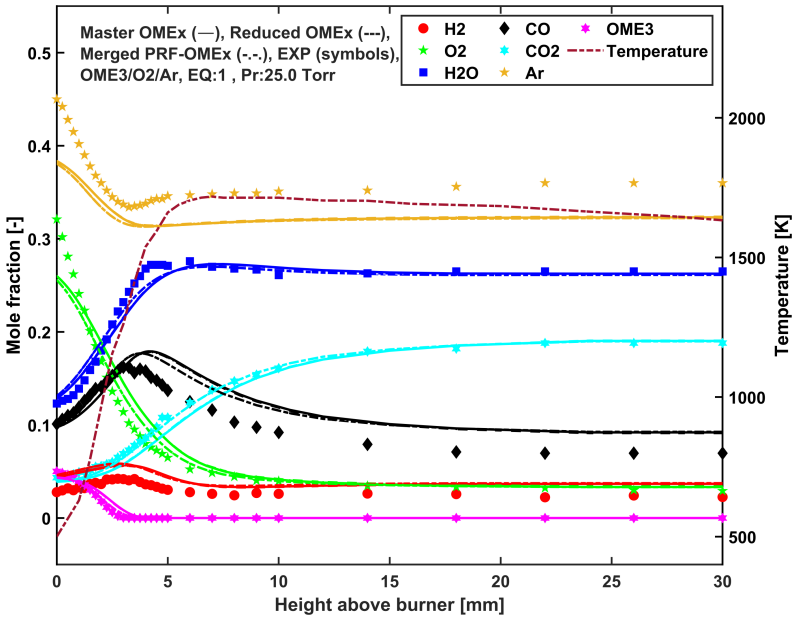

Figure 4.8: Species concentration profile validations of masterOME_x, reduced OME_x and merged PRF-OME_x mechanism against experimental data for the case of $OME_3/O_2/Ar$ mixtures at 25 torr pressure and equivalence ratio of 1.

The species concentration profile validations were also extended to PRF mixtures in Figure 4.9. Experimental data is acquired from [33, 34]. It can be seen that both merged PRF-OME_x and base PRF mechanism are able to replicate experimental data related to n-heptane and iso-octane's reactants and products reasonably well. In general, it can be said that the developed PRF-OME_x mechanism reproduces the experimental data related to flame species of n-heptane and iso-octane in a very reasonable manner except for a few discrepancies.

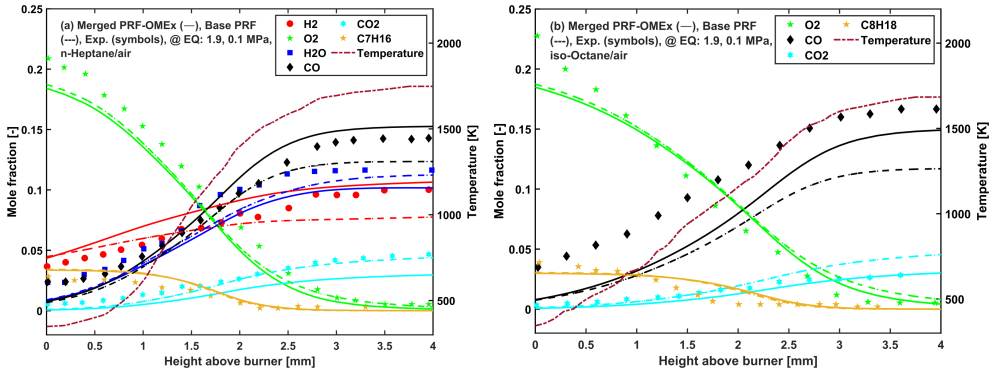

Figure 4.9: Species concentration profile validations of base PRF and merged PRF-OME$_x$ mechanism against experimental data for the case of n-heptane/air (a) and iso-octane/air (b) mixtures at 0.1MPa pressure and equivalence ratio of 1.9.

These all validations including ignition delay, laminar flame speed, and species profile concentrations show the accuracy of the developed PRF-OME$_x$ mechanism. Hence in the proceeding section, the detailed analysis of Diesel-OME$_x$ blends is carried out through 3D CFD simulations performed with the developed mechanism consisting of 213 species and 840 reactions.

4.2.2 Analysis of blends performed through numerical simulations

As described earlier, the developed PRF-OME$_x$ mechanism was utilized to perform the 3D CFD simulations of blends of Diesel-OME$_x$. The CFD model that has been utilized in performing simulations has been described in detail in the 3D CFD model development part of section 3.4. The operating conditions correspond to the one described earlier in section 4.1.

It must be taken into account that in doing the CFD simulations as established earlier, the liquid phase of fossil diesel was modeled by using a pre-defined fluid found in CONVERGE CFD named DIESEL2, however, n-heptane was chosen as a surrogate to model the vapor phase. For the case of OME$_x$, the definition of the surrogate was done according to the experimental fuel utilized which consisted of a mixture of different OMEs where larger fractions corresponded to OME$_3$ and OME$_4$ (see Table 3.1). This was possible thanks to the developed PRF-OME$_x$ mechanism in this work, where OME$_x$ part consisted of different OMEs including OME$_2$, OME$_3$ and OME$_4$.

It must be noted that as the developed PRF-OME_x mechanism consisted of only $OME_{2\text{-}4}$ molecules, the surrogate definition was limited to only these OME molecules. The fractions where $x \geq 4$, was modeled by OME_4. This practice has already been done in previous works [19]. The experimental fuel and its surrogate composition are highlighted in Table 4.4.

Table 4.4: Composition of OME_x fuel and its surrogate $OME_{2\text{-}4}$ utilized.

OME_x molecule	**OME_x experimental fuel (% by weight)**	**OME_x surrogate fuel (% by weight)**
OME_1	0.01	0
OME_2	< 0.01	0
OME_3	57.90	57.9
OME_4	28.87	42.1
OME_5	10.08	0
OME_6	1.91	0

Simulations were performed for D90O10, D80O20, D70O30, and D50O50 as described in the beginning. The analysis can be divided into two separate sections namely combustion characteristics and emissions analysis.

4.2.2.1 Combustion characteristics

- **Ignition delay**

The simulation analysis can be started in a chronological order of the events happening after the start of injection. Figure 4.10 depicts the ignition delays obtained for both numerical and experimental cases. The ignition delay here is defined as the time interval in crank angle degrees between the SOI, which occurs at -6.8 °aTDC, and the SOC. The SOC is calculated based on the extrapolation of the maximum slope of the in-cylinder pressure curve (reactive case) to the non-reactive pressure curve. This method is utilized in experiments and is well-documented by Rothamer and Murphy [35]. It is possible to see that ID decreases when OME_x content in the blend is increased. Despite the difference between both data sources, it can be stated that the trend obtained with the numerical simulations regarding the fuel composition is corroborated by experiments. This behavior could be related to the fact that

as OME$_x$ content is decreased in the blend, the oxygen supplied by the fuel itself also decreases making the blend less reactive and delaying combustion. A similar influence of the OME$_x$ fraction over the ignitability of the blends was reported by Liu et al. [36], who reported a reduction of the cetane number of the blends as this fraction decreased. Hence, it can be stated that an addition of OME$_x$ progressively decreases ID. In fact, when the OME$_x$ percentage in the blend raises from 10% to 50%, a decrease of 19% in ignition delay is observed numerically. The experimental value observed in experiments for D50O50 is not consistent with other blends, which will be analysed in more detail in the following paragraphs.

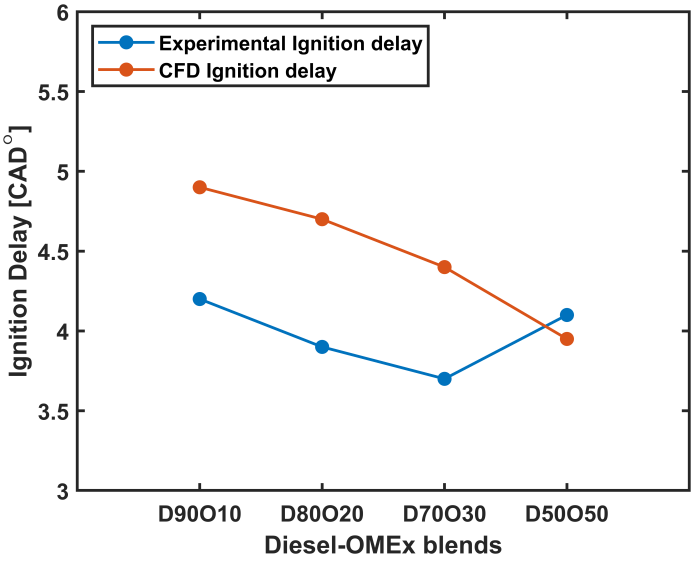

Figure 4.10: Numerical and Experimental ignition delay for Diesel-OME$_x$ blends.

- **Heat Release Rate and In-cylinder Pressure**

The results obtained with the developed PRF-OME$_x$ mechanism for the four blends related to the in-cylinder heat release rate and pressure evolution are compared with experimental data in Figure 4.11. The numerical results obtained by utilizing the PRF-OME$_3$ mechanism by Lin et al. [6] are also included here in dotted lines, as it was the most appropriate mechanism among all the mechanisms tested before (see Figure 4.1). It must be taken into account that simulations with PRF-OME$_3$ mechanism by [6] were performed by considering only OME$_3$ as a surrogate for OME$_x$. While for the case of

the developed PRF-OME$_x$ mechanism, as described earlier, the composition of the surrogate highlighted in Table 4.4 has been utilized which consists of both OME$_3$ and OME$_4$ and replicates the experimental fuel.

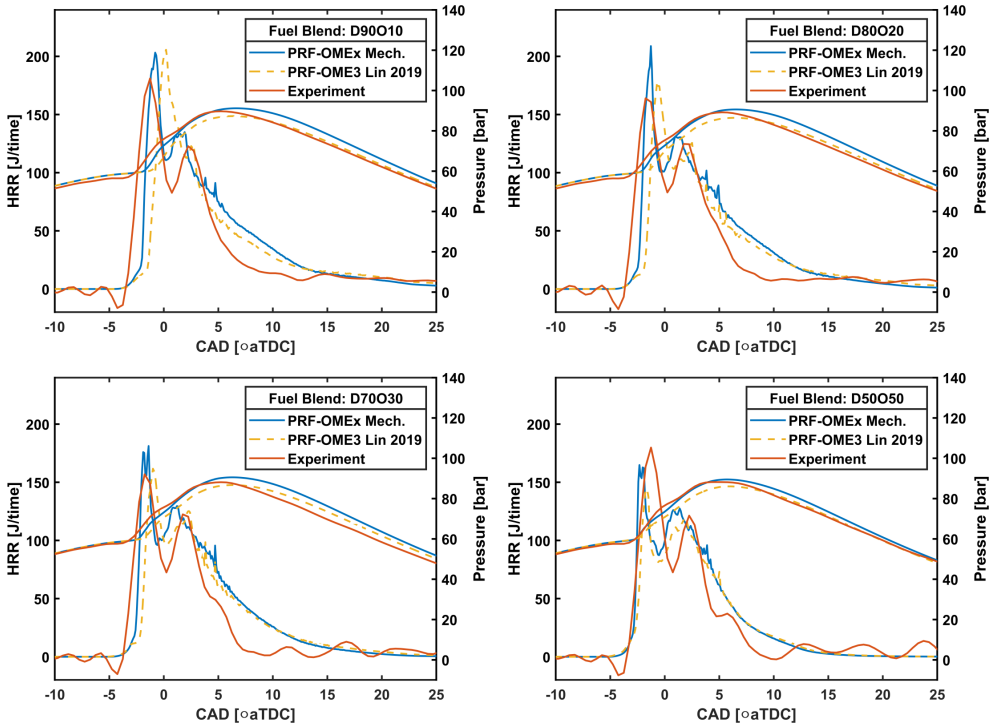

Figure 4.11: Numerical and Experimental Heat release rate and in-cylinder pressure for Diesel-OME$_x$ blends.

Primarily when comparing the mechanisms, it is possible to see that for all the blended cases including D90O10, D80O20, D70O30 and D50O50, the developed PRF-OME$_x$ mechanism not only replicates the experimental behavior in terms of in-cylinder pressure and heat release rate but exhibits a better in-cylinder pressure prediction and combustion phasing closer to experimental data in HRR curve including ignition delay, premixed and diffusion combustion peaks etc. when compared with PRF-OME$_3$ mechanism by [6] regarded here as Lin 2019. It should be noted that according to the physical properties of OME molecules as described in [37], the cetane number of the molecule increases with increasing OME chain length. Hence, a mixture having OME$_{2\text{-}4}$ instead of only OME$_3$ will have a higher cetane number and will ultimately

result in a shorter ID. Therefore, the PRF-OME_x mechanism shows closer ID with respect to experimental data as compared to the PRF-OME_3 mechanism. Furthermore, it should be noted that the lower heating values of OME_3 and OME_4 are not that different (19.6 MJ/kg for OME_3 and 19.0 MJ/kg for OME_4) [37]. Therefore, after the ignition happens, a similar energy release can be expected on pressure and HRR profiles for both mechanisms. Also, during the later stages of combustion, the differences are subtle between mechanisms, as during that phase the reactivity is not dominant, instead the diffusion process is dominant which depends upon physical processes, and it is not much affected by the reaction mechanism itself. However, in general, this discussion goes to show the better performance of the developed PRF-OME_x mechanism in replicating global combustion behavior and this can be directly linked towards the proper surrogate definition of OME_x as close as possible to experimental fuel, which this mechanism offers as compared to other mechanisms.

When comparing the different blends, taking the numerical simulations from the PRF-OME_x mechanism and experimental data, the effect of blends composition starts to be visible when the premixed combustion phase is taking place (between -3° and 0°aTDC). The HRR maximum peak decreases when increasing the OME_x content in the blend. On one hand, this can be related to the fact that the LHV of this fuel is lower than that of pure diesel and, therefore, the energy released by each blend at this stage will be different (see Table 3.2). In this sense, the increase in the injected mass previously reported while describing the injection profile (see Figure 3.15) seems to not be enough to compensate for the energy difference. On the other hand, the ID has an impact on the amount of fuel that mixes with air before combustion and, as a consequence, the energy released in the premixed phase. Thus, the higher ID observed when decreasing the OME_x content is coherent with the more intense HRR peak observed in both CFD and experimental data. Moving further into the diffusion stage, it can be observed that all the fuels present a similar HRR. However, after 5°aTDC the decrease of energy release is more abrupt for the blends with higher OME_x content. This is especially visible when comparing D50O50 and D70O30 with the other two blends and suggests a faster late oxidation stage. This behavior is clearly visible in the numerical simulation results and is corroborated by experiments, despite the larger oscillations and the discrepancies observed for D50O50. It is important to mention that experimental D5050 deviates from other blends showing a similar energy release as D90O10 (and also an ID higher than expected as seen in Figure 4.10). This has been related to experimental errors in [1] since this behavior can not be explained by the fuel properties.

At this point, a strategy was defined to quantify how fast combustion is progressing with each blend with respect to D90O10, chosen as a reference. The fraction of energy released at 15°aTDC from the total energy released at the end of combustion was calculated, to evaluate how far combustion was completed. This instant was chosen as a reference since it corresponds to the late stages of combustion. Figure 4.12 shows a comparison of the experimental and numerical data, including the percentage of total energy released (TER) for each fuel at 15°aTDC as well as the percentage of its variation with respect to the reference case (D90O10). It can be seen that the percentage of energy released is higher for the case of the largest OME_x fraction and decreases when OME_x fraction is decreased. In fact, by looking at the percentage of variation, D50O50 combustion is on average 5% more complete at 15°aTDC than D90O10. It can be also observed that the trend obtained with CFD is again corroborated by experimental data. Therefore, it can be concluded that combustion is accelerated when increasing the OME_x fraction in the blend.

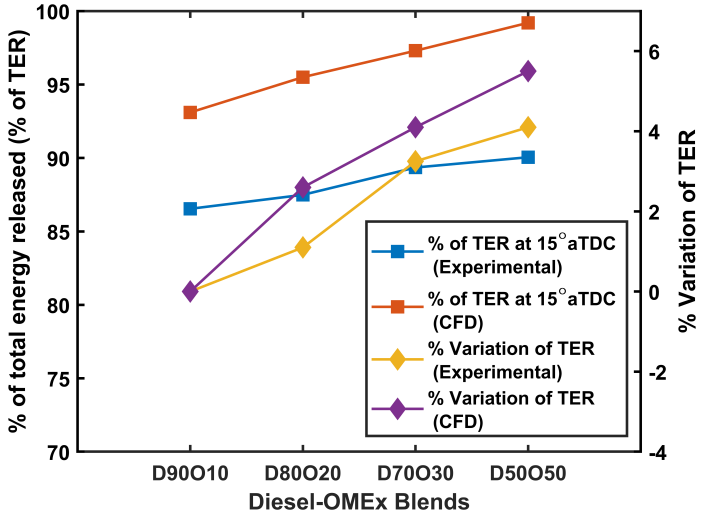

Figure 4.12: Numerical vs experimental percentage of total energy released (TER) at 15°aTDC for each blend and the percentage variation of this parameter w.r.t D90O10 results.

- **Equivalence ratio, Temperature and Fuel Mass**

One of the main differences of OME_x when compared to fossil diesel is its molecular composition, which will affect the stoichiometry of the air/fuel mixture and will have an impact on the combustion process. Thus, to get a deeper insight into the stoichiometry of the blends, the spatial distribution of the equivalence ratio (EQ) inside the combustion chamber is shown in Figure 4.13. During this thesis, the equivalence ratio represents the total equivalence ratio of the gaseous phase of fuel in the corresponding cell as given in the CONVERGE CFD manual [38]. Equation 4.1 describes the equivalence ratio definition utilized in this thesis, where C represents the number of carbon atoms, H represents the number of hydrogen atoms and O represents the number of oxygen atoms.

$$\text{Equivalence ratio} = \left[\frac{2C + \frac{H}{2}}{O}\right] \tag{4.1}$$

The data presented in Figure 4.13 corresponds to the average equivalence ratio calculated between the piston and cylinder head. The inner dotted line in the figure represents the field of view of experimental OH* chemiluminescence visualization presented in [1], the middle one represents the bowl radius and the outer line represents the piston radius. Besides, it has been decided to represent only a quarter of the bowl to match the experimental data available in [1].

It is possible to see that higher EQ values are located at the periphery of the bowl for all the cases. In general, D50O50 shows lower equivalence ratios than the other blends. In fact, it is possible to see that the more the OME_x is in the blend, the lesser equivalence ratios obtained. At 2°aTDC (the beginning of the diffusion stage), all the blends seem to reach equivalence ratio values above 2, which decrease as the combustion progresses. At 5°aTDC, the differences among blends are significant with D50O50 showing large regions where the equivalence ratio was below 1. In contrast, D80O20 and D90O10 still show regions where EQ is close to or even above 2. According to Kitamura et al., [39], more soot is likely to be formed in the regions where EQ is higher than 2. So, based on this, it can be expected that the lower EQ fields achieved thanks to the OME_x content in the blend would result in less soot formation.

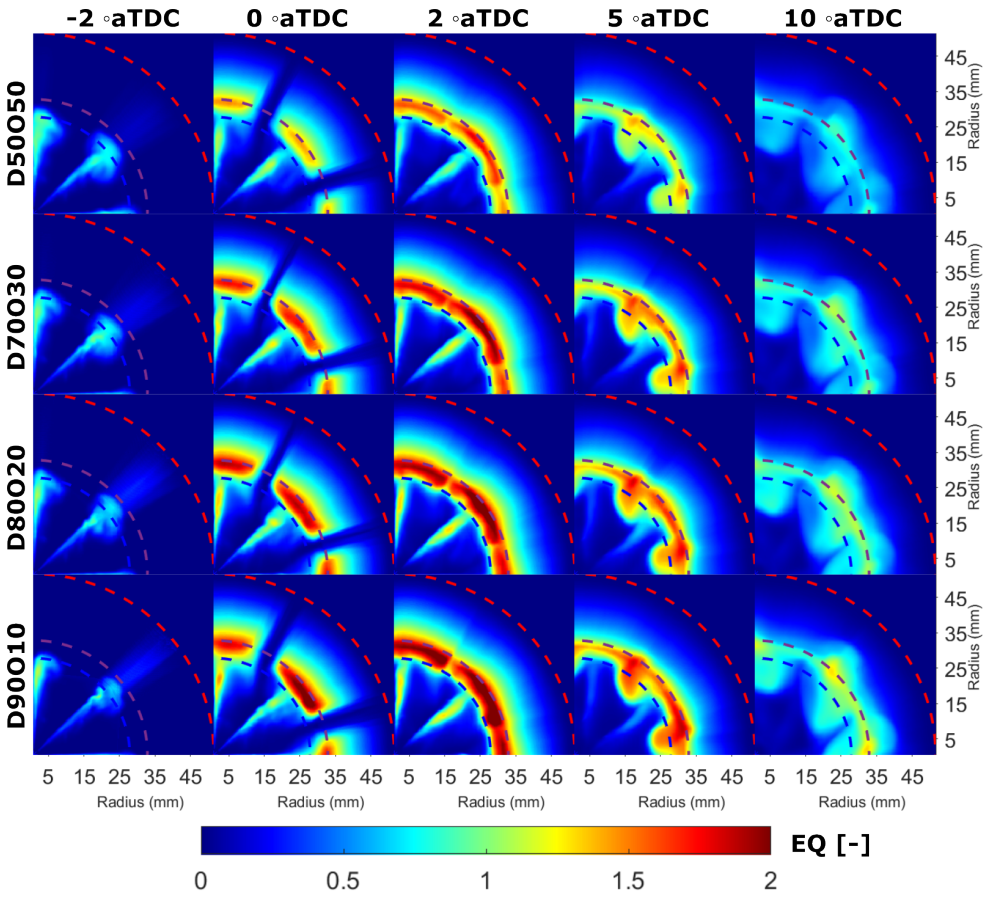

Figure 4.13: Numerically calculated average equivalence ratio distribution inside the combustion chamber for Diesel-OME$_x$ blends.

Figure 4.14 represents the EQ-Temperature diagrams for all the blends at different CADs. Each point corresponds to one of the cells of the computational domain while the dashed lines represent the soot and NO_x peninsulas identified by [40].

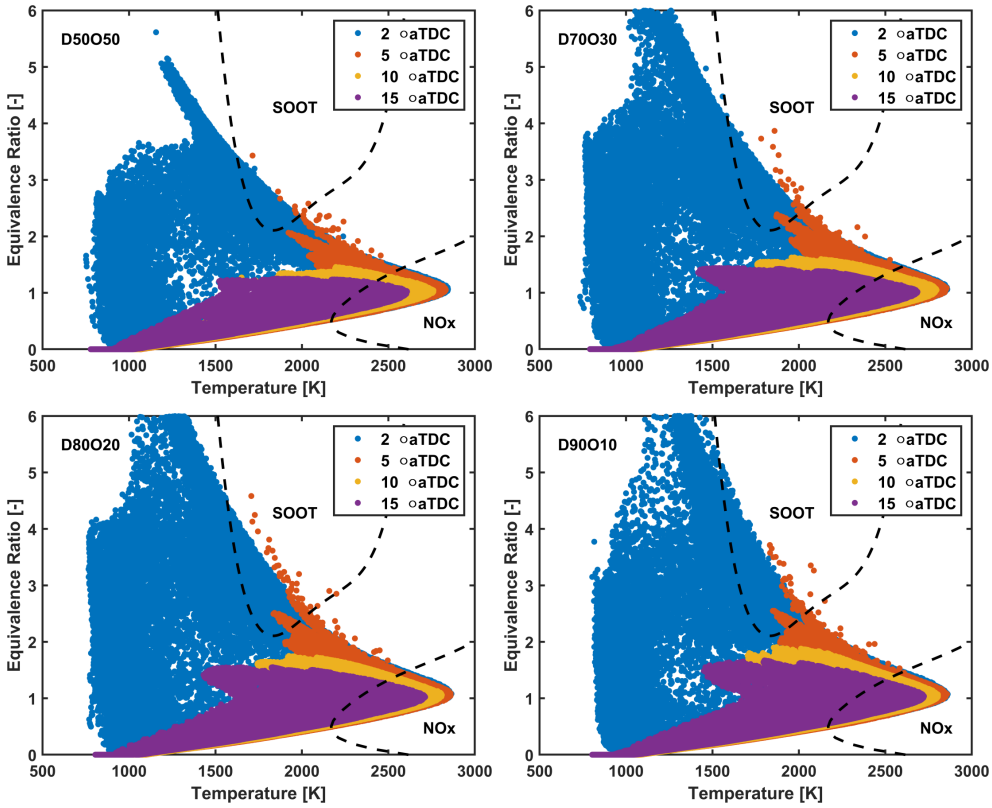

Figure 4.14: Numerically calculated Equivalence ratio vs temperature distribution for Diesel-OME$_x$ blends.

As it can be seen, despite using this oxygenated fraction, all blends end up inside the soot peninsula. Notice that only at 2°aTDC points in the soot peninsula are visible for every case, with D90O10 and D80O20 showing more points in this region than the other blends. This indicates that soot is likely to be formed at around 2°aTDC. When looking at later instants, it is possible to see that an increase in the oxygenated fraction reduces the EQ field inside the soot peninsula. For example, when looking at the 5°aTDC case, it can be observed that D50O50 is not reaching EQ values above 2, while less oxygenated blends exceed 2.

To get more clearer insight, a comparison of accumulated mass versus the equivalence ratio range for each blend at two instants is plotted in Figure 4.15. The y-axis range has been limited to allow a more accurate interpretation of

results corresponding to higher EQ values. It is quite evident that in the case of blends having less OME_x in them, the accumulated mass quantity is displaced to equivalence ratios above 2. This is true for both 2°aTDC and 5°aTDC. So, these maps confirm that even though all blends end up in the soot peninsula as seen in Figure 4.14, the amount of fuel present at EQ above 2 is higher for blends having less OME_x in them. So, these less oxygenated blends are likely to form soot.

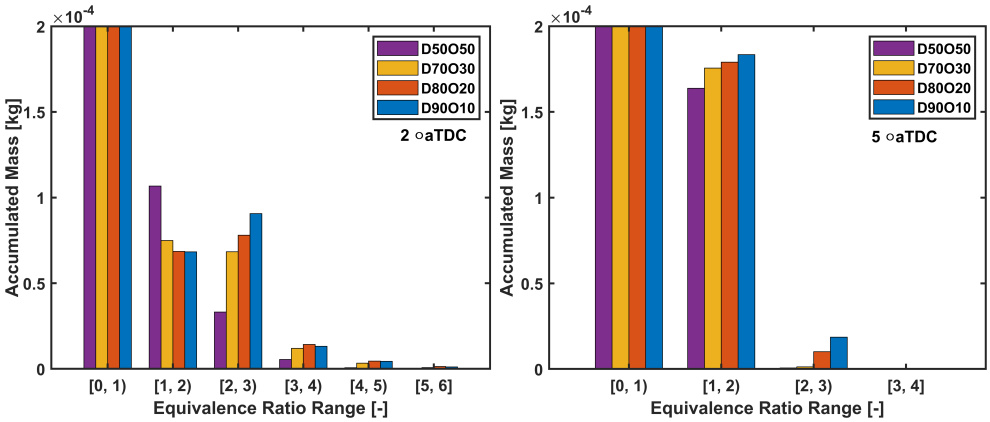

Figure 4.15: Equivalence ratio vs Accumulated mass Maps for Diesel-OME_x blends.

- **OH Distributions**

The OH radical is considered as a good tracer of high-temperature oxidation reactions. Its spatial distribution identifies the regions where oxidation is taking place. For this reason, it has been decided to investigate the evolution of this radical. In the first approach, Figure 4.16 (a) represents the accumulated OH mass inside the combustion chamber obtained by CFD for each blend. This data should be comparable with the OH* accumulated intensity in Figure 4.16 (b) presented by Pastor et al. [1]. It is possible to see that until 5°aTDC all the fuels provide a similar amount of OH mass which is corroborated by the OH* radiation. However, differences appear after 5°aTDC when a decrease of the OME_x content in the blend results in an increase of the in-cylinder OH mass (D90O10 and D80O20 show rather similar peak OH mass). This is observable with the CFD data but not with experiments. In fact, until 15°aTDC, the second source shows a different trend. However, it was stated by the authors of the experimental work that at this stage of combustion

(interval delimited by the dotted rectangle) the soot peak was reached and the images were contaminated by soot radiation [1]. The OH content starts decreasing earlier for D50O50 and the lesser content of OME$_x$ in the blend seems to delay it more. This results in a sooner disappearance of OH from the combustion chamber, which is coherent with the faster combustion process that was previously mentioned. After 15°aTDC, experimental data provide again a similar trend among the blends as CFD (once soot radiation is not so intense) showing a sooner decay of the signal when the OME$_x$ content is increased. Only experimental D50O50 shows a different behaviour, which has been already discussed in the previous section.

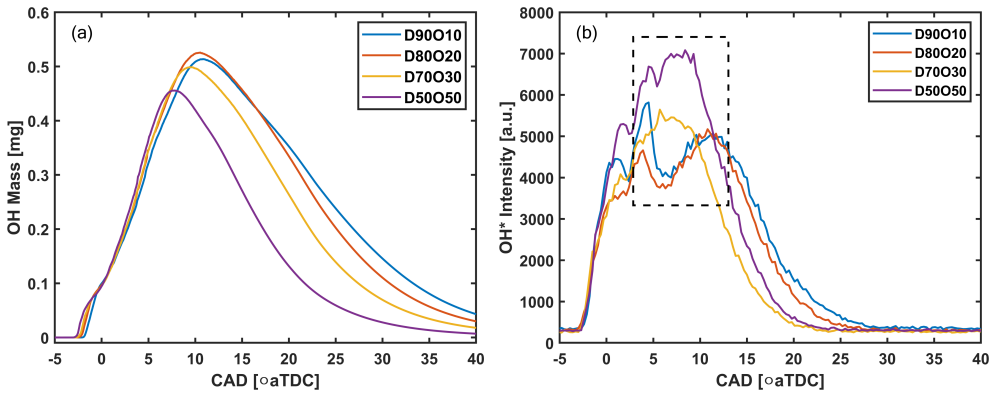

Figure 4.16: In-cylinder accumulated OH mass from numerical simulations (a) and experimental accumulated OH radiation (b) for Diesel-OME$_x$ blends.*

To analyse in more detail how the OH radical is distributed within the combustion chamber, Figure 4.17 represents the spatial distribution of this radical obtained with numerical simulations. The represented data corresponds to the accumulated OH mass between the piston and the head surfaces, for all the blends at different instants. Notice that here again only a quarter of the combustion chamber has been represented to match the field of view reported in [1]. The inner dashed line represents the limit of the field of view of the OH* chemiluminescence experimental visualization, the middle dashed line represents the piston bowl radius and the outer dashed line represents the piston radius.

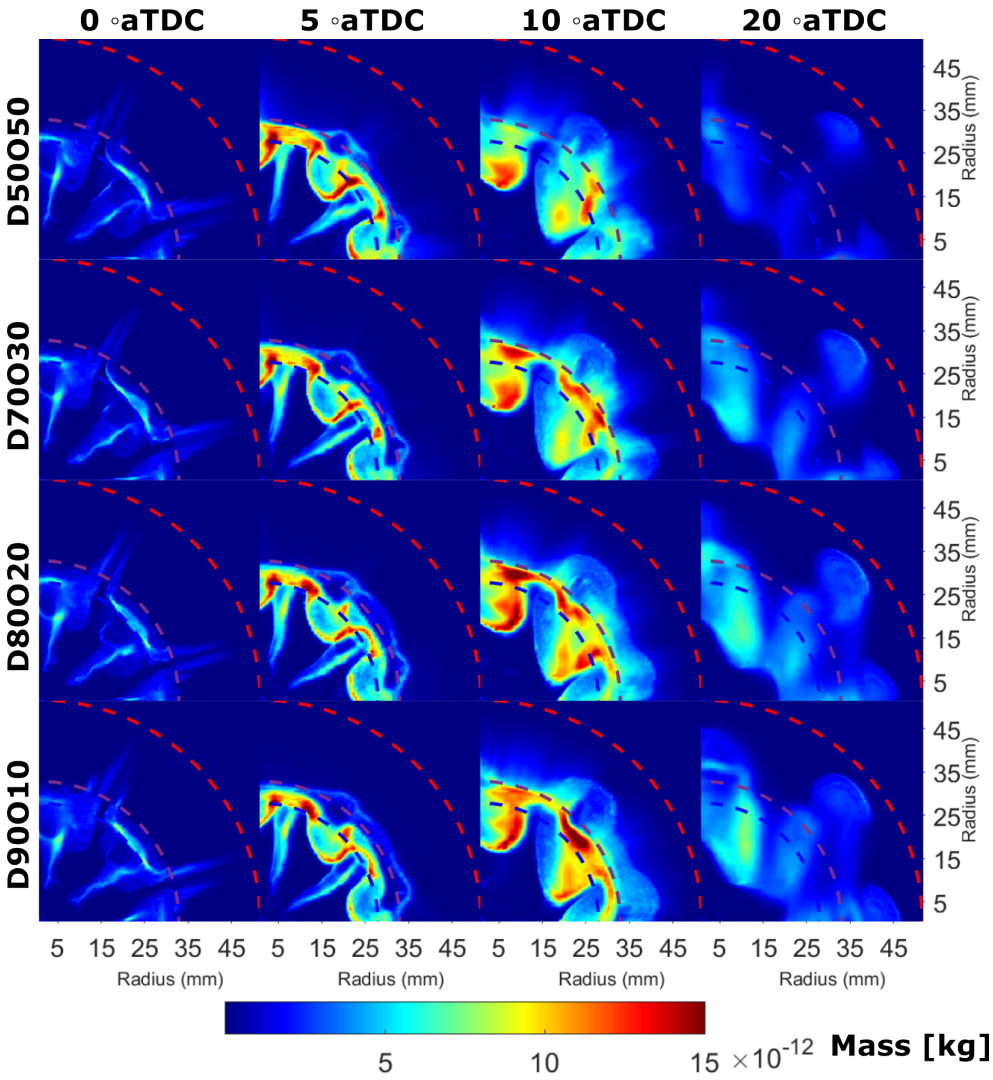

Figure 4.17: Numerically calculated accumulated OH mass distribution inside the combustion chamber for Diesel-OME$_x$ blends

At the first instants, OH seems to be accumulated close to the periphery of the bowl, which was also observed in the OH* chemiluminescence images from [1]. Moving further, at 10°aTDC significant differences start to appear among blends. D50O50 shows spots of lower OH mass close to the bowl wall while this is not observable for the rest of the blends. Besides, in general,

the OH field of this blend is lower than the rest. This can be related to the different equivalence ratio distributions reported in Figure 4.15. Those spots correspond to the regions where EQ was close to 1. The sooner disappearance of OH observed in Figure 4.16 is also visible here.

At 20°aTDC, the major part of OH has disappeared for D50O50 and only small isolated clouds remain. In contrast, the other blends still show larger clouds of higher OH mass which take longer to disappear. For these fuels, the OH clouds seem to evolve from regions where EQ reached the higher values in previous instants, e.g. 5°aTDC. However, for D50O50 they seem to evolve from regions where EQ was significantly below 1.

Considering all the above mentioned, there is a relation between the blend composition, the EQ distribution and the OH distribution. The more OME_x in the blend results in a lower EQ field, thanks to its different stoichiometry (the oxygen content). D90O10, D80O20 and D70O30 provided regions of EQ close or higher than 2 even at 5°aTDC. However, at this stage for D50O50, EQ is lower and closer to 1. This promotes more oxidation in comparison with the other blends, which results in a faster combustion completion (see Figure 4.11 and Figure 4.12 and a sooner OH disappearance.

4.2.2.2 Emissions Analysis

- **Soot Formation**

As has been already mentioned in the previous paragraphs, the different EQ fields obtained by each blend will have an impact on soot formation. To analyse this, Figure 4.18 shows the net amount of soot formed (a), the amount of soot produced (b), the amount of soot oxidized (c) and its percentage in relation to the total soot produced (d). The net amount of soot formed is the difference between the soot produced and oxidized. These values correspond to numerical simulations where the Hiroyasu model is utilized to model soot formation as described earlier in section 3.4

As it can be observed, with the increase of OME_x in the blend, the amount of soot produced decreases while the proportion of soot that is being oxidized increases. This agrees with the EQ-T maps presented in Figure 4.14, where it was observed that the less OME_x content resulted in a larger number of points within the soot peninsula at 2°aTDC. In fact, this is the instant when the soot production starts to increase faster for the blends with the lower OME_x fraction. Later, at 5°aTDC, the EQ values decrease (see Figure 4.14) for all the fuels and the soot production stops and oxidation becomes dominant. The lower EQ field provided by D50O50 allows it to oxidise the soot faster than the

other blends as in can be seen in Figure 4.18 (d). Besides, the results also show that the effectiveness of oxidizing soot increases with the OME_x content which is consistent with the progressive decrease of EQ values observed previously.

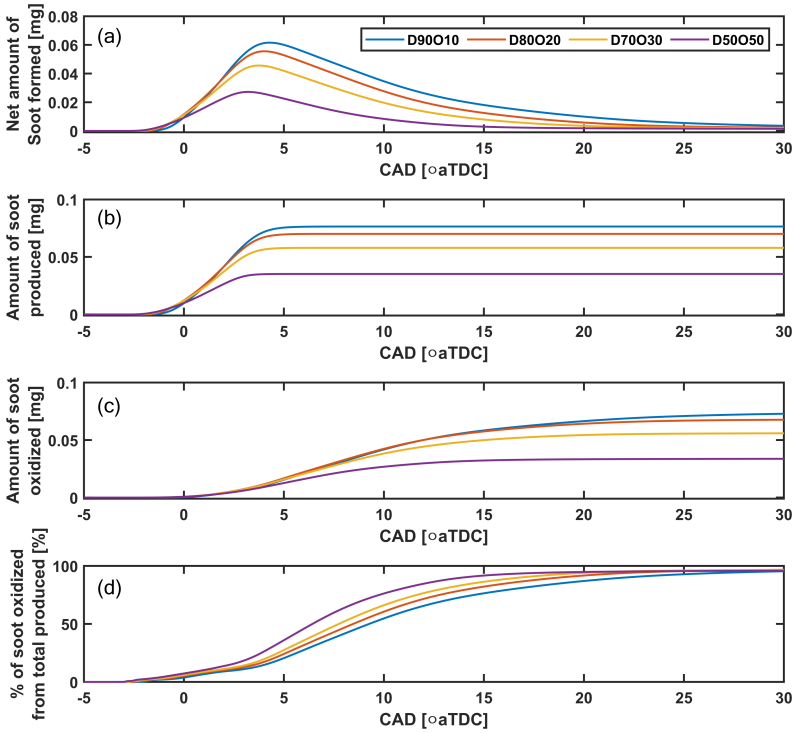

Figure 4.18: Evolution of the net amount of soot formed (a),the amount of soot produced (b), the amount of soot oxidized (c), and the percentage of soot oxidized from the total produced (d) for Diesel-OME_x blends.

The spatial distribution of soot is presented in Figure 4.19, where the net soot formed inside the combustion chamber is shown. Data corresponds to the accumulation of soot mass between the piston and the head surface. Only a quarter of the combustion chamber has been represented as in Figure 4.17. These distributions show that at the beginning (close to TDC) the soot distribution is similar for all blends. At 2°aTDC differences appear, as stated previously. In all the cases, soot is mainly formed near the bowl walls which correlates with the experimentally obtained high-speed natural luminosity images found in [1]. Besides, it corresponds with the regions of higher EQ values in Figure 4.13.

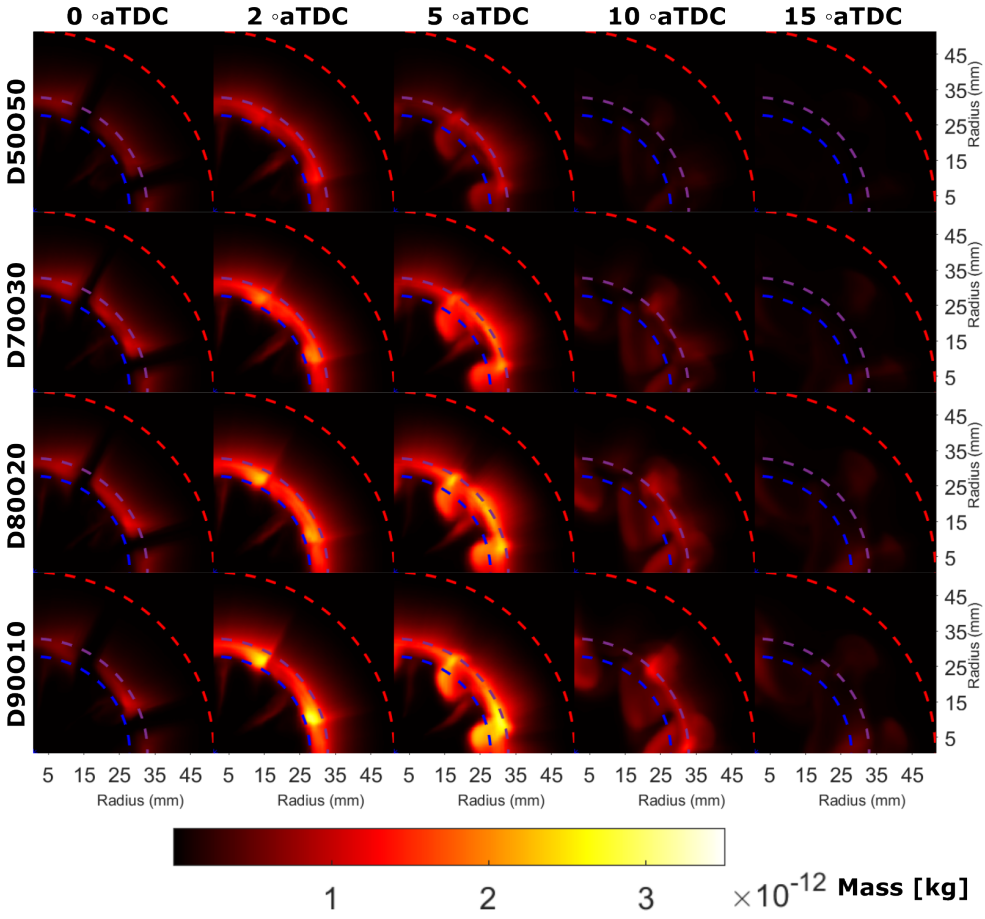

Figure 4.19: Numerically calculated accumulated soot mass distribution inside the combustion chamber for Diesel-OME$_x$ blends

The differences among blends are then mostly related to the amount of soot but not with its distribution. When combustion progresses, it can be seen for D70O30, D80O20 and D90O30 that soot clouds move towards the piston center while this is not visible for D50O50. This can be related to the fact that, due to the air and spray dynamics, the flames are pushed towards this region. As soot lasts longer when the OME_x content is decreased, these clouds are able to travel longer distances while for the last blend i.e. D50O50 they disappear before the other three blends.

- **NO_x Formation**

To model the NO_x formation, as mentioned in section 3.4, the extended Zeldovich model was utilized. Figure 4.20 shows the net NO_x mass produced for each blend along with the maximum in-cylinder temperature. D90O10 and D80O20 show similar levels of NO_x. In general, a 50% addition of OME_x content in the blend reduces the NO_x emissions by almost 30%.

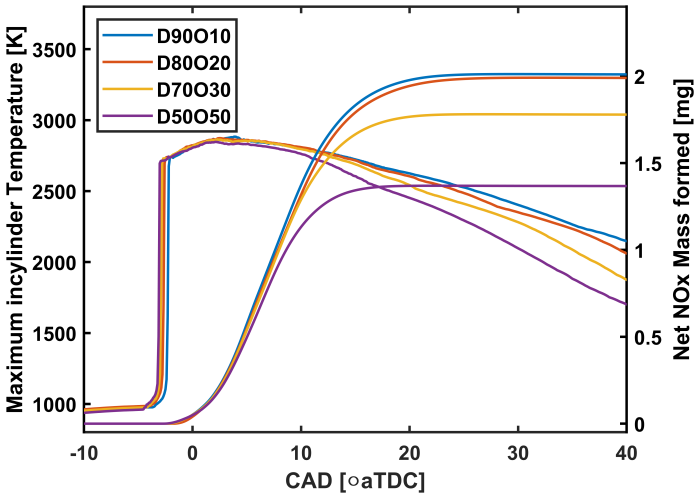

Figure 4.20: Numerically obtained net NO_x mass and maximum in-cylinder temperature for Diesel-OME_x blends.

The NO_x emissions are generally related to the maximum in-cylinder temperature reached inside the combustion chamber. Thus looking at Figure 4.20 an evolution of the maximum temperature values reached for each blend shows the decrement of maximum temperature, as the percentage of OME_x in the blend rises from 10 to 50%. This temperature reduction is particularly evident between 10°aTDC to 20°aTDC, where the NO_x formation differences also appear among blends. Hence, it can be said that the addition of OME_x in the blend reduces the maximum temperature reached inside the cylinder, which contributes to NO_x reduction. However, some authors report that the addition OME_x in diesel infact doesn't significantly affect the NO_x emissions [7]. Hence, these values reported should be validated via experimental data from an actual engine running on Diesel-OME_x blends.

4.2.2.3 Discussion

One of the disadvantages the OME$_x$ blending presents is that it decreases the total LHV of the blend, which in turn leads to a reduction of energy injected into the cylinder. Therefore, it has been decided to compare the maximum energy released by each blend with the maximum net soot and NO$_x$ mass formed along with the corresponding percentages of reduction with respect to D90O10. All this information is summarized in Figure 4.21.

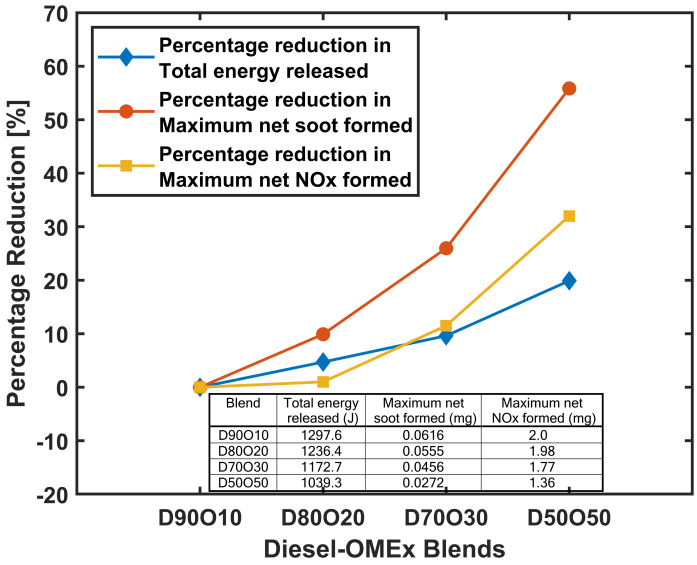

Blend	Total energy released (J)	Maximum net soot formed (mg)	Maximum net NOx formed (mg)
D90O10	1297.6	0.0616	2.0
D80O20	1236.4	0.0555	1.98
D70O30	1172.7	0.0456	1.77
D50O50	1039.3	0.0272	1.36

Figure 4.21: Percentage reduction in total energy released, maximum net soot formed, and maximum net NO$_x$ formed w.r.t D90O10 for Diesel-OME$_x$ blends.

The percentage of reduction of soot formation increases sharply when the blend contains 70% or more OME$_x$ in it. At first, it can be seen that there is almost no difference between D90O10 and D80O20, although, in comparison, the D50O50 blend produces almost 56% less soot than D90O10. This reduction for NO$_x$ formation stands at 32%. However, when looking at the total energy released reduction, the variation is much lower. Between D90O10 and D50O50, only 19.9% of reduction was obtained. It must be considered that based on the experimental data, more fuel mass was injected with D50O50 which compensated for part of the expected energy loss. In terms of LHV, the difference should be close to 24%. Thus, it can be concluded that reductions in soot formation of up to 50% and NO$_x$ formation of up to 30% would only require modifying injection strategy to compensate for a 19% of energy loss.

4.3 HVO-OME_1 Blends

The detailed literature review and the advantages achieved in terms of using HVO and OME_1 in CI engines have been discussed in detail in section 2.3. For this reason, different blends of HVO-OME_1 blends have been utilized in the context of this thesis in order to combine the advantages both from HVO, which has similar physical properties as diesel, and from OME_1 which is an oxygenated fuel. Specifically, the blends of HVO with OME_1 ranging from 0% to 30% have been utilized. These different blends are identified as neat HVO (H100), H90M10, H80M20 and H70M30. The OME_1 fraction in blends has been limited up to 30% owing to both energy reduction caused by the lower LHV of this fuel and its high volatile characteristics as discussed in chapter 3.

4.3.1 Fuel Definition and Mechanism development

In contrast to the work performed related to Diesel-OME_x blends, where different chemical mechanisms were already available in the literature, in this current case, no chemical mechanism existed in the literature that could be utilized to perform detailed numerical simulations of HVO-OME_1 blends. Hence, it was necessary to develop a reaction mechanism from scratch that could be utilized for this purpose. Following a similar approach, primarily surrogates are identified for utilized fuels, and then individual mechanisms are selected based on the surrogate definition. These are further combined to form a combined reaction mechanism that is used to perform simulations for the said blends.

4.3.1.1 n-Dodecane as HVO surrogate

HVO is a complex blend of different paraffin molecules. Thus, to be able to simulate its behavior, a more simple surrogate fuel was defined. This has been a common practice in literature with other fuels with similar characteristics, such as in the case of Diesel–OME_x blends, n-heptane was used as a surrogate for diesel. For this work, neat n-Dodecane was proposed as a surrogate fuel for HVO. This proposal is based on two arguments. The first one is that n-Dodecane belongs to one of the most abundant molecular classes within HVO [41]. Therefore, both present certain similarities in terms of physical and chemical properties (see Table 3.2). The second one is the high similarities experimentally observed between them. Pastor et al. [42] reported that both fuels exhibit similar combustion characteristics like ignition delay, lift-off length, and spray tip penetration under well-controlled spray vessel operating conditions. Hence, with the experimental setup defined in the section 3.3,

tests were performed for both these fuels to extend these conclusions to an engine application utilizing optical setup A (see Figure 3.2) and operating conditions mentioned in Table 4.1.

The comparison can be started by analyzing the combustion process, through the HRR. Figure 4.22 depicts that only minor differences can be observed between them. The ID is very similar, which is represented by the same start of the HRR curve. Besides, the development of both the premixed and diffusion phases is very similar. In contrast, when looking at the integrated heat release rate (IHRR) a difference of 0.8% between both fuels is observed. This can be related to the higher LHV of n-Dodecane as compared to HVO, as reported previously in Table 3.2. However, based on this, only a difference of 0.35% between both fuels should be expected. Therefore, additional effects like different injection durations (for the same injection strategy) could be taking place due to the different viscosity among them. Nevertheless, this seems to not have an impact on combustion progression.

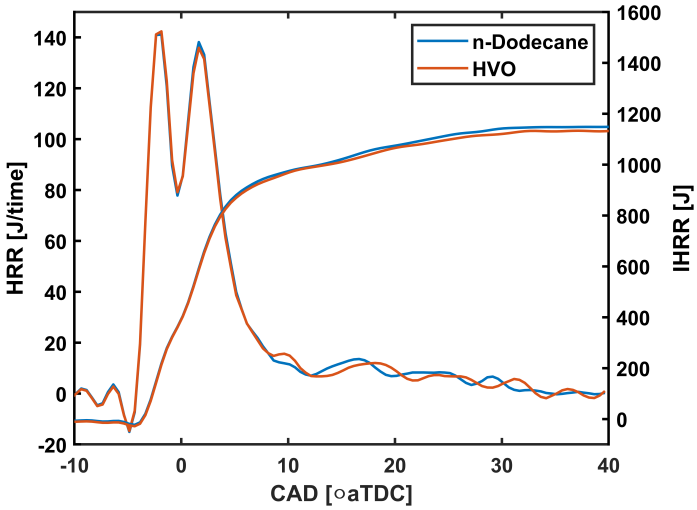

Figure 4.22: Experimentally measured HRR and IHRR for n-Dodecane and HVO.

To get a deeper insight into the combustion characteristics of these two fuels, the NL signal can be analyzed as an indicator of soot distribution. For this purpose, NL maps for both HVO and n-Dodecane have been constructed utilizing the methodology depicted in Figure 3.8. Figure 4.23 shows these NL maps.

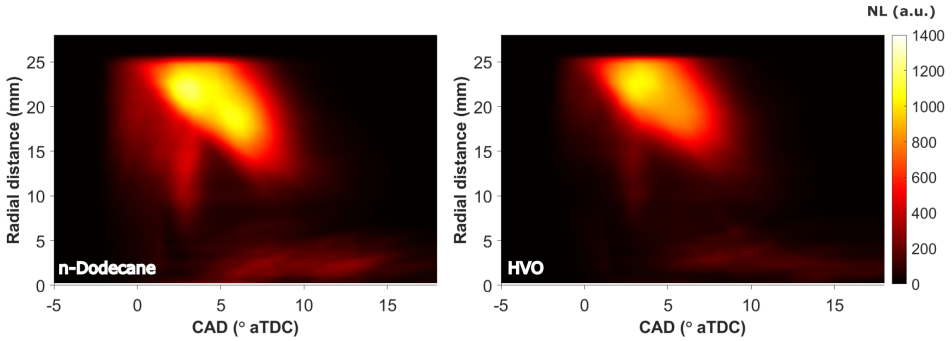

Figure 4.23: 2D NL experimental maps of n-Dodecane and HVO.

When compared, similarities can be observed in terms of soot evolution. Its formation starts from the periphery of the bowl and extends slowly towards the center. The region of highest NL radiation (and presumably soot) during the diffusion phase (between 0 and 5°aTDC) is located close to the periphery of the flame and extends some millimeters towards the center of the bowl at the late combustion stage. However, some differences can be observed too. The maximum intensity of the NL signal from n-Dodecane is 14% higher in comparison to HVO. Besides, the signal reaches a region closer to the injector.

The comparison of both fuels presented by Pastor et al. [42] under a variety of operating conditions confirms that the relative behavior between both fuels was not substantially altered. In this case, these authors reported that HVO produced slightly more soot than n-Dodecane. Nevertheless, the differences found between them were much more reduced than those found when comparing both fuels with fossil diesel.

Therefore, considering all the above mentioned, n-Dodecane is proposed as a surrogate of HVO. However, regarding soot formation, it must be considered that it could be slightly overpredicted as certain fuel properties could impact the mixing process, the equivalence ratio achieved, and the later soot formation.

4.3.1.2 n-Dodecane sub-mechanism

After proposing n-Dodecane as a surrogate fuel for HVO, a literature review was done to find the most appropriate n-Dodecane mechanism suitable for 3D CFD simulations. Two skeletal mechanisms were selected among the numerous mechanisms that are available in the literature: the one of Yao et al. [43] and

the one of Wang et al. [44] (which includes PAH chemistry to enable soot predictions). Other mechanisms include that of Lawrence Livermore National Laboratory [45] (2885 species), Narayanaswamy et al. [46] (225 species), and Cai et al. [47] (1692 species) which were not utilized in this study due to their large size in terms of number of species and reactions. Table 4.5 summarizes the reaction mechanisms of n-Dodecane tested in this investigation, including the number of species and reactions in them.

Table 4.5: Details of n-Dodecane reaction mechanisms utilized.

Mechanism	**Number of species**	**Number of reactions**
Yao [43]	54	269
Wang [44]	100	432

Ignition delay calculations over a wide range of conditions were performed with both Yao's and Wang's mechanisms following the methodology described in section 3.4, and results were compared against experimental data taken from literature [48]. Figure 4.24 shows the ignition delay as a function of the inverse of temperature for experiments and simulations at a pressure of 20 bar and an EQ of 1.0. Yao's mechanism shows a better agreement with experimental values than Wang's mechanism, especially at the medium and low temperatures important for spray ignition. These results are consistent with those of Payri et al. [49], who also preferred Yao's mechanism due to its shorter ignition delay at temperatures lower than 1000 K compared to other mechanisms. Moreover, Desantes et al. [50] evaluated seven different n-Dodecane mechanisms by comparison against experimental rapid compression-expansion machine ignition delay data, concluding that Yao's is the most accurate mechanism among those with less than 1000 species. Finally, Yao's mechanism is more compact than Wang's, which makes it a more suitable choice for CFD simulations.

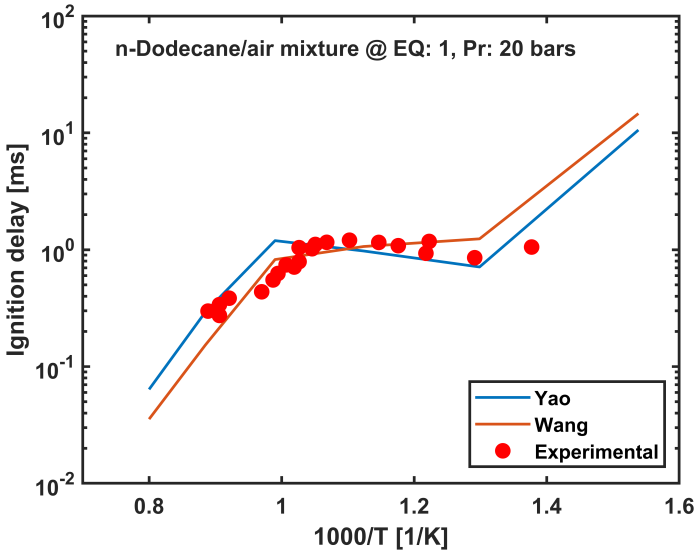

Figure 4.24: Numerical and experimental ignition delay of n-Dodecane/air mixture at a pressure of 20 bar and equivalence ratio of 1.0.

4.3.1.3 OME_1 sub-mechanism

Only a few chemical mechanisms for OME_1 can be found in the literature. Two different mechanisms were tested in this study, and they are summarized in Table 4.6. First, Ren et al. [5] developed a Primary reference fuel-oxymethylene dimethyl ethers mechanism for engine applications. Although the ignition delay of pure OME_1 was not considered during the mechanism development procedure, it contains the chemistry of this molecule, so it was evaluated in this study. Second, the comprehensive mechanism for OME_1 developed by Jacob et al. [51] was tested, which includes a detailed description of both the low and high-temperature oxidation processes of OME_1.

Table 4.6: Details of OME_1 reaction mechanisms utilized.

Mechanism	Number of species	Number of reactions
Ren [5]	145	585
Jacob [51]	530	2889

Figure 4.25 shows the ignition delay of OME_1 versus the inverse of temperature obtained with both Ren's and Jacob's mechanisms at a pressure of

20 bar and an equivalence ratio of 1.0. Experimental data from [51] was also included in the figure. Results show that Jacob's mechanism reproduces the experimental measurements with high accuracy. Unfortunately, Jacob's mechanism is too large to be implemented in 3D CFD engine simulations, since it would lead to a prohibitive computational cost. For this reason, it was decided to reduce Jacob's detailed mechanism.

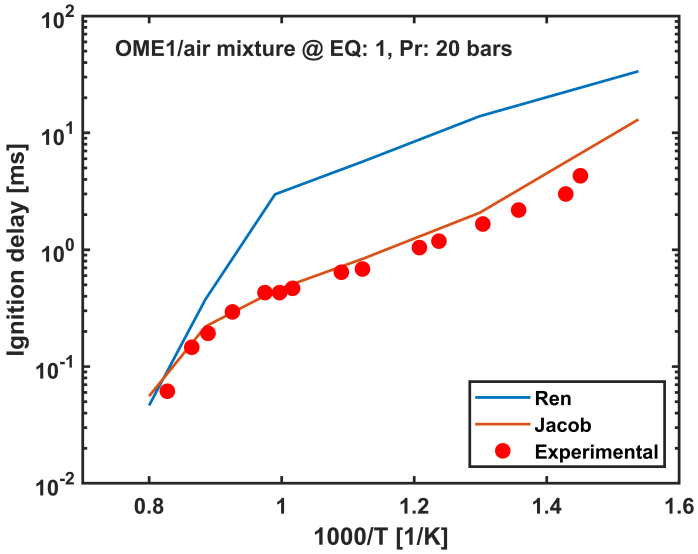

Figure 4.25: Numerical and experimental ignition delay of OME$_1$/air mixture at a pressure of 20 bar and equivalence ratio of 1.0.

Jacob's mechanism reduction is based on a large dataset of ignition delay data calculated in an adiabatic, closed, constant-volume, homogeneous reactor at the following conditions:

- Pressure variation: 50, 60, and 75 bar.
- Temperature variation: from 500 K to 1100 K.
- Equivalence ratio variation: from 0.2 to 5.0.
- Oxygen concentration variation: 21% and 15% (N_2 dilution) in mole basis.

Note that the test matrix derived from the above parametric ranges covers the typical conditions of ignition for fuel sprays in compression-ignition

engines. The reduction techniques described in section 3.4 were utilized here. DRGEP was applied to reduce Jacob's mechanism. During the iterative process, ignition delay was used as the target parameter with a relative tolerance of 20%. Special attention was paid to the chemistry OH, CH_2O and C_2H_2 as they are representative of fuel's exothermicity, fuel's low-temperature chemistry and soot formation, respectively, which are important parameters for the analysis of combusting sprays. The resulting reduced mechanism consisted of 285 species and 1695 reactions. Then, the DRGEP with sensitivity analysis (DRGEPSA) method was used to further reduce the mechanism with the same targeting settings described above, resulting in a skeletal mechanism that consisted of 91 species and 505 reactions (hereafter referred to as SNL mechanism named after Sandia national laboratories).

Figure 4.26 shows a comparison between Jacob's and SNL mechanisms. More specifically, the ignition delay and peak concentrations of OH, CH_2O, and C_2H_2 for OME_1 autoignition are shown at 50, 60, and 75 bar and 15% O2. In contrast to the work with Diesel-OME_x blends, where species concentration validations were carried out using the CHEMKIN premixed model, to replicate experimental data of burner, in this case, the validations were carried out using the CHEMKIN homogenous reactor model. The results were compared between detailed Jacobs and reduced SNL mechanism due to the unavailability of experimental data for OME_1. Calculations were performed at several temperatures–equivalence ratio combinations representative of the temperature distribution that could be found in a fuel spray. They were estimated by a 1D spray model described in [52]. Thus, leaner conditions have higher temperatures and vice versa. It must be noted that the 1D spray model used here is only confined to the mechanism validation part. This 1D model has been extensively used in literature [53–55]. It is based on assuming an adiabatic mixing between fuel and air where each equivalence ratio is related to only one temperature value. The SNL mechanism shows a very good agreement with Jacob's mechanism at all these conditions.

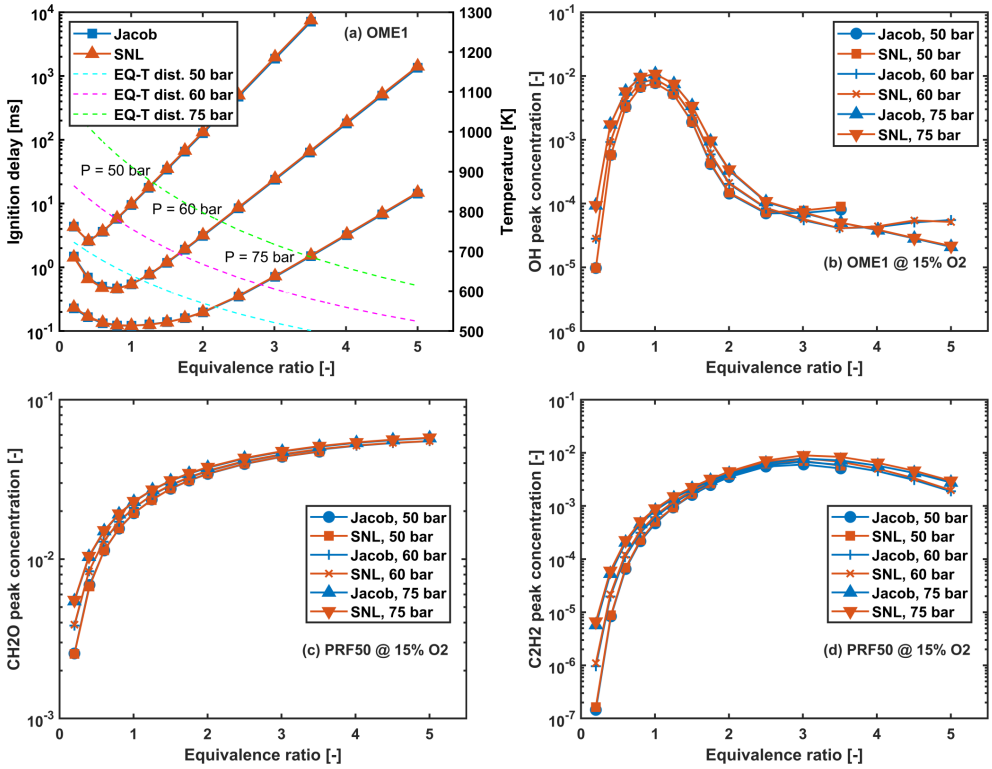

Figure 4.26: Ignition delay (a) and maximum concentration of OH (b), CH_2O (c) and C_2H_2 (d) obtained with Jacob's (blue) and SNL (orange) mechanisms for OME$_1$ at 15% O_2 condition and different pressures.

Figure 4.27 shows the ignition delay of OME$_1$ versus the inverse of temperature experimentally obtained from [51] and obtained numerically with both Jacob's and SNL mechanisms at a pressure of 20 bar and an equivalence ratio of 1.0. Results show that the SNL mechanism reproduces both Jacob's mechanism and the experiments with high accuracy.

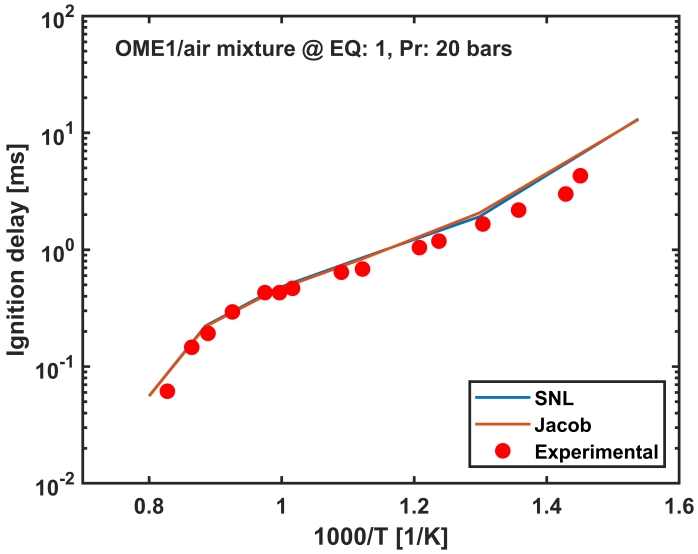

Figure 4.27: Numerical and experimental ignition delay of OME_1/air mixture at a pressure of 20 bar and equivalence ratio of 1.0.

4.3.1.4 Mechanism Merging

To have a single mechanism for n-Dodecane and OME_1 blends, Yao's mechanism for n-Dodecane and SNL mechanism for OME_1 were merged using the Ansys CHEMKIN Pro merging tool [20]. Yao's mechanism was chosen as the master mechanism and SNL as the doner mechanism with preference given to retaining the master mechanism thermodynamic data. The final mechanism, namely the Yao-SNL mechanism, consists of 121 species and 678 reactions. Experimental data from [48], which includes ignition delay data of a blend of 35% OME_1 and 65% n-Dodecane by volume at a pressure of 20 bar and an equivalence ratio of 1.0, were used to validate the Yao-SNL mechanism. Figure 4.28 depicts the simulated ignition delay behavior of the merged mechanism in comparison with experimentally obtained data. Except at low temperatures, the merged mechanism behaved in accordance with the experimental data. This is likely because the radical consumption ratio between the two fuels during the low-temperature regime is not well captured by the mechanism. To solve this issue, the Yao-SNL mechanism was optimized in this study.

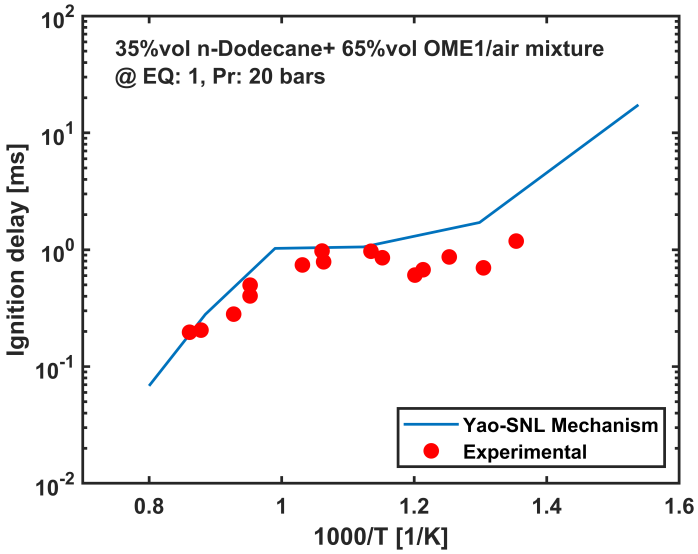

Figure 4.28: Numerical and experimental ignition delay of the blend of 35%vol OME$_1$ and 65%vol n-Dodecane with air at a pressure of 20 bar and equivalence ratio of 1.0.

4.3.1.5 Mechanism Optimization and Validations

As mentioned before, the Yao-SNL mechanism exhibited longer ignition delays than experimental data at lower temperatures, likely because the radical consumption ratio between OME$_1$ and n-Dodecane was not well captured by the mechanism. Results suggest that, at low-temperature conditions, OME$_1$ captures more radicals than expected, reducing the number of radicals available for n-Dodecane ignition and, therefore, decreasing the overall reactivity of the fuel blend. Therefore, an optimization was needed to obtain a combined reaction mechanism that behaves according to the experimental data. For this purpose, first a detailed sensitivity analysis was carried out to point out the reactions responsible for this delayed ignition observed at a low-temperature regime as seen in Figure 4.28.

The Arrhenius equation (Equation 3.16) represents the exponential relationship between reaction rate and temperature. In the equation, factor A known as the pre-exponential factor, represents the frequency of collisions and successful reactions between reactant molecules. During the optimization process, this parameter in the relevant reactions was adjusted. Furthermore, the necessary validations were carried out to have an optimized reaction mechanism that behaves in a similar way as experiments.

- **Optimization through Sensitivity analysis**

Sensitivity analysis for ignition delay was performed for the Yao-SNL mechanism at the same conditions as included in Figure 4.28 i.e., a blend of 35%vol. OME_1 and 65%vol. n-Dodecane with air at a pressure of 20 bar and an equivalence ratio of 1.0 with an addition of three different initial temperatures (700K, 900K, 1100K). Figure 4.29 shows the sensitivity coefficient for the 6 most sensitive reactions at three temperatures representative of different ignition regimes: 700K (low-temperature regime), 900K (Negative temperature coefficient (NTC) regime), and 1100K (high-temperature regime).

Based on the performance of the original mechanism as seen in Figure 4.28, it needs to be improved at low temperatures without largely modifying its performance at medium at high temperatures. Thus, optimization was applied to specific reaction rates of OME_1 + OH reactions, since at low temperatures, ignition becomes extremely sensitive to attack of OH radical present in the fuel [6, 7]. The ignition could also become sensitive to HCHO radicals, however as depicted in Figure 4.29, the reactions involving OH are more relevant at low temperatures (700K). Specifically, the focus was on the reactions that have high ignition delay sensitivity coefficients at low temperatures and much lower coefficients at medium and high temperatures. This happens for R1 and R2, which are dehydrogenation reactions of OME_1 (as highlighted in the Figure 4.29). For this reason, the pre-exponential coefficients of the specific reaction rates of R1 and R2 reactions were adjusted in an iterative process to minimize the deviation between the mechanism and the experimental data. The pre-exponential factors were reduced to make more OH radicals available for oxidation of n-Dodecane, compensating for excessively long ignition predictions at low temperatures.

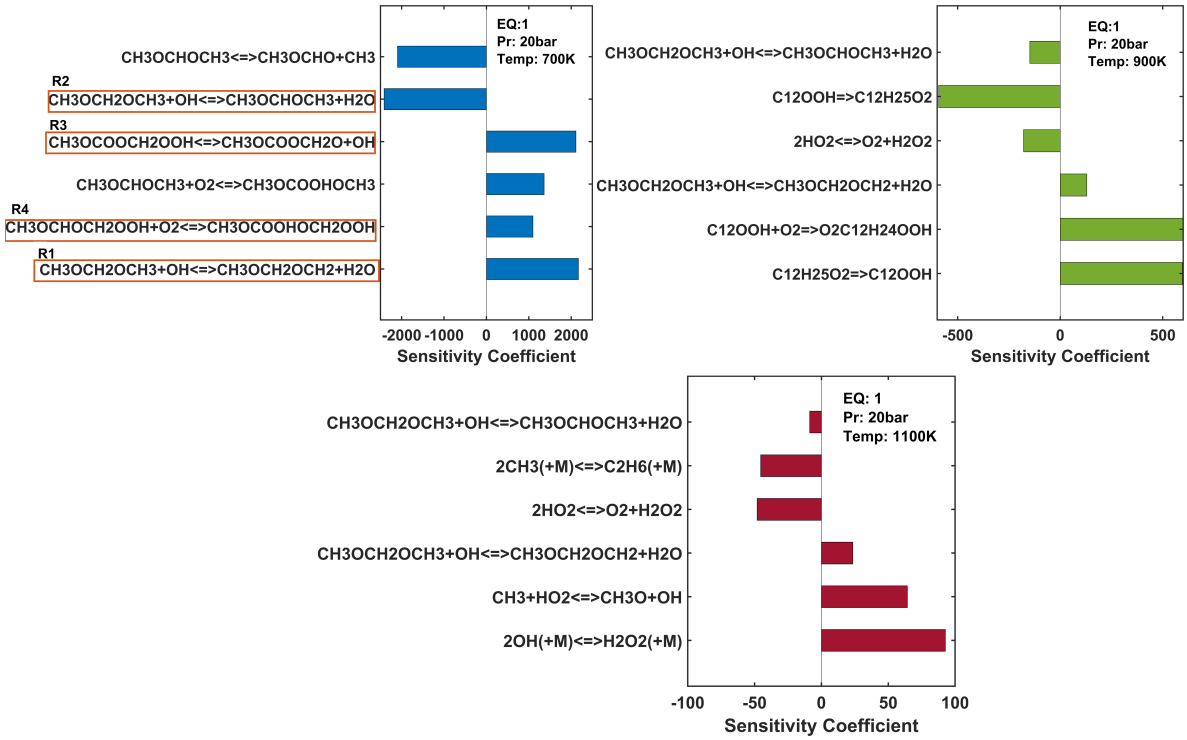

Figure 4.29: Sensitivity analysis for 35%vol OME$_1$ and 65%vol n-Dodecane mixture with air to ignition delay at an equivalence ratio of 1, the pressure of 20 bar and temperatures of 700,900 and 1100K.

Note that only the pre-exponential coefficients (A) were adjusted for each reaction, while it was not necessary to modify the temperature index and activation energy to obtain good results. However, by only modifying this, the pure OME$_1$ performance was affected. So, to accurately simulate pure OME$_1$, further improvement was made and the pre-exponential coefficients of R3 and R4 were also adjusted in an iterative procedure. This was done in order to make sure that the mechanism works both for single-component fuel and its blends. Table 4.7 summarizes the old and new pre-exponential coefficients of these 4 reactions.

Table 4.7: Modified Arrhenius rate constants.

Reaction Number	**Reaction**	A	n	$E_a(KJ/mol)$	**Modified** A
R1	CH3OCH2OCH3+OH= CH3OCH2OCH2+H2O	6.06×10^1	3.49	-2.20$\times 10^3$	6.06$\times 10^0$
R2	CH3OCH2OCH3+OH= CH3OCHOCH3+H2O	1.41×10^4	2.72	-1.24$\times 10^3$	1.41×10^2
R3	CH3OCOOCH2OOH= CH3OCOOCH2O+OH	2.0×10^{16}	0.0	4.20×10^4	5.0×10^{15}
R4	CH3OCHOCH2OOH+O2= CH3OCOOHOCH2OOH	1.0$\times 10^0$	1.0	1.0$\times 10^0$	—
		PLOG/1.0$\times 10^{-3}$ 3.36$\times 10^{18}$	-3.37	-4.294$\times 10^3$/	PLOG/1.0$\times 10^{-3}$ 2.69$\times 10^{19}$
		PLOG/1.0$\times 10^{-2}$ 3.99$\times 10^{21}$	-3.95	-2.615$\times 10^3$/	PLOG/1.0$\times 10^{-2}$ 3.19$\times 10^{22}$
		PLOG/1.0$\times 10^0$ 3.39$\times 10^{28}$	-5.24	4.088$\times 10^3$/	PLOG/1.0$\times 10^0$ 2.71$\times 10^{29}$
		PLOG/2.0$\times 10^0$ 1.173$\times 10^{28}$	-5.0	4.512$\times 10^3$/	PLOG/2.0$\times 10^0$ 9.38$\times 10^{28}$
		PLOG/1.0$\times 10^1$ 8.25$\times 10^{24}$	-3.87	-4.29$\times 10^3$/	PLOG/1.0$\times 10^1$ 6.60$\times 10^{25}$
		PLOG/2.0$\times 10^1$ 8.91$\times 10^{22}$	-3.23	3.781$\times 10^3$/	PLOG/2.0$\times 10^1$ 7.13$\times 10^{23}$
		PLOG/5.0$\times 10^1$ 1.557$\times 10^{20}$	-2.35	2.908$\times 10^3$/	PLOG/5.0$\times 10^1$ 1.26$\times 10^{21}$
		PLOG/1.0$\times 10^2$ 1.629 $\times 10^{18}$	-1.73	2.21$\times 10^3$/	PLOG/1.0$\times 10^2$ 1.30$\times 10^{19}$

- **Ignition delay validations**

Figure 4.30 shows the ignition delays obtained by the application of optimized reaction mechanism for the case of pure OME_1 (a) pure n-Dodecane (b) and a blend of 35% vol OME_1 and 65% vol n-Dodecane (c). Note that this validation is not limited to only the mixture dataset on which optimization is applied. In fact, the other two datasets (pure n-Dodecane and pure OME_1) have also been utilized. It is possible to see that for the three cases, the newly optimized reaction mechanism performed accurately in accordance with experimental data. So, it can be said that the optimization worked quite well for both single-component fuels and the blend.

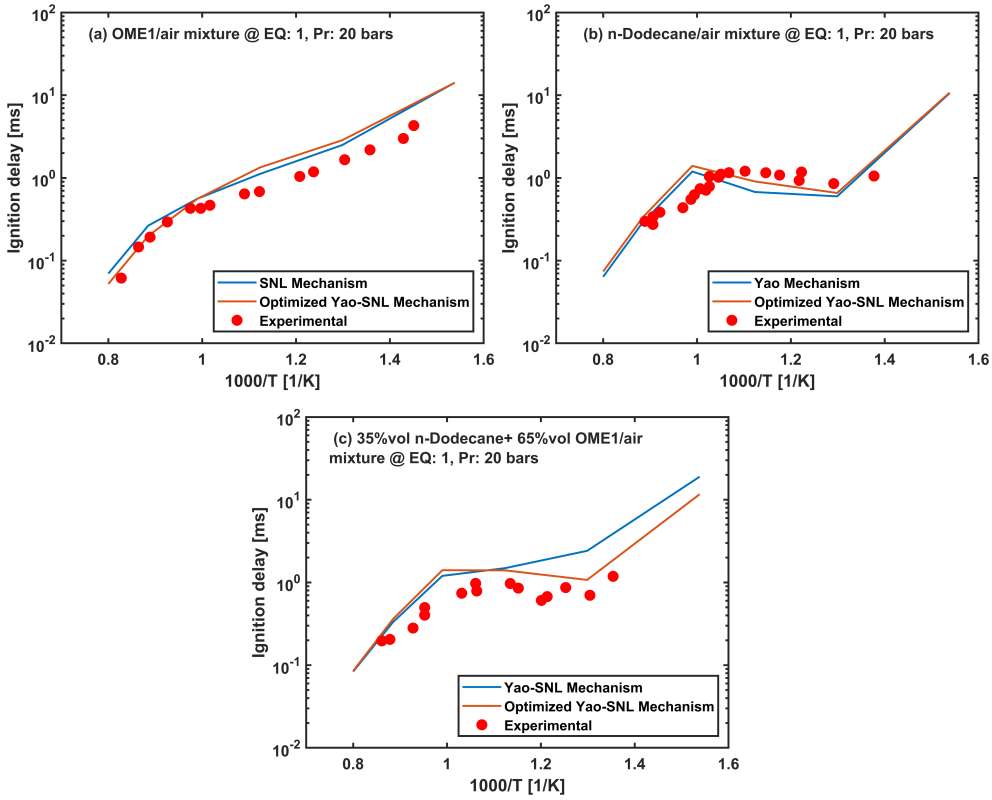

Figure 4.30: Numerical and Experimental ignition delay for OME_1/air (a) for n-Dodecane/air (b) for 35%vol OME_1+65%vol n-Dodecane blend with air (c).

- **Laminar flame speed validations**

The developed optimized Yao-SNL mechanism was also validated with regard to laminar flame speed predictions. Simulations were carried out utilizing a similar methodology as done for PRF-OME_x blends as described in the section 3.4.Figure 4.31 shows the flame speed analysis done (a) for the case of pure OME_1 and (b) for the case of n-Dodecane using the developed optimized Yao-SNL mechanism. For the case of n-Dodecane, 1D simulations were performed at a pressure of 1 atm and different initial temperatures of 403K and 470K replicating the experimental conditions available at [56]. Similarly, the experimental conditions of a pressure of 1 atm and two different initial temperatures of 298K and 358K from [57] were replicated for the case of pure OME_1. For the case of blends, simulations weren't performed due to the unavailability of experimental data. Nevertheless, it is possible to see that the numerical predictions are well in line with experimental data for both cases. Therefore, it can be stated that these validations are quite acceptable for engine-level applications.

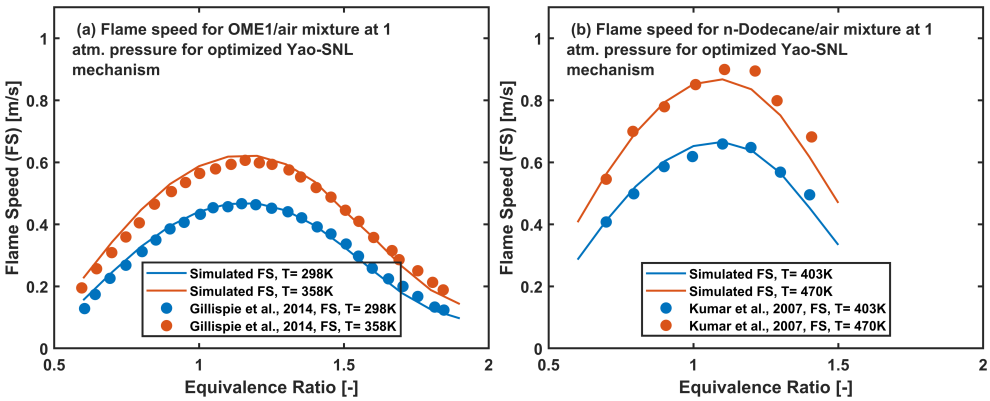

Figure 4.31: Numerically obtained laminar flame speeds alongside experimental data for the case of OME_1/air (a) and for n-Dodecane/air (b).

- **Species concentration profile validations**

Similar to Figure 4.26, here the validations are carried out for OME_1 between the detailed Jacobs OME_1 mechanism and the optimized Yao-SNL mechanism. The methodology utilized is the same as described while validating the reduced SNL mechanism when compared with the detailed Jacobs mechanism in Figure 4.26. Figure 4.32 shows the comparison of ignition delay and peak concentrations for the case of CH_2O, OH and C_2H_2 for OME_1

autoignition at three different pressures of 50,60 and 75 bar and 15% O_2 for Jacobs OME_1 mechanism and optimized Yao-SNL mechanism. The results show that the optimized Yao-SNL mechanism exhibits a very good agreement with Jacob's mechanism at all conditions. Small divergences appear related to OH peak concentration at larger equivalence ratios, which despite the differences, are still below 0.001 for the case of optimized mechanism.

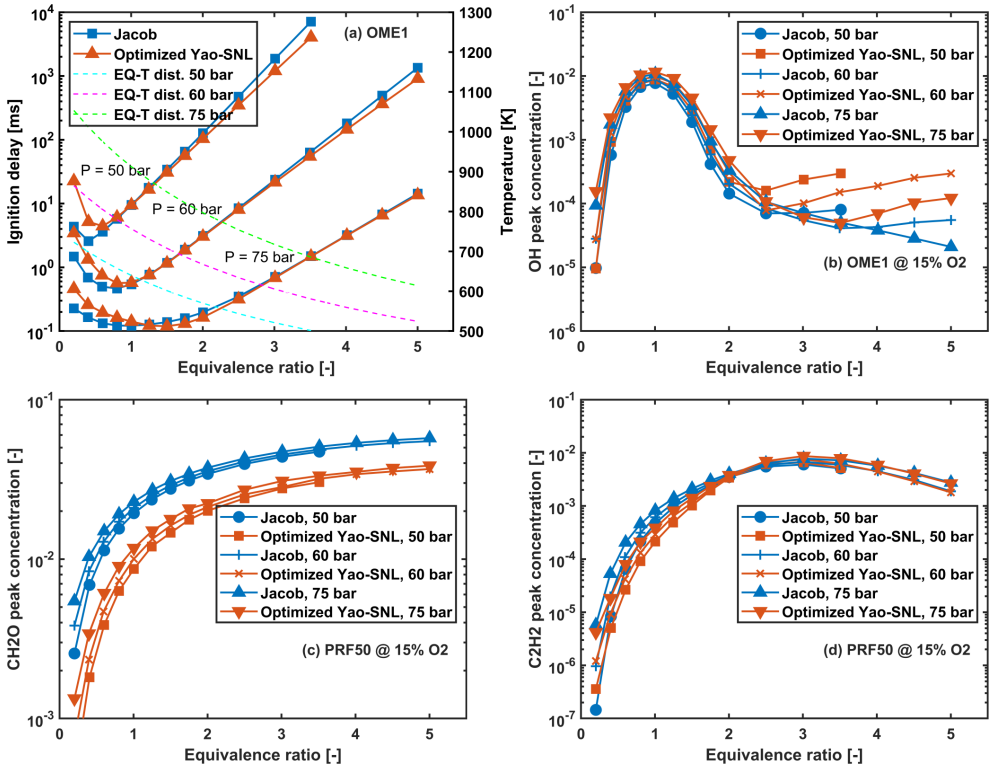

Figure 4.32: Ignition delay (a) and maximum concentration of OH (b), CH_2O (c) and C_2H_2 (d) obtained with Jacob's (blue) and optimized Yao-SNL (orange) mechanisms for OME_1 at 15% O_2 condition and different pressures.

These all validations including ignition delay, laminar flame speed, and species profile concentrations show the accuracy of the developed optimized Yao-SNL mechanism. Figure 4.33 summarizes the pathway followed in developing the optimized Yao-SNL mechanism.

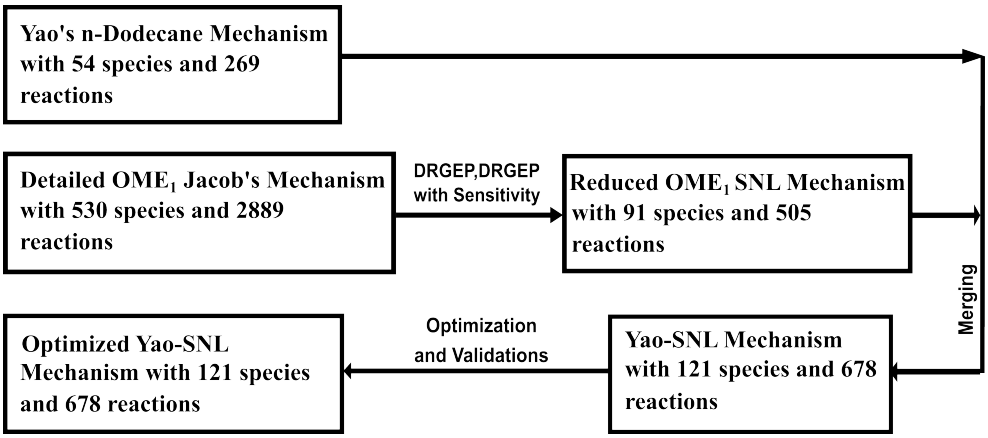

Figure 4.33: Pathway followed to develop Optimized Yao-SNL mechanism required for HVO-OME$_1$ blends simulations.

Hence in the proceeding section, the detailed analysis of HVO-OME$_1$ blends is carried out through 3D CFD simulations performed with the developed mechanism consisting of 121 species and 678 reactions.

4.3.2 Analysis of blends performed through numerical simulations

As described earlier, the developed optimized Yao-SNL mechanism was utilized to perform the 3D CFD simulations of blends of HVO-OME$_1$. The CFD model that has been utilized in performing simulations has been described in detail in the 3D CFD model development part of section 3.4. The operating conditions correspond to the one described earlier in section 4.1.

It must be taken into account that in doing the CFD simulations as established, n-Dodecane was used as a surrogate to model both the liquid and vapour phase of HVO and OME$_1$ was used to represent itself. Simulations were performed for pure HVO (H100), H90M10, H80M20, and H70M30 as described in the beginning. The analysis can be divided into two separate sections namely combustion characteristics and emissions analysis.

4.3.2.1 Combustion Characteristics

- **Ignition delay**

The simulation analysis can be started in chronological order of the events happening after the start of the injection. Figure 4.34 depicts the ignition delays obtained for both numerical and experimental cases. The ignition delay here is defined according to the same definition as done for Diesel-OME$_x$ blends, the time interval in crank angle degrees between SOI and SOC, where SOC is calculated according to the method documented by Rothamer and Murphy [35]. It is possible to see that an increment of OME$_1$ percentage in the blend increases ignition delay. This occurs both in the case of simulations and experiments with a slight difference among them. This confirms that the numerical simulations using the developed optimized reaction mechanism were able to replicate the blend's experimental behavior in this regard and reflects the improvement obtained by the optimization process applied to adjust the reaction mechanism. The increase in ID while increasing the OME$_1$ percentage in the blend can be related to many facts. Primarily, the blend's cetane number can affect the ID. As the percentage of OME$_1$ in the blend increases, its cetane number decreases because this fuel has a very low cetane number as compared to HVO (28 as compared to 75.5). This means that the reactivity of the blends is affected, in turn slowing down the ignition process.

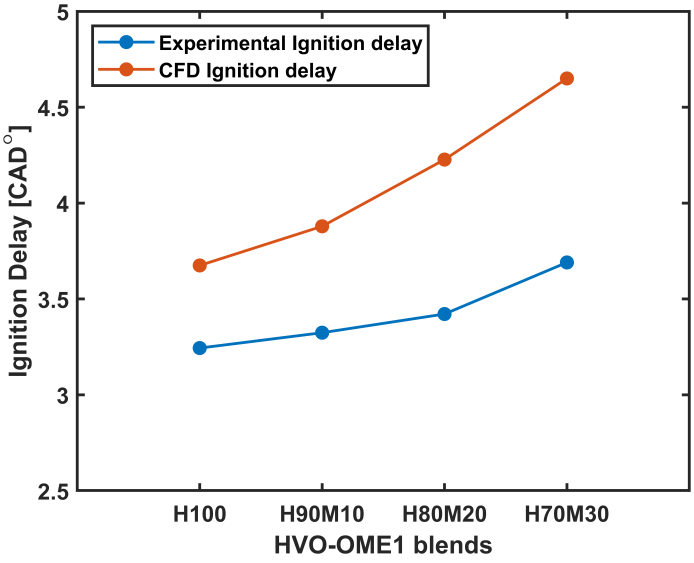

Figure 4.34: Numerical and Experimental ignition delay for HVO-OME$_1$ blends.

Furthermore, as can be seen in the properties of the fuels described in Table 3.2, a rather higher value of latent heat of evaporation (318.6 KJ/kg for OME_1 as compared to 256 KJ/kg for HVO) and a lower boiling point for OME_1, help lower the overall in-cylinder temperature hence leading to longer ignition delay. The same trends when adding OME_1 in diesel were observed by authors in [58]. Since HVO and diesel resemble a lot in physical properties, the established results for Diesel-OME_1 blends can be referred to validate current results. Hence, it can be stated that an addition of OME_1 progressively increases ID. In fact, when the OME_1 percentage in the blend raises from 0% to 30%, an increase of 26% in ignition delay is observed numerically.

- **Lift-off Length**

Lift-off length (LOL) is an important parameter to analyze the combustion behavior because it affects the quality of the air-fuel mixing process before initial combustion starts. LOL has been numerically calculated as the axial distance from the exit of the nozzle to 14% of the maximum OH mass fraction [59]. This definition is chosen due to two reasons, one being the OH* radical absence in the mechanism and the other being the correlation of 14% OH with 50% of OH* level-off value as documented by [59]. Experimentally LOL is calculated by using the specific algorithm described in [60], where the LOL was defined as the distance between the nozzle tip and the first point at the flame axis where the intensity of OH* radiation reaches a fixed threshold value of 200 over the background noise level, which was found to be 500 in this work.

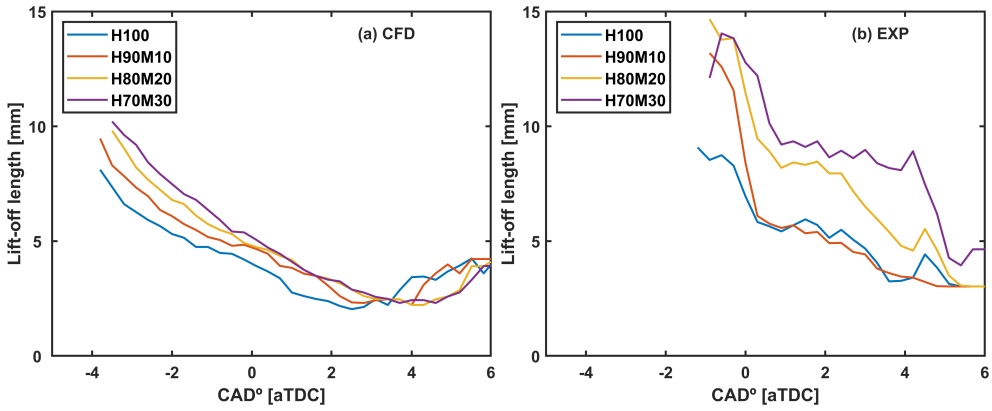

Figure 4.35: Numerical (a) and Experimental (b) Lift-off Length for HVO-OME_1 blends.

Figure 4.35 (a) depicts the numerically calculated LOL values plotted with respect to CAD for all 4 blends. Similarly, Figure 4.35 (b) shows the experimental LOL values. Setting aside the differences between numerical and experiment results, it is possible to see that LOL increases with the increment of OME_1 in the blend. This is particularly evident from -3°aTDC to around 2°aTDC (where injection stops). During this span, the trend seems to be stable and can give rather accurate measurements of LOL for both numerical and experimental cases. This increase in LOL with an increment of OME_1 content in the blend can be related to the variation in the reactivity as discussed earlier. The reactivity is decreased as OME_1 content in the blend increases, thereby increasing ignition delay as observed in Figure 4.34, and ultimately leading to ignition happening farther from the nozzle. The differences between numerically and experimentally obtained LOL could be related to the approach utilized to calculate LOL or due to few discrepancies found in terms of OH peak species concentration in Figure 4.32. However, considering the observed trend, it can be said that the 3D model in combination with the optimized mechanism is able to reflect the influence of OME_1 content on the LOL. In addition, it can be stated that blending OME_1 with HVO increases the LOL which gives an indication of less soot formation that will be analyzed later.

- **Heat Release Rate and In-cylinder Pressure**

Moving further into the combustion process, the results obtained by using the developed optimized Yao-SNL mechanism in terms of pressure inside the cylinder and heat release rate are compared with experimental results for all the blends in Figure 4.36.

In general, it can be said that numerical simulations are able to replicate the behavior observed in experimental results in terms of pressure and heat release rate quite accurately highlighting the accuracy of the developed mechanism. As discussed above, increasing OME_1 percentage in the blend delays the ignition which in turn affects the premixed combustion peak. The longer ID gives more time for the fuel to mix with air which results in a much more intense premixed combustion phase. Furthermore, the oxygen content present in the blend due to OME_1, triggers the chemical reaction and improves the premixed combustion, resulting in a higher heat release rate peak as well. After the premixed phase, no visible differences can be observed between blends both in the case of numerical simulations and experiments. Small discrepancies appear in later stages of combustion between simulations and experiments, where the experimental HRR slope seems to be higher than the numerical simulations, in turn leading to zero HRR earlier. This effect

can most probably be related to the performance of different sub-models for spray modeling utilized in CFD. In contrast to the phenomenon of increase in combustion speed observed in the work involving Diesel-OME_x blends, here almost no effect can be seen in terms of shortening of combustion duration (increase in combustion speed) with the addition of OME_1 in the blend. In the first case, this phenomenon was clearly observable when OME_x content in the blend reached 50%. However, in the present case, the maximum OME_1 fraction is 30%, which could limit the effect of this fuel specifically in the combustion duration as it was observed also with the Diesel-OME_x blends.

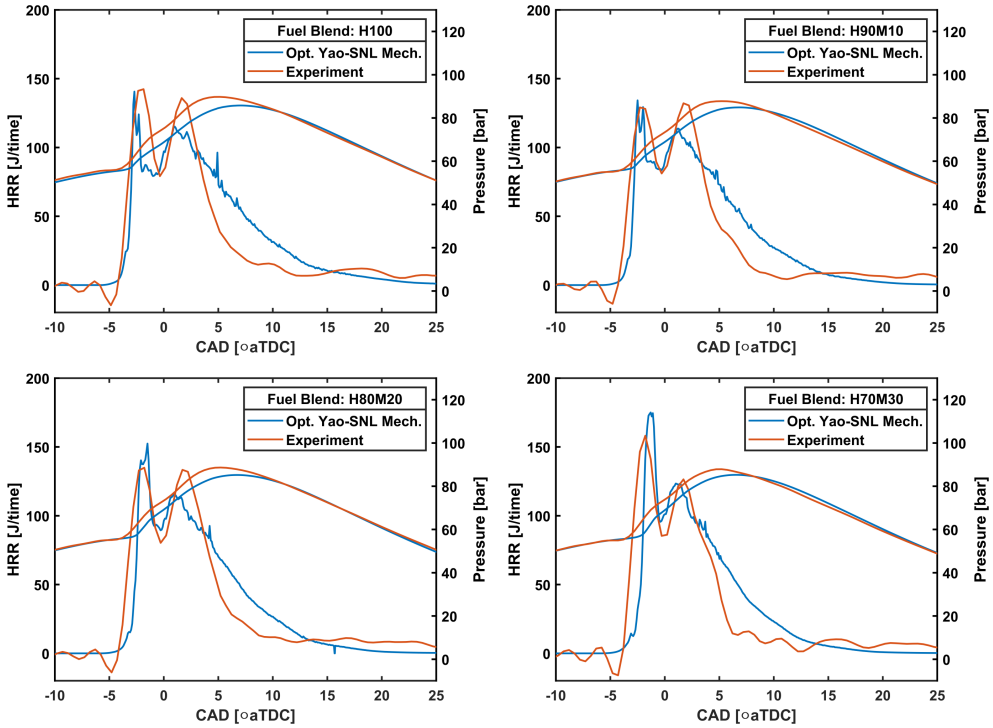

Figure 4.36: Numerical and Experimental Heat release rate and in-cylinder pressure for HVO-OME_1 blends.

- **Equivalence ratios and Fuel Mass**

The presence of OME_1 in the blends due to its oxygen content can affect the stoichiometry of the blend. It has been observed in the past that the presence of oxygenated fuels can alter the equivalence ratio fields achieved in the

cylinder as in the case of Diesel-OME$_x$ blends. Figure 4.37 shows the comparison of accumulated mass plotted versus the equivalence ratio range for each blend at two instants as done for Diesel-OME$_x$ blends. The y-axis range has been limited to allow a more accurate interpretation of results corresponding to higher EQ values. It is quite evident that in the case of blends having less or no OME$_1$ in them, the accumulated mass quantity is displaced to equivalence ratios above 2. This is true for both 2°aTDC and 5°aTDC, however, it is more evident for the first one. Literature shows that soot is expected to be formed at equivalence ratios above 2 [39] as also discussed earlier in the case of Diesel-OME$_x$ blends, so it can be said that having more mass at higher equivalence ratios for blends having less or no OME$_1$ in them will likely form more soot.

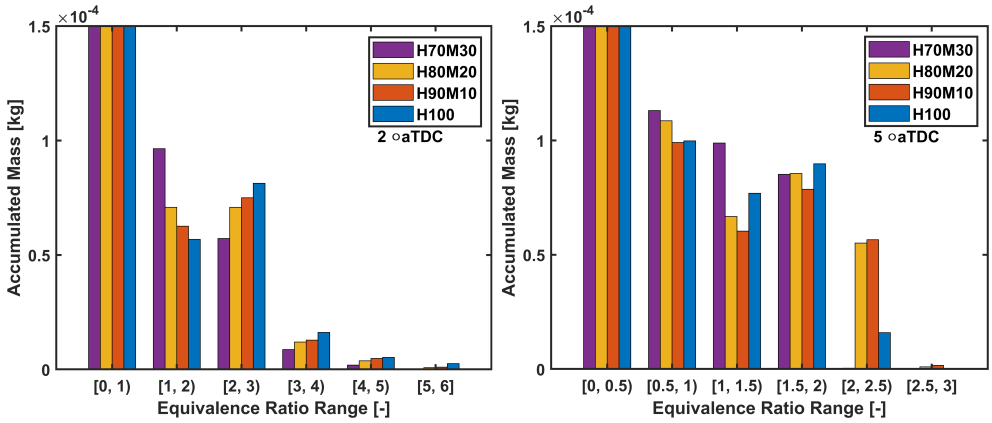

Figure 4.37: Equivalence ratio vs Accumulated mass Maps for HVO-OME$_1$ blends.

Kamimoto et al. [40] identified different combinations of EQ and temperature which would likely result in the formation of soot and NO$_x$. The groups of different combinations are commonly known as soot and NO$_x$ peninsula which has been plotted already in Figure 4.14 for Diesel-OME$_x$ blends. In this case, a different approach is taken. The total fuel mass present within these peninsulas was calculated and plotted for a range of CAD (0, 2, 5, and 10 °aTDC) in Figure 4.38. Primarily it is evident that despite having OME$_1$ in the mixture, all the blends exhibit a certain amount of fuel mass inside both soot and NO$_x$ peninsula which gradually diminishes as combustion progresses. However, looking at the accumulated fuel mass inside the soot peninsula, increment of OME$_1$ greatly reduces it (evident at 2°aTDC).

This can be correlated with the accumulated mass observed at 2°aTDC in Figure 4.37, which shows less mass at equivalence ratios above 2 (which is likely to form soot) for blends having more OME_1 in them. The same occurs for the fuel mass inside the NO_x region (evident at 5°aTDC). Therefore, this comparison suggests that the presence of less fuel inside the soot and NO_x peninsula for the cases of blend having more OME_1 can lead towards lesser soot and NO_x formation respectively.

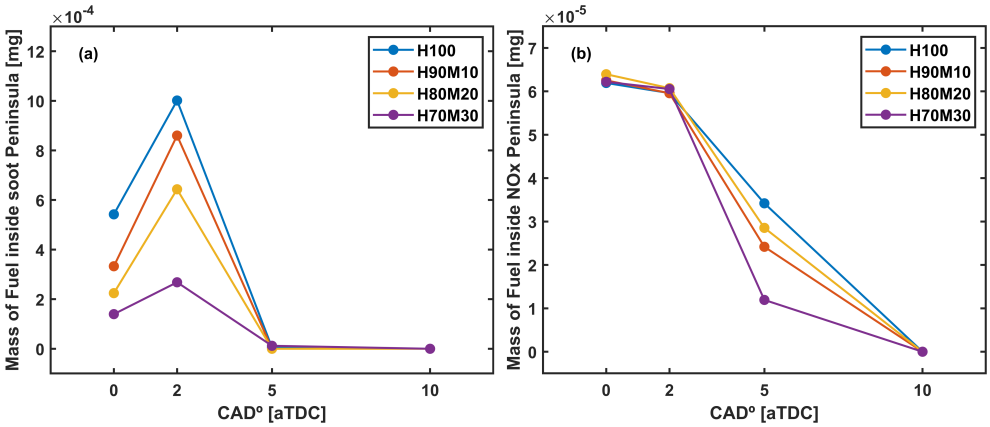

Figure 4.38: Accumulated Fuel mass present inside soot peninsula (a) and present inside NO_x Peninsula (b) for HVO-OME_1 blends.

4.3.2.2 Emissions Analysis

- **Soot Formation**

As mentioned in the section 3.4, Hiroysou model was utilized in 3D CFD simulations to analyze soot formation. Figure 4.39 shows (a) the normalized net soot mass with respect to H100 maximum value plotted versus CAD and (b) the normalized experimental NL accumulated intensity obtained from experiments with regard to the H100 maximum value plotted versus CAD for each blend. A qualitative analysis can be done between both experimental NL intensity and simulated net soot mass. Primarily a few similarities can be observed, i.e., the maximum net soot mass as well as maximum experimental NL accumulated intensity occur just before 5°aTDC. Further increasing of OME_1 content by 30% in the blend reduces maximum net soot mass by almost 50% as compared to pure HVO. The reduction achieved by increasing OME_1 to 30% stands at 43% for the case of NL, which corroborates well with numerical simulation results.

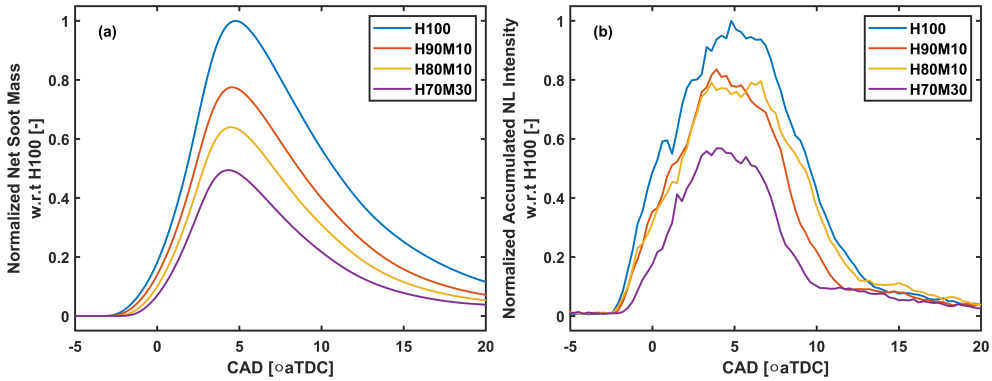

Figure 4.39: Numerically obtained normalized net soot mass w.r.t H100 (a) and experimentally obtained normalized net NL intensity w.r.t H100 (b) for HVO-OME$_1$ blends.

For a more detailed analysis of soot distribution inside the combustion chamber, a strategy has been developed for summarizing all the combustion chamber information related to soot into 2D soot maps which resembles the experimental strategy as described in Figure 3.8. In this strategy, the combustion chamber is divided into rings of different radii for each CAD. Then an average net soot mass for each ring is calculated corresponding to each CAD by using the formula shown in Equation 4.2.

$$\text{Average soot mass}_r = \frac{\text{Accumulated soot mass}_r}{A_r} \tag{4.2}$$

Where A_r represents the total area of the ring and Accumulated soot mass$_r$ represents the accumulation of net soot mass present inside each ring. Following the procedure for each CAD, a 1D vector is created which consists of average net soot mass values distributed through the whole combustion duration (CAD). This vector then allows the creation of a 2D map of average soot mass distribution where CADs are shown on the x-axis and the distance from the nozzle spanning until the bowl radius is represented on the y-axis.

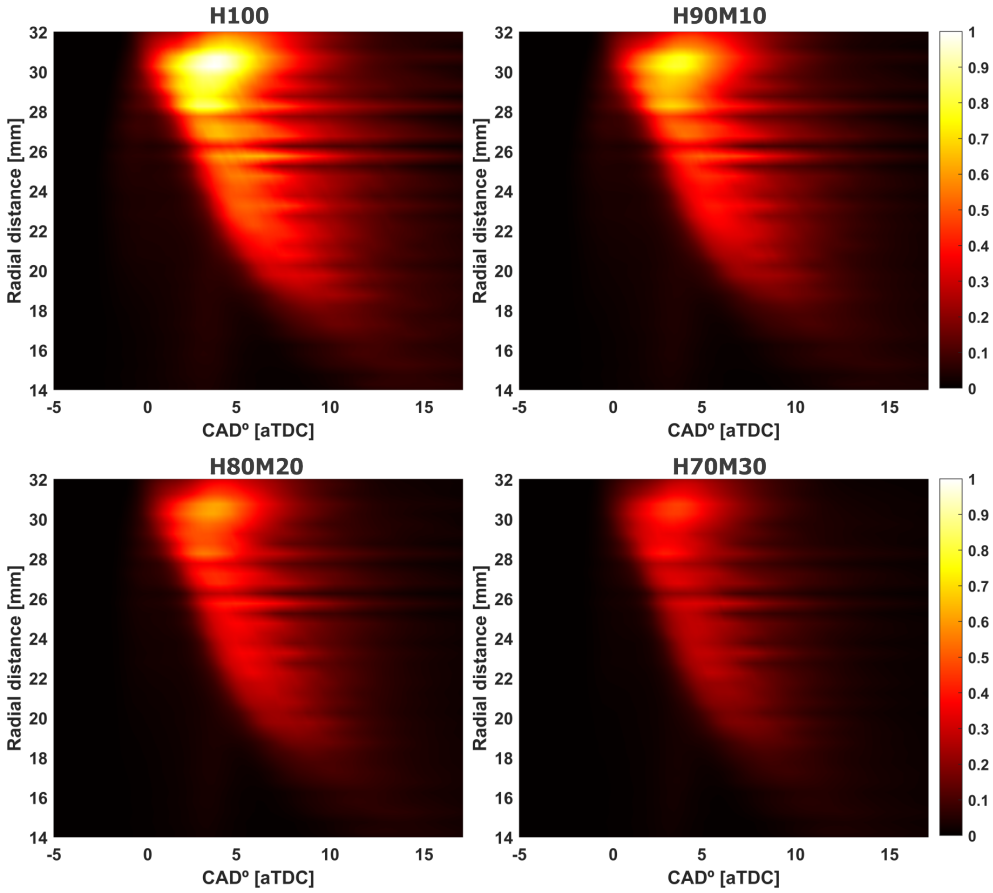

Figure 4.40: Numerically obtained Average Soot Mass Maps normalized w.r.t H100 for HVO-OME$_1$ blends.

For the present case, the chamber was divided into rings of thickness of 0.5mm. The soot mass maps normalized with respect to the maximum value of H100 are shown in Figure 4.40. Similarities can be observed for all the blends with regards to the evolution of soot. It appears from the periphery of the bowl primarily due to flame/wall interaction and moves towards the nozzle in all cases, with maximum values occurring near the periphery of the bowl. The soot cloud never reaches its center rather it seems to be oxidized close to the center. So, these maps suggest the maximum soot mass is accumulated near the bowl walls. Further as observed in Figure 4.39, they also confirm that the maximum soot is formed around 5°aTDC for all the cases. When

comes to analyzing differences, a clear variation in terms of total soot mass can be observed. H70M30 case shows almost half of the maximum soot mass compared to H100 case. Further, soot cloud seems to last less amount of time for H70M30 as compared to H100. This confirms that not only less amount of soot is formed with H70M30 but also that it is oxidized faster as compared to H100. A progressive decrement in soot cloud intensity and duration can be seen as OME_1 percentage in the blend is increased. This confirms a clear advantage in terms of soot reduction for the case of blends having more OME_1.

- **NO_x Formation**

To model the NO_x formation, as mentioned in section 3.4, the extended Zeldovich model was utilized. Figure 4.41 shows the net NO_x mass produced for each blend along with the maximum in-cylinder temperature. In general, a 30% addition of OME_1 content in the blend reduces the NO_x emissions by almost 35%.

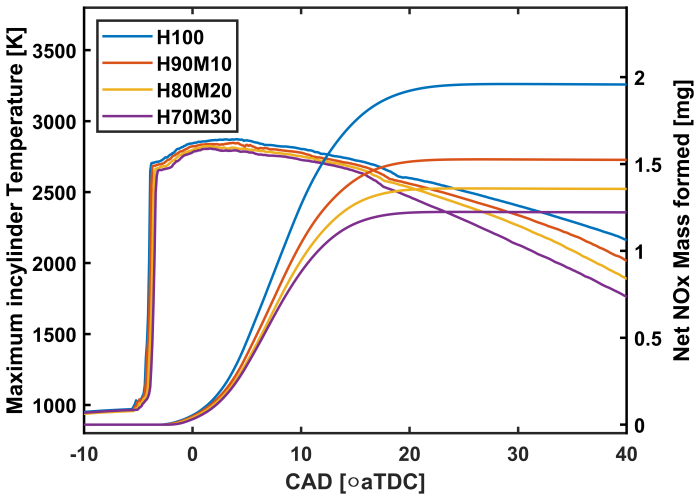

Figure 4.41: Numerically obtained net NO_x mass and maximum in-cylinder temperature for HVO-OME$_1$ blends.

The NO_x emissions are generally related to the maximum in-cylinder temperature reached inside the combustion chamber. Thus looking at Figure 4.41 an evolution of the maximum temperature values reached for each blend shows the decrement of maximum temperature, as the percentage of OME_1 in the blend rises from 0 to 30%. This temperature reduction is particularly evident between 10°aTDC to 20°aTDC, where the NO_x formation differences also appear among blends. This reduction in temperature can be related to the higher

latent heat of evaporation of OME_1 and the fact that OME_1 releases less energy as compared to HVO. Hence, it can be said that the addition of OME_1 in the blend reduces the maximum temperature reached inside the cylinder, which contributes to NO_x reduction. A similar trend in terms of NO_x reduction was observed by [61] where authors studied Diesel-OME_1 blends and increment of OME_1 decreased the in-cylinder temperature, thereby reducing NO_x emissions.

4.3.2.3 Discussion

One of the disadvantages the OME_1 blending presents is that it decreases the total LHV of the blend, which in turn leads to a reduction of energy injected into the cylinder. Therefore, it has been decided to compare the maximum energy released by each blend with the maximum net soot and NO_x mass formed along with the corresponding percentages of reduction with respect to H100. All this information is summarized in Figure 4.42.

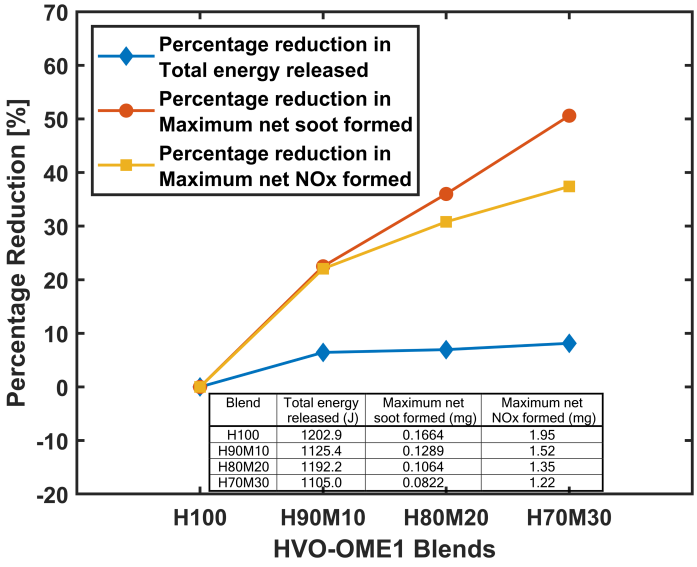

Blend	Total energy released (J)	Maximum net soot formed (mg)	Maximum net NOx formed (mg)
H100	1202.9	0.1664	1.95
H90M10	1125.4	0.1289	1.52
H80M20	1192.2	0.1064	1.35
H70M30	1105.0	0.0822	1.22

Figure 4.42: Percentage reduction in total energy released, maximum net soot formed, and maximum net NO_x formed w.r.t H100 for HVO-OME_1 blends.

It is possible to see that even a 10% addition of OME_1 percentage in the blend leads to a drastic reduction of 20% in both soot and NO_x formation. Furthermore, a progressive reduction is observed in both pollutants, as the OME_1 content in the blend increases. This reduction achieved by blending of

30% OME_1 stands at 50% and 37% for soot and NO_x formation respectively, however, only a decrease of 8% is observed in terms of energy release. This energy release reduction is much lower as compared to the benefits in terms of soot and NO_x achieved. Due to this reason, this comparison between blends could be considered fair, as the advantages achieved in terms of pollutant reduction surpass the energy reduction, which is quite low. Furthermore, it reflects a possible strategy to implement the blends in real applications. It must be considered that based on the experimental data, more fuel mass was injected with H70O30 which compensated for part of the expected energy loss. In terms of LHV, the difference should be close to 17%. In summary, it can be concluded from the discussion that reductions in soot and NO_x formation of up to 50% and 37% respectively would only require modifying the injection strategy to compensate for 8% of energy loss.

4.4 Summary and conclusions

In this chapter, a detailed numerical study was conducted regarding the blends of different fuels i.e, Diesel-OME_x and HVO-OME_1. The analysis began with the identification and development of a reaction mechanism necessary for numerical simulations of blends. Later on, results from 3D CFD simulations were presented and combustion evolution and emissions formation inside the combustion chamber was studied. It is convenient to summarize the main conclusions obtained from the study.

4.4.1 Diesel-OME_x blends

For the case of Diesel-OME_x blends, primarily different reaction mechanisms from the literature were evaluated. The results showed that the most compact reaction mechanism provided by Lin 2019 [6] was able to closely reproduce a global combustion behavior similar to the one observed with the experimental data. However the OME_x part of the mechanisms only considered OME_3 molecule. Hence to better represent the real OME_x behavior (formed by a mixture of different OME molecules), a new PRF-OME_x mechanism was constructed including molecules ranging from $OME_{2\text{-}4}$. It was constructed by reducing a detailed OME_x mechanism and combining it with a PRF mechanism. The developed PRF-OME_x consisting of 213 species and 840 reactions was widely validated over fundamental experimental data including ignition delay times, laminar flame speeds, and species profile concentrations. Then the mechanism was used to perform detailed numerical simulations for blends

of Diesel-OME_x blends i.e., D90O10, D80O20, D70O30, and D50O50, to analyze their combustion and emissions behavior. The following conclusions can be drawn from the study related to these blends.

- The developed PRF-OME_x mechanism offers good predictions matching experimental data for OME_2, OME_3, OME_4 and PRF mixtures in terms of ignition delay times, laminar flame speeds and species concentration profiles.
- Numerical simulations performed using the developed PRF-OME_x mechanism show that it not only replicates the experimental behavior in terms of heat release rate and in-cylinder pressure but also exhibits a more accurate prediction (closer to experimental data) when compared with PRF-OME_3 mechanism from [6]. This primarily confirms the accuracy and the robustness of the developed mechanism and secondly highlights the importance of the definition of the proper surrogate of OME_x (i.e., $OME_{2\text{-}4}$) as close as possible to experimental fuel. Hence, the compact mechanism comprising of 213 species and 840 reactions can be utilized for Diesel-OME_x blends irrespective of the initial conditions, and CI engine hardware used.
- The ignition delay of the blend decreases when increasing the OME_x content. This primarily relates to the higher oxygen content present in the blends when increasing the fraction of this fuel. Numerically, increasing the OME_x percentage in the blend from 10% to 50%, decreases the ignition delay by almost 19%.
- The HRR at the premixed combustion phase increased when decreasing the OME_x fraction, which can be related to the lower LHV of this fuel but also to the different ID of the blends. On the other hand, the HRR levels reached during the diffusion phase are more similar despite the difference in terms of LHV. In addition, it has been also observed at the late stages of combustion that an increase of OME_x content also increases the combustion speed up to 5% for D50O50 when compared to D90O10.
- The different stoichiometry of OME_x leads to a decrease in the EQ field. In this sense, D50O50 provides a different behaviour than the other blends. The fact that it reaches lower EQ values (closer to 1) promotes oxidation reaction which results in a faster combustion completion and sooner OH disappearance.

- The higher EQ values reached when reducing the OME_x content has been related with the higher net soot formation. On one hand, the soot formation increases as the amount of mixture under EQ > 2 increases. On the other hand, the percentage of soot oxidation decreases too. This leads to a higher amount of soot in the cylinder, which lasts longer before being oxidized.

- In general, the addition of OME_x content in Diesel from 10% to 50% results in a decrease of soot and NO_x emissions by 56% and 32% respectively, with a much lower reduction of total energy release of 19%.

4.4.2 HVO-OME_1 blends

For the case of HVO-OME_1 blends, primarily n-Dodecane was proposed as a surrogate for HVO based on similar experimental behavior observed between them. Then a compact mechanism was constructed reducing a detailed OME_1 mechanism and combining it with an n-Dodecane mechanism. It was further optimized to better replicate the behavior of HVO-OME_1 blends at various fuel compositions. The developed optimized Yao-SNL mechanism consisting of 121 species and 678 reactions was widely validated over fundamental experimental data including ignition delay times, laminar flame speeds, and species profile concentrations. Then the mechanism was used to perform detailed numerical simulations for blends of HVO-OME_1 blends i.e., H100, H90M10, H80O20, and H70M30, to analyze their combustion and emissions behavior. The following conclusions can be drawn from the study related to these blends.

- The developed optimized Yao-SNL mechanism works well both for the case of single component fuel i.e., HVO and OME_1 and for their blends. All the necessary validations in terms of ignition delay, laminar flame speed, and species concentration profiles show a good agreement with regard to the experimental data available. Further, the developed mechanism when coupled with 3D CFD to simulate an actual diesel engine combustion shows realistic results as compared to experimental data for all the blends. Hence, the compact mechanism comprising of 121 species and 678 reactions can be utilized by HVO-OME_1 blends irrespective of the initial conditions, and CI engine hardware used.

- The ignition delay shows a progressive increment as the percentage of OME_1 in the blend is increased, making the higher OME_1 blends less reactive. Numerically, increasing the OME_1 percentage in the blend to

30%, prolongs the ignition delay by almost 26%. Furthermore, the lift-off length is also increased for the blends having more OME_1 in them, suggesting less soot formation.

- The stoichiometry of the blend is affected with the addition of OME_1 in the blend with HVO, which in turn, affects soot formation. The quantity of total fuel mass present at equivalence ratios above 2 drops, when the OME_1 content in the blend is increased. This is also linked to the total fuel mass present inside the soot peninsula which decreases when OME_1 percentage in the blend is increased. This decrement in fuel mass at equivalence ratios above 2 and inside the soot peninsula suggests less soot formation for OME_1 rich blends.

- The spatial and temporal distribution of soot is quite similar, where soot is formed close to the periphery of the piston bowl for all the cases. However, a higher soot concentration appears for pure HVO as compared to blends having more OME_1 in them.

- In general, the addition of OME_1 content in HVO from 0% to 30% results in a decrease of soot and NO_x emissions by 50% and 37% respectively, with a much lower reduction of total energy release of 8%.

References

[1] Pastor, Jose V, Garcia-Oliver, Jose M, Micó, Carlos, and Tejada, Francisco J. *Combustion behaviour of blends of synthetic fuels in an optical single cylinder engine.* Tech. rep. SAE Technical Paper, 2021.

[2] Pitz, William J and Mueller, Charles J. "Recent progress in the development of diesel surrogate fuels". In: *Progress in Energy and Combustion Science* 37.3 (2011), pp. 330–350.

[3] Diez, Alvaro, Crookes, Roy J, and Løvås, Terese. "Experimental studies of autoignition and soot formation of diesel surrogate fuels". In: *Proceedings of the Institution of Mechanical Engineers, Part D: Journal of Automobile Engineering* 227.5 (2013), pp. 656–664.

[4] He, Tanjin et al. "Development of surrogate model for oxygenated wide-distillation fuel with polyoxymethylene dimethyl ether". In: *SAE International Journal of Fuels and Lubricants* 10.3 (2017), pp. 803–814.

[5] Ren, Shuojin, Wang, Zhi, Li, Bowen, Liu, Haoye, and Wang, Jianxin. "Development of a reduced polyoxymethylene dimethyl ethers (PODEn) mechanism for engine applications". In: *Fuel* 238 (2019), pp. 208–224.

[6] Lin, Qinjie, Tay, Kun Lin, Zhou, Dezhi, and Yang, Wenming. "Development of a compact and robust Polyoxymethylene Dimethyl Ether 3 reaction mechanism for internal combustion engines". In: *Energy Conversion and Management* 185 (2019), pp. 35–43.

[7] Lv, Delin et al. "Development of a reduced diesel/PODEn mechanism for diesel engine application". In: *Energy Conversion and Management* 199 (2019), p. 112070.

[8] Lin, Qinjie, Tay, Kun Lin, Zhao, Feiyang, and Yang, Wenming. "Enabling robust simulation of polyoxymethylene dimethyl ether 3 (PODE3) combustion in engines". In: *International Journal of Engine Research* 23.9 (2022), pp. 1522–1542.

[9] Klotz, Stephen D, Brezinsky, Kenneth, and Glassman, Irvin. "Modeling the combustion of toluene-butane blends". In: *Symposium (International) on Combustion*. Vol. 27. 1. Elsevier. 1998, pp. 337–344.

[10] Tanaka, Shigeyuki, Ayala, Ferran, and Keck, James C. "A reduced chemical kinetic model for HCCI combustion of primary reference fuels in a rapid compression machine". In: *Combustion and flame* 133.4 (2003), pp. 467–481.

[11] Ra, Youngchul and Reitz, Rolf D. "A reduced chemical kinetic model for IC engine combustion simulations with primary reference fuels". In: *Combustion and Flame* 155.4 (2008), pp. 713–738.

[12] Tsurushima, Tadahi. "A new skeletal PRF kinetic model for HCCI combustion". In: *Proceedings of the Combustion Institute* 32.2 (2009), pp. 2835–2841.

[13] Liu, Yao-Dong, Jia, Ming, Xie, Mao-Zhao, and Pang, Bin. "Enhancement on a skeletal kinetic model for primary reference fuel oxidation by using a semidecoupling methodology". In: *Energy & Fuels* 26.12 (2012), pp. 7069–7083.

[14] Wang, Hu, Yao, Mingfa, and Reitz, Rolf D. "Development of a reduced primary reference fuel mechanism for internal combustion engine combustion simulations". In: *Energy & Fuels* 27.12 (2013), pp. 7843–7853.

[15] Chang, Yachao et al. "Development of a skeletal mechanism for diesel surrogate fuel by using a decoupling methodology". In: *Combustion and Flame* 162.10 (2015), pp. 3785–3802.

[16] Cai, Liming et al. "Auto-ignition of oxymethylene ethers (OMEn, n= 2–4) as promising synthetic e-fuels from renewable electricity: shock tube experiments and automatic mechanism generation". In: *Fuel* 264 (2020), p. 116711.

[17] Benajes, Jesus, Garcia-Oliver, Jose M, Pastor, Jose M, and De Leon-Ceriani, Daiana. "Unsteady Flamelet modeling study on OMEx-type fuels under Engine Combustion Network Spray A conditions". In: *Fuel* 331 (2023), p. 125458.

[18] Haspel, Philip et al. "Large eddy simulation of OME3 and OME4 spray combustion under heavy-duty conditions". In: *Fuel* 353 (2023), p. 129097.

[19] García-Oliver, José M, Novella, Ricardo, Micó, Carlos, and De Leon-Ceriani, Daiana. "Numerical analysis of the combustion process of oxymethylene ethers as low-carbon fuels for compression ignition engines". In: *International Journal of Engine Research* 24.5 (2023), pp. 2175–2186.

[20] ANSYS, Chemkin. *Reaction Workbench 17.0*. 2016.

[21] Shen, Hsi-Ping S, Steinberg, Justin, Vanderover, Jeremy, and Oehlschlaeger, Matthew A. "A shock tube study of the ignition of n-heptane, n-decane, n-dodecane, and n-tetradecane at elevated pressures". In: *Energy & Fuels* 23.5 (2009), pp. 2482–2489.

[22] Fieweger, K, Blumenthal, Ro, and Adomeit, G. "Self-ignition of SI engine model fuels: a shock tube investigation at high pressure". In: *Combustion and Flame* 109.4 (1997), pp. 599–619.

[23] Hartmann, M et al. "Auto-ignition of toluene-doped n-heptane and iso-octane/air mixtures: High-pressure shock-tube experiments and kinetics modeling". In: *Combustion and Flame* 158.1 (2011), pp. 172–178.

[24] Herzler, J, Jerig, L, and Roth, P. "Shock tube study of the ignition of lean n-heptane/air mixtures at intermediate temperatures and high pressures". In: *Proceedings of the Combustion Institute* 30.1 (2005), pp. 1147–1153.

[25] Eckart, Sven et al. "Laminar burning velocities, CO, and NOx emissions of premixed polyoxymethylene dimethyl ether flames". In: *Fuel* 293 (2021), p. 120321.

[26] Shrestha, Krishna P et al. “A comprehensive kinetic modeling of oxymethylene ethers (OMEn, n= 1–3) oxidation-laminar flame speed and ignition delay time measurements”. In: *Combustion and Flame* 246 (2022), p. 112426.

[27] Wang, Qiao et al. “Experimental and kinetic study on the laminar burning speed, Markstein length and cellular instability of oxygenated fuels”. In: *Fuel* 297 (2021), p. 120754.

[28] Richter, Sandra, Kathrotia, Trupti, Braun-Unkhoff, Marina, Naumann, Clemens, and Köhler, Markus. “Influence of oxymethylene ethers (OMEn) in mixtures with a diesel surrogate”. In: *Energies* 14.23 (2021), p. 7848.

[29] Davis, Scott G and Law, Chung King. “Laminar flame speeds and oxidation kinetics of iso-octane-air and n-heptane-air flames”. In: *Symposium (international) on combustion*. Vol. 27. 1. Elsevier. 1998, pp. 521–527.

[30] Van Lipzig, JPJ, Nilsson, EJK, De Goey, Laurentius PH, and Konnov, Alexander A. “Laminar burning velocities of n-heptane, iso-octane, ethanol and their binary and tertiary mixtures”. In: *Fuel* 90.8 (2011), pp. 2773–2781.

[31] Dirrenberger, Patricia et al. “Laminar burning velocity of gasolines with addition of ethanol”. In: *Fuel* 115 (2014), pp. 162–169.

[32] Sun, Wenyu et al. “Speciation and the laminar burning velocities of poly (oxymethylene) dimethyl ether 3 (POMDME3) flames: An experimental and modeling study”. In: *Proceedings of the Combustion Institute* 36.1 (2017), pp. 1269–1278.

[33] Bakali, A El, Delfau, J-L, and Vovelle, Christian. “Experimental study of 1 atmosphere, rich, premixed n-heptane and iso-octane flames”. In: *Combustion science and technology* 140.1-6 (1998), pp. 69–91.

[34] Marchal, Caroline et al. “Modelling of aromatics and soot formation from large fuel molecules”. In: *Proceedings of the Combustion Institute* 32.1 (2009), pp. 753–759.

[35] Rothamer, David A and Murphy, Lucas. “Systematic study of ignition delay for jet fuels and diesel fuel in a heavy-duty diesel engine”. In: *Proceedings of the combustion institute* 34.2 (2013), pp. 3021–3029.

[36] Liu, Junheng, Sun, Ping, Huang, He, Meng, Jian, and Yao, Xiaohua. "Experimental investigation on performance, combustion and emission characteristics of a common-rail diesel engine fueled with polyoxymethylene dimethyl ethers-diesel blends". In: *Applied Energy* 202 (2017), pp. 527–536.

[37] Wu, Yixuan, Ays, Isabelle, and Geimer, Marcus. *Analysis and Preliminary Design of Oxymethylene ether (OME) Driven Mobile Machines*. Tech. rep. 2019. DOI: 10.5445/IR/1000097941.

[38] Richards, KJ, Senecal, PK, and Pomraning, E. "CONVERGE (v3. 0), Convergent Science". In: *Inc., Madison, WI* (2021).

[39] Kitamura, Takaaki, Ito, T, Senda, Jiro, and Fujimoto, Hajime. "Mechanism of smokeless diesel combustion with oxygenated fuels based on the dependence of the equivalence ration and temperature on soot particle formation". In: *International Journal of Engine Research* 3.4 (2002), pp. 223–248.

[40] Kamimoto, Takeyuki and Bae, Myurng-hoan. "High combustion temperature for the reduction of particulate in diesel engines". In: *SAE transactions* (1988), pp. 692–701.

[41] Hartikka, Tuukka, Kuronen, Markku, and Kiiski, Ulla. *Technical performance of HVO (hydrotreated vegetable oil) in diesel engines*. Tech. rep. SAE Technical Paper, 2012.

[42] Pastor, José V, García-Oliver, José M, Micó, Carlos, García-Carrero, Alba A, and Gómez, Arantzazu. "Experimental study of the effect of hydrotreated vegetable oil and oxymethylene ethers on main spray and combustion characteristics under engine combustion network spray a conditions". In: *Applied Sciences* 10.16 (2020), p. 5460.

[43] Yao, Tong et al. "A compact skeletal mechanism for n-dodecane with optimized semi-global low-temperature chemistry for diesel engine simulations". In: *Fuel* 191 (2017), pp. 339–349.

[44] Wang, Hu, Ra, Youngchul, Jia, Ming, and Reitz, Rolf D. "Development of a reduced n-dodecane-PAH mechanism and its application for n-dodecane soot predictions". In: *Fuel* 136 (2014), pp. 25–36.

[45] Sarathy, S Mani et al. "Comprehensive chemical kinetic modeling of the oxidation of 2-methylalkanes from C7 to C20". In: *Combustion and flame* 158.12 (2011), pp. 2338–2357.

[46] Narayanaswamy, Krithika, Pepiot, Perrine, and Pitsch, Heinz. "A chemical mechanism for low to high temperature oxidation of n-dodecane as a component of transportation fuel surrogates". In: *Combustion and Flame* 161.4 (2014), pp. 866–884.

[47] Cai, Liming et al. "Optimized reaction mechanism rate rules for ignition of normal alkanes". In: *Combustion and Flame* 173 (2016), pp. 468–482.

[48] Goeb, Dominik et al. "Oxymethylene ether–n-dodecane blend spray combustion: Experimental study and large-eddy simulations". In: *Proceedings of the Combustion Institute* 38.2 (2021), pp. 3417–3425.

[49] Payri, Francisco, García-Oliver, Jose M, Novella, Ricardo, and Pérez-Sánchez, Eduardo J. "Influence of the n-dodecane chemical mechanism on the CFD modelling of the diesel-like ECN Spray A flame structure at different ambient conditions". In: *Combustion and Flame* 208 (2019), pp. 198–218.

[50] Desantes, José M, López, J Javier, García-Oliver, José M, and López-Pintor, Darío. "Experimental validation and analysis of seven different chemical kinetic mechanisms for n-dodecane using a rapid compression-expansion machine". In: *Combustion and Flame* 182 (2017), pp. 76–89.

[51] Jacobs, Sascha et al. "Detailed kinetic modeling of dimethoxymethane. Part II: Experimental and theoretical study of the kinetics and reaction mechanism". In: *Combustion and Flame* 205 (2019), pp. 522–533.

[52] Pastor, Jose V, Garcia-Oliver, Jose M, Pastor, Jose M, and Vera-Tudela, W. "One-dimensional diesel spray modeling of multicomponent fuels". In: *Atomization and sprays* 25.6 (2015).

[53] Garcia-Oliver, Jose M, Novella, Ricardo, Pastor, Jose M, Pachano, Leonardo, and Naud, Bertrand. "A quasi-1D model for the description of ECN spray a combustion process". In: *SAE International Journal of Advances and Current Practices in Mobility* 2.2020-01-0661 (2020), pp. 1974–1985.

[54] Garcia-Oliver, Jose Maria et al. "An experimental and one-dimensional modeling analysis of turbulent gas ejection in pre-chamber engines". In: *Fuel* 299 (2021), p. 120861.

[55] Monsalve-Serrano, Javier, Belgiorno, Giacomo, Di Blasio, Gabriele, and Guzmán-Mendoza, María. "1D simulation and experimental analysis on the effects of the injection parameters in methane–diesel dual-fuel combustion". In: *Energies* 13.14 (2020), p. 3734.

[56] Gillespie, Fiona Rita. "An experimental and modelling study of the combustion of oxygenated hydrocarbons". In: *National University of Ireland* (2014).

[57] Kumar, Kamal and Sung, Chih-Jen. "Laminar flame speeds and extinction limits of preheated n-decane/O2/N2 and n-dodecane/O2/N2 mixtures". In: *Combustion and Flame* 151.1-2 (2007), pp. 209–224.

[58] Zhu, RJ, Wang, XB, Miao, Haiyan, and Huang, ZH. "Combustion and particulate emission characteristics of a diesel engine fuelled with diesel—dimethoxymethane blends". In: *Proceedings of the Institution of Mechanical Engineers, Part D: Journal of Automobile Engineering* 224.4 (2010), pp. 521–531.

[59] Payri, Raúl, Viera, Juan Pablo, Pei, Yuanjiang, and Som, Sibendu. "Experimental and numerical study of lift-off length and ignition delay of a two-component diesel surrogate". In: *Fuel* 158 (2015), pp. 957–967.

[60] Pastor, Jose V, García-Oliver, Jose M, Micó, Carlos, and Tejada, Francisco J. "Characterization of the oxymethylene ether fuels flame structure for ECN Spray A and Spray D nozzles". In: *Applied Energy* 332 (2023), p. 120475.

[61] Ghadamkheir, Kourosh, Zareei, J, Yang, Xiaohu, and Hatami, Mohammad. "The effects of diesel-OME1 blended fuel on combustion characteristics of a heavy-duty compression ignition engine by a numerical study". In: *Alexandria Engineering Journal* 64 (2023), pp. 493–503.

Chapter 5

Ducted fuel injection (DFI) application applied to CI engines to reduce pollutant emissions

5.1 Introduction

In this chapter, a detailed experimental study has been carried out regarding the Ducted fuel injection concept applied in CI engines to tackle pollutant

emissions. The DFI device, its implementation inside the optical engine, and the methodology for analysis of KL (soot) have already been explained in section 3.3. The different DFI designs that are tested here against Free spray (FS) configuration are also listed already in Table 3.4.

The discussion starts with enlisting the general operating conditions utilized for the study. This is followed by the analysis of the global behavior of combustion (HRR and pressure) and emission (KL) parameters for a base DFI and FS configuration. As discussed earlier in the literature review section regarding DFI section 2.4, the geometry of the ducts has been identified as a key parameter to optimize the performance of DFI in terms of soot reduction. For this reason, a parametric evaluation of the main geometrical parameters including L, D, and G in terms of both combustion and emission parameters is presented afterward to better understand their effect on the overall performance of the device in the context of the current work (relatively small bowl diameter and more nozzle holes). The parametric evaluation ends with a quantitative reduction analysis in terms of KL between DFI configurations and FS done to identify the optimal duct design. After the identification of the optimal design, the analysis is extended to utilizing different blends of fuels, identified in previous chapter chapter 4 i.e., D70O30 and D50O50 with the DFI to understand their effect on DFI performance. In the end, a summary and conclusions are made regarding the whole study carried out.

5.2 Operating Conditions

The experimental analysis has been carried out inside the same optical engine as shown in Figure 3.1. The Optical setup B explained previously in Figure 3.3 has been utilized to analyze the combustion and emission evolution inside the combustion chamber. As mentioned earlier in section 3.3, a skip fire mode was chosen to operate the engine which means only 1 out of 20 cycles was a firing cycle. In the study, fossil diesel along with two blends of Diesel-OME_x i.e., D70O30 and D50O50 have been utilized as a fuel, the properties of which have been described in Table 3.2. The fuel was injected via a common rail delivering fuel to the injector having a standard 8-hole conical nozzle with an orifice diameter of approximately 138 μm. Regarding the injection strategy, a rather simpler injection strategy was utilized to evaluate the DFI performance. It consisted of one main and one pilot injection. The energizing signal for the case of D100, D70O30, and D50O50 is represented in Figure 5.1. It must be noted that for the case of blends, the strategy has been altered (pilot and main injection duration have been increased) in order to match the overall

IMEP to have a realistic comparison between blends and fossil diesel. This has been done because of the lower LHV of OME_x as compared to diesel (see Table 3.2).

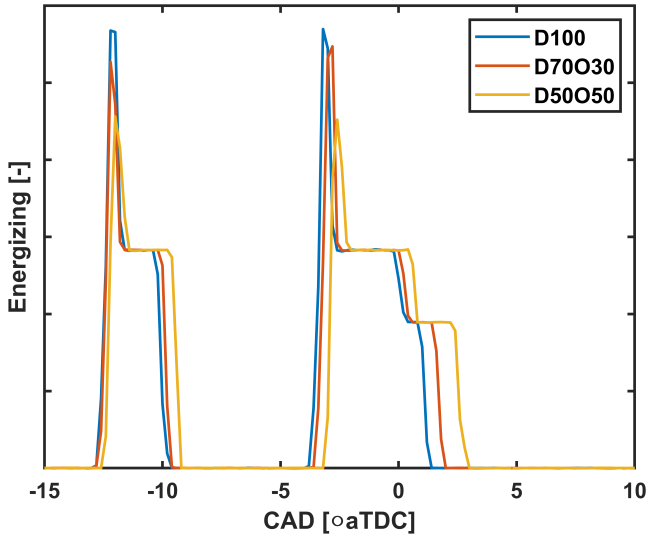

Figure 5.1: Energizing signal utilized for injection for DFI evaluation for the case of D100, D70O30, and D50O50.

Table 5.1: Engine operating conditions for DFI evaluation.

Parameter	**Value**
Injection profile (-)	Multi pulse
Engine speed (rpm)	1200
Intake pressure (bar)	1.34
Exhaust pressure (bar)	1.54
Injection pressure (bar)	1200
SOE (°aTDC)	-12
Indicated mean effective pressure (bar)	7.6
Oxygen concentration (% O_2)	21,18, and 15

Table 5.1 summarizes the main operating conditions utilized in this work. It corresponded to 7.6 bar indicated mean effective pressure (IMEP), which can be considered medium load conditions. In addition, three different oxygen concentrations i.e., 21%, 18% and 15% O_2 were used to simulate the effect of EGR. This reduction in O_2 concentration was accomplished by the dilution of airflow with nitrogen at the intake port.

5.3 DFI vs Free Spray

Discussion can be started by looking at the effect of the DFI device when compared to a FS configuration. For this purpose, duct L8D2G4.28 is chosen as the baseline design and fossil diesel has been used. Figure 5.2 shows the in-cylinder pressure and heat release rate signal for the case of 21% O_2 concentration.

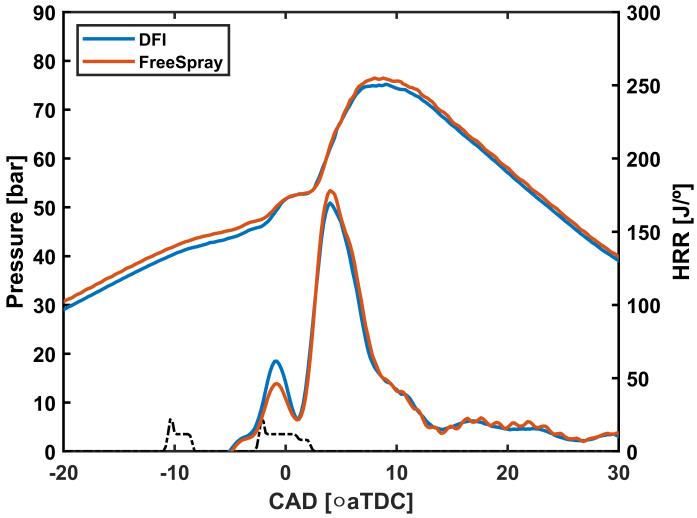

Figure 5.2: Comparison of In-cylinder pressure and Heat release rate signal between base DFI (L8D2G4.28) and Free Spray for 21% oxygen concentration case.

It can be observed that there are not so many differences between DFI and FS in terms of global combustion behavior. The ignition delay and combustion duration seem to be quite similar in both cases. However, literature has reported that the DFI increases the ignition delay [1–3], while combustion duration is decreased. A possible reason for not observing a similar effect in this work is the frequency of the data acquisition. In this work, a measuring

resolution of 0.5 CAD was used which was in the order of magnitude of the differences observed thanks to the OH^* chemiluminescence signal in this regard. Another reason could be the injection strategy used. On one hand, the pilot injection is burning under the premixed regime, in which the DFI effect could be not so noticeable. On the other hand, the first combustion increases temperature and pressure inside the combustion chamber which increases reactivity of the air-fuel mixture and reduces differences between DFI and FS in this regard.

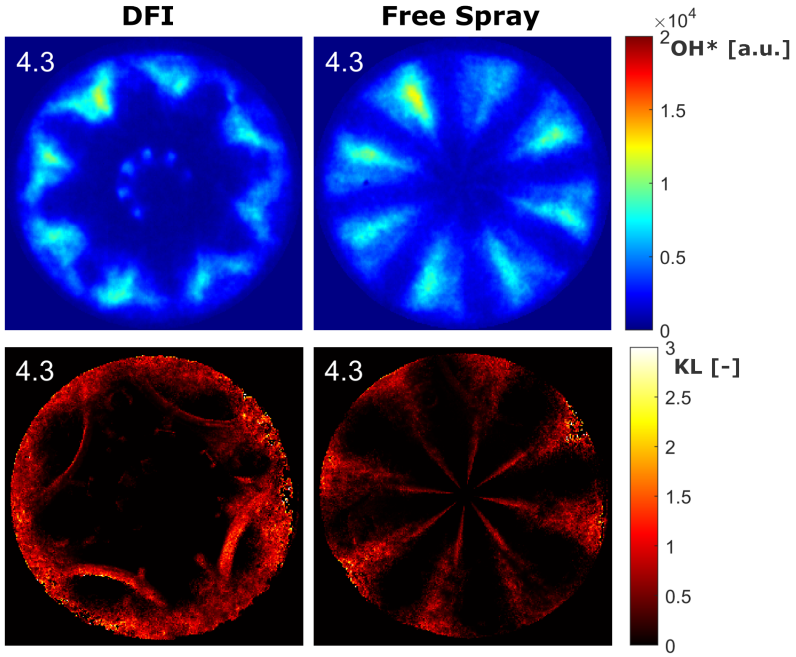

Figure 5.3: Comparison of OH^* and KL images at 4.3 CAD between base DFI (L8D2G4.28) and Free Spray for 21% oxygen concentration case.

Moving further, by looking at the radiation from combustion, significant differences arise. Figure 5.3 shows the OH^* and KL images obtained at 4.3 CAD, both for DFI and FS. Focusing on the OH^* signal, a clear difference in terms of flame structure and lift-off length is visible between both configurations. DFI increases the LOL and moves the OH^* signal toward the bowl wall when compared to FS. This coincides with the literature findings [1, 2]. Another phenomenon that is visible when using DFI is the appearance of weak OH^* areas near some duct inlets. This indicates that a small amount of fuel could not be entering into the ducts and is being oxidized there. However, it is

a small percentage that is not affecting combustion performance and achieved IMEP.

Figure 5.4 shows the Mean Accumulated KL ($\overline{KL}_{\text{acc}}$) (see Equation 3.7) for the same DFI design (L8D2G4.28) and FS. The first thing that can be observed is that a lower $\overline{KL}_{\text{acc}}$ peak is reached with the DFI. At this stage of combustion, when soot levels increase, the formation of this pollutant dominates over its oxidation although both processes are taking place simultaneously. Thus, the lower peak observed indicates a lower net soot formation within the combustion which is in agreement with the soot reductions reported in literature. However, the reduction observed here (in terms of in-cylinder KL) seems to not be as important as the one reported in previous works. A more detailed quantification has been included in further sections.

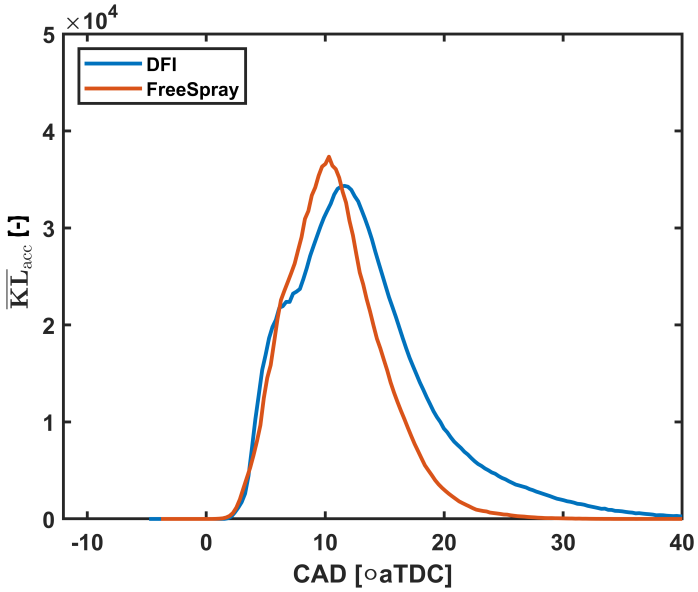

Figure 5.4: Comparison of Mean Accumulated KL ($\overline{KL}_{acc}$) between base DFI (L8D2G4.28) and Free Spray for 21% oxygen concentration case.

After the KL peak is reached, the decrease of the KL curve, corresponding to the soot oxidation phase, seems to be delayed for the DFI case as compared to FS. This behavior could be caused by several factors. Primarily the DFI device utilized in this study was relatively larger in volume as compared to the whole combustion chamber. This larger volume could hinder the oxidation of the soot that is re-directed from the re-entrant bowl walls towards the

center of the piston, because of less fresh air presence near the DFI device. In contrast to DFI, in the case of FS this reflected soot cloud could be oxidized by fresh air still present at the center of the bowl. Piano et al. [4] observed the late oxidation problem of DFI, where they performed a detailed CFD analysis under similar operating conditions as those considered in present thesis, including the bore/stroke ratio of the considered engine. They stated that the relatively small size of the combustion chamber could hinder the potential of DFI due to earlier interaction of the flame with the bowl wall and later with the device. These findings, which have not been observed previously in bigger engines, are corroborated by the results reported here.

To get a deeper insight into the OH^* and KL spatial evolution, Figure 5.5 shows the radial maps for both the cases of DFI and FS, built following the methodology described in Figure 3.8. The maps on the left represent OH^* evolution while on the right highlight the KL evolution. The OH^* maps highlight the high-temperature oxidation activity happening inside the combustion chamber while the evolution of soot is represented by the KL maps.

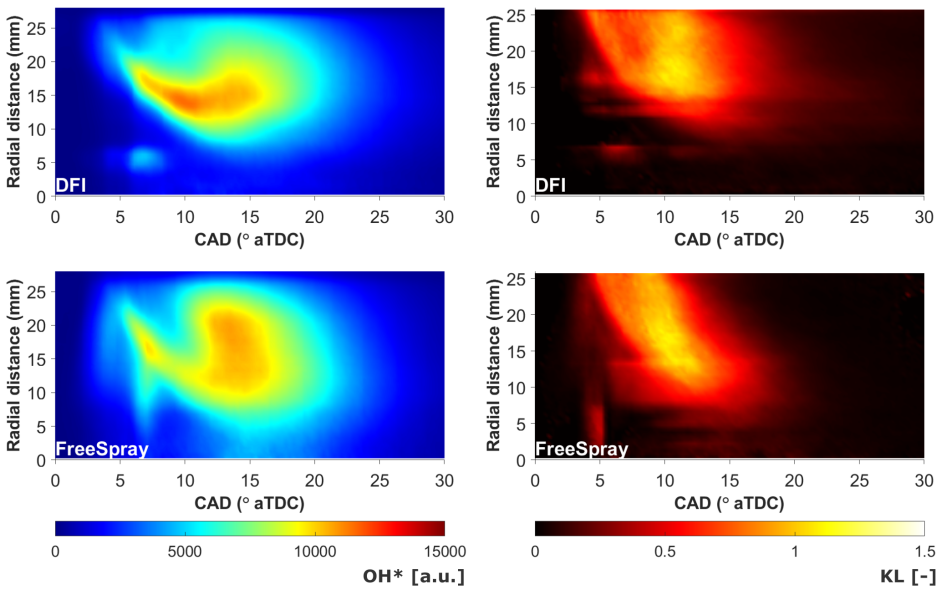

Figure 5.5: OH^* and KL radial maps obtained for base DFI (L8D2G4.28) and Free Spray at 21% oxygen concentration case.

It can be observed that the OH^* cloud for the case of DFI, when compared to the FS case, shows intense oxidation activity during the angle span where the KL peak is reached (see Figure 5.4). This leads to a lower $\overline{KL}_{\text{acc}}$ (lower soot) in the combustion chamber as reported previously, which suggests that the DFI decreases net soot formation when compared to FS. Moving to later stages of combustion, more differences between both configurations arise. The flame front for FS, as observed in KL maps, seems to be moving closer toward the bowl center as compared to DFI. In fact, in the DFI case, the soot cloud seems to drastically stop progression between 10 and 5 mm, due to the presence of the device. It is worth mentioning that the outer radius of the holder is close to 12 mm. It can also be observed that for the FS the higher OH^* radiation starts after 10°aTDC in contrast with DFI, where at the same angle the signal starts to decrease. In addition, the region of intense OH^* radiation with the FS extends from the periphery of the bowl to almost 10 mm from the nozzle, while with DFI seems to concentrate between 10 and 15 mm. In terms of KL, it is also possible to see that especially in the region between 15 and 25 mm KL seems to disappear faster for the FS case when compared to DFI, with which it is possible to see that KL remains visible for more time. All of this indicates that with FS a higher oxidation activity is achieved during later stages of combustion which leads to a faster soot oxidation in a wider region of the combustion chamber, as it was observed in Figure 5.4.

5.4 Parametric Evaluation of DFI geometry

The discussion is started by presenting a global overview of the effect of geometrical parameters on combustion development and performance. Then, it is followed by an analysis of soot (KL) and OH^* chemiluminescence in the combustion chamber. It should be taken into account that here also fossil diesel has been utilized for the parametric evaluation of the DFI geometry.

5.4.1 Thermodynamic analysis

Figure 5.6 shows the in-cylinder pressure and HRR for all the ducts and FS for three different oxygen concentration cases.

Primarily, a clear effect of decreasing the oxygen concentration can be seen with both DFI and FS. The ignition delay is increased as the oxygen concentration is decreased. The energy released by the pilot injection tends to weaken and even disappear in some cases. However, as stated previously, no clear and consistent differences between DFI and FS can be observed in this regard. Only the L10D2G4.28 configurations seem to cause a longer ignition

delay for all conditions. With the rest, it can be concluded that combustion evolution is similar to FS.

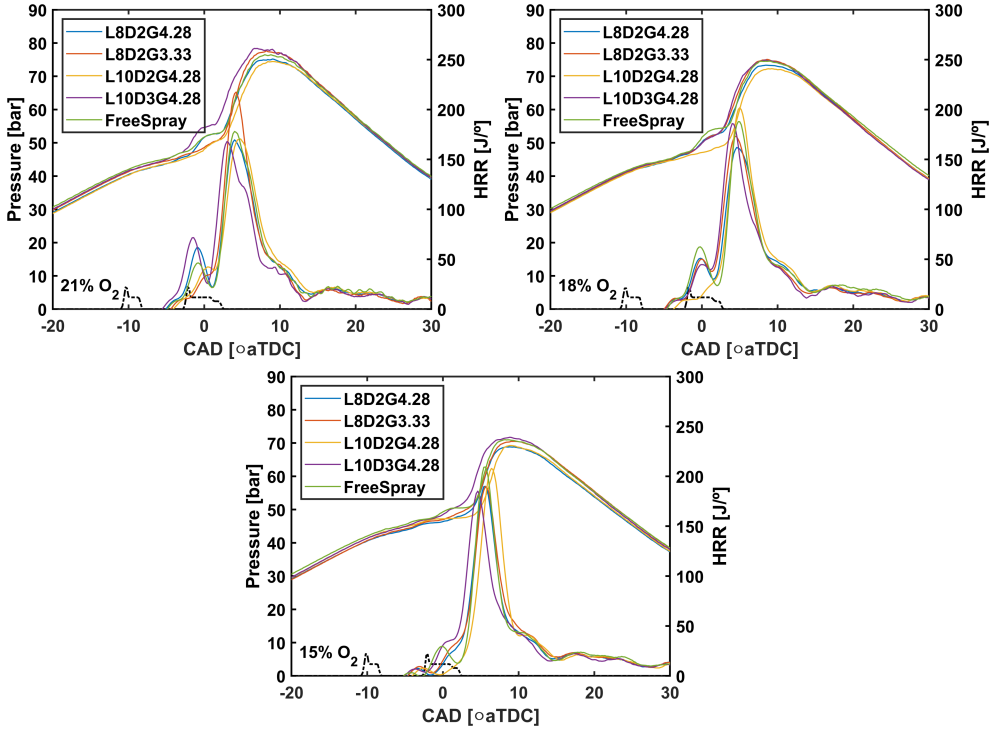

Figure 5.6: In-cylinder pressure and Heat release rate signals for all the ducts utilized and Free Spray configuration including all three oxygen concentrations (21, 18, and 15%).

5.4.2 In-cylinder KL analysis

In this section, the effect of the duct geometrical parameters on the DFI performance in terms of soot reduction will be analyzed. Figure 5.7 shows the $\overline{KL}_{\text{acc}}$ obtained for all four different duct configurations and FS in all three O_2 concentration conditions.

In general, all the geometries tested provide a reduction of the KL maximum peak and hence a reduction of soot formation as discussed previously. However, it can be seen that the duct L10D3G4.28 is consistent in reducing the maximum KL more than the other designs when compared to FS in all 3 oxygen concentration cases. Furthermore, all ducts show the limitations

with the late oxidation of soot. However, some duct designs seem to improve it when compared to the others. In this regard, the L10D3G4.28 and the L8D2G3.33 provide the best performance as a larger reduction of KL during the oxidation stage is reported.

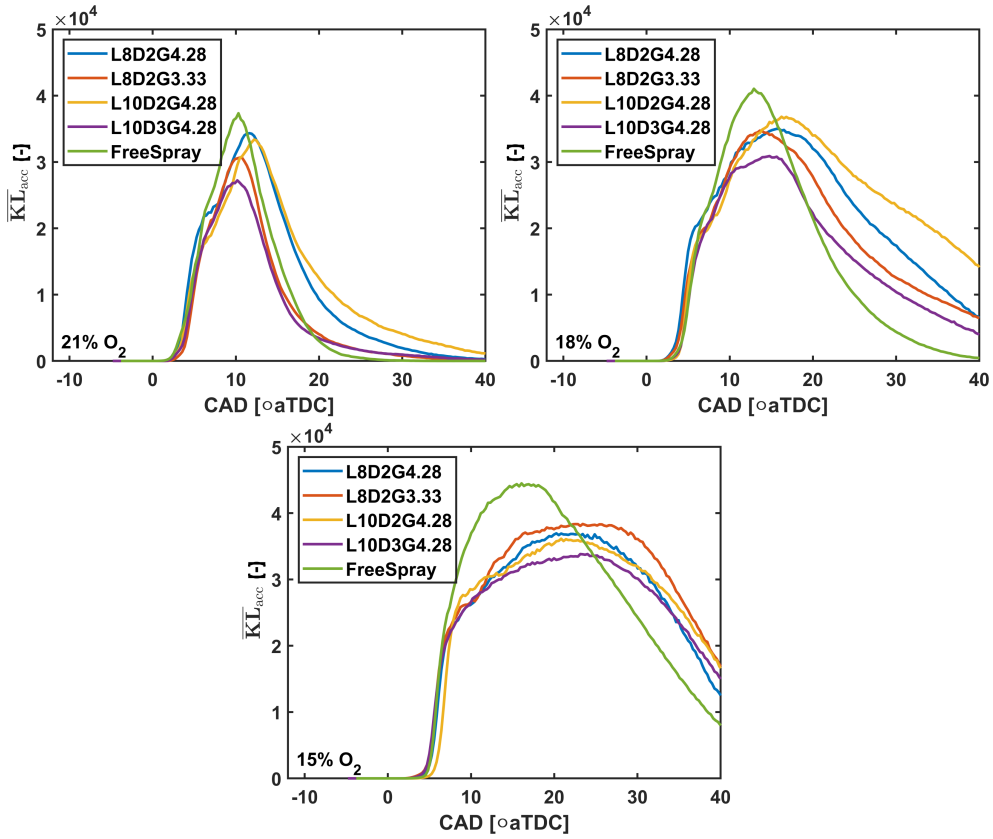

Figure 5.7: Mean Accumulated KL ($\overline{KL}_{acc}$) signal for all the ducts utilized and Free Spray configuration including all three oxygen concentrations (21, 18 and 15%).

To look at the spatial evolution of the combustion process, the analysis is complemented with the corresponding OH^* and KL radial maps for 21% O_2 (Figure 5.8). Thanks to these maps, it is possible to see large differences in terms of OH^* chemiluminescence among ducts. With L10D3G4.28 and L8D2G3.33, a much more intense activity is observed between 10 and 15°aTDC, extending among a wider region of the piston bowl between 15 and

25 mm radius from the nozzle. This is accompanied by a faster reduction of KL when compared to the other two cases, with which KL remains longer in the cycle at positions above 15 mm. The effect of each dimensional parameter has been discussed in more detail in the following paragraphs.

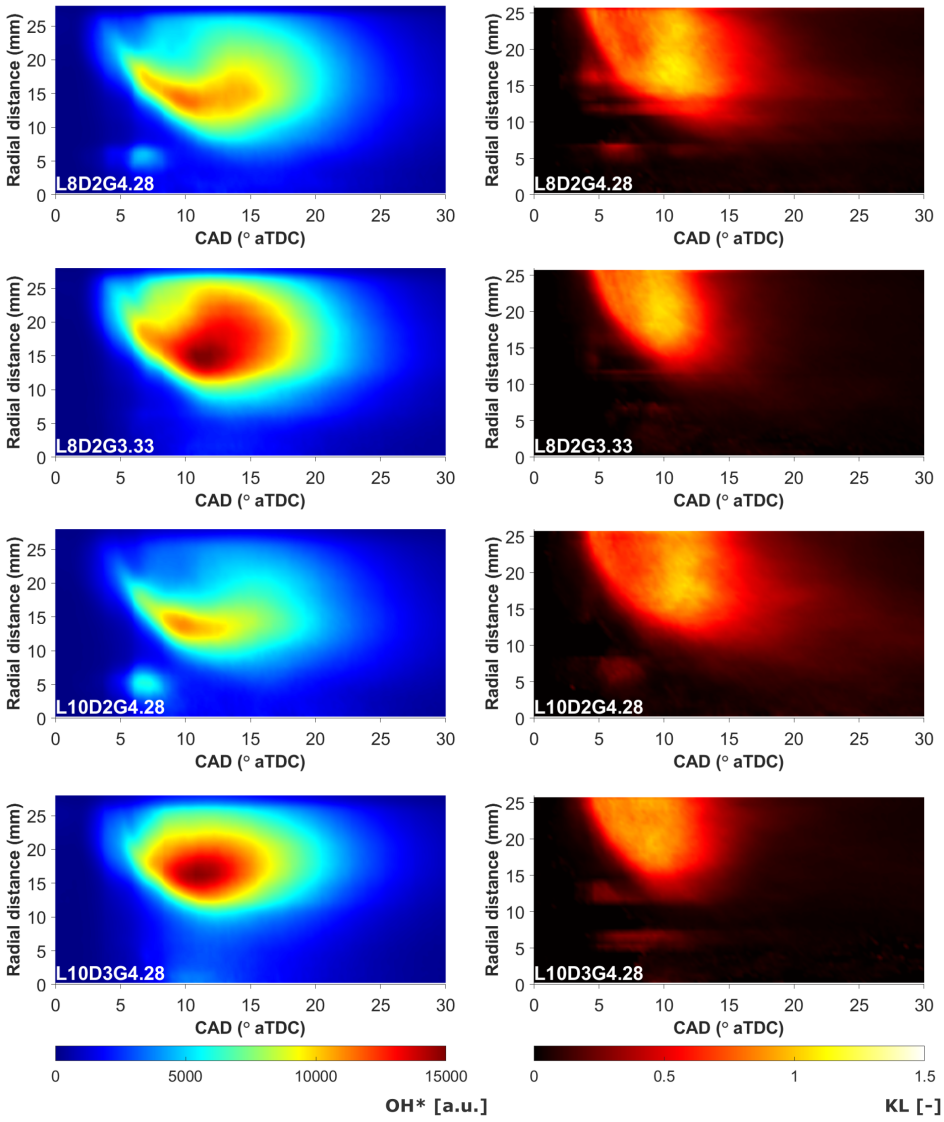

Figure 5.8: OH and KL radial maps obtained for all ducts and Free Spray at 21% oxygen concentration case.*

- **Influence of Stand-off Distance (G)**

Looking at Figure 5.7 and focusing on 21% O_2, by only decreasing the stand-off distance (G) from 4.28 mm (blue curve) to 3.33 mm (orange curve), the overall peak of the KL is decreased indicating lower net soot formation inside the cylinder. Improvement is also seen in terms of late oxidation. Therefore, it can be stated that reducing G helps both to reduce the overall KL and the speeding up the late oxidation of soot.

This can be explained by the fact that, as the duct inlet gets closer to the nozzle, the cross-section of the spray is smaller at the duct inlet leaving more space and improving air entrainment towards the duct, resulting in better air-fuel mixing and hence leaner combustion and lower soot formation. These results coincide with the literature, where it has been reported that lower G decreases soot formation while larger G has the opposite effect[5]. However, these authors also highlighted that a much smaller axial gap (G $<$ 2 mm) could reverse this relation because it will limit the entrainment of the air into the duct, resulting in higher soot formation. In this sense, Svensson et al. [3] evaluated G in a range from 0.1 to 6 mm in a high-temperature pressure vessel reporting similar conclusions despite not observing this change of trend. In applications like the one presented in this work, it is not possible to assemble the ducts so close, especially with multiple nozzle holes. Considering this limitation, it can be concluded that the duct should be mounted as close as possible to the nozzle exit which, in practice is limited to 3-4 mm for an 8-hole nozzle. Looking at the radial maps in Figure 5.8, it is quite clear when comparing OH^* chemiluminescence that decreasing G increases oxidation activity. This contributes towards the lower KL and faster decrease as discussed previously.

Moving towards lower oxygen concentrations, the trends observed for the case of 21% O_2 seem to hold only for 18% O_2. When reaching 15% O_2, the smaller G seems to become ineffective both in terms of decreasing the maximum KL and improving the late oxidation. The current author considers that the combination of a smaller G and lower oxygen concentration would make it difficult to entrain enough O_2 before duct inlet which would potentially lead to richer mixtures downstream the duct and hence more soot formation than the other duct configuration. The effect would be like the one described in [5] when decreasing G. Therefore, in general, it can be stated that the decrement of G, with constant L and D, improves the oxidation activity and results in a lower KL peak when compared with longer G as long as oxygen concentration is above 15%.

- **Influence of Duct Length (L)**

In this study, two different duct lengths have been tested: 8 mm and 10 mm. As mentioned in the device description, 10 mm was the maximum possible length to avoid interference with the valves. By looking at Figure 5.7 and focusing first on 21% O_2, small differences can be seen when comparing L8D2G4.28 (blue curve) and L10D2G4.28 (yellow curve). Primarily, when increasing L, the KL maximum peak is delayed and slightly decreased. Regarding late oxidation, the same behavior is observed or even slightly worsened. The OH^* chemiluminescence (Figure 5.8) shows a slightly less intense region for the longer duct suggesting lower oxidation activity. In addition, KL maps show a wider cloud for a longer time indicating slower oxidation of soot. When comparing with the literature, authors in [5] reported that no significant differences were observed in terms of soot reduction when duct length was changed from 8 to 16 mm keeping the G and D same. Similar results were observed by Nilsen et al. [6] where the difference in terms of soot attenuation was not significant when comparing larger and shorter ducts. Henceforth, the findings in the current work in terms of net soot formation are consistent with the literature. However, some problems arise for L = 10 mm which have not been observed in other applications. The trends observed for the case of 21% O_2 are held for 18% and 15% O_2 cases. A longer L provides a slightly lower maximum KL peak but slows down the oxidation process as compared to a shorter L. However, the differences reported are subtle.

- **Influence of Duct Diameter (D)**

As it was highlighted previously, duct L10D3G4.28 provided the best improvement in terms of KL among all the designs tested when compared to FS. Keeping the L and G constant, the $\overline{KL}_{\text{acc}}$ evolution curves for L10D2G4.28 (yellow) and L10D3G4.28 (purple) for 21% O_2 can be compared in Figure 5.7. A significant reduction is achieved when duct diameter is increased by 1 mm, keeping the other parameters constant. This could be related to the fact that as the nozzle orifice diameter is larger in this work (138 μm), more fuel is injected, and hence more air is required to be entertained at the duct inlet to achieve better mixing. In this regard, a larger diameter of the duct is beneficial. In addition, an improvement in oxidation is also observed. These findings are consistent with the literature as reported in [6]. Their results indicated that a larger diameter with a larger nozzle orifice diameter worked better in terms of soot attenuation as compared to a smaller diameter when keeping L and G the same. The OH^* chemiluminescence maps in Figure 5.8 also highlight significant differences in terms of signal intensity. For the case of D = 3 mm, the OH^* signal is much more intense, highlighting a stronger

oxidation activity. This is also reflected in KL evolution maps in Figure 5.8, where KL cloud is much smaller and extinguishes faster compared to D = 2 mm, indicating faster oxidation.

The same trend is also observed for 18% and 15% O_2 cases. Hence, in general, it can be stated that the increment of D, with constant G and L, results in a lower KL peak and higher oxidation activity when compared with smaller D.

5.4.3 Quantification of in-cylinder KL reduction achieved with DFI

To get a better understanding of global behavior in terms of reduction in KL by utilizing different ducts, the Mean Accumulated KL ($\overline{KL}_{\text{acc}}$) reduction is plotted for all ducts calculated with respect to FS and for three different O_2 concentrations. This reduction has been calculated according to Equation 5.1 by subtracting the $\overline{KL}_{\text{acc}}$ obtained by each DFI from the FS values and then normalized by the $\overline{KL}_{\text{acc}}$ achieved with FS. It must be noted that the calculation is performed per each crank angle degree (CAD).

$$\overline{KL}_{\text{acc}}Reduction = \frac{\overline{KL}_{\text{acc.FS}} - \overline{KL}_{\text{acc.DFI}}}{\overline{KL}_{\text{acc.FS}}} \tag{5.1}$$

Figure 5.9 shows the $\overline{KL}_{\text{acc}}$ reduction evolution obtained for each of the four duct designs utilized in this work and for three different oxygen concentrations discussed previously. In all three cases, it can be seen that the maximum KL reduction is achieved by L10D3G4.28 where it varies from 30-35% with respect to FS. In contrast, the worst performance is obtained with the L8D2G4.28 for which the maximum values vary between 15-20% and are visible for a shorter range of CAD. The advantages reported for L8D2G3.33 and L10D3G4.28 are related to lower maximum KL achieved but are also observable for a longer part of the combustion cycle (up to 20°aTDC) thanks to the fewer oxidation difficulties reported. Nevertheless, for all the geometries the KL decreases slower than with FS and, at a certain point, measured KL levels become higher, as can be observed in Figure 5.9 when the reduction values become negative. This effect was also reported by Piano et al. [4] under similar geometrical and operating conditions.

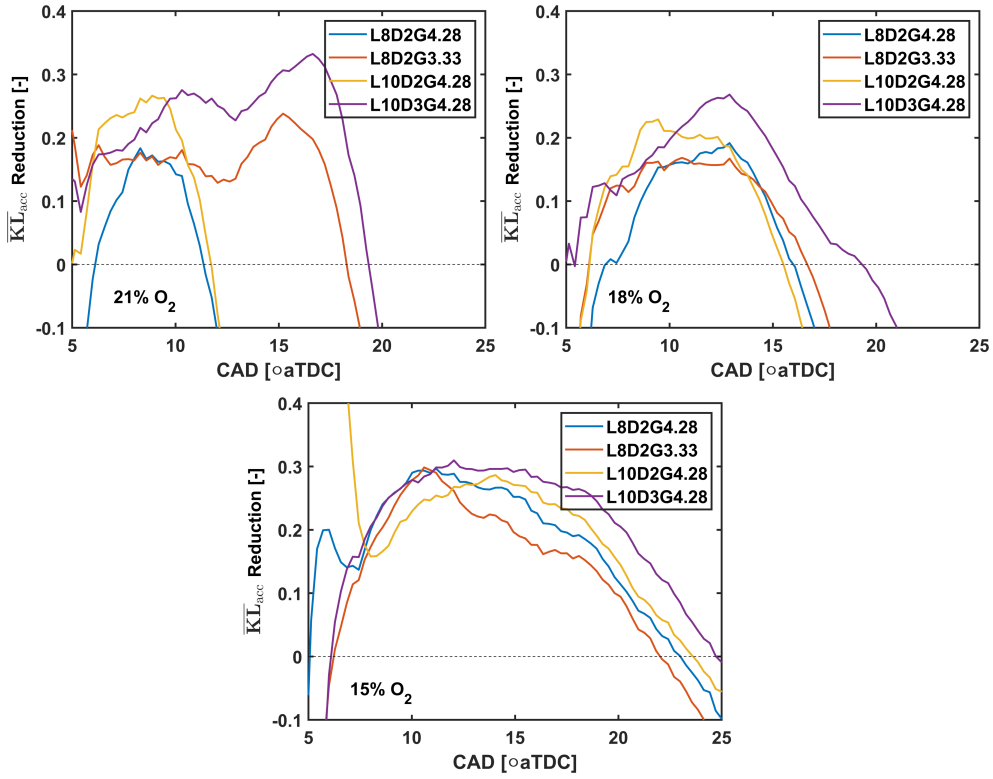

Figure 5.9: Mean Accumulated KL ($\overline{KL}_{acc}$) reduction obtained for each duct with respect to Free Spray case at all three oxygen concentrations (21, 18 and 15%).

5.5 Application of fuel blends to DFI

Based on the results established earlier during the parametric evaluation of DFI geometry, the duct L10D3G4.28 performs better in terms of KL reduction as compared to other designs. Therefore, this duct was further utilized with the blends of Diesel-OME_x i.e., D70O30 and D50O50 as described in the introduction section, to understand their effect on DFI performance. As observed earlier, DFI exhibits late oxidation problems. On the other hand as reported previously in chapter 4, these blends promote the oxidation reaction which results in a faster combustion and in turn lesser soot formation. Therefore, this approach of utilizing DFI with these specific blends was followed in order to overcome the drawbacks observed with DFI while improving the soot reduction observed with these fuels.

Figure 5.10 shows the in-cylinder pressure and heat release rate signal for the case of fossil diesel (D100), D70O30 and D50O50 for both 21% and 15% O_2 concentration. As mentioned in the introduction section, the injection strategy was modified for the case of blends in order to achieve the same IMEP for every case, therefore, not so many differences are visible in terms of combustion evolution for the case of pure diesel and its blends with OME_x for each O_2 concentration case. Ignition delay is however shortened while utilizing these blends as compared to pure diesel for both oxygen concentration cases, which has been already discussed in previous chapter 4 while discussing the combustion characteristics of these blends (see Figure 4.10).

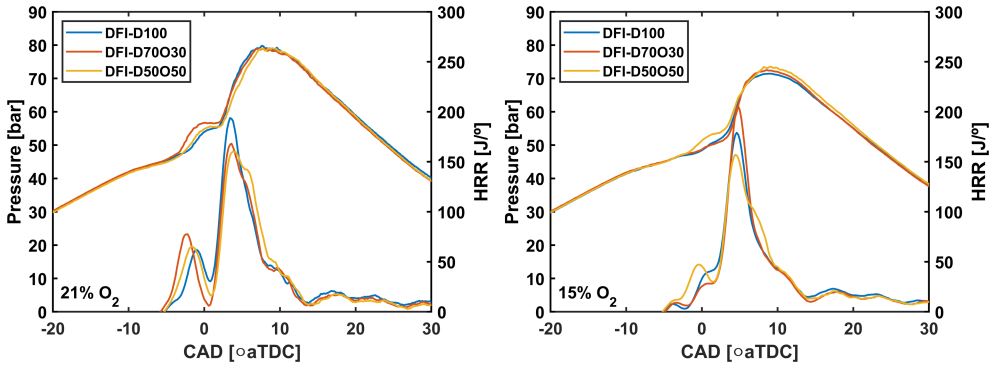

Figure 5.10: In-cylinder pressure and Heat release rate signals for L10D3G4.28 duct case for three fuel blends (D100,D70O30 and D50O50) and two oxygen concentrations (21 and 15%).

Figure 5.11 shows the $\overline{KL}_{\text{acc}}$ obtained for all the fuel blends for L10D3G4.28 in both O_2 concentration conditions. In general, it can be seen that the blend having the most OME_x in it provides the maximum KL reduction i.e., D50O50. The KL peak decreases with the increase in the OME_x content in the blend. Furthermore, the late oxidation problems are also tackled while using the blends along with DFI. It can be seen that both less soot KL is formed and it is oxidized earlier when compared to the D100 case. This is true for both O_2 concentrations, however, it is more prominent for the 21% oxygen concentration case.

The reasons for this behavior can be traced back to chapter 4 where a detailed numerical analysis for Diesel- OME_x blends was carried out. The addition of OME_x in the blend with diesel, as established earlier, alters the stoichiometry of the blend, displacing the equivalence ratios regions to below

2 which promotes lower soot formation. Furthermore, the presence of oxygen speeds up the oxidation process of the soot. Therefore, it can be said that the performance of the DFI (L10D3G4.28) is improved in terms of KL reduction and late soot oxidation when utilized alongside the Diesel-OME_x blends.

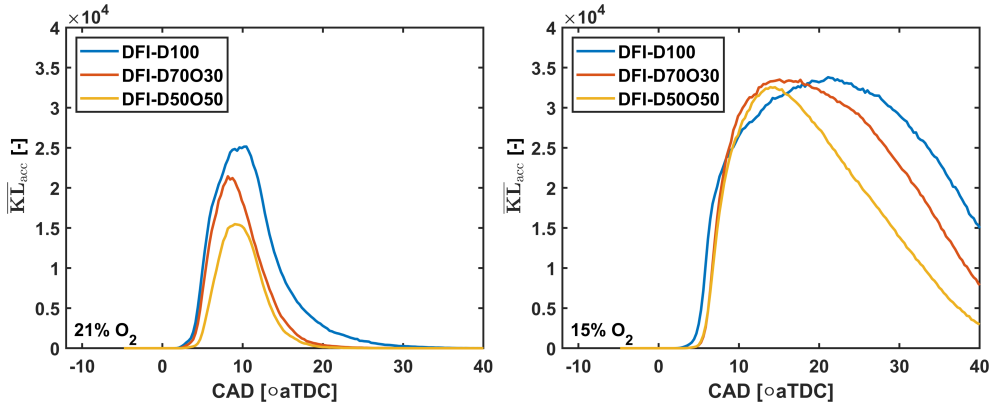

Figure 5.11: Mean Accumulated KL ($\overline{KL}_{acc}$) signal for L10D3G4.28 duct case for three fuel blends (D100,D70O30 and D50O50) and two oxygen concentrations (21 and 15%).

5.6 Summary and conclusions

The DFI concept has been evaluated experimentally to reduce pollutant (soot) emissions inside a medium-duty optical engine with a nozzle having 8 holes. It represents a particular application different from those reported previously in the literature. Four different duct designs were utilized in this study among which the most relevant geometrical parameters (G, D, and L) were modified to evaluate its influence on DFI performance. The first analysis comparing one of the duct designs (L8D2G4.28) with the FS configuration confirmed the influence of DFI on combustion evolution, especially in terms of spatial development. The results confirmed also that net soot formation was attenuated but some problems were observed during the late oxidation stage. When analyzing the influence of G, L, and D on DFI performance, the following conclusions can be established:

- Reduction of stand-off distance (G), improves the late oxidation and also decreases the maximum KL peak. This agrees with the results observed in literature in larger engines and combustion vessels. However, some

limitations have been observed when O_2 concentration is reduced below 18%.

- Increment in duct length (L), has almost no effect on reducing net soot formation (KL peak) and worsens the oxidation.
- Increasing the duct diameter (D), improves the late oxidation to quite an extent and decreases the maximum KL peak. This behavior is consistent with literature for large nozzle orifices and is maintained even when decreasing O_2 concentration up to 15%.

From these conclusions, L10D3G4.28 can be identified as an optimum duct geometry as it provides the lowest soot formation and faster oxidation than the other designs. Furthermore, the performance of the said duct, when utilized with fuel blends (D70O30 and D50O50), is improved significantly in terms of soot reduction and late oxidation. However, a further combination of the designs proposed here could perform better. A lower G (3.33 mm) combined with a shorter duct length (8 mm) and larger diameter (3 mm) seems to be the way to find the optimum design for this application. Further exploration in this regard including detailed CFD simulations would be required to improve this definition.

Based on the experimental results reported, it can be stated that DFI does reduce net soot formation when utilized with fossil diesel. However, reduction levels achieved (based on KL) are not as high as those reported in the literature. The use of a relatively small-bore size compared to other applications could be a critical aspect as well as the amount of nozzle orifices. Further, the late oxidation problems reported in this thesis were not observed previously in other scenarios. The blends of Diesel-OME_x blends could be used to improve the DFI performance in terms of soot reduction and late oxidation problem. However, in general, this stage of the combustion process would require a deeper investigation in future works to better understand the reasons after these observations.

References

[1] Mueller, Charles J et al. “Ducted fuel injection: A new approach for lowering soot emissions from direct-injection engines”. In: *Applied energy* 204 (2017), pp. 206–220.

[2] Fitzgerald, Russell, Svensson, Kenth, Martin, Glen, Qi, Yongli, and Koci, Chad. "Early investigation of ducted fuel injection for reducing soot in mixing-controlled diesel flames". In: *SAE International Journal of Engines* 11.6 (2018), pp. 817–834.

[3] Svensson, Kenth I and Martin, Glen C. "Ducted fuel injection: effects of stand-off distance and duct length on soot reduction". In: *SAE International Journal of Advances and Current Practices in Mobility* 1.2019-01-0545 (2019), pp. 1074–1083.

[4] Piano, Andrea, Segatori, Cristiano, Millo, Federico, Pesce, Francesco Concetto, and Vassallo, Alberto Lorenzo. "Investigation of Ducted Fuel Injection Implementation in a Retrofitted Light-Duty Diesel Engine through Numerical Simulation". In: *SAE International Journal of Engines* 16.03-16-05-0038 (2022).

[5] Gehmlich, RK et al. "Using ducted fuel injection to attenuate or prevent soot formation in mixing-controlled combustion strategies for engine applications". In: *Applied energy* 226 (2018), pp. 1169–1186.

[6] Nilsen, Christopher W, Biles, Drummond E, Wilmer, Brady M, and Mueller, Charles J. "Investigating the effects of duct length and diameter and fuel-injector orifice diameter in a compression-ignition engine equipped with ducted fuel injection". In: *Applications in Energy and Combustion Science* 7 (2021), p. 100030.

Chapter 6

Conclusions and future works

6.1 Introduction

This chapter aims to summarize the main findings reported in the previous chapters of the thesis. It starts by outlining the conclusions obtained by both the numerical study carried out on the potential of different fuel blends in chapter 4 and experimental analysis carried out on the DFI concept in chapter 5. The chapter concludes by offering recommendations for potential future research directions within the scope of the thesis.

6.2 Conclusions

The main goal of this thesis as already established was the assessment of different solutions to reduce pollutant emission in compression ignition engines by utilizing both numerical and optical techniques. A detailed literature

review was first carried out. It put in evidence the necessity of finding new strategies to mitigate pollutant formation in CI engines. Two promising approaches including utilization of alternative fuels and implementation of hardware improvements inside CI engine were identified as potential pathways for reducing the pollutant emissions in diesel engines in the context of current thesis.

The research on utilization of alternative fuels inside CI engines has been widely explored. These alternative fuels present themselves as a viable choice over the traditional fossil-based fuels which are constantly depleting and significantly contribute towards global GHG as well as tail pipe emissions. Alternative fuels including both biofuels and efuels are of significant importance as they help in achieving energy sustainability, enhancing engine efficiency and reducing emissions as well as alleviating the disproportionate reliance on traditional petroleum-based fossil fuels. During the context of this thesis, the potential of alternative fuels including Hydrotreated vegetable oil and Oxymethylene dimethyl ethers has been explored. The literature research related to these fuels was mainly focused on experimental studies, with a few numerical studies. Furthermore, the literature was also confined to the use of specific blends of these fuels due to the absence of reduced chemical reaction mechanisms necessary to perform numerical simulations. So, a different perspective in terms of numerical modeling of fuel blends of Diesel-OME_x and HVO-OME_1 was explored in chapter 4, which involved the development of a reduced and robust chemical reaction mechanism followed by detailed combustion and emission analysis performed by doing detailed 3D CFD simulations on the basis of a medium-duty optical CI engine.

In conjunction with the exploration of alternative fuels for CI engines, the development of combustion system hardware offers itself a promising strategy to mitigate pollutant emissions. In this context, research work has already been carried out mainly on approaches like changes applied to piston bowl design, optimization of the combustion chamber, optimizing cylinder head design and changing the injector nozzle design, etc. During the context of this thesis, a relatively new concept namely Ducted fuel injection was explored in chapter 5. In the case of the use of the DFI concept, the literature was also focused mainly on experimental studies and was mainly confined to heavy-duty engines as it is a relatively new concept. Hence, a different perspective in terms of experimental modeling of the DFI concept applied to a medium-duty optical CI engine was explored, which improved the understanding of the working principle and combustion and emission behavior of DFI.

The important conclusions of these two different approaches i.e., a numer-

ical study on blends of different fuels and an experimental study of the DFI concept are summarized in the following subsections.

6.2.1 Potential of blends of different fuels to tackle pollutant emissions

A detailed numerical analysis regarding the blends of different fuels including Diesel-OME_x and HVO-OME_1 blends was carried out. For both cases, the analysis began with the identification and development of a reaction mechanism necessary for numerical simulations of blends, and later on, combustion evolution and emissions formation inside the combustion chamber were studied through numerical simulations utilizing the developed reaction mechanism. The following major conclusions (listed here comparatively) can be drawn from the numerical analysis of these blends.

- The developed PRF-OME_x mechanism and the developed Optimized Yao-SNL mechanism necessary for simulations of Diesel-OME_x and HVO-OME_1 blends respectively performed quite accurately. The results obtained with both of them were compared with experimental data, showing capabilities to reproduce fundamental combustion parameters such as ignition delay, laminar flame speeds and chemical species evolution in a wide range of operating conditions. All this is an indication of their robustness and accuracy. These mechanisms were then utilized to perform accurate 3D CFD simulations of the respective blends and the results were validated thanks to the experimental data acquired in the optical engine.

- The ignition delay for the case of Diesel-OME_x blends decreases when increasing the OME_x content. This primarily relates to the higher oxygen percentage present in the blends having higher OME_x content in them. Numerically, increasing the OME_x percentage in the blend from 10% to 50%, decreases the ignition delay by almost 19%. However, in contrast, the ignition delay for the case of HVO-OME_1 blends increases when increasing the OME_1 content. This primarily relates to the lesser reactivity of blends having higher OME_1 content in them. Numerically, increasing the OME_1 percentage in the blend to 30% prolongs the ignition delay by almost 26%.

- In terms of heat release rate, an increase of OME_x content from 10% to 50% increases the combustion speed (late stage of combustion) up to 5%. This is corroborated by the faster disappearance of OH signal

for blends having higher OME_x content in them. In contrast, no such phenomenon is observed while analyzing HVO-OME_1 primarily because OME_1 content in those blends is restricted to a maximum of 30%.

- The addition of oxygenated fuel both OME_x in Diesel and OME_1 in HVO effects the stoichiometry of the blends. The quantity of total fuel mass present at equivalence ratios above 2 drops, when the OME_x or OME_1 content in the respective blend is increased. The lower equivalence ratios reached promote oxidation reaction which corroborate with sooner OH disappearance. This particular phenomenon hints towards lesser soot formation.

- The evolution of soot, both spatial and temporal, is similar for both blends. Soot is formed close to the periphery of the piston bowl for both Diesel-OME_x and HVO-OME_1 blend cases. However, a higher soot concentration appears for blends having lesser OME_x or OME_1 in them.

- A drop in maximum in-cylinder temperature is observed when adding OME_x in Diesel and OME_1 in HVO. This in turn related to lesser NO_x formation for the highly oxygenated blends.

- The diminished lower heating value of both OME_x and OME_1 serves as a constraint, resulting in achieving less heat released during the combustion process however this is insignificant as compared to advantages achieved in terms of soot and NO_x emissions reduction. In general, the addition of OME_x content in Diesel from 10% to 50% results in a decrease of soot and NO_x emissions by 56% and 32% respectively, with a much lower reduction of total energy release of 19%. Similarly, the addition of OME_1 content in HVO from 0% to 30% results in a decrease of soot and NO_x emissions by 50% and 37% respectively, with a much lower reduction of total energy release of 8%.

As a general conclusion from this part of this thesis, it can be said that the blends of these different fuels studied here i.e., Diesel-OME_x and HVO-OME_1 present themselves as a potential solution to tackle major pollutant emissions including soot and NO_x in CI engines. The lower LHV of these oxygenated fuels is a constraint, however it can be compensated by modifying the injection strategy. The advantages achieved in terms of pollutant reduction including both soot and NO_x surpass the energy reduction caused by these fuels, which is quite low and can be compensated. Furthermore, the comparison presented here reflects a possible strategy to implement these blends in

real applications. In addition, the reaction mechanisms developed herein can be utilized for application in engine combustion simulations irrespective of the initial conditions and CI engine hardware utilized.

6.2.2 Ducted fuel injection (DFI) concept applied to CI engines to reduce pollutant emissions

A detailed experimental analysis was carried out regarding the ducted fuel injection during the second part of this thesis. In this context, a prototype was designed, manufactured, tested and adapted to the optical engine. The prototype consisted of two distinct parts named duct and holder and it was designed in such a way that it was easy remove and replace the different ducts utilized. The design was proven to be successful in terms of implementation and testing inside the optical engine. The DFI concept was then evaluated experimentally in a medium-duty optical engine with a nozzle having 8 holes fuelled with fossil diesel and Diesel-OME_x blends. It should be highlighted that, this work was different when compared to what was already done in literature in terms of the size of engine platform and number of injector holes utilized. In doing so, four different duct designs were utilized in this study among which the most relevant geometrical parameters (G, D, and L) were modified to evaluate its influence on DFI performance in terms of reduction in soot KL. The following major conclusions can be drawn from this analysis.

- In general, the DFI does attenuate the soot when applied in the particular application tested during this thesis however, it suffers from late soot oxidation problems which can be related to the particular design constraints including the piston geometry utilized and the relatively larger size of the DFI geometry as compared to the combustion chamber.
- Reduction of stand-off distance (G) and increasing the duct diameter (D) improves the late oxidation to quite an extent and decreases the maximum KL peak. However, Increment in duct length (L), has almost no effect on reducing net soot formation (KL peak) and it worsens the oxidation.
- L10D3G4.28 is identified as an optimum duct geometry as it provides the lowest soot formation and faster oxidation than the other designs as it provides almost 30-35% reduction in soot KL as compared to free spray configuration.

- The performance of L10D3G4.28 duct when utilized along with blends of Diesel-OME_x i.e, D70O30 and D50O50, is improved significantly in terms of soot reduction and late oxidation.

As a general conclusion from this part of this thesis, it can be said that DFI does work in terms of reducing soot emissions when applied in a CI engine application. However, reduction levels achieved (based on KL) herein are not as high as those reported in the literature. The use of a relatively small-bore size as well as the amount of nozzle orifices compared to other applications could be a critical aspect in DFI application as it leads to an earlier interaction of the flame with the bowl wall and later with the relatively larger DFI device in the center which hinders late oxidation.

6.3 Future works

The present thesis has evaluated the potential of blends of different fuels as well as new hardware improvement i.e., DFI concept with the objective of reducing pollutant emissions in compression ignition engines. Even though the study has provided interesting results regarding the potential of Diesel-OME_x and HVO-OME_1 blends as well as the DFI concept, there are certain features that have an extensive field to be investigated and better understood. Some suggestions for future works are provided in the following paragraphs.

- **Evaluation of fuel blends on a wide range of engine operating conditions and validation of pollutant prediction with exhaust emissions**

Although different fuel blends are numerically investigated during this thesis however the application herein is limited to a single injection strategy and single medium-duty alike engine load. The application of the developed CFD model and the developed chemical mechanisms could be extended to conditions having a range of engine load and multiple injection strategies including pilot and main injections. This would on one hand improve the understanding and performance of these fuel blends at a wide range of operating conditions and on the other hand help in validating the developed reaction mechanisms. Furthermore, the pollutant predictions done by the numerical model could be compared with exhaust measurements. The development of an experimental methodology by CMT research group is necessary to accomplish this task. This will further help in validating the numerical model in terms of real engine exhaust emissions.

- **Investigation of DFI concept via CFD simualations**

The DFI concept during this thesis is evaluated experimentally with room given to future CFD studies. The already developed CFD model of the optical engine could be extended to include the DFI device in it and then a detailed numerical analysis could be carried out to better understand the working principle of the DFI, as 3D CFD gives detailed information about the in-cylinder combustion phenomenon. This is important because the experimental analysis carried out in this thesis wasn't able to provide enough information regarding the problems associated with DFI performance as in terms of late oxidation. In this context, the CFD approach can shed light as a it can provide detailed information about different parameters like equivalence ratios fields achieved after the duct and inside the chamber, flame-wall interaction, fuel mass accumulation near the holder and inside the duct, the alignment of the injector with the duct, etc. These open points along with many other which were not investigated via experimental analysis could be addressed by utilizing detailed CFD simulations.

- **Utilization of new piston geometries alongside the DFI concept**

Last but not least, the application of the DFI concept could be extended to different piston geometries in contrast to flat piston studied in this thesis. This could result in a substantial improvement in DFI performance in terms of soot reduction. Furthermore, these sophisticated piston geometries could be effective in terms of speeding up late soot oxidation which has been the problem associated with flat piston utilized in this thesis. In this context different pistons like wave piston geometry by VOLVO, a re-entrant piston with a bump in the middle instead of a flat bowl, a stepped lip piston, etc could be explored along with DFI.

Global Bibliography

Aatola, Hannu, Larmi, Martti, Sarjovaara, Teemu, and Mikkonen, Seppo. "Hydrotreated vegetable oil (HVO) as a renewable diesel fuel: trade-off between NOx, particulate emission, and fuel consumption of a heavy duty engine". In: *SAE International Journal of Engines* 1.1 (2009), pp. 1251–1262.

Agarwal, Avinash Kumar et al. "Ultra-low soot/particulate emissions from a dimethyl ether-fueled agricultural tractor engine". In: *Fuel* 356 (2024), p. 129637.

Aithal, SM. "Modeling of NOx formation in diesel engines using finite-rate chemical kinetics". In: *Applied Energy* 87.7 (2010), pp. 2256–2265.

Alozie, Nehemiah Sabinus and Ganippa, Lionel Christopher. "Diesel Exhaust Emissions and Mitigations". In: *Introduction to Diesel Emissions*. Ed. by Richard Viskup. Rijeka: IntechOpen, 2019. Chap. 1. DOI: 10.5772/intechopen.85248.

Amsden, Anthony A and Findley, Margaret. *KIVA-3V: A block-structured KIVA program for engines with vertical or canted valves*. Tech. rep. Lawrence Livermore National Lab.(LLNL), Livermore, CA (United States), 1997. DOI: 10.2172/505339.

ANSYS, Chemkin. *Reaction Workbench 17.0*. 2016.

Arunkumar, M, Kannan, M, and Murali, G. "Experimental studies on engine performance and emission characteristics using castor biodiesel as fuel in CI engine". In: *Renewable Energy* 131 (2019), pp. 737–744.

Bae, Choongsik and Kim, Jaeheun. "Alternative fuels for internal combustion engines". In: *Proceedings of the Combustion Institute* 36.3 (2017), pp. 3389–3413.

Bakali, A El, Delfau, J-L, and Vovelle, Christian. “Experimental study of 1 atmosphere, rich, premixed n-heptane and iso-octane flames”. In: *Combustion science and technology* 140.1-6 (1998), pp. 69–91.

Barro, Christophe, Parravicini, Matteo, and Boulouchos, Konstantinos. “Neat polyoxymethylene dimethyl ether in a diesel engine; part 1: Detailed combustion analysis”. In: *Fuel* 256 (2019), p. 115892.

Bartok, William and Sarofim, Adel F. “Fossil fuel combustion: a source book”. In: (1991).

Benajes, Jesus, Garcia-Oliver, Jose M, Pastor, Jose M, and De Leon-Ceriani, Daiana. “Unsteady Flamelet modeling study on OMEx-type fuels under Engine Combustion Network Spray A conditions”. In: *Fuel* 331 (2023), p. 125458.

Bjørgen, Karl Oskar Pires, Emberson, David Robert, and Løvås, Terese. “Combustion and soot characteristics of hydrotreated vegetable oil compression-ignited spray flames”. In: *Fuel* 266 (2020), p. 116942.

Boccardo, Giulio et al. “Experimental investigation on a 3000 bar fuel injection system for a SCR-free non-road diesel engine”. In: *Fuel* 243 (2019), pp. 342–351.

Bortel, Ivan, Vávra, Jiří, and Takáts, Michal. “Effect of HVO fuel mixtures on emissions and performance of a passenger car size diesel engine”. In: *Renewable Energy* 140 (2019), pp. 680–691.

Burger, Jakob, Siegert, Markus, Ströfer, Eckhard, and Hasse, Hans. “Poly (oxymethylene) dimethyl ethers as components of tailored diesel fuel: Properties, synthesis and purification concepts”. In: *Fuel* 89.11 (2010), pp. 3315–3319.

Burger, Jakob, Ströfer, Eckhard, and Hasse, Hans. “Production process for diesel fuel components poly (oxymethylene) dimethyl ethers from methane-based products by hierarchical optimization with varying model depth”. In: *Chemical Engineering Research and Design* 91.12 (2013), pp. 2648–2662.

Cai, Liming et al. “Optimized reaction mechanism rate rules for ignition of normal alkanes”. In: *Combustion and Flame* 173 (2016), pp. 468–482.

Cai, Liming et al. “Auto-ignition of oxymethylene ethers (OMEn, n= 2–4) as promising synthetic e-fuels from renewable electricity: shock tube experiments and automatic mechanism generation”. In: *Fuel* 264 (2020), p. 116711.

Cai, Panpan et al. “Effects of Fischer-Tropsch diesel blending in petrochemical diesel on combustion and emissions of a common-rail diesel engine”. In: *Fuel* 305 (2021), p. 121587.

Cant, Stewart. “SB Pope, Turbulent Flows, Cambridge University Press, Cambridge, UK, 2000, 771 pp.” In: *Combustion and Flame* 4.125 (2001), pp. 1361–1362.

Cepsa begins supply of HVO (100% renewable diesel) for professional customers. 2023.

Chang, Yachao et al. “Development of a skeletal mechanism for diesel surrogate fuel by using a decoupling methodology”. In: *Combustion and Flame* 162.10 (2015), pp. 3785–3802.

Chau, Vo Tan, Chinda, Charoenphonphanich, Preechar, Karin, Sato, Susumu, and Kosaka, Hidenori. “Optical study on combustion characteristics of hydrotreated vegetable oil and blends under simulated CI engine conditions and various EGR”. In: *Journal of Mechanical Science and Technology* 31 (2017), pp. 4521–4531.

Chen, Hao, He, Jingjing, and Zhong, Xianglin. “Engine combustion and emission fuelled with natural gas: a review”. In: *Journal of the Energy Institute* 92.4 (2019), pp. 1123–1136.

Cheng, Song et al. “Autoignition and preliminary heat release of gasoline surrogates and their blends with ethanol at engine-relevant conditions: Experiments and comprehensive kinetic modeling”. In: *Combustion and Flame* 228 (2021), pp. 57–77.

Chiong, Meng-Choung et al. “Advancements of combustion technologies in the ammonia-fuelled engines”. In: *Energy Conversion and Management* 244 (2021), p. 114460.

Chum, Helena L and Overend, Ralph P. “Biomass and renewable fuels”. In: *Fuel processing technology* 71.1-3 (2001), pp. 187–195.

Davis, Scott G and Law, Chung King. “Laminar flame speeds and oxidation kinetics of iso-octane-air and n-heptane-air flames”. In: *Symposium (international) on combustion*. Vol. 27. 1. Elsevier. 1998, pp. 521–527.

Dec, John E. “A conceptual model of DL diesel combustion based on laser-sheet imaging”. In: *SAE transactions* (1997), pp. 1319–1348.

Dec, John E and Coy, Edward B. “OH radical imaging in a DI diesel engine and the structure of the early diffusion flame”. In: *SAE transactions* (1996), pp. 1127–1148.

Deepanraj, B, Sankaranarayanan, G, Senthilkumar, N, and Pugazhvadivu, M. "Influence of dimethoxymethane addition on performance, emission and combustion characteristics of the diesel engine". In: *International Journal of Ambient Energy* 38.6 (2017), pp. 622–626.

Dempsey, Adam B, Seiler, Patrick J, Svensson, Kenth I, and Qi, Yongli. "A comprehensive evaluation of diesel engine CFD modeling predictions using a semi-empirical soot model over a broad range of combustion systems". In: *SAE International Journal of Engines* 11.6 (2018), pp. 1399–1420.

Desantes, José M, López, J Javier, García-Oliver, José M, and López-Pintor, Darío. "Experimental validation and analysis of seven different chemical kinetic mechanisms for n-dodecane using a rapid compression-expansion machine". In: *Combustion and Flame* 182 (2017), pp. 76–89.

Diez, Alvaro, Crookes, Roy J, and Løvås, Terese. "Experimental studies of autoignition and soot formation of diesel surrogate fuels". In: *Proceedings of the Institution of Mechanical Engineers, Part D: Journal of Automobile Engineering* 227.5 (2013), pp. 656–664.

Dimitriadis, Athanasios et al. "Improving PM-NOx trade-off with paraffinic fuels: A study towards diesel engine optimization with HVO". In: *Fuel* 265 (2020), p. 116921.

Dimitriou, Pavlos and Javaid, Rahat. "A review of ammonia as a compression ignition engine fuel". In: *International Journal of Hydrogen Energy* 45.11 (2020), pp. 7098–7118.

Dirrenberger, Patricia et al. "Laminar burning velocity of gasolines with addition of ethanol". In: *Fuel* 115 (2014), pp. 162–169.

Eckart, Sven et al. "Laminar burning velocities, CO, and NOx emissions of premixed polyoxymethylene dimethyl ether flames". In: *Fuel* 293 (2021), p. 120321.

Eismark, Jan and Balthasar, Michael. *Device for reducing emissions in a vehicle combustion engine*. US Patent 8,499,735. 2013.

Eismark, Jan, Christensen, Magnus, Andersson, Mats, Karlsson, Anders, and Denbratt, Ingemar. "Role of fuel properties and piston shape in influencing soot oxidation in heavy-duty low swirl diesel engine combustion". In: *Fuel* 254 (2019), p. 115568.

ERTRAC Working Group. Energy Carriers for Powertrains for a clean and efficient mobility. European Road Transport Research Advisory Council (ERTRAC) Working Group: Energy and Environment. 2014.

Euro 7: Deal on new EU rules to reduce road transport emissions, Dec 2023, https://www.europarl.europa.eu/news/en.

Farzaneh, Farhad and Jung, Sungmoon. "Lifecycle carbon footprint comparison between internal combustion engine versus electric transit vehicle: A case study in the US". In: *Journal of Cleaner Production* 390 (2023), p. 136111.

Fieweger, K, Blumenthal, Ro, and Adomeit, G. "Self-ignition of SI engine model fuels: a shock tube investigation at high pressure". In: *Combustion and Flame* 109.4 (1997), pp. 599–619.

Fitzgerald, Russell, Svensson, Kenth, Martin, Glen, Qi, Yongli, and Koci, Chad. "Early investigation of ducted fuel injection for reducing soot in mixing-controlled diesel flames". In: *SAE International Journal of Engines* 11.6 (2018), pp. 817–834.

Flynn, Patrick F et al. "Diesel combustion: an integrated view combining laser diagnostics, chemical kinetics, and empirical validation". In: *SAE transactions* (1999), pp. 587–600.

Fraioli, Valentina, Mancaruso, Ezio, Migliaccio, Marianna, and Vaglieco, Bianca Maria. "Ethanol effect as premixed fuel in dual-fuel CI engines: experimental and numerical investigations". In: *Applied energy* 119 (2014), pp. 394–404.

Gao, Wanying et al. "Numerical simulation on NO and soot formation process of a diesel engine with polyoxymethylene dimethyl ethers-diesel blend fuel". In: *Energy Sources, Part A: Recovery, Utilization, and Environmental Effects* (2020), pp. 1–16.

Garcia, Antonio, Monsalve-Serrano, Javier, Villalta, David, and Guzman-Mendoza, Maria. "Parametric assessment of the effect of oxygenated low carbon fuels in a light-duty compression ignition engine". In: *Fuel Processing Technology* 229 (2022), p. 107199.

García, Antonio, Monsalve-Serrano, Javier, Sari, Rafael Lago, and Martinez-Boggio, Santiago. "Energy sustainability in the transport sector using synthetic fuels in series hybrid trucks with RCCI dual-fuel engine". In: *Fuel* 308 (2022), p. 122024.

Garcia-Oliver, Jose M, Novella, Ricardo, Pastor, Jose M, Pachano, Leonardo, and Naud, Bertrand. "A quasi-1D model for the description of ECN spray a combustion process". In: *SAE International Journal of Advances and Current Practices in Mobility* 2.2020-01-0661 (2020), pp. 1974–1985.

Garcia-Oliver, Jose Maria et al. “An experimental and one-dimensional modeling analysis of turbulent gas ejection in pre-chamber engines”. In: *Fuel* 299 (2021), p. 120861.

García-Oliver, José M, Novella, Ricardo, Micó, Carlos, and De Leon-Ceriani, Daiana. “Numerical analysis of the combustion process of oxymethylene ethers as low-carbon fuels for compression ignition engines”. In: *International Journal of Engine Research* 24.5 (2023), pp. 2175–2186.

Gaydon, A. *The Spectroscopy of Flames*. Springer Netherlands, 2012.

Gehmlich, RK et al. “Using ducted fuel injection to attenuate or prevent soot formation in mixing-controlled combustion strategies for engine applications”. In: *Applied energy* 226 (2018), pp. 1169–1186.

Ghadamkheir, Kourosh, Zareei, J, Yang, Xiaohu, and Hatami, Mohammad. “The effects of diesel-OME1 blended fuel on combustion characteristics of a heavy-duty compression ignition engine by a numerical study”. In: *Alexandria Engineering Journal* 64 (2023), pp. 493–503.

Gill, SS, Tsolakis, Athanasios, Dearn, KD, and Rodríguez-Fernández, J. “Combustion characteristics and emissions of Fischer–Tropsch diesel fuels in IC engines”. In: *Progress in Energy and Combustion Science* 37.4 (2011), pp. 503–523.

Gillespie, Fiona Rita. “An experimental and modelling study of the combustion of oxygenated hydrocarbons”. In: *National University of Ireland* (2014).

Girardi, Pierpaolo, Gargiulo, Alessia, and Brambilla, Paola Cristina. “A comparative LCA of an electric vehicle and an internal combustion engine vehicle using the appropriate power mix: the Italian case study”. In: *The International Journal of Life Cycle Assessment* 20 (2015), pp. 1127–1142.

Goeb, Dominik et al. “Oxymethylene ether–n-dodecane blend spray combustion: Experimental study and large-eddy simulations”. In: *Proceedings of the Combustion Institute* 38.2 (2021), pp. 3417–3425.

Gong, Y, Kaario, O, Tilli, A, Larmi, M, and Tanner, FX. *A computational investigation of hydrotreated vegetable oil sprays using RANS and a modified version of the RNG k-ε model in OpenFOAM*. Tech. rep. SAE Technical Paper, 2010.

Grützner, Thomas, Hasse, Hans, Lang, Neven, Siegert, Markus, and Ströfer, Eckhard. “Development of a new industrial process for trioxane production”. In: *Chemical Engineering Science* 62.18-20 (2007), pp. 5613–5620.

Hartikka, Tuukka, Kuronen, Markku, and Kiiski, Ulla. *Technical performance of HVO (hydrotreated vegetable oil) in diesel engines.* Tech. rep. SAE Technical Paper, 2012.

Härtl, Martin, Seidenspinner, Philipp, Jacob, Eberhard, and Wachtmeister, Georg. "Oxygenate screening on a heavy-duty diesel engine and emission characteristics of highly oxygenated oxymethylene ether fuel OME1". In: *Fuel* 153 (2015), pp. 328–335.

Hartmann, M et al. "Auto-ignition of toluene-doped n-heptane and iso-octane/air mixtures: High-pressure shock-tube experiments and kinetics modeling". In: *Combustion and Flame* 158.1 (2011), pp. 172–178.

Haspel, Philip et al. "Large eddy simulation of OME3 and OME4 spray combustion under heavy-duty conditions". In: *Fuel* 353 (2023), p. 129097.

Hawkins, Troy R, Singh, Bhawna, Majeau-Bettez, Guillaume, and Strømman, Anders Hammer. "Comparative environmental life cycle assessment of conventional and electric vehicles". In: *Journal of industrial ecology* 17.1 (2013), pp. 53–64.

He, Tanjin et al. "Development of surrogate model for oxygenated wide-distillation fuel with polyoxymethylene dimethyl ether". In: *SAE International Journal of Fuels and Lubricants* 10.3 (2017), pp. 803–814.

Heavy-duty Vehicles - AECC - Legislative updates Feb 2024, https://www.aecc.eu/legislation/heavy-duty-vehicles/.

Herzler, J, Jerig, L, and Roth, P. "Shock tube study of the ignition of lean n-heptane/air mixtures at intermediate temperatures and high pressures". In: *Proceedings of the Combustion Institute* 30.1 (2005), pp. 1147–1153.

Heywood, John B. "Automotive engines and fuels: a review of future options". In: *Progress in Energy and Combustion Science* 7.3 (1981), pp. 155–184.

Heywood, John B. *Internal combustion engine fundamentals.* McGraw-Hill Education, 2018.

Higgins, Brian and Siebers, Dennis. "Measurement of the flame lift-off location on DI diesel sprays using OH chemiluminescence". In: *SAE Transactions* (2001), pp. 739–753.

Higgins, Brian, Siebers, Dennis, and Aradi, Allen. "Diesel-spray ignition and premixed-burn behavior". In: *SAE transactions* (2000), pp. 961–984.

Hiroyasu, H and Kadota, To. "Models for combustion and formation of nitric oxide and soot in direct injection diesel engines". In: *SAE transactions* (1976), pp. 513–526.

Hottel, Hoyt C and Broughton, FP. "Determination of true temperature and total radiation from luminous gas flames". In: *Industrial & Engineering Chemistry Analytical Edition* 4.2 (1932), pp. 166–175.

Howden Backing Bioenergy for a Low Carbon Future,2023, https://www.howden.com/en-us/articles/renewables/backing-bioenergy.

Iannuzzi, Stefano Emanuele, Barro, Christophe, Boulouchos, Konstantinos, and Burger, Jakob. "Combustion behavior and soot formation/oxidation of oxygenated fuels in a cylindrical constant volume chamber". In: *Fuel* 167 (2016), pp. 49–59.

Ibrahim, Fadzli, Mahmood, Wan Mohd Faizal Wan, Abdullah, Shahrir, and Mansor, Mohd Radzi Abu. *Comparison of simple and detailed soot models in the study of soot formation in a compression ignition diesel engine.* Tech. rep. SAE Technical Paper, 2017.

Jacobs, Sascha et al. "Detailed kinetic modeling of dimethoxymethane. Part II: Experimental and theoretical study of the kinetics and reaction mechanism". In: *Combustion and Flame* 205 (2019), pp. 522–533.

Jakob, Markus et al. "Simultaneous high-speed visualization of soot luminosity and OH* chemiluminescence of alternative-fuel combustion in a HSDI diesel engine under realistic operating conditions". In: *Combustion and Flame* 159.7 (2012), pp. 2516–2529.

Jalilimehr, M, Behzadan, H, Javadi Mal Abad, SM, Moghiman, M, and Niazmand, H. "Investigating the effects of natural gas preheating on soot formation, flame luminosity, and nox emissions: a combined experimental and numerical approach". In: *Heat Transfer—Asian Research* 46.7 (2017), pp. 895–912.

Jamuwa, DK, Sharma, D, and Soni, SL. "Performance, emission and combustion analysis of an ethanol fuelled stationary CI engine". In: *Biofuels* (2016).

Jing, Zheng, Zhang, Chunhua, Cai, Panpan, Li, Yangyang, and Wang, Jibai. "Construction of a Reduced Diesel/Polyoxymethylene Dimethyl Ether 3 (PODE3) Reaction Mechanism for Combustion and Emission Analysis". In: *Energy & Fuels* 35.5 (2021), pp. 4437–4446.

Kamimoto, Takeyuki and Bae, Myurng-hoan. "High combustion temperature for the reduction of particulate in diesel engines". In: *SAE transactions* (1988), pp. 692–701.

Karavalakis, George et al. “Emissions and fuel economy evaluation from two current technology heavy-duty trucks operated on HVO and FAME blends”. In: *SAE International Journal of Fuels and Lubricants* 9.1 (2016), pp. 177–190.

Kawamoto, Ryuji et al. “Estimation of CO2 emissions of internal combustion engine vehicle and battery electric vehicle using LCA”. In: *Sustainability* 11.9 (2019), p. 2690.

Khan, Nida, Sudhakar, Kumarasamy, and Mamat, Rizalman. “Role of biofuels in energy transition, green economy and carbon neutrality”. In: *Sustainability* 13.22 (2021), p. 12374.

Kim, Duckhan, Kim, Seonghwan, Oh, Sehun, and No, Soo-Young. “Engine performance and emission characteristics of hydrotreated vegetable oil in light duty diesel engines”. In: *Fuel* 125 (2014), pp. 36–43.

Kitamura, Takaaki, Ito, T, Senda, Jiro, and Fujimoto, Hajime. “Mechanism of smokeless diesel combustion with oxygenated fuels based on the dependence of the equivalence ration and temperature on soot particle formation”. In: *International Journal of Engine Research* 3.4 (2002), pp. 223–248.

Klotz, Stephen D, Brezinsky, Kenneth, and Glassman, Irvin. “Modeling the combustion of toluene-butane blends”. In: *Symposium (International) on Combustion*. Vol. 27. 1. Elsevier. 1998, pp. 337–344.

Kokjohn, Sage L, Hanson, Reed M, Splitter, DA, and Reitz, RD. “Fuel reactivity controlled compression ignition (RCCI): a pathway to controlled high-efficiency clean combustion”. In: *International Journal of Engine Research* 12.3 (2011), pp. 209–226.

Kranenburg-Bruinsma, KJ van et al. “E-fuels-Towards a more sustainable future for truck transport, shipping and aviation”. In: (2020).

Kumar, Kamal and Sung, Chih-Jen. “Laminar flame speeds and extinction limits of preheated n-decane/O2/N2 and n-dodecane/O2/N2 mixtures”. In: *Combustion and Flame* 151.1-2 (2007), pp. 209–224.

Launder, Brian Edward and Spalding, Dudley Brian. “The numerical computation of turbulent flows”. In: *Numerical prediction of flow, heat transfer, turbulence and combustion*. Elsevier, 1983, pp. 96–116.

Leach, Felix, Kalghatgi, Gautam, Stone, Richard, and Miles, Paul. “The scope for improving the efficiency and environmental impact of internal combustion engines”. In: *Transportation Engineering* 1 (2020), p. 100005.

Lepperhoff, Gerhard et al. *Potential of synthetic fuels in future combustion systems for HSDI diesel engines*. Tech. rep. SAE Technical Paper, 2006.

Li, Feng, Lee, Chia-fon, Wang, Ziman, Liu, Fushui, and Lu, Guoxiang. "Optical investigation on impacts of ambient pressure on macroscopic spray characteristics of ducted fuel injection under non-vaporizing conditions". In: *Fuel* 268 (2020), p. 117192.

Li, Feng, Lee, Chia-fon, Wang, Ziman, Pei, Yiqiang, and Lu, Guoxiang. "Impacts of duct inner diameter and standoff distance on macroscopic spray characteristics of ducted fuel injection under non-vaporizing conditions". In: *International Journal of Engine Research* 22.5 (2021), pp. 1702–1713.

Li, Feng, Lee, Chia-fon, Wu, Han, Wang, Ziman, and Liu, Fushui. "An optical investigation on spray macroscopic characteristics of ducted fuel injection". In: *Experimental Thermal and Fluid Science* 109 (2019), p. 109918.

Li, Zheming et al. *Comparison of laser-extinction and natural luminosity measurements for soot probing in diesel optical engines*. Tech. rep. SAE Technical Paper, 2016.

Lin, Qinjie, Tay, Kun Lin, Zhao, Feiyang, and Yang, Wenming. "Enabling robust simulation of polyoxymethylene dimethyl ether 3 (PODE3) combustion in engines". In: *International Journal of Engine Research* 23.9 (2022), pp. 1522–1542.

Lin, Qinjie, Tay, Kun Lin, Zhou, Dezhi, and Yang, Wenming. "Development of a compact and robust Polyoxymethylene Dimethyl Ether 3 reaction mechanism for internal combustion engines". In: *Energy Conversion and Management* 185 (2019), pp. 35–43.

Liu, Haoye, Wang, Zhi, Wang, Jianxin, and He, Xin. "Improvement of emission characteristics and thermal efficiency in diesel engines by fueling gasoline/diesel/PODEn blends". In: *Energy* 97 (2016), pp. 105–112.

Liu, Jialin et al. "Effects of diesel/PODE (polyoxymethylene dimethyl ethers) blends on combustion and emission characteristics in a heavy duty diesel engine". In: *Fuel* 177 (2016), pp. 206–216.

Liu, Junheng, Sun, Ping, Huang, He, Meng, Jian, and Yao, Xiaohua. "Experimental investigation on performance, combustion and emission characteristics of a common-rail diesel engine fueled with polyoxymethylene dimethyl ethers-diesel blends". In: *Applied Energy* 202 (2017), pp. 527–536.

Liu, Junheng et al. "Effects of PODE/diesel blends on particulate matter emission and particle oxidation characteristics of a common-rail diesel engine". In: *Fuel processing technology* 212 (2021), p. 106634.

Liu, Junheng et al. “An overview of polyoxymethylene dimethyl ethers as alternative fuel for compression ignition engines”. In: *Fuel* 318 (2022), p. 123582.

Liu, Xinlei, Im, Hong G, Mueller, Charles J, and Nyrenstedt, Gustav. “A computational parametric study of ducted fuel injection implementation in a heavy-duty diesel engine”. In: *Fuel* 358 (2024), p. 130228.

Liu, Xinlei, Mohan, Balaji, and Im, Hong G. “Numerical investigation of the free and ducted fuel injections under compression ignition conditions”. In: *Energy & Fuels* 34.11 (2020), pp. 14832–14842.

Liu, Yao, Tan, Jianguo, Wan, Minggang, Zhang, Lang, and Yao, Xiao. “Quantitative measurement of OH* and CH* chemiluminescence in jet diffusion flames”. In: *ACS omega* 5.26 (2020), pp. 15922–15930.

Liu, Yao-Dong, Jia, Ming, Xie, Mao-Zhao, and Pang, Bin. “Enhancement on a skeletal kinetic model for primary reference fuel oxidation by using a semidecoupling methodology”. In: *Energy & Fuels* 26.12 (2012), pp. 7069–7083.

Lopez, J Javier et al. *Characterization of in-cylinder soot oxidation using two-color pyrometry in a production light-duty diesel engine*. Tech. rep. SAE Technical Paper, 2016.

Lv, Delin et al. “Development of a reduced diesel/PODEn mechanism for diesel engine application”. In: *Energy Conversion and Management* 199 (2019), p. 112070.

MAN Engines approves off-road engines for use with regenerative diesel/HVO, 2023, https://press.mantruckandbus.com/corporate/man-engines-approves-off-road-engines-for-use-with-regenerative-dieselhvo/.

Manin, Julien, Skeen, Scott, Pickett, Lyle, Kurtz, Eric, and Anderson, James E. “Effects of oxygenated fuels on combustion and soot formation/oxidation processes”. In: *SAE International Journal of Fuels and Lubricants* 7.3 (2014), pp. 704–717.

Marchal, Caroline et al. “Modelling of aromatics and soot formation from large fuel molecules”. In: *Proceedings of the Combustion Institute* 32.1 (2009), pp. 753–759.

Masamoto, Junzo and Matsuzaki, Kazuhiko. “Development of methylal synthesis by reactive distillation”. In: *Journal of chemical engineering of Japan* 27.1 (1994), pp. 1–5.

Mathews, John A. “Carbon-negative biofuels”. In: *Energy policy* 36.3 (2008), pp. 940–945.

McCaffery, Cavan, Karavalakis, George, Durbin, Tom, Jung, Heejung, and Johnson, Kent. *Engine-out emissions characteristics of a light duty vehicle operating on a hydrogenated vegetable oil renewable diesel*. Tech. rep. SAE Technical Paper, 2020.

Mikkonen, Seppo, Honkanen, Markku, and Kuronen, Markku. "HVO, hydrotreated vegetable oil. A premium renewable biofuel for diesel engines". In: (2013).

Millo, F et al. "Ducted fuel injection: Experimental and numerical investigation on fuel spray characteristics, air/fuel mixing and soot mitigation potential". In: *Fuel* 289 (2021), p. 119835.

Mollenhauer, Klaus, Tschöke, Helmut, and Johnson, Krister GE. *Handbook of diesel engines*. Vol. 1. Springer Berlin, 2010.

Monsalve-Serrano, Javier, Belgiorno, Giacomo, Di Blasio, Gabriele, and Guzmán-Mendoza, María. "1D simulation and experimental analysis on the effects of the injection parameters in methane–diesel dual-fuel combustion". In: *Energies* 13.14 (2020), p. 3734.

Mueller, Charles J and Martin, Glen C. "Effects of oxygenated compounds on combustion and soot evolution in a DI diesel engine: broadband natural luminosity imaging". In: *SAE Transactions* (2002), pp. 518–537.

Mueller, Charles J, Nilsen, Christopher W, Biles, Drummond E, and Yraguen, Boni F. "Effects of fuel oxygenation and ducted fuel injection on the performance of a mixing-controlled compression-ignition optical engine with a two-orifice fuel injector". In: *Applications in Energy and Combustion Science* 6 (2021), p. 100024.

Mueller, Charles J et al. "Ducted fuel injection: A new approach for lowering soot emissions from direct-injection engines". In: *Applied energy* 204 (2017), pp. 206–220.

Musculus, Mark PB, Miles, Paul C, and Pickett, Lyle M. "Conceptual models for partially premixed low-temperature diesel combustion". In: *Progress in energy and combustion science* 39.2-3 (2013), pp. 246–283.

Musculus, Mark PB, Singh, Satbir, and Reitz, Rolf D. "Gradient effects on two-color soot optical pyrometry in a heavy-duty DI diesel engine". In: *Combustion and flame* 153.1-2 (2008), pp. 216–227.

Nadimi, Ebrahim et al. "Effects of using ammonia as a primary fuel on engine performance and emissions in an ammonia/biodiesel dual-fuel CI engine". In: *International Journal of Energy Research* 46.11 (2022), pp. 15347–15361.

Nagle, J and Strickland-Constable, RF. "Oxidation of carbon between 1000–2000 C". In: *Proceedings of the fifth conference on carbon*. Elsevier. 1962, pp. 154–164.

Narayanaswamy, Krithika, Pepiot, Perrine, and Pitsch, Heinz. "A chemical mechanism for low to high temperature oxidation of n-dodecane as a component of transportation fuel surrogates". In: *Combustion and Flame* 161.4 (2014), pp. 866–884.

New Generation DAF trucks ready for 100% HVO, 2023, https://www.daf.com/en/news-and-media/news-articles/global/2023/20-07-2023-new-generation-daf-trucks-ready-for-100-procent-hvo.

Niemeyer, Kyle E, Sung, Chih-Jen, and Raju, Mandhapati P. "Skeletal mechanism generation for surrogate fuels using directed relation graph with error propagation and sensitivity analysis". In: *Combustion and flame* 157.9 (2010), pp. 1760–1770.

Nilsen, Christopher W, Biles, Drummond E, and Mueller, Charles J. "Using ducted fuel injection to attenuate soot formation in a mixing-controlled compression ignition engine". In: *SAE International Journal of Engines* 12.3 (2019), pp. 309–322.

Nilsen, Christopher W, Biles, Drummond E, Wilmer, Brady M, and Mueller, Charles J. "Investigating the effects of duct length and diameter and fuel-injector orifice diameter in a compression-ignition engine equipped with ducted fuel injection". In: *Applications in Energy and Combustion Science* 7 (2021), p. 100030.

Nilsen, Christopher W, Biles, Drummond E, Yraguen, Boni F, and Mueller, Charles J. "Ducted Fuel Injection versus Conventional Diesel Combustion". In: *SAE International Journal of Engines* 13.3 (2020), pp. 345–362.

Novella, Ricardo, Bracho, Gabriela, Gomez-Soriano, Josep, Fernandes, Cássio S, and Lucchini, Tommaso. "Combustion system optimization for the integration of e-fuels (Oxymethylene Ether) in compression ignition engines". In: *Fuel* 305 (2021), p. 121580.

Nyrenstedt, Gustav, Nilsen, Christopher W, Biles, Drummond E, and Mueller, Charles J. "Ducted fuel injection with Low-Net-Carbon fuels as a solution for meeting future emissions regulations". In: *Fuel* 338 (2023), p. 127167.

O'rourke, PJ and Amsden, AA. "A particle numerical model for wall film dynamics in port-injected engines". In: *SAE transactions* (1996), pp. 2000–2013. DOI: 10.4271/961961.

Ogawa, Hideyuki, Nabi, Md Nurun, Minami, Masahiro, Miyamoto, Noboru, and Bong-Seock, Kim. "Ultra low emissions and high performance diesel combustion with a combination of high EGR, three-way catalyst, and a highly oxygenated fuel, dimethoxy methane (DMM)". In: *SAE transactions* (2000), pp. 1019–1027.

Omari, Ahmad, Heuser, Benedikt, Pischinger, Stefan, and Rüdinger, Christoph. "Potential of long-chain oxymethylene ether and oxymethylene ether-diesel blends for ultra-low emission engines". In: *Applied energy* 239 (2019), pp. 1242–1249.

Pan, Mingzhang, Qian, Weiwei, Wang, Yuke, Wu, Changkun, and Huang, Haozhong. "Effect of dimethoxymethane (DMM) additive on combustion and emission characteristics under different working conditions in CI engines". In: *Fuel* 284 (2021), p. 119304.

Park, Su Han and Lee, Chang Sik. "Applicability of dimethyl ether (DME) in a compression ignition engine as an alternative fuel". In: *Energy Conversion and Management* 86 (2014), pp. 848–863.

Pastor, Jose V, Garcia-Oliver, Jose M, Garcia, Antonio, Mico, Carlos, and Möller, Sebastian. "Application of optical diagnostics to the quantification of soot in n-alkane flames under diesel conditions". In: *Combustion and Flame* 164 (2016), pp. 212–223.

Pastor, Jose V, Garcia-Oliver, Jose M, Micó, Carlos, and Tejada, Francisco J. *Combustion behaviour of blends of synthetic fuels in an optical single cylinder engine*. Tech. rep. SAE Technical Paper, 2021.

Pastor, Jose V, Garcia-Oliver, Jose M, Pastor, Jose M, and Vera-Tudela, W. "One-dimensional diesel spray modeling of multicomponent fuels". In: *Atomization and sprays* 25.6 (2015).

Pastor, Jose V, García-Oliver, Jose M, Micó, Carlos, and Tejada, Francisco J. "Characterization of the oxymethylene ether fuels flame structure for ECN Spray A and Spray D nozzles". In: *Applied Energy* 332 (2023), p. 120475.

Pastor, José V, García, Antonio, Micó, Carlos, and Lewiski, Felipe. "An optical investigation of Fischer-Tropsch diesel and Oxymethylene dimethyl ether impact on combustion process for CI engines". In: *Applied Energy* 260 (2020), p. 114238.

Pastor, José V, García-Oliver, José M, Micó, Carlos, García-Carrero, Alba A, and Gómez, Arantzazu. "Experimental study of the effect of hydrotreated vegetable oil and oxymethylene ethers on main spray and combustion characteristics under engine combustion network spray a conditions". In: *Applied Sciences* 10.16 (2020), p. 5460.

Pastor, José V et al. “Effect of a novel piston geometry on the combustion process of a light-duty compression ignition engine: An optical analysis”. In: *Energy* 221 (2021), p. 119764.

Pastor, José V et al. “Influence of the radial-lip concept design to achieve ultra-low soot emission reductions: An optical analysis”. In: *Fuel* 345 (2023), p. 128161.

Payri, Francisco, García-Oliver, Jose M, Novella, Ricardo, and Pérez-Sánchez, Eduardo J. “Influence of the n-dodecane chemical mechanism on the CFD modelling of the diesel-like ECN Spray A flame structure at different ambient conditions”. In: *Combustion and Flame* 208 (2019), pp. 198–218.

Payri, Francisco, Olmeda, Pablo, Martín, Jaime, and García, Antonio. “A complete 0D thermodynamic predictive model for direct injection diesel engines”. In: *Applied Energy* 88.12 (2011), pp. 4632–4641.

Payri, Raúl, Viera, Juan Pablo, Pei, Yuanjiang, and Som, Sibendu. “Experimental and numerical study of lift-off length and ignition delay of a two-component diesel surrogate”. In: *Fuel* 158 (2015), pp. 957–967.

Pélerin, Dominik, Gaukel, Kai, Härtl, Martin, Jacob, Eberhard, and Wachtmeister, Georg. “Potentials to simplify the engine system using the alternative diesel fuels oxymethylene ether OME1 and OME3- 6 on a heavy-duty engine”. In: *Fuel* 259 (2020), p. 116231.

Pellegrini, Leonardo et al. *Combustion behaviour and emission performance of neat and blended polyoxymethylene dimethyl ethers in a light-duty diesel engine*. Tech. rep. SAE Technical Paper, 2012.

Pepiot-Desjardins, Perrine and Pitsch, Heinz. “An efficient error-propagation-based reduction method for large chemical kinetic mechanisms”. In: *Combustion and Flame* 154.1-2 (2008), pp. 67–81.

Peters, N. “Turbulent combustion. Cambridge, UK: Cambridge University Press."” In: (2000).

Piano, A et al. “Numerical and optical soot characterization through 2-color pyrometry technique for an innovative diesel piston bowl design”. In: *Fuel* 333 (2023), p. 126347.

Piano, Andrea, Segatori, Cristiano, Millo, Federico, Pesce, Francesco Concetto, and Vassallo, Alberto Lorenzo. “Investigation of Ducted Fuel Injection Implementation in a Retrofitted Light-Duty Diesel Engine through Numerical Simulation”. In: *SAE International Journal of Engines* 16.03-16-05-0038 (2022).

Pickett, Lyle M, Kook, Sanghoon, and Williams, Timothy C. "Visualization of diesel spray penetration, cool-flame, ignition, high-temperature combustion, and soot formation using high-speed imaging". In: *SAE international journal of engines* 2.1 (2009), pp. 439–459.

Pickett, Lyle M and Siebers, Dennis L. "Non-sooting, low flame temperature mixing-controlled DI diesel combustion". In: *SAE transactions* (2004), pp. 614–630.

Pinto, GM et al. "Combustion, performance and emission analyses of a CI engine operating with renewable diesel fuels (HVO/FARNESANE) under dual-fuel mode through hydrogen port injection". In: *International Journal of Hydrogen Energy* 48.51 (2023), pp. 19713–19732.

Pitz, William J and Mueller, Charles J. "Recent progress in the development of diesel surrogate fuels". In: *Progress in Energy and Combustion Science* 37.3 (2011), pp. 330–350.

Plee, Steven L and Ahmad, Tanvir. "Relative roles of premixed and diffusion burning in diesel combustion". In: *SAE transactions* (1983), pp. 892–909.

Polonowski, Christopher J et al. "An experimental investigation of low-soot and soot-free combustion strategies in a heavy-duty, single-cylinder, direct-injection, optical diesel engine". In: *SAE International Journal of Fuels and Lubricants* 5.1 (2012), pp. 51–77.

Posada, Francisco, Chambliss, Sarah, and Blumberg, Kate. "Costs of emission reduction technologies for heavy-duty diesel vehicles". In: *ICCT White paper* (2016).

Putrasari, Yanuandri and Lim, Ocktaeck. "Dimethyl ether as the next generation fuel to control nitrogen oxides and particulate matter emissions from internal combustion engines: A review". In: *ACS omega* 7.1 (2021), pp. 32–37.

Ra, Youngchul and Reitz, Rolf D. "A reduced chemical kinetic model for IC engine combustion simulations with primary reference fuels". In: *Combustion and Flame* 155.4 (2008), pp. 713–738.

Rajasekar, E and Selvi, S. "Review of combustion characteristics of CI engines fueled with biodiesel". In: *Renewable and Sustainable Energy Reviews* 35 (2014), pp. 390–399.

Rao, Varun and Honnery, Damon. "A comparison of two NOx prediction schemes for use in diesel engine thermodynamic modelling". In: *Fuel* 107 (2013), pp. 662–670.

Reitz, Rolf D et al. *IJER editorial: The future of the internal combustion engine*. 2020.

Ren, Shuojin, Wang, Zhi, Li, Bowen, Liu, Haoye, and Wang, Jianxin. "Development of a reduced polyoxymethylene dimethyl ethers (PODEn) mechanism for engine applications". In: *Fuel* 238 (2019), pp. 208–224.

Richards, KJ, Senecal, PK, and Pomraning, E. "CONVERGE (v3. 0), Convergent Science". In: *Inc., Madison, WI* (2021).

Richter, Sandra, Kathrotia, Trupti, Braun-Unkhoff, Marina, Naumann, Clemens, and Köhler, Markus. "Influence of oxymethylene ethers (OMEn) in mixtures with a diesel surrogate". In: *Energies* 14.23 (2021), p. 7848.

Riedl, Max J. *Optical design fundamentals for infrared systems*. Vol. 48. SPIE press, 2001.

Ritchie, Hannah. "Sector by sector: where do global greenhouse gas emissions come from?" In: *Our World in Data* (2020). https://ourworldindata.org/ghg-emissions-by-sector.

Ritchie, Hannah, Rosado, Pablo, and Roser, Max. "Energy Production and Consumption". In: *Our World in Data* (2020). https://ourworldindata.org/energy-production-consumption.

Ritchie, Hannah, Rosado, Pablo, and Roser, Max. "CO2 and Greenhouse Gas Emissions". In: *Our World in Data* (2023). https://ourworldindata.org/co2-and-greenhouse-gas-emissions.

Ritchie, Hannah, Rosado, Pablo, and Roser, Max. "Energy". In: *Our World in Data* (2023). https://ourworldindata.org/energy.

Rothamer, David A and Murphy, Lucas. "Systematic study of ignition delay for jet fuels and diesel fuel in a heavy-duty diesel engine". In: *Proceedings of the combustion institute* 34.2 (2013), pp. 3021–3029.

Sarathy, S Mani et al. "Comprehensive chemical kinetic modeling of the oxidation of 2-methylalkanes from C7 to C20". In: *Combustion and flame* 158.12 (2011), pp. 2338–2357.

Sattarzadeh, Mehran, Ebrahimi, Mojtaba, and Jazayeri, Seyed Ali. "A detail study of a RCCI engine performance fueled with diesel fuel and natural gas blended with syngas with different compositions". In: *International Journal of Hydrogen Energy* 47.36 (2022), pp. 16283–16296.

Schemme, Steffen, Samsun, Remzi Can, Peters, Ralf, and Stolten, Detlef. "Power-to-fuel as a key to sustainable transport systems–An analysis of diesel fuels produced from CO2 and renewable electricity". In: *Fuel* 205 (2017), pp. 198–221.

Senecal, PK et al. “Multi-dimensional modeling of direct-injection diesel spray liquid length and flame lift-off length using CFD and parallel detailed chemistry”. In: *SAE transactions* (2003), pp. 1331–1351.

Şener, R. “Numerical investigation of ducted fuel injection strategy for soot reduction in compression ignition engine”. In: *Journal of Applied Fluid Mechanics* 15.2 (2022), pp. 475–489.

Şener, Ramazan. “Ducted fuel injection: Numerical study of soot formation and oxidation using detailed soot modeling approach in a compression ignition engine at different loads”. In: *Journal of the Brazilian Society of Mechanical Sciences and Engineering* 44.1 (2022), p. 45.

Shahir, VK, Jawahar, CP, and Suresh, PR. “Comparative study of diesel and biodiesel on CI engine with emphasis to emissions—a review”. In: *Renewable and Sustainable Energy Reviews* 45 (2015), pp. 686–697.

Shen, Hsi-Ping S, Steinberg, Justin, Vanderover, Jeremy, and Oehlschlaeger, Matthew A. “A shock tube study of the ignition of n-heptane, n-decane, n-dodecane, and n-tetradecane at elevated pressures”. In: *Energy & Fuels* 23.5 (2009), pp. 2482–2489.

Shrestha, Krishna P et al. “A comprehensive kinetic modeling of oxymethylene ethers (OMEn, n= 1–3) oxidation-laminar flame speed and ignition delay time measurements”. In: *Combustion and Flame* 246 (2022), p. 112426.

Singh, Rahul Kumar and Agarwal, Avinash Kumar. “Soot and NOx modelling for diesel engines”. In: *Engine Modeling and Simulation*. Springer, 2021, pp. 195–217.

Skeen, Scott, Manin, Julien, and Pickett, Lyle M. “Visualization of ignition processes in high-pressure sprays with multiple injections of n-dodecane”. In: *SAE International Journal of Engines* 8.2 (2015), pp. 696–715.

Song, Ki Hoon and Litzinger, Thomas A. “Effects of dimethyoxymethane blending into diesel fuel on soot in an optically accessible DI diesel engine”. In: *Combustion science and technology* 178.12 (2006), pp. 2249–2280.

Stone, R. and Ball, J.K. *Automotive Engineering Fundamentals*. Premiere Series Bks. SAE International, 2004.

Sugiyama, Kouseki, Goto, Isamu, Kitano, Koji, Mogi, Kazuhisa, and Honkanen, Markku. “Effects of hydrotreated vegetable oil (HVO) as renewable diesel fuel on combustion and exhaust emissions in diesel engine”. In: *SAE International Journal of Fuels and Lubricants* 5.1 (2012), pp. 205–217.

Sun, Wenting, Chen, Zheng, Gou, Xiaolong, and Ju, Yiguang. "A path flux analysis method for the reduction of detailed chemical kinetic mechanisms". In: *Combustion and Flame* 157.7 (2010), pp. 1298–1307.

Sun, Wenyu et al. "Speciation and the laminar burning velocities of poly (oxymethylene) dimethyl ether 3 (POMDME3) flames: An experimental and modeling study". In: *Proceedings of the Combustion Institute* 36.1 (2017), pp. 1269–1278.

Svensson, Kenth, Fitzgerald, Russell, and Martin, Glen. *Ducted Fuel Injection: An Experimental Study on Optimal Duct Size*. Tech. rep. SAE Technical Paper, 2022.

Svensson, Kenth, Kim, Charlie, Seiler, Patrick, Martin, Glen, and Koci, Chad. *Performance and emission results from a heavy-duty diesel engine with ducted fuel injection*. Tech. rep. SAE Technical Paper, 2021.

Svensson, Kenth I and Martin, Glen C. "Ducted fuel injection: effects of standoff distance and duct length on soot reduction". In: *SAE International Journal of Advances and Current Practices in Mobility* 1.2019-01-0545 (2019), pp. 1074–1083.

Szeto, Wai and Leung, Dennis YC. "Is hydrotreated vegetable oil a superior substitute for fossil diesel? A comprehensive review on physicochemical properties, engine performance and emissions". In: *Fuel* 327 (2022), p. 125065.

Taghizadeh-Alisaraei, Ahmad and Rezaei-Asl, Abbas. "The effect of added ethanol to diesel fuel on performance, vibration, combustion and knocking of a CI engine". In: *Fuel* 185 (2016), pp. 718–733.

Tanaka, Shigeyuki, Ayala, Ferran, and Keck, James C. "A reduced chemical kinetic model for HCCI combustion of primary reference fuels in a rapid compression machine". In: *Combustion and flame* 133.4 (2003), pp. 467–481.

Tang, Meng et al. "Numerical Investigation of Fuel Effects on Soot Emissions at Heavy-Duty Diesel Engine Conditions". In: *Internal Combustion Engine Division Fall Technical Conference*. Vol. 51999. American Society of Mechanical Engineers. 2018, V002T06A019.

Tejada Magraner, Francisco José. "Analysis of Fuel Effects on the Diffusive Flame Structure Using Advanced Optical Techniques in a Single Cylinder Optical Engine". PhD thesis. Universitat Politècnica de València, 2024.

Tiemin, Xuan. "Optical investigations on diesel spray dynamics and in-flame soot formation". PhD thesis. Universitat Polit'ecnica de Val'encia, 2017.

Transport sector contribution to total GHG emissions, 2009 (EEA-32) — European Environment Agency, https://www.eea.europa.eu/data-and-maps/figures/transport-sector-contribution-to-total.

Tree, Dale R and Svensson, Kenth I. "Soot processes in compression ignition engines". In: *Progress in energy and combustion science* 33.3 (2007), pp. 272–309.

Tsurushima, Tadahi. "A new skeletal PRF kinetic model for HCCI combustion". In: *Proceedings of the Combustion Institute* 32.2 (2009), pp. 2835–2841.

Turns, Stephen R et al. *Introduction to combustion.* Vol. 287. McGraw-Hill Companies New York, NY, USA, 1996.

Ueckerdt, Falko et al. "Potential and risks of hydrogen-based e-fuels in climate change mitigation". In: *Nature Climate Change* 11.5 (2021), pp. 384–393.

Van Lipzig, JPJ, Nilsson, EJK, De Goey, Laurentius PH, and Konnov, Alexander A. "Laminar burning velocities of n-heptane, iso-octane, ethanol and their binary and tertiary mixtures". In: *Fuel* 90.8 (2011), pp. 2773–2781.

Vargas Lewiski, Felipe de. "Analysis of the combustion process and soot formation in a single cylinder optical engine fueled with e-fuels and using different piston geometries". PhD thesis. Universitat Politècnica de València, 2021.

Verhelst, Sebastian, Turner, James WG, Sileghem, Louis, and Vancoillie, Jeroen. "Methanol as a fuel for internal combustion engines". In: *Progress in Energy and Combustion Science* 70 (2019), pp. 43–88.

Verma, Shrey, Dwivedi, Gaurav, and Verma, Puneet. "Life cycle assessment of electric vehicles in comparison to combustion engine vehicles: A review". In: *Materials Today: Proceedings* 49 (2022), pp. 217–222.

Versteeg, Henk Kaarle and Malalasekera, Weeratunge. *An introduction to computational fluid dynamics: the finite volume method.* Pearson education, 2007.

Volvo Trucks certify HVO synthetic diesel for all engines, 2015, https://www.fleetnews.co.uk/news/latest-news/2015/06/25/volvo-trucks-certify-hvo-synthetic-diesel-for-all-engines.

Wahbi, A, Tsolakis, A, and Herreros, J. "Emissions control technologies for natural gas engines". In: *Natural Gas Engines: For Transportation and Power Generation* (2019), pp. 359–379.

Walker, Joseph Frederic and Frederic, Joseph. *Formaldehyde*. Vol. 26. Reinhold New York, 1964.

Wang, Hu, Ra, Youngchul, Jia, Ming, and Reitz, Rolf D. "Development of a reduced n-dodecane-PAH mechanism and its application for n-dodecane soot predictions". In: *Fuel* 136 (2014), pp. 25–36.

Wang, Hu, Yao, Mingfa, and Reitz, Rolf D. "Development of a reduced primary reference fuel mechanism for internal combustion engine combustion simulations". In: *Energy & Fuels* 27.12 (2013), pp. 7843–7853.

Wang, Qiao et al. "Experimental and kinetic study on the laminar burning speed, Markstein length and cellular instability of oxygenated fuels". In: *Fuel* 297 (2021), p. 120754.

Wei, Jiangjun et al. "Impact of methanol alternative fuel on oxidation reactivity of soot emissions from a modern CI engine". In: *Fuel* 268 (2020), p. 117352.

Wei, Wu, Zhou, Tingyu, Zhao, Lun, Ba, Jin, and Zhang, Long. "Numerical study on the injection strategy on combustion and emission characteristics of a non-road diesel engine under different altitude conditions". In: *Case Studies in Thermal Engineering* 53 (2024), p. 103838.

Westbrook, CK et al. "The effects of pressure, temperature, and concentration on the reactivity of alkanes: Experiments and modeling in a rapid compression machine". In: *Symposium (international) on combustion*. Vol. 27. 1. Elsevier. 1998, pp. 371–378.

White, CM. "OH* chemiluminescence measurements in a direct injection hydrogen-fuelled internal combustion engine". In: *International Journal of Engine Research* 8.2 (2007), pp. 185–204.

Wu, Yixuan, Ays, Isabelle, and Geimer, Marcus. *Analysis and Preliminary Design of Oxymethylene ether (OME) Driven Mobile Machines*. Tech. rep. 2019. DOI: 10.5445/IR/1000097941.

Xuan, Tiemin et al. "In-flame soot quantification of diesel sprays under sooting/non-sooting critical conditions in an optical engine". In: *Applied Thermal Engineering* 149 (2019), pp. 1–10.

Yakhot, VSASTBCG, Orszag, SA, Thangam, Siva, Gatski, TB, and Speziale, CG1167781. "Development of turbulence models for shear flows by a double expansion technique". In: *Physics of Fluids A: Fluid Dynamics* 4.7 (1992), pp. 1510–1520.

Yang, Qirui, Grill, Michael, and Bargende, Michael. *The application of e-fuel oxymethylene ether OME1 in a virtual heavy-duty diesel engine for ultra-low emissions*. Tech. rep. SAE Technical Paper, 2020.

Yao, Tong et al. "A compact skeletal mechanism for n-dodecane with optimized semi-global low-temperature chemistry for diesel engine simulations". In: *Fuel* 191 (2017), pp. 339–349.

Yu, Xin, Zha, Kan, Luo, Xi, Taraza, Dinu, and Jansons, Marcis. *Simulation and experimental measurement of CO2*, OH* and CH2O* chemiluminescence from an optical diesel engine fueled with n-heptane*. Tech. rep. SAE Technical Paper, 2013.

Zhang, Zhichao et al. "Investigation of the macroscopic characteristics of Hydrotreated Vegetable Oil (HVO) spray using CFD method". In: *Fuel* 237 (2019), pp. 28–39.

Zhao, Fuquan et al. "Homogeneous charge compression ignition (HCCI) engines". In: (2003).

Zhao, Hua and Ladommatos, Nicos. "Optical diagnostics for soot and temperature measurement in diesel engines". In: *Progress in energy and combustion science* 24.3 (1998), pp. 221–255.

Zhao, Mengmeng, Buttsworth, David, and Choudhury, Rishabh. "Experimental and numerical study of OH* chemiluminescence in hydrogen diffusion flames". In: *Combustion and Flame* 197 (2018), pp. 369–377.

Zheng, Yanyan, Tang, Qiang, Wang, Tiefeng, Liao, Yuhui, and Wang, Jinfu. "Synthesis of a green fuel additive over cation resins". In: *Chemical Engineering & Technology* 36.11 (2013), pp. 1951–1956.

Zhou, Feng et al. "The application prospect and challenge of the alternative methanol fuel in the internal combustion engine". In: *Science of The Total Environment* (2023), p. 169708.

Zhu, RJ, Wang, XB, Miao, Haiyan, and Huang, ZH. "Combustion and particulate emission characteristics of a diesel engine fuelled with diesel—dimethoxymethane blends". In: *Proceedings of the Institution of Mechanical Engineers, Part D: Journal of Automobile Engineering* 224.4 (2010), pp. 521–531.

Zhu, Ruijun, Wang, Xibin, Miao, Haiyan, Yang, Xiaofeng, and Huang, Zuohua. "Effect of dimethoxy-methane and exhaust gas recirculation on combustion and emission characteristics of a direct injection diesel engine". In: *Fuel* 90.5 (2011), pp. 1731–1737.

UNIVERSITAT POLITÈCNICA DE VALÈNCIA

DOCTORAL THESIS

NUMERICAL AND OPTICAL ASSESSMENT OF DIFFERENT SOLUTIONS FOR POLLUTANT EMISSION REDUCTION IN COMPRESSION IGNITION ENGINES

USAMA BIN KHALID

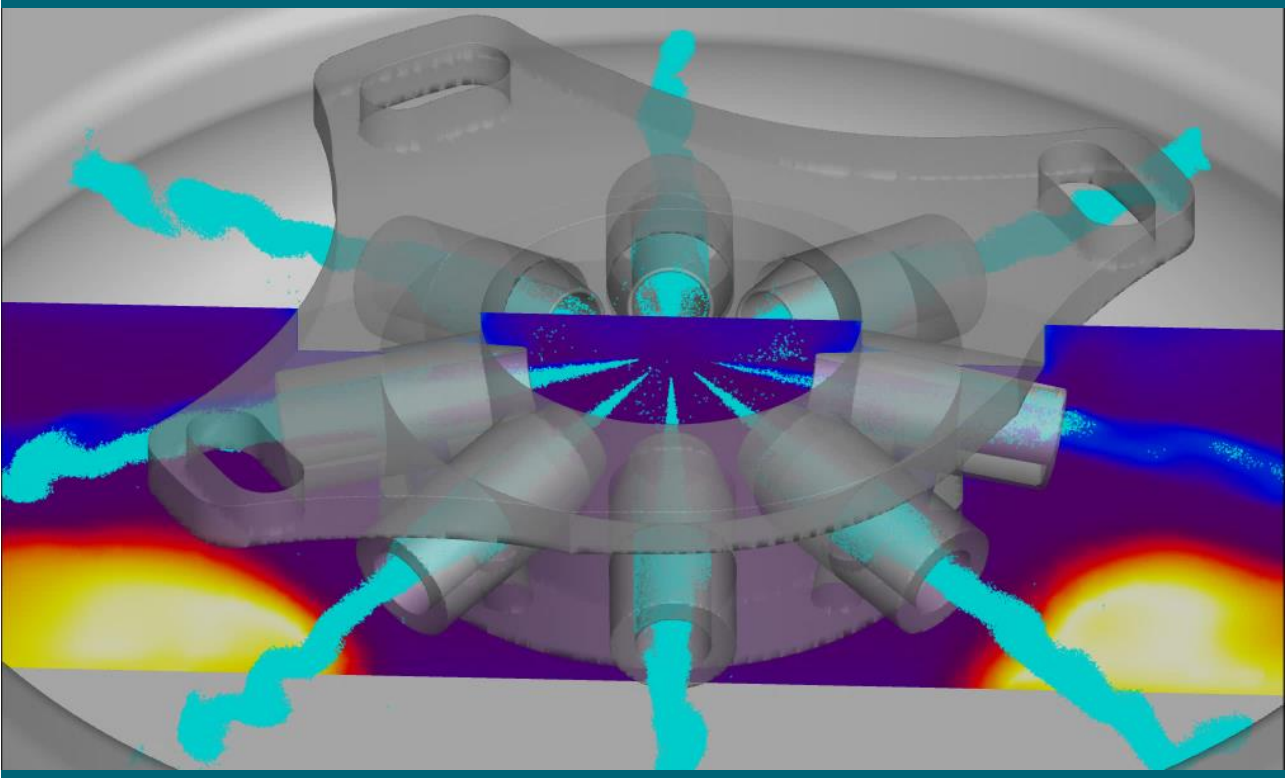

JUNE 2024

CMT - CLEAN MOBILITY & THERMOFLUIDS